



## INTERIM REPORT

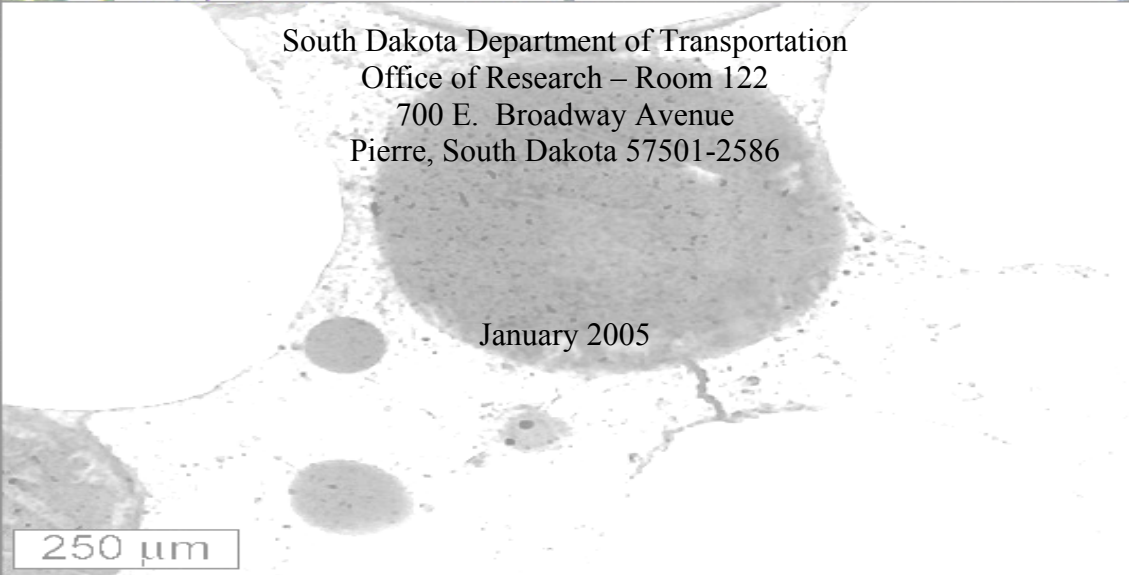
Investigation of the Long Term Effects of Magnesium Chloride and  
Other Concentrated Salt Solutions on Pavement and Structural  
Portland Cement Concrete



SD2002-01  
Submitted by:

Lawrence L. Sutter, Ph.D.  
Michigan Tech Transportation Institute  
Michigan Technological University  
1400 Townsend Dr.  
Houghton, MI 49931  
Voice: 906-487-2268  
FAX: 906-487-2583

Submitted to:



South Dakota Department of Transportation  
Office of Research – Room 122  
700 E. Broadway Avenue  
Pierre, South Dakota 57501-2586

January 2005

250  $\mu\text{m}$

# Table of Contents

<b>TABLE OF CONTENTS</b> .....	<b>I</b>
<b>LIST OF TABLES</b> .....	<b>IV</b>
<b>LIST OF FIGURES</b> .....	<b>VI</b>
<b>SECTION 1. INTRODUCTION</b> .....	<b>1</b>
1.0. PROBLEM STATEMENT .....	1
1.1. SUMMARY OF WORK.....	2
1.2. ORGANIZATION OF THIS REPORT .....	3
<b>SECTION 2. BACKGROUND</b> .....	<b>4</b>
2.1. REVIEW OF PAST AND CURRENT SNOW AND ICE REMOVAL MAINTENANCE PRACTICES.....	4
2.1.1 <i>Traditional Winter Maintenance Practices</i> .....	4
2.1.2 <i>What Led to Change</i> .....	5
2.1.3 <i>Modified &amp; Current Winter Maintenance Practices</i> .....	7
2.1.3.1 Deicing.....	8
2.1.3.2 Pre-wetting.....	10
2.1.3.3 Anti-icing.....	11
2.2. CONCRETE PROPERTIES THAT AFFECT FREEZE-THAW AND CHEMICAL RESISTANCE.....	14
2.2.1 <i>Permeability</i> .....	14
2.2.1.1 Chloride Diffusion .....	14
2.2.2 <i>Air Content</i> .....	17
2.2.3 <i>Cement Chemistry</i> .....	19
2.2.3.1 Dedolomitization.....	20
2.2.4 <i>Cracking</i> .....	21
2.3. TYPES OF INTERACTIONS.....	22
2.3.1. <i>Physical Mechanisms of Paste Freeze-Thaw Attack</i> .....	22
2.3.2 <i>Chemical Mechanisms of Paste Freeze-Thaw Attack</i> .....	25
2.4 PAVEMENT CONSTRUCTION PRACTICES – EFFECTS ON DEICER SCALING/DETERIORATION .....	33
2.4.1 <i>Overview</i> .....	33
2.4.2 <i>Materials</i> .....	33
2.4.2.1 Cementitious and Supplementary Cementitious Materials.....	33
2.4.2.2 Cement .....	33
2.4.2.3 Ground Granulated Blast Furnace Slag.....	34
2.4.2.4 Silica Fume .....	35
2.4.3 <i>Test Methods to Evaluate Concrete Mixture Designs</i> .....	35
2.4.3.1 Diagnostic Methods for Identifying Deicer Scaling/Deterioration.....	35
2.4.3.2 Diagnostic Methods for Determining Permeability.....	39

2.4.4	<i>Construction Considerations for Preventing Deicer Distress</i> .....	41
2.4.4.1	Ambient and Seasonal Construction Conditions .....	41
2.4.4.2	Consolidation .....	41
2.4.4.3	Steel Placement .....	42
2.4.4.4	Finishing.....	42
2.4.4.5	Curing .....	43
2.4.5	<i>Preventive Strategies for Controlling Specific Types of Materials-Related Distress</i> .....	44
2.4.5.1	Deicer Scaling/Deterioration .....	44
2.4.5.2	Corrosion of Embedded Steel.....	46
2.5	STATE-OF-THE PRACTICE CONSTRUCTION OF CONCRETE PAVEMENTS .....	49
2.6	LITERATURE REVIEW SUMMARY .....	52
<b>SECTION 3. WORK TO DATE .....</b>		<b>54</b>
3.1	EXAMINATION OF FIELD CORES .....	54
3.1.1	<i>Idaho, westbound Interstate Highway 184 west of Boise, near milepost 3.</i> .....	54
3.1.2	<i>Iowa, eastbound US Highway 34, western end of the Burlington Bridge.</i> .....	59
3.1.3	<i>Montana, westbound Interstate Highway 90 bridge deck near milepost 117.</i> .....	64
3.1.4	<i>Colorado, State Highway 83, south of Denver near milepost 57.</i> .....	68
3.1.5	<i>South Dakota, eastbound 26th Street left-turn lane onto northbound Interstate Highway 29.</i> ..	73
3.2	LABORATORY EXPERIMENT - PHASE I.....	83
3.2.1	<i>Mix Design</i> .....	83
3.2.2	<i>Testing Regimes</i> .....	84
3.2.3	<i>Deicer Solution Strength</i> .....	84
3.2.4	<i>Rapid Chloride Ion Penetration Test</i> .....	86
3.2.5	<i>Analysis of Specimens Exposed to Deicer Solutions</i> .....	87
3.2.6	<i>Cyclical Temperature Experiment</i> .....	87
3.2.6.1	Observations.....	87
3.2.6.2	Split Tensile Strength Testing .....	94
3.2.6.3	Petrographic Analysis .....	94
3.2.7	<i>Low Temperature Experiment</i> .....	111
3.2.7.1	Observations.....	111
3.2.7.2	Split Tensile Strength Testing .....	115
3.2.7.3	Petrographic Analysis .....	117
3.2.8	<i>High Temperature Experiment</i> .....	155
3.2.8.1	Observations.....	155
3.2.8.2	Split Tensile Strength Testing .....	158
3.2.8.3	Petrographic Analysis .....	158

3.3 PHASE I ADDITIONAL EXPERIMENTS .....	162
3.3.1 <i>Cyclical Temperature Experiments</i> .....	162
3.3.1.1 Additional Tests Performed .....	162
3.3.1.2 Results of Additional Tests .....	162
3.3.2 <i>Cold Temperature Experiment</i> .....	165
3.3.2.1 Additional Tests Performed .....	165
3.3.2.2 Results of Additional Tests .....	165
<b>SECTION 4. PHASE II PROPOSAL .....</b>	<b>169</b>
4.1 PHASE II BACKGROUND .....	169
4.2 PHASE II EXPERIMENTAL PLAN .....	169
4.2.1 <i>Overview</i> .....	169
4.2.2 <i>Sample Preparation</i> .....	169
4.2.3 <i>Scaling Resistance Testing</i> .....	170
4.2.4 <i>Low Temperature Test</i> .....	171
4.2.5 <i>Diffusion and Permeability Assessment</i> .....	171
4.2.6 <i>Analytical Methods</i> .....	172
<b>SECTION 5. REVISED SCHEDULE .....</b>	<b>173</b>
<b>SECTION 6. BIBLIOGRAPHY .....</b>	<b>174</b>

## List of Tables

TABLE 1.1. SUMMARY OF TASK PROGRESS TO DATE .....	2
TABLE 2.1. DEICING CHEMICAL CONCENTRATIONS USED BY VARIOUS AGENCIES .....	8
TABLE 2.2. PRE-WETTING CHEMICALS THAT ARE USED BY AGENCIES .....	11
TABLE 2.3. ANTI-ICING CHEMICAL CONCENTRATIONS USED BY VARIOUS AGENCIES .....	11
TABLE 2.4. OPERATION METHODS AS PER STORM EVENT .....	12
TABLE 2.5. EFFECTS OF W/C RATIO ON THE AIR VOID SYSTEM IN CONCRETE .....	18
TABLE 2.6. CAUSES OF CRACKING IN INDIVIDUAL COMPONENTS OF CONCRETE DUE TO INTERACTIONS WITH SURROUNDINGS .....	22
TABLE 2.7. CHLORIDE ION PENETRABILITY BASED ON CHARGE PASSED .....	40
TABLE 2.8. RECOMMENDED AIR CONTENTS FOR FREEZE-THAW DISTRESS RESISTANT CONCRETE .....	45
TABLE 2.9. CONCRETE MIXTURE PARAMETERS OBTAINED FROM SHA STANDARD SPECIFICATIONS .....	51
TABLE 3.1. RESULTS OF MODIFIED POINT-COUNTS ON CORES FROM IDAHO SITE .....	57
TABLE 3.2. RESULTS OF MODIFIED POINT-COUNTS ON CORES FROM IOWA SITE .....	62
TABLE 3.3. RESULTS OF MODIFIED POINT-COUNTS ON CORES FROM MONTANA SITE .....	67
TABLE 3.4. RESULTS OF MODIFIED POINT-COUNTS ON CORES FROM COLORADO SITE .....	71
TABLE 3.5. RESULTS OF MODIFIED POINT-COUNTS ON CORES FROM SOUTH DAKOTA SITE .....	76
TABLE 3.6. TESTING DETAILS ASSOCIATED WITH THE LABORATORY EVALUATION .....	83
TABLE 3.7 THEORETICAL VOLUME PERCENT OF PHASES FORMED IN THE VARIOUS DEICER SOLUTIONS USED AND THE COMPOSITION OF THE NON-ICE PHASE FORMED. ALSO, SATURATION CONCENTRATIONS AT TWO TEMPERATURES. ....	86
TABLE 3.8. RCPT RESULTS FOR DIFFERENT W/C RATIO MORTARS .....	87
TABLE 3.9. LIST OF VISUAL RATINGS FOR ALL MORTAR CYLINDERS FROM THE CYCLIC TEMPERATURE TESTS. RATING SCALE: 0 - NO VISIBLE CHANGE, 1 – SOME CRACKING, 2 - VISIBLE EXPANSION AND CRACKING, 3 - SEVERE EXPANSION AND CRACKING, 4 - PARTIAL DISINTEGRATION, 5 - TOTAL DISINTEGRATION, X – TEST ABORTED. ....	93
TABLE 3.10 LIST OF VISUAL RATINGS FOR ALL MORTAR CYLINDERS FROM THE LOW TEMPERATURE TESTS. RATING SCALE: 0 - NO VISIBLE CHANGE, 1 – SOME CRACKING, 2 - VISIBLE EXPANSION AND CRACKING, 3 - SEVERE EXPANSION AND CRACKING, 4 - PARTIAL DISINTEGRATION, 5 - TOTAL DISINTEGRATION, X – TEST ABORTED. ....	115
TABLE 3.11 SPLITTING TENSILE STRENGTH OF MORTAR CYLINDERS EXPOSED TO LIME WATER SOLUTION FOR 28 DAYS IN THE CONSTANT LOW TEMPERATURE TEST .....	116
TABLE 3.12 SPLITTING TENSILE STRENGTH OF MORTAR CYLINDERS EXPOSED TO NaCl SOLUTION FOR 28 DAYS IN THE CONSTANT LOW TEMPERATURE TEST .....	116
TABLE 3.13 SPLITTING TENSILE STRENGTH OF MORTAR CYLINDERS EXPOSED TO MgCl <sub>2</sub> SOLUTION FOR 28 DAYS IN THE CONSTANT LOW TEMPERATURE TEST .....	116

TABLE 3.14 SPLITTING TENSILE STRENGTH OF MORTAR CYLINDERS EXPOSED TO $\text{CMA}$ SOLUTION FOR 28 DAYS IN THE CONSTANT LOW TEMPERATURE TEST. ....	117
TABLE 3.15 SPLITTING TENSILE STRENGTH OF MORTAR CYLINDERS EXPOSED TO $\text{CaCl}_2$ SOLUTION FOR 28 DAYS IN THE CONSTANT LOW TEMPERATURE TEST. ....	117
TABLE 3.16 LIST OF VISUAL RATINGS FOR ALL MORTAR CYLINDERS FROM THE HIGH TEMPERATURE TESTS. RATING SCALE: 0 - NO VISIBLE CHANGE, 1 – SOME CRACKING, 2 - VISIBLE EXPANSION AND CRACKING, 3 - SEVERE EXPANSION AND CRACKING, 4 - PARTIAL DISINTEGRATION, 5 - TOTAL DISINTEGRATION, $X$ – TEST ABORTED. ....	158
TABLE 4.1. EXPERIMENTAL DESIGN FOR UNSEALED ASTM C 672 TESTING. ....	170
TABLE 4.2. DEICER CONCENTRATIONS TO BE USED IN THE PHASE II TESTING. ....	170
TABLE 4.3. EXPERIMENTAL DESIGN FOR SEALED ASTM C 672 TESTING. ....	171
TABLE 4.4. EXPERIMENTAL DESIGN FOR CYLINDRICAL SPECIMENS TESTED AT 40 °F. ....	171

## List of Figures

FIGURE 2.1 THE PARTIAL PHASE DIAGRAMS FOR THE COMMON DEICER SOLUTIONS.....	9
FIGURE 2.2. EFFECT OF ENTRAINED AIR ON DURABILITY AND STRENGTH.....	18
FIGURE 2.3. SCHEMATIC REPRESENTATION OF THE HYDRAULIC PRESSURE THEORY. ....	23
FIGURE 2.4. ETTRINGITE (A) AND HYDROCALUMITE (B) IN-FILLING IN VOID AND CRACK, RESPECTIVELY. EXAMPLE SPECTRA FROM EACH PHASE ARE SHOWN IN (C) AND (D), RESPECTIVELY. ....	28
FIGURE 3.1. CORE AS RECEIVED FROM IDAHO SITE, LEFT-MOST LANE, AT JOINT, (ID_L06). ....	54
FIGURE 3.2. CORE AS RECEIVED FROM IDAHO SITE, LEFT-MOST LANE, AWAY FROM JOINT, (ID_L04). ....	55
FIGURE 3.3. CORE AS RECEIVED FROM IDAHO SITE, RIGHT-MOST LANE, AT JOINT, (ID_R07). ....	55
FIGURE 3.4. CORE AS RECEIVED FROM IDAHO SITE, LEFT-MOST LANE, AT JOINT, (ID_R03). ....	56
FIGURE 3.5. STEREOMICROSCOPE IMAGE OF POLISHED SURFACE FROM CORE ID_R07, MAGNIFIED HERE APPROXIMATELY 4X.....	58
FIGURE 3.6. STEREOMICROSCOPE IMAGE OF POLISHED SURFACE FROM CORE ID_R07, MAGNIFIED HERE APPROXIMATELY 22X.....	58
FIGURE 3.7. CORE AS RECEIVED FROM IOWA SITE, WITH SURFACE CRACK, (IA_07). ....	59
FIGURE 3.8. CORE AS RECEIVED FROM IOWA SITE, WITHOUT SURFACE CRACK, (IA_04). ....	60
FIGURE 3.9. PHOTOGRAPH OF CRACK AT IOWA SITE.....	60
FIGURE 3.10. STEREOMICROSCOPE IMAGE OF POLISHED SURFACE FROM CORE IA_04, MAGNIFIED HERE APPROXIMATELY 4X.....	61
FIGURE 3.11. STEREOMICROSCOPE IMAGE OF POLISHED SURFACE FROM CORE IA_04, MAGNIFIED HERE APPROXIMATELY 22X.....	61
FIGURE 3.12. STEREOMICROSCOPE IMAGE OF POLISHED SURFACE FROM CORE IA_07 SHOWING ALKALI- SILICA REACTIVE SAND PARTICLE BEFORE STAINING PROCEDURE. ....	63
FIGURE 3.13. STEREOMICROSCOPE IMAGE OF POLISHED SURFACE FROM CORE IA_07 SHOWING ALKALI- SILICA REACTIVE SAND PARTICLE AFTER STAINING PROCEDURE. ....	63
FIGURE 3.14. VARIABLE WEAR OF PAVEMENT SURFACE AT MONTANA SITE. ....	64
FIGURE 3.15. CORE AS RECEIVED FROM MONTANA SITE, WITH LITTLE SURFACE WEAR (MT_02). ....	65
FIGURE 3.16. CORE AS RECEIVED FROM MONTANA SITE, WITH SOME SURFACE WEAR (MT_08). ....	65
FIGURE 3.17. STEREOMICROSCOPE IMAGE OF POLISHED SURFACE FROM CORE MT_02, MAGNIFIED HERE APPROXIMATELY 4X.....	66
FIGURE 3.18. STEREOMICROSCOPE IMAGE OF POLISHED SURFACE FROM CORE MT_02, MAGNIFIED HERE APPROXIMATELY 22X.....	66
FIGURE 3.19. CORE AS RECEIVED FROM COLORADO SITE, AT JOINT (CO_01). ....	68
FIGURE 3.20. CORE AS RECEIVED FROM COLORADO SITE, AWAY FROM JOINT (CO_05). ....	69
FIGURE 3.21. PHOTOGRAPH OF CRACKS IN PAVEMENT AT COLORADO SITE. ....	69
FIGURE 3.22. STEREOMICROSCOPE IMAGE OF POLISHED SURFACE FROM CORE CO_01, MAGNIFIED HERE APPROXIMATELY 4X.....	70

FIGURE 3.23. STEREOMICROSCOPE IMAGE OF POLISHED SURFACE FROM CORE CO_01, MAGNIFIED HERE APPROXIMATELY 22X.....	70
FIGURE 3.24. STEREOMICROSCOPE IMAGE OF POLISHED SURFACE FROM CORE CO_05 SHOWING ALKALI- SILICA REACTIVE SAND PARTICLE BEFORE STAINING PROCEDURE.....	72
FIGURE 3.25. STEREOMICROSCOPE IMAGE OF POLISHED SURFACE FROM CORE CO_05 SHOWING ALKALI- SILICA REACTIVE SAND PARTICLE AFTER STAINING PROCEDURE.....	72
FIGURE 3.26. CORE AS RECEIVED FROM SOUTH DAKOTA SITE, AT JOINT (SD_01).....	74
FIGURE 3.27. CORE AS RECEIVED FROM SOUTH DAKOTA SITE, AWAY FROM JOINT (SD_04).....	74
FIGURE 3.28. PHOTOGRAPH OF SOUTH DAKOTA CORING SITE.....	75
FIGURE 3.29. PHOTOGRAPH OF SOUTH DAKOTA CORING SITE.....	75
FIGURE 3.30. STEREOMICROSCOPE IMAGE OF POLISHED SURFACE FROM CORE SD_04, MAGNIFIED HERE APPROXIMATELY 4X.....	77
FIGURE 3.31. STEREOMICROSCOPE IMAGE OF POLISHED SURFACE FROM CORE SD_04, MAGNIFIED HERE APPROXIMATELY 22X.....	77
FIGURE 3.32. A 5 X 6 MOSAIC OF 30 EPIFLUORESCENT MODE IMAGES FROM THIN SECTIONS PREPARED FROM CORE SD_01, MAGNIFIED 17X.....	78
FIGURE 3.33. A 5 X 6 MOSAIC OF 30 EPIFLUORESCENT MODE IMAGES FROM THIN SECTIONS PREPARED FROM CORE SD_01 AFTER MASKING OUT SAND AND AIR VOIDS, MAGNIFIED 17X.....	79
FIGURE 3.34. A 5 X 6 MOSAIC OF 30 EPIFLUORESCENT MODE IMAGES FROM THIN SECTIONS PREPARED FROM CORE SD_04, MAGNIFIED 17X.....	80
FIGURE 3.35. A 5 X 6 MOSAIC OF 30 EPIFLUORESCENT MODE IMAGES FROM THIN SECTIONS PREPARED FROM CORE SD_01 AFTER MASKING OUT SAND AND AIR VOIDS, MAGNIFIED 17X.....	81
FIGURE 3.36. CEMENT PASTE FLUORESCENCE INTENSITY HISTOGRAMS FOR IMAGES COLLECTED FROM CORES AT JOINT, (SD_01) AND AWAY FROM THE JOINT (SD_04).....	82
FIGURE 3.37. CYCLIC TEMPERATURE TEST PROCEDURE FOR ONE CYCLE FOR CYLINDERS EXPOSED TO DEICER SOLUTIONS AND A CONTROL SOLUTION.....	84
FIGURE 3.38 THE PARTIAL PHASE DIAGRAMS FOR THE DEICER SOLUTIONS TESTED SHOWING THE EUTECTIC POINTS FOR EACH SOLUTION. CONCENTRATIONS USED ARE SHOWN WITH VERTICAL DOTTED LINES. THE TEMPERATURE -15 °F IS SHOWN AS A DOTTED HORIZONTAL LINE.....	85
FIGURE 3.39. A MORE COMPLETE PHASE DIAGRAM FOR THE NaCl - WATER SYSTEM (SOURCE: <a href="http://www.phasediagram.dk/binary/">HTTP://WWW.PHASEDIAGRAM.DK/BINARY/</a> ).....	86
FIGURE 3.40. CYLINDERS EXPOSED TO ROCK SALT NaCl SOLUTION AFTER 8 DAYS OF CYCLIC TEMPERATURE TEST. FROM LEFT TO RIGHT: 0.40, 0.50, AND 0.60 w/c MORTAR CYLINDERS.....	88
FIGURE 3.41. CYLINDERS EXPOSED TO FOOD GRADE NaCl SOLUTION AFTER 8 DAYS OF CYCLIC TEMPERATURE TEST. FROM LEFT TO RIGHT: 0.40, 0.50, AND 0.60 w/c MORTAR CYLINDERS. .....	89



FIGURE 3.42	CYLINDERS EXPOSED TO ROCK SALT NaCl SOLUTION IN DRAINED TRAY AFTER 28 DAYS OF CYCLIC TEMPERATURE TEST.....	89
FIGURE 3.43	CYLINDERS EXPOSED TO FOOD GRADE NaCl SOLUTION IN DRAINED TRAY AFTER 28 DAYS OF CYCLIC TEMPERATURE TEST.....	90
FIGURE 3.44	CYLINDERS EXPOSED TO MgCl <sub>2</sub> SOLUTION AFTER 56 DAYS OF CYCLIC TEMPERATURE TEST. FROM LEFT TO RIGHT: 0.40, 0.50, AND 0.60 w/c MORTAR CYLINDERS.....	90
FIGURE 3.45	CYLINDERS EXPOSED TO CaCl <sub>2</sub> SOLUTION AFTER 56 DAYS OF CYCLIC TEMPERATURE TEST. FROM LEFT TO RIGHT: 0.40, 0.50, AND 0.60 w/c MORTAR CYLINDERS.....	91
FIGURE 3.46	CYLINDERS EXPOSED TO MgCl <sub>2</sub> SOLUTION AFTER 84 DAYS OF CYCLIC TEMPERATURE TEST. FROM LEFT TO RIGHT: 0.40, 0.50, AND 0.60 w/c MORTAR CYLINDERS.....	91
FIGURE 3.47	CYLINDERS EXPOSED TO CaCl <sub>2</sub> SOLUTION AFTER 84 DAYS OF CYCLIC TEMPERATURE TEST. FROM LEFT TO RIGHT: 0.40, 0.50, AND 0.60 w/c MORTAR CYLINDERS.....	92
FIGURE 3.48	CYLINDERS EXPOSED TO CMA SOLUTION AFTER 84 DAYS OF CYCLIC TEMPERATURE TEST. FROM LEFT TO RIGHT: 0.40, 0.50, AND 0.60 w/c MORTAR CYLINDERS.....	92
FIGURE 3.49	CONTROL CYLINDERS EXPOSED TO LIME WATER SOLUTION AFTER 84 DAYS OF CYCLIC TEMPERATURE TEST. FROM LEFT TO RIGHT 0.40, 0.50, AND 0.60 w/c MORTAR CYLINDERS.....	93
FIGURE 3.50A:	PLANE POLARIZED LIGHT IMAGE FROM CONTROL CYLINDER.....	95
FIGURE 3.50B:	PLANE POLARIZED LIGHT IMAGE FROM ROCK SALT NaCl DEICER-EXPOSED CYLINDER.....	95
FIGURE 3.51A:	CROSS POLARIZED LIGHT IMAGE FROM CONTROL CYLINDER.....	96
FIGURE 3.51B:	CROSS POLARIZED LIGHT IMAGE FROM ROCK SALT NaCl DEICER-EXPOSED CYLINDER.....	96
FIGURE 3.52A:	EPIFLUORESCENT IMAGE FROM CONTROL CYLINDER.....	97
FIGURE 3.52B:	EPIFLUORESCENT IMAGE FROM ROCK SALT NaCl DEICER-EXPOSED CYLINDER.....	97
FIGURE 3.53A:	CARBON K $\alpha$ X-RAY MAP FROM CONTROL CYLINDER. DARKER AREAS CORRESPOND TO HIGHER K $\alpha$ X-RAY COUNTS.....	98
FIGURE 3.53B:	CARBON K $\alpha$ X-RAY MAP FROM ROCK SALT NaCl DEICER-EXPOSED CYLINDER. DARKER AREAS CORRESPOND TO HIGHER K $\alpha$ X-RAY COUNTS.....	98
FIGURE 3.54A:	OXYGEN K $\alpha$ X-RAY MAP FROM CONTROL CYLINDER. DARKER AREAS CORRESPOND TO HIGHER K $\alpha$ X-RAY COUNTS.....	99
FIGURE 3.54B:	OXYGEN K $\alpha$ X-RAY MAP FROM ROCK SALT NaCl DEICER-EXPOSED CYLINDER. DARKER AREAS CORRESPOND TO HIGHER K $\alpha$ X-RAY COUNTS.....	99
FIGURE 3.55A:	SODIUM K $\alpha$ X-RAY MAP FROM CONTROL CYLINDER. DARKER AREAS CORRESPOND TO HIGHER K $\alpha$ X-RAY COUNTS.....	100
FIGURE 3.55B:	SODIUM K $\alpha$ X-RAY MAP FROM ROCK SALT NaCl DEICER-EXPOSED CYLINDER. DARKER AREAS CORRESPOND TO HIGHER K $\alpha$ X-RAY COUNTS.....	100
FIGURE 3.56A:	MAGNESIUM K $\alpha$ X-RAY MAP FROM CONTROL CYLINDER. DARKER AREAS CORRESPOND TO HIGHER K $\alpha$ X-RAY COUNTS.....	101

FIGURE 3.56B: MAGNESIUM $K\alpha$ X-RAY MAP FROM ROCK SALT NaCl DEICER-EXPOSED CYLINDER. DARKER AREAS CORRESPOND TO HIGHER $K\alpha$ X-RAY COUNTS.....	101
FIGURE 3.57A: ALUMINUM $K\alpha$ X-RAY MAP FROM CONTROL CYLINDER. DARKER AREAS CORRESPOND TO HIGHER $K\alpha$ X-RAY COUNTS.....	102
FIGURE 3.57B: ALUMINUM $K\alpha$ X-RAY MAP FROM ROCK SALT NaCl DEICER-EXPOSED CYLINDER. DARKER AREAS CORRESPOND TO HIGHER $K\alpha$ X-RAY COUNTS.....	102
FIGURE 3.58A: SILICON $K\alpha$ X-RAY MAP FROM CONTROL CYLINDER. DARKER AREAS CORRESPOND TO HIGHER $K\alpha$ X-RAY COUNTS.....	103
FIGURE 3.58B: SILICON $K\alpha$ X-RAY MAP FROM ROCK SALT NaCl DEICER-EXPOSED CYLINDER. DARKER AREAS CORRESPOND TO HIGHER $K\alpha$ X-RAY COUNTS.....	103
FIGURE 3.59A: SULFUR $K\alpha$ X-RAY MAP FROM CONTROL CYLINDER. DARKER AREAS CORRESPOND TO HIGHER $K\alpha$ X-RAY COUNTS.....	104
FIGURE 3.59B: SULFUR $K\alpha$ X-RAY MAP FROM ROCK SALT NaCl DEICER-EXPOSED CYLINDER. DARKER AREAS CORRESPOND TO HIGHER $K\alpha$ X-RAY COUNTS.....	104
FIGURE 3.60A: CHLORINE $K\alpha$ X-RAY MAP FROM CONTROL CYLINDER. DARKER AREAS CORRESPOND TO HIGHER $K\alpha$ X-RAY COUNTS.....	105
FIGURE 3.60B: CHLORINE $K\alpha$ X-RAY MAP FROM ROCK SALT NaCl DEICER-EXPOSED CYLINDER. DARKER AREAS CORRESPOND TO HIGHER $K\alpha$ X-RAY COUNTS.....	105
FIGURE 3.61A: POTASSIUM $K\alpha$ X-RAY MAP FROM CONTROL CYLINDER. DARKER AREAS CORRESPOND TO HIGHER $K\alpha$ X-RAY COUNTS.....	106
FIGURE 3.61B: POTASSIUM $K\alpha$ X-RAY MAP FROM ROCK SALT NaCl DEICER-EXPOSED CYLINDER. DARKER AREAS CORRESPOND TO HIGHER $K\alpha$ X-RAY COUNTS.....	106
FIGURE 3.62A: CALCIUM $K\alpha$ X-RAY MAP FROM CONTROL CYLINDER. DARKER AREAS CORRESPOND TO HIGHER $K\alpha$ X-RAY COUNTS.....	107
FIGURE 3.62B: CALCIUM $K\alpha$ X-RAY MAP FROM ROCK SALT NaCl DEICER-EXPOSED CYLINDER. DARKER AREAS CORRESPOND TO HIGHER $K\alpha$ X-RAY COUNTS.....	107
FIGURE 3.63A: IRON $K\alpha$ X-RAY MAP FROM CONTROL CYLINDER. DARKER AREAS CORRESPOND TO HIGHER $K\alpha$ X-RAY COUNTS.....	108
FIGURE 3.63B: IRON $K\alpha$ X-RAY MAP FROM ROCK SALT NaCl DEICER-EXPOSED CYLINDER. DARKER AREAS CORRESPOND TO HIGHER $K\alpha$ X-RAY COUNTS.....	108
FIGURE 3.64: PETROGRAPHIC MICROSCOPE IMAGES OF EARLY ONSET OF CRACKING IN $MgCl_2$ EXPOSED SAMPLE FROM CYCLIC EXPERIMENT. WHITE ARROWS INDICATE CRYSTALLINE MATERIAL FILLING CRACKS. FROM TOP TO BOTTOM: PLANE POLARIZED LIGHT, CROSS POLARIZED LIGHT, AND EPIFLUORESCENT MODE.....	109

FIGURE 3.65: PETROGRAPHIC MICROSCOPE IMAGES OF EARLY ONSET OF CRACKING IN NaCl EXPOSED SAMPLE FROM CYCLIC EXPERIMENT. FROM TOP TO BOTTOM: PLANE POLARIZED LIGHT, CROSS POLARIZED LIGHT, AND EPIFLUORESCENT MODE.....	110
FIGURE 3.66 CYLINDERS EXPOSED TO NaCl SOLUTION AFTER 84 DAYS OF CONSTANT LOW TEMPERATURE TEST. FROM LEFT TO RIGHT: 0.40, 0.50, AND 0.60 w/c MORTAR CYLINDERS. ....	111
FIGURE 3.67. CYLINDERS EXPOSED TO MgCl <sub>2</sub> SOLUTION AFTER 56 DAYS OF CONSTANT LOW TEMPERATURE TEST. FROM LEFT TO RIGHT: 0.40, 0.50, AND 0.60 w/c MORTAR CYLINDERS. ....	112
FIGURE 3.68 CYLINDERS EXPOSED TO CaCl <sub>2</sub> SOLUTION AFTER 56 DAYS OF CONSTANT LOW TEMPERATURE TEST. FROM LEFT TO RIGHT: 0.40, 0.50, AND 0.60 w/c MORTAR CYLINDERS. ....	112
FIGURE 3.69 CYLINDERS EXPOSED TO MgCl <sub>2</sub> SOLUTION AFTER 84 DAYS OF CONSTANT LOW TEMPERATURE TEST. FROM LEFT TO RIGHT: 0.40, 0.50, AND 0.60 w/c MORTAR CYLINDERS. ....	113
FIGURE 3.70. CYLINDERS EXPOSED TO CaCl <sub>2</sub> SOLUTION AFTER 84 DAYS OF CONSTANT LOW TEMPERATURE TEST. FROM LEFT TO RIGHT: 0.40, 0.50, AND 0.60 w/c MORTAR CYLINDERS. ....	113
FIGURE 3.71. CYLINDERS EXPOSED TO CMA SOLUTION AFTER 84 DAYS OF CONSTANT LOW TEMPERATURE TEST. FROM LEFT TO RIGHT: 0.40, 0.50, AND 0.60 w/c MORTAR CYLINDERS. ....	114
FIGURE 3.72 CONTROL CYLINDERS EXPOSED TO LIME WATER SOLUTION AFTER 84 DAYS OF CONSTANT LOW TEMPERATURE TEST. FROM LEFT TO RIGHT: 0.40, 0.50, AND 0.60 w/c MORTAR CYLINDERS. ....	114
FIGURE 3.73: EPIFLUORESCENT MODE IMAGES OF THIN SECTIONS PREPARED FROM MORTAR CYLINDERS IMMERSSED IN THE FOLLOWING SOLUTIONS, FROM TOP TO BOTTOM: MAGNESIUM CHLORIDE, CALCIUM CHLORIDE, SODIUM CHLORIDE, CALCIUM MAGNESIUM ACETATE, AND LIME WATER. ....	119
FIGURE 3.74: BACK-SCATTERED ELECTRON IMAGES OF THIN SECTIONS PREPARED FROM MORTAR CYLINDERS IMMERSSED IN THE FOLLOWING SOLUTIONS, FROM TOP TO BOTTOM: MAGNESIUM CHLORIDE, CALCIUM CHLORIDE, SODIUM CHLORIDE, CALCIUM MAGNESIUM ACETATE, AND LIME WATER. ....	120
FIGURE 3.75: ELEMENTAL MAP FOR CARBON COLLECTED FROM THIN SECTIONS PREPARED FROM MORTAR CYLINDERS IMMERSSED IN THE FOLLOWING SOLUTIONS, FROM TOP TO BOTTOM: MAGNESIUM CHLORIDE, CALCIUM CHLORIDE, SODIUM CHLORIDE, CALCIUM MAGNESIUM ACETATE, AND LIME WATER. ....	121
FIGURE 3.76: CROSS-POLARIZED LIGHT IMAGES OF THIN SECTIONS PREPARED FROM MORTAR CYLINDERS IMMERSSED IN THE FOLLOWING SOLUTIONS, FROM TOP TO BOTTOM: MAGNESIUM CHLORIDE, CALCIUM CHLORIDE, SODIUM CHLORIDE, CALCIUM MAGNESIUM ACETATE, AND LIME WATER. ....	122
FIGURE 3.77: CRACKS AND AIR VOIDS FILLED WITH REMNANT CALCIUM OXYCHLORIDE CRYSTALS IN THIN SECTION PREPARED FROM MAGNESIUM CHLORIDE SOLUTION IMMERSSED SAMPLE. FROM TOP	

TO BOTTOM: PLANE POLARIZED LIGHT, CROSS POLARIZED LIGHT, AND EPIFLUORESCENT MODE. ....	123
FIGURE 3.78 CRACKS AND AIR VOIDS FILLED WITH REMNANT CALCIUM OXYCHLORIDE CRYSTALS IN THIN SECTION PREPARED FROM CALCIUM CHLORIDE SOLUTION IMMersed SAMPLE. FROM TOP TO BOTTOM: PLANE POLARIZED LIGHT, CROSS POLARIZED LIGHT, AND EPIFLUORESCENT MODE. ....	124
FIGURE 3.79 REMNANT CALCIUM OXYCHLORIDE CRYSTALS THAT ARE PSEUDOMORPHS OF SECONDARY CALCIUM HYDROXIDE CRYSTALS INITIALLY FORMED IN AN AIR VOID FROM THIN SECTION PREPARED FROM MAGNESIUM CHLORIDE SOLUTION IMMersed SAMPLE. FROM TOP TO BOTTOM: PLANE POLARIZED LIGHT, CROSS POLARIZED LIGHT, AND EPIFLUORESCENT MODE. ....	125
FIGURE 3.80 ELEMENTAL MAP FOR MAGNESIUM COLLECTED FROM THIN SECTIONS PREPARED FROM MORTAR CYLINDERS IMMersed IN THE FOLLOWING SOLUTIONS, FROM TOP TO BOTTOM: MAGNESIUM CHLORIDE, CALCIUM CHLORIDE, SODIUM CHLORIDE, CALCIUM MAGNESIUM ACETATE, AND LIME WATER. ....	126
FIGURE 3.81 BRUCITE, (MAGNESIUM HYDROXIDE) CRYSTALS IN AIR VOID AND SEAM BENEATH SAND GRAIN NEAR EXTERIOR IN THIN SECTION PREPARED FROM CYLINDER IMMersed IN MAGNESIUM CHLORIDE SOLUTION. FROM TOP TO BOTTOM: PLANE POLARIZED LIGHT, CROSS POLARIZED LIGHT, AND EPIFLUORESCENT MODE. ....	127
FIGURE 3.82: MAGNESIUM CHLORIDE HYDRATE CRYSTALS IN AIR VOIDS NEAR EXTERIOR IN THIN SECTION PREPARED FROM CYLINDER IMMersed IN MAGNESIUM CHLORIDE SOLUTION. FROM TOP TO BOTTOM: PLANE POLARIZED LIGHT, CROSS POLARIZED LIGHT, AND EPIFLUORESCENT MODE. ....	128
FIGURE 3.83: ELEMENTAL MAP FOR CHLORINE COLLECTED FROM THIN SECTIONS PREPARED FROM MORTAR CYLINDERS IMMersed IN THE FOLLOWING SOLUTIONS, FROM TOP TO BOTTOM: MAGNESIUM CHLORIDE, CALCIUM CHLORIDE, SODIUM CHLORIDE, CALCIUM MAGNESIUM ACETATE, AND LIME WATER. ....	129
FIGURE 3.84: FROM LEFT TO RIGHT: PLANE POLARIZED LIGHT, CROSS POLARIZED LIGHT, AND EPIFLUORESCENT MODE IMAGES OF A THIN SECTION PREPARED FROM A CYLINDER IMMersed IN MAGNESIUM CHLORIDE SOLUTION. ....	130
FIGURE 3.85: FROM LEFT TO RIGHT: BACK SCATTERED ELECTRON IMAGE, ELEMENTAL MAP FOR CARBON, AND ELEMENTAL MAP FOR OXYGEN. IMAGES WERE COLLECTED FROM A THIN SECTION PREPARED FROM A CYLINDER IMMersed IN MAGNESIUM CHLORIDE SOLUTION. ....	131
FIGURE 3.86: ELEMENTAL MAPS, FROM LEFT TO RIGHT: SODIUM, MAGNESIUM, AND ALUMINUM. THE ELEMENTAL MAPS WERE COLLECTED FROM A THIN SECTION PREPARED FROM A CYLINDER IMMersed IN MAGNESIUM CHLORIDE SOLUTION. ....	132

FIGURE 3.87: ELEMENTAL MAPS, FROM LEFT TO RIGHT: SILICON, SULFUR, AND CHLORINE. THE ELEMENTAL MAPS WERE COLLECTED FROM A THIN SECTION PREPARED FROM A CYLINDER IMMERSSED IN MAGNESIUM CHLORIDE SOLUTION. ....	133
FIGURE 3.88: ELEMENTAL MAPS, FROM LEFT TO RIGHT: POTASSIUM, CALCIUM, AND IRON. THE ELEMENTAL MAPS WERE COLLECTED FROM A THIN SECTION PREPARED FROM A CYLINDER IMMERSSED IN MAGNESIUM CHLORIDE SOLUTION. ....	134
FIGURE 3.89: FROM LEFT TO RIGHT: PLANE POLARIZED LIGHT, CROSS POLARIZED LIGHT, AND EPIFLUORESCENT MODE IMAGES OF A THIN SECTION PREPARED FROM A CYLINDER IMMERSSED IN CALCIUM CHLORIDE SOLUTION. ....	135
FIGURE 3.90: FROM LEFT TO RIGHT: BACK SCATTERED ELECTRON IMAGE, ELEMENTAL MAP FOR CARBON, AND ELEMENTAL MAP FOR OXYGEN. IMAGES WERE COLLECTED FROM A THIN SECTION PREPARED FROM A CYLINDER IMMERSSED IN CALCIUM CHLORIDE SOLUTION. ....	136
FIGURE 3.91: ELEMENTAL MAPS, FROM LEFT TO RIGHT: SODIUM, MAGNESIUM, AND ALUMINUM. THE ELEMENTAL MAPS WERE COLLECTED FROM A THIN SECTION PREPARED FROM A CYLINDER IMMERSSED IN CALCIUM CHLORIDE SOLUTION. ....	137
FIGURE 3.92: ELEMENTAL MAPS, FROM LEFT TO RIGHT: SILICON, SULFUR, AND CHLORINE. THE ELEMENTAL MAPS WERE COLLECTED FROM A THIN SECTION PREPARED FROM A CYLINDER IMMERSSED IN CALCIUM CHLORIDE SOLUTION. ....	138
FIGURE 3.93: ELEMENTAL MAPS, FROM LEFT TO RIGHT: POTASSIUM, CALCIUM, AND IRON. THE ELEMENTAL MAPS WERE COLLECTED FROM A THIN SECTION PREPARED FROM A CYLINDER IMMERSSED IN CALCIUM CHLORIDE SOLUTION. ....	139
FIGURE 3.94: FROM LEFT TO RIGHT: PLANE POLARIZED LIGHT, CROSS POLARIZED LIGHT, AND EPIFLUORESCENT MODE IMAGES OF A THIN SECTION PREPARED FROM A CYLINDER IMMERSSED IN SODIUM CHLORIDE SOLUTION. ....	140
FIGURE 3.95: FROM LEFT TO RIGHT: BACK SCATTERED ELECTRON IMAGE, ELEMENTAL MAP FOR CARBON, AND ELEMENTAL MAP FOR OXYGEN. IMAGES WERE COLLECTED FROM A THIN SECTION PREPARED FROM A CYLINDER IMMERSSED IN SODIUM CHLORIDE SOLUTION. ....	141
FIGURE 3.96: ELEMENTAL MAPS, FROM LEFT TO RIGHT: SODIUM, MAGNESIUM, AND ALUMINUM. THE ELEMENTAL MAPS WERE COLLECTED FROM A THIN SECTION PREPARED FROM A CYLINDER IMMERSSED IN SODIUM CHLORIDE SOLUTION. ....	142
FIGURE 3.97: ELEMENTAL MAPS, FROM LEFT TO RIGHT: SILICON, SULFUR, AND CHLORINE. THE ELEMENTAL MAPS WERE COLLECTED FROM A THIN SECTION PREPARED FROM A CYLINDER IMMERSSED IN SODIUM CHLORIDE SOLUTION. ....	143
FIGURE 3.98: ELEMENTAL MAPS, FROM LEFT TO RIGHT: POTASSIUM, CALCIUM, AND IRON. THE ELEMENTAL MAPS WERE COLLECTED FROM A THIN SECTION PREPARED FROM A CYLINDER IMMERSSED IN SODIUM CHLORIDE SOLUTION. ....	144

FIGURE 3.99: FROM LEFT TO RIGHT: PLANE POLARIZED LIGHT, CROSS POLARIZED LIGHT, AND EPIFLUORESCENT MODE IMAGES OF A THIN SECTION PREPARED FROM A CYLINDER IMMERS	
ED IN CALCIUM MAGNESIUM ACETATE SOLUTION. ....	145
FIGURE 3.100: FROM LEFT TO RIGHT: BACK SCATTERED ELECTRON IMAGE, ELEMENTAL MAP FOR CARBON, AND ELEMENTAL MAP FOR OXYGEN. IMAGES WERE COLLECTED FROM A THIN SECTION PREPARED FROM A CYLINDER IMMERS	
ED IN CALCIUM MAGNESIUM ACETATE SOLUTION. ...	146
FIGURE 3.101: ELEMENTAL MAPS, FROM LEFT TO RIGHT: SODIUM, MAGNESIUM, AND ALUMINUM. THE ELEMENTAL MAPS WERE COLLECTED FROM A THIN SECTION PREPARED FROM A CYLINDER IMMERS	
ED IN CALCIUM MAGNESIUM ACETATE SOLUTION. ....	147
FIGURE 3.102: ELEMENTAL MAPS, FROM LEFT TO RIGHT: SILICON, SULFUR, AND CHLORINE. THE ELEMENTAL MAPS WERE COLLECTED FROM A THIN SECTION PREPARED FROM A CYLINDER IMMERS	
ED IN CALCIUM MAGNESIUM ACETATE SOLUTION. ....	148
FIGURE 3.103: ELEMENTAL MAPS, FROM LEFT TO RIGHT: POTASSIUM, CALCIUM, AND IRON. THE ELEMENTAL MAPS WERE COLLECTED FROM A THIN SECTION PREPARED FROM A CYLINDER IMMERS	
ED IN CALCIUM MAGNESIUM ACETATE SOLUTION. ....	149
FIGURE 3.104: FROM LEFT TO RIGHT: PLANE POLARIZED LIGHT, CROSS POLARIZED LIGHT, AND EPIFLUORESCENT MODE IMAGES OF A THIN SECTION PREPARED FROM A CYLINDER IMMERS	
ED IN LIME WATER .....	150
FIGURE 3.105: FROM LEFT TO RIGHT: BACK SCATTERED ELECTRON IMAGE, ELEMENTAL MAP FOR CARBON, AND ELEMENTAL MAP FOR OXYGEN. IMAGES WERE COLLECTED FROM A THIN SECTION PREPARED FROM A CYLINDER IMMERS	
ED IN LIME WATER . ....	151
FIGURE 3.106: ELEMENTAL MAPS, FROM LEFT TO RIGHT: SODIUM, MAGNESIUM, AND ALUMINUM. THE ELEMENTAL MAPS WERE COLLECTED FROM A THIN SECTION PREPARED FROM A CYLINDER IMMERS	
ED IN LIME WATER . ....	152
FIGURE 3.107: ELEMENTAL MAPS, FROM LEFT TO RIGHT: SILICON, SULFUR, AND CHLORINE. THE ELEMENTAL MAPS WERE COLLECTED FROM A THIN SECTION PREPARED FROM A CYLINDER IMMERS	
ED IN LIME WATER . ....	153
FIGURE 3.108: ELEMENTAL MAPS, FROM LEFT TO RIGHT: POTASSIUM, CALCIUM, AND IRON. THE ELEMENTAL MAPS WERE COLLECTED FROM A THIN SECTION PREPARED FROM A CYLINDER IMMERS	
ED IN LIME WATER . ....	154
FIGURE 3.109. CYLINDERS EXPOSED TO NaCl SOLUTION AFTER 84 DAYS OF CONSTANT HIGH TEMPERATURE TEST. FROM LEFT TO RIGHT: 0.40, 0.50, AND 0.60 w/c MORTAR CYLINDERS. ....	155
FIGURE 3.110. CYLINDERS EXPOSED TO MgCl <sub>2</sub> SOLUTION AFTER 84 DAYS OF CONSTANT HIGH TEMPERATURE TEST. FROM LEFT TO RIGHT: 0.40, 0.50, AND 0.60 w/c MORTAR CYLINDERS. ....	156

FIGURE 3.111. CYLINDERS EXPOSED TO $\text{CaCl}_2$ SOLUTION AFTER 84 DAYS OF CONSTANT HIGH TEMPERATURE TEST. FROM LEFT TO RIGHT: 0.40, 0.50, AND 0.60 <i>w/c</i> MORTAR CYLINDERS. ....	156
FIGURE 3.112. CYLINDERS EXPOSED TO CMA SOLUTION AFTER 28 DAYS OF CONSTANT HIGH TEMPERATURE TEST. FROM LEFT TO RIGHT: 0.40, 0.50, AND 0.60 <i>w/c</i> MORTAR CYLINDERS. ....	157
FIGURE 3.113. CONTROL CYLINDERS EXPOSED TO LIME SOLUTION AFTER 84 DAYS OF CONSTANT HIGH TEMPERATURE TEST. FROM LEFT TO RIGHT: 0.40, 0.50, AND 0.60 <i>w/c</i> MORTAR CYLINDERS. ....	157
FIGURE 3.114: STEREOMICROSCOPE IMAGE OF NEEDLES OF TRANSLUCENT CRYSTALS ON DISINTEGRATED MASS OF MORTAR. ....	159
FIGURE 3.115: X-RAY DIFFRACTION PATTERN SHOWING MATCH FOR CALCIUM ACETATE HYDRATE. ....	159
FIGURE 3.116: SECONDARY ELECTRON IMAGE OF CRYSTALS PLUCKED FROM DISINTEGRATED MORTAR. ..	160
FIGURE 3.117: X-RAY ENERGY SPECTRUM, (IN UNITS OF K $\alpha$ ) SHOWING COUNTS FOR CARBON $\text{K}\alpha$ , OXYGEN $\text{K}\alpha$ , CALCIUM $\text{K}\alpha$ , AND CALCIUM $\text{K}\beta$ X-RAYS, COLLECTED FROM CRYSTALS PLUCKED FROM DISINTEGRATED MORTAR. ....	160
FIGURE 3.118: PETROGRAPHIC MICROSCOPE IMAGE, TRANSMITTED PLANE POLARIZED LIGHT, OF THIN SECTION PREPARED FROM CYLINDER FROM CALCIUM MAGNESIUM ACETATE CONSTANT HOT TEMPERATURE EXPERIMENT. ....	161
FIGURE 3.119: PETROGRAPHIC MICROSCOPE IMAGE, CROSS POLARIZED LIGHT, OF THIN SECTION PREPARED FROM CYLINDER FROM CALCIUM MAGNESIUM ACETATE CONSTANT HOT TEMPERATURE EXPERIMENT. ....	161
FIGURE 3.120: PETROGRAPHIC MICROSCOPE IMAGE, EPIFLUORESCENT MODE, OF THIN SECTION PREPARED FROM CYLINDER FROM CALCIUM MAGNESIUM ACETATE CONSTANT HOT TEMPERATURE EXPERIMENT. ....	162
FIGURE 3.121. CYLINDERS EXPOSED TO ROCK SALT $\text{NaCl}$ SOLUTION AFTER 28 DAYS OF CYCLIC TEMPERATURE TEST WITHOUT THE OVEN STEP. FROM LEFT TO RIGHT: 0.40, 0.50, AND 0.60 <i>w/c</i> MORTAR CYLINDERS. ....	163
FIGURE 3.122. CYLINDERS EXPOSED TO ROCK SALT $\text{NaCl}$ SOLUTION AFTER 28 DAYS OF CYCLIC TEMPERATURE TEST WITHOUT THE OVEN STEP OR THE CONDITIONING IN LIME WATER STEP. FROM LEFT TO RIGHT: 0.40, 0.50, AND 0.60 <i>w/c</i> MORTAR CYLINDERS. ....	164
FIGURE 3.123. CYLINDERS EXPOSED TO ROCK SALT $\text{NaCl}$ SOLUTION AFTER 56 DAYS OF CYCLIC TEMPERATURE TEST WITHOUT THE OVEN STEP. FROM LEFT TO RIGHT: 0.40, 0.50, AND 0.60 <i>w/c</i> MORTAR CYLINDERS. ....	164
FIGURE 3.124. CYLINDERS EXPOSED TO ROCK SALT $\text{NaCl}$ SOLUTION AFTER 56 DAYS OF CYCLIC TEMPERATURE TEST WITHOUT THE OVEN STEP OR THE CONDITIONING IN LIME WATER STEP. FROM LEFT TO RIGHT: 0.40, 0.50, AND 0.60 <i>w/c</i> MORTAR CYLINDERS. ....	165

FIGURE 3.125. CYLINDERS EXPOSED TO $\text{CaCl}_2$ SOLUTION AFTER 56 DAYS OF CONSTANT LOW TEMPERATURE TEST. FROM LEFT TO RIGHT: 0.40, 0.50, AND 0.60 <i>w/c</i> MORTAR CYLINDERS. SOLUTION STRENGTH WAS 3% $\text{CaCl}_2$ .	166
FIGURE 3.126. CYLINDERS EXPOSED TO $\text{CaCl}_2$ SOLUTION AFTER 56 DAYS OF CONSTANT LOW TEMPERATURE TEST. FROM LEFT TO RIGHT: 0.40, 0.50, AND 0.60 <i>w/c</i> MORTAR CYLINDERS. SOLUTION STRENGTH WAS 7% $\text{CaCl}_2$ .	166
FIGURE 3.127. CYLINDERS EXPOSED TO $\text{CaCl}_2$ SOLUTION AFTER 56 DAYS OF CONSTANT LOW TEMPERATURE TEST. FROM LEFT TO RIGHT: 0.40, 0.50, AND 0.60 <i>w/c</i> MORTAR CYLINDERS. SOLUTION STRENGTH WAS 10% $\text{CaCl}_2$ .	167
FIGURE 3.128. CYLINDERS EXPOSED TO $\text{CaCl}_2$ SOLUTION AFTER 56 DAYS OF CONSTANT LOW TEMPERATURE TEST. FROM LEFT TO RIGHT: 0.40, 0.50, AND 0.60 <i>w/c</i> MORTAR CYLINDERS. SOLUTION STRENGTH WAS 14% $\text{CaCl}_2$ .	167
FIGURE 3.129. CYLINDERS EXPOSED TO $\text{CaCl}_2$ SOLUTION AFTER 56 DAYS OF CONSTANT LOW TEMPERATURE TEST. FROM LEFT TO RIGHT: 0.40, 0.50, AND 0.60 <i>w/c</i> MORTAR CYLINDERS. SOLUTION STRENGTH WAS 17% $\text{CaCl}_2$ .	168
FIGURE 5.1 REVISED PROJECT SCHEDULE FROM OCTOBER 1, 2004 TO PROJECT END.	173



## **Section 1. Introduction**

### **1.0. Problem Statement**

Keeping roads safe and passable are key concerns for any State Highway Agency (SHA), especially during the winter season when ice and snow accumulation on roads and bridges can create hazardous driving conditions. To accomplish these goals, SHAs are constantly seeking out, evaluating, and adapting new winter maintenance strategies that are cost effective and environmentally friendly. One such area where new strategies are being employed is the broad area of deicing and anti-icing. Deicing is defined as any effort to remove ice from roads and bridges after ice deposition on those surfaces has occurred. This is in contrast to anti-icing, which is defined as a surface treatment applied prior to ice formation that eliminates ice accumulation or facilitates ice removal by lessening the bond between the ice and the pavement surface. In general, deicing and anti-icing are accomplished through the use of various chemicals including aqueous solutions of various chlorides (e.g. magnesium chloride, sodium chloride, and calcium chloride) or other chemicals such as calcium magnesium acetate (CMA), urea, or others. Although the efficacy of these chemicals for deicing and anti-icing has been clearly demonstrated, possible detrimental effects to concrete in transportation structures have not been fully examined and documented. In this sense, the true cost effectiveness has not been determined as chemical attack on concrete structures is a possibility and in turn, the resulting deterioration of the structures from these chemical attacks may lead to costly rehabilitation or replacement. Based upon published research, the most problematic chemicals appear to be the chlorides of magnesium, calcium, and sodium and other chemicals containing calcium and magnesium (e.g. CMA). Use of these chemicals has increased given their relatively low cost, ease of use, and effectiveness for deicing and anti-icing, in certain applications. Use of alternative chemicals such as propylene glycol and ethylene glycol have not occurred given concerns about their environmental impact. In the end, chloride-based deicers appear to be the best choice if they can be used in such a way as to minimize possible chemical attacks to concrete structures.

The degradation of concrete used in pavements and bridges that may occur as a result of chemical attack by deicing chemicals is the result of an increase in concentration of dissociated calcium and magnesium ions in the concrete pore water. In theory, these free ions are available to combine with materials in the concrete to form expansive or weak products such as brucite or magnesium silicate hydrates, respectively. Of course, the dissociation of chlorides into ionic species also increases the concentration of chloride in the pore water solution, which has been well documented as a primary cause of scaling and corrosion of reinforcing steel. These possible and known effects must be fully understood if these chemicals are to be used as a mainstay of any deicing or anti-icing strategy. The goal of this proposed research is to examine the effects of deicing and anti-icing chemicals on portland cement concrete and to recommend changes to concrete mixture designs, construction practices, and winter maintenance procedures that will make these solutions non-detrimental to concrete durability.

## 1.1 Summary of Work

Table 1.1 shows a summary of the individual tasks for this project and the status of each Task. Tasks 5 through 8 are the heart of the remaining research and all of those tasks are under way. Tasks 5 and 6 are approximately 50% completed and the results to date are included in this report. In the case of Task 6, a proposal for the final phase of this task (Phase II) is included in this interim report. Tasks 7 and 8 are approximately 20% completed and the remainder will follow after completion of Tasks 5 and 6. The remaining Tasks will be started as data is received and processed. At this time, the results of Task 5 do not indicate any clear indication of deicer distress in the field. However, all results are not in and a final assessment of the field cores will be forthcoming. In the case of Task 6, some very interesting results have been observed that do indicate that there are chemical interactions between the various deicers tested and hardened portland cement paste. Caution should be exercised in reading too much into these preliminary results as the Phase I testing involved mortars only. Phase II will involve concrete testing and will help focus the results obtained from Phase I and put those results in the proper context.

Table 1.1. Summary of Task Progress to Date.

TASK	STATUS
TASK 1: LITERATURE REVIEW	DONE
TASK 2: CONDUCT SURVEY	DON
TASK 3: SITE SELECTION	DONE
TASK 4: MEETING WITH TECHNICAL PANEL	DONE
TASK 5: CHARACTERIZATION OF FIELD SPECIMENS	PARTIAL
TASK 6: LABORATORY EXPERIMENT	PARTIAL
TASK 7: ASSESSING AND MINIMIZING THE IMPACT OF DEICING/ANTI-ICING CHEMICALS	PARTIAL
TASK 8: EFFECTS OF VARIOUS DEICING/ANTI-ICING CHEMICALS	PARTIAL
TASK 9. LIFE CYCLE COST ANALYSES	PENDING
TASK 10: DEVELOPMENT OF GUIDELINES	PENDING
TASK 11: SUBMIT INTERIM REPORT	DONE
TASK 12: MEETING WITH TECHNICAL PANEL AT MICHIGAN TECH	DONE
TASK 13: PREPARE AND SUBMIT FINAL REPORT	PENDING
TASK 14: EXECUTIVE PRESENTATION TO RESEARCH PANEL	PENDING
TASK 15: EXECUTIVE PRESENTATION TO SDDOT EXECUTIVE REVIEW BOARD	PENDING

As a result of the Task 11 Panel meeting, it is expected that Phase II will be finalized and work will commence immediately. It is the goal of the research team to finish the project at the originally scheduled date of September 30, 2005.

## **1.2 Organization of This Report**

This report is organized into 5 sections. Section 1 is this brief introduction. Section 2 provides background for the project and represents the results of the Task 1 literature review. Section 3 is a comprehensive summary of the work to date. Section 4 is a summary of the Phase II proposal designed to complete Task 6. Section 5 is the project schedule from October 1, 2004 to project end and Section 6 is a bibliography. Also included at the end are a number of appendices that summarize raw data presented in the report.

## **Section 2. Background**

The purpose of this background section is to summarize past research efforts regarding concrete damage resulting from the use of various deicing agents on transportation structures. In order to understand the potential damage that deicers may cause, this literature review will discuss the following topics:

- Past and current winter maintenance practices and what led to changes in these practices over the years.
- Concrete properties (i.e. permeability, aggregates, and air content) and their impact on concrete's resistance to freeze-thaw and deicer attack.
- Physical interactions that occur in the concrete as a result of freeze-thaw cycling in the presence of deicing chemicals.
- Chemical interactions between deicing chemicals and concrete and how they complicate the physical interactions.
- Deleterious effects that deicing chemicals have on both the hydrated cement paste and the aggregate.

In addition, this report will include a review of the maintenance and construction practices that affect deicer application. Such practices include chemical type, application rates, or other variables in the area of maintenance, and the use of sealants or coatings to protect against future degradation as part of construction.

### **2.1. Review of Past and Current Snow and Ice Removal Maintenance Practices**

The purpose of winter snow and ice removal maintenance is to provide safe roadways for the traveling public by re-establishing traction on frozen pavement surfaces as quickly as possible. Reasonably, the majority of information pertaining to the maintenance practices for snow and ice control is documented at state Departments of Transportation (DOTs). Overwhelmingly, most DOTs currently use NaCl, CaCl<sub>2</sub>, MgCl<sub>2</sub>, and CMA (or blends of these materials) as deicing chemicals. Knowing the effectiveness and cost of each of these deicing chemicals helps determine which one is used in practice.

A major source of information used in this section of the report is from a maintenance survey that was conducted in 2003. The intent of the survey was to obtain information from transportation agencies (US and Canada) about current deicing/anti-icing chemical usage, their application rates to structural portland cement concrete (PCC) and any observed distresses in PCC pavements. A total of 31 agencies responded to the survey including 20 states and 1 province of Canada. This survey is located in Appendix A of this report.

#### ***2.1.1 Traditional Winter Maintenance Practices***

Traditionally, winter maintenance entails plowing snow and applying chemicals and/or abrasives to melt the ice cover and re-establish traction. DOTs across the country use the "same basic types of equipment for handling snow; dump trucks with plows, motor

patrols, rotary plows (blowers), loaders and equipment to spread liquid and solid chemicals and abrasives” (Williams 2001). Typically, rock salt (sodium chloride) is the least expensive deicing chemical and therefore most often used by DOTs to remove snow and ice. However, NaCl does not adequately melt ice at temperatures below 20 °F. It has been found that CaCl<sub>2</sub> has the ability to generate heat and when combined with rock salt, the two work in combination enhancing the performance of ice removal. Although, considered highly corrosive to vehicles and bridge decks, CaCl<sub>2</sub> is still applied to roads to quickly attain a safe riding surface.

In the past, many DOTs favored the use of rock salt, although methods of snow and ice removal may vary across the thirty States that practice winter maintenance. For example, Montana (William 2001) and Iowa (Nixon 2001) have used sand or other abrasive materials in order to create traction on ice or snow covered pavements for the traveling public. The abrasives are generally applied “on the road up to 1,200 lbs. per lane mile (340 kg per lane km)” (Nixon 2001). The methods in which sand may be applied to roadways include: “straight”, pre-wet with a liquid deicer, or mixed with salt (Nixon 2001).

### ***2.1.2 What Led to Change***

A study by Minsk (1998) reports that, up until the 1970’s the use of sand or other abrasives was a major part of winter maintenance procedures in the United States. As abrasives were found to have little effectiveness, the use of deicing chemicals became a more common practice. However, there are still many agencies that use abrasives in winter maintenance.

In addition, there are considerable problems with using abrasives. Primarily, they do not adhere well to frozen surfaces thus frequent replacement is required. Despite the labor that goes into stockpiling and applying these abrasives, once it has been applied only about 20-30% actually adheres to the hard frozen pavement. The rest is lost “during the first few minutes of traffic” (Perchanok 1997), lowering the cost effectiveness of this type of practice.

A study by Kuemmael and Bari (1996) included a cost/benefit analysis of abrasives or abrasive/salt mixtures for winter maintenance. They found that this type of practice can be economically justified for use on freeways, however not on two lane highways. These findings are based on the amount of traffic on such roadways. In a study from Germany, Hanke (1998) reports that abrasives will cost more than salt in the long run. This is primarily because more applications are required and yet there is no remarkable improvement in road safety.

Furthermore, the use of abrasives has raised much concern about environmental issues, such as air, water, soil and vegetation quality as well as the impact it has on animals and infrastructure.

Therefore, the Guide of Snow and Ice Control (AASHTO 1999) recommends that special environmental considerations should be given to:

- Minimizing air quality and highway safety impacts associated with the use of abrasives.
- Controlling runoff from roadway applications.
- Protecting surface water quality.
- Protecting groundwater, including wells and aquifers.
- Proper storage of chemicals and abrasives.
- Protecting vegetation.
- Protecting habitat quality.
- Protecting maintenance facilities and equipment against weather, corrosion.
- Protecting transportation facilities (bridges, pavement, appurtenances) against corrosion.

With regard to air quality, winter maintenance using abrasives tends to generate a microscopic air pollutant, commonly known as PM10. According to the European Environment Agency these small, textured particles have a diameter less than or equal to 10 microns (about 1/7 the diameter of a single human hair). Among other sources, PM10 is emitted from vehicles traveling on unpaved roads, crushing and grinding operations, as well as windblown dust, causing visibility reduction. Furthermore, their small size allows them to make their way to the air sacs deep within the lungs where they may be deposited, leading to adverse health effects<sup>1</sup>.

Water quality, including surface and ground water has been affected by the use of abrasives and chemicals in winter maintenance practice. This is due to poor storage and handling methods, as well as improper pavement application and neglecting post-storm sweeping and cleanup. Although, some runoff from roadways cannot be avoided, it is possible to control application to minimize runoff. In addition, proper storage will help improve water quality near maintenance facilities.

In order to have effective pollution control at facilities, it is important to practice proper collection, treatment and disposal of wash water, oils and other waste substances. However the abrasives and solid chemicals that are stored on site have not always been contained properly due to low storage capacity. Usually winter treated abrasives are stockpiled outside on an impermeable pad and covered with a waterproof material. This method has proved faulty since the chemicals in the open will attract moisture, which can then leach from the stockpile and drain into the watercourses and aquifers (AASHTO 1999). Other potential problems with outside storage of bulk chemical stockpiling comes from brine runoff caused by rain and snowmelt. These quantities can be sufficient enough to harm surface water supplies, aquifers and vegetation. Therefore, indoor

---

<sup>1</sup> [glossary.eea.eu.int/EEAGlossary/P/PM10](http://glossary.eea.eu.int/EEAGlossary/P/PM10)

storage in a structure with a permanent roof, impervious floor, and protection from wind and precipitation is highly recommended for chemicals and abrasives when possible (AASHTO 1999).

### ***2.1.3 Modified & Current Winter Maintenance Practices***

Over the years, traditional snow and ice removal methods have been modified in order to comply with environmental regulations, reduce corrosive damage to vehicles, and provide a more economical method to maintain safe roads. Current methods of snow and ice removal include deicing, pre-wetting salt or abrasive material, and anti-icing.

Deicing is a reactive strategy in which the application of chemicals occurs after the ice bonds to the pavement. Pre-wetting is simply the application of deicing chemicals to salt and/or sand, which helps to keep the granular materials on the road. In contrast to deicing and pre-wetting, anti-icing is primarily a preventative maintenance strategy, in that it is the application of freezing-point suppressant chemicals (solid or liquid) to paved surfaces before ice forms a bond to the pavement.

The transition from traditional to current winter maintenance practices is a two-way street. The benefits are debatable, especially among chemical manufacturers and the DOTs maintaining safe roads. Contradicting studies are evidence that anti-icing in particular, may not be the most appropriate method for winter maintenance. Both sides are presented within this report in order to inform the reader of potential benefits as well as impediments these approaches may exhibit.

According to Colorado's Standard Operating Guide, "each winter storm is unique and should be treated as such". Each storm is dependent on several factors including temperature, elevation, location, intensity and duration of the storm. Knowing how to treat the pavement for a given weather condition is the first step in winter maintenance. With that in mind, many agencies, like Colorado are developing guidelines or "toolboxes" that are intended to assist the maintenance professionals in winter maintenance practices. These guides typically contain procedures for the application rates of both anti-icing and deicing chemicals and information about the products themselves. Furthermore, it is important that all maintenance personnel of each agency understand and implement those guidelines when performing winter maintenance operations.

The following are a sample from guidelines from the Colorado DOT Standard Operating Guide:

- Under application will cause a premature re-freezing of the roadway surface, leading to icy conditions that must be avoided.
- Over-application of deicer during storms leads to excessive residue on the roadway after the storm. This has significant effect on the corrosion to metal parts on vehicles using the highways.
- The anti-icing use of these materials places material on the roadway prior to the storm and causes the strongest concentrations of materials to come (into) contact with vehicles because there is no moisture to dilute the material. Timing of the anti-icing phase as close to the start of the storm as is possible is crucial in keeping corrosion at a minimum.

### 2.1.3.1 Deicing

Of the 31 agencies that responded to the maintenance survey, 91% use deicing chemicals for road maintenance. This represents approximately 35,569 of 37,706 miles or 94.3% of PCC pavement that will be exposed to deicing chemicals annually. Table 2.1 below lists the deicing chemicals and the average concentration of each that are commonly used by these agencies. See Appendix A for details on application rates used by each participating agency.

Table 2.1. Deicing chemical concentrations used by various agencies.

Chemical	Average Application (%)	Lbs. chemical/gal	No. of Agencies
NaCl	23.3	1.94	10
CaCl <sub>2</sub>	32.9	2.75	13
MgCl <sub>2</sub>	29.2	2.44	9
CMA	29.5	2.46	2
KA (Potassium Acetate)	50	4.17	1



The following summarizes a common view regarding the effectiveness of NaCl, CaCl<sub>2</sub> and MgCl<sub>2</sub> used as deicing chemicals (The Dow Chemical Company, 1999):

*In their solid form, deicers are incapable of melting snow or ice; they must be in the form of liquid brine. In this form, deicers effectively lower the freezing point of water in order to melt ice and snow on contact. How quickly a deicer becomes a brine depends on how quickly it takes up moisture. Where NaCl must come into direct contact with moisture in order to dissolve into liquid brine, MgCl<sub>2</sub> and CaCl<sub>2</sub> actually attract moisture from the atmosphere to form brine very quickly. In addition to their fast brine formation, these two chemicals also generate heat as they melt ice. This exothermic reaction differs from that of NaCl, in that it undergoes an endothermic reaction that absorbs heat from its surroundings. At low temperatures, the rate of heat pickup from snow and ice slows to a point where it can not form brine and therefore cannot melt snow and ice. MgCl<sub>2</sub> and CaCl<sub>2</sub> effectively melt snow at much lower temperatures than NaCl. It has been found that MgCl<sub>2</sub> and CaCl<sub>2</sub> can effectively dissolve ice at (eutectic) temperatures as low as -28°C and -59°C, respectively.*

A study by Gilfillam (2001) confirmed that deicing chemicals “will work until the eutectic temperature of the solution meets the pavement surface temperature”. At this point, the chemical has become diluted to a concentration where it no longer effectively melts ice and re-freezing may even occur. This process is the same for all deicing chemicals. However, the rate at which it occurs for each deicer varies greatly. Figure 2.11 presents a partial phase diagram that shows the freezing point depression (eutectic point) of anti-icing/deicing chemicals in water.

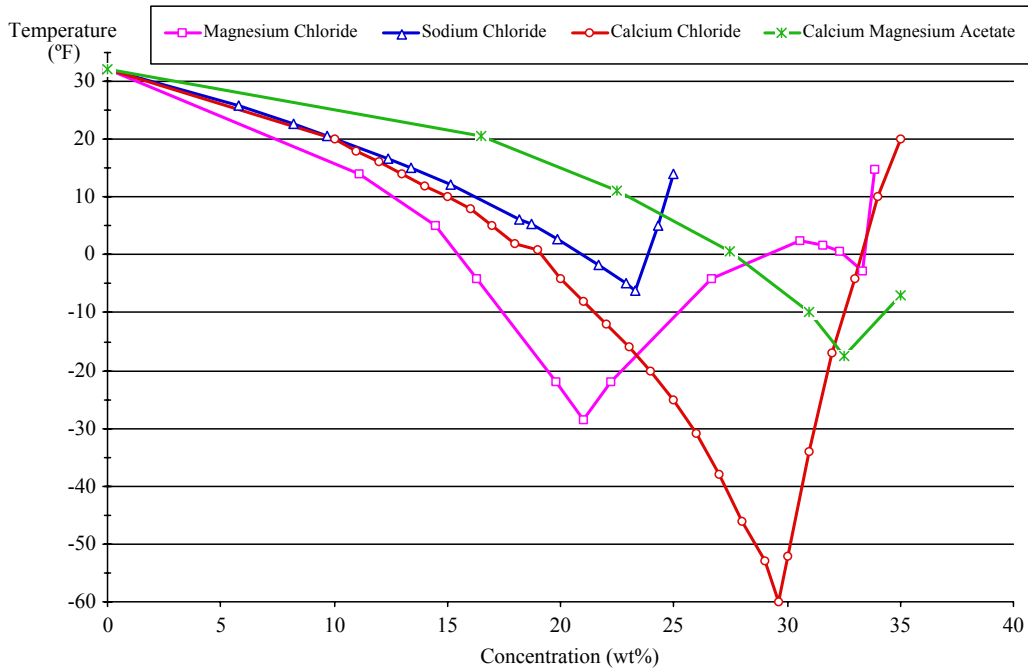


Figure 2.1 The partial phase diagrams for the common deicer solutions

One study, which led to the development of Caltrans (California DOT) Snow and Ice Policy, tested CMA as an alternative deicing material. When compared with salt, CMA penetrates snow at a much slower rate and is ineffective at temperatures below 24 °F. In addition to its relatively high cost, CMA requires more frequent applications than salt<sup>2</sup>.

### 2.1.3.2 Pre-wetting

The traditional use of chemical deicers as snow and ice treatment has since been modified by pre-wetting sand or salt with deicing chemicals. According to studies conducted by Gilfillam (2000, 2001), there are many benefits for using pre-wetted materials. For instance, pre-wetting sand and/or salt is more efficient both in “volume and maintenance worker time” (Gilfillam, 2001). The pre-wetting chemicals are the same as the deicing chemicals; only the application to the road differs between the two methods. The pre-wetting treatment essentially envelops each granule of salt and aggregate “so that when it hits the road surface, it burns its way into the snow and ice to provide a greater level of friction as well as stay on the road for a longer period of time” (Gilfillam, 2001). As with ordinary deicing applications, pre-wetting techniques are also used in conjunction with plowing. The following is a list of benefits of the pre-wetting application with both salt and sand (Gilfillam 2001):

- Reduces material loss, cost, and use.
- Material burns in.
- Improves traction.
- Easily modified.
- Reduces sweeping.
- Minimum change in operations.
- Reduced environmental impact.
- Increased effectiveness and service level.

There are several methods in which pre-wetting abrasives can be accomplished. One way is to inject a chemical into a stockpile of sand or salt at a specified dosage. Another method is to spray the liquid chemical either directly into a loaded spreader or “on the material as it is being loaded into the spreader” (AASHTO 1999). Lastly, the chemical can be sprayed on to the dry material as it is being spread onto the roadway (AASHTO 1999).

---

<sup>2</sup> <http://www.dot.ca.gov/hq/roadinfo/snvicecontrol.pdf>

Today, only about 58% of the agencies that participated in the survey, pre-wet solids for deicing purposes. Below, Table 2.2 represents of the types of pre-wetting chemicals used by participating agencies. Appendix A also gives details about application rates and types of materials that these agencies pre-wet.

Table 2.2. Pre-wetting chemicals that are used by agencies.

Chemical	No. of Agencies
NaCl	5
CaCl <sub>2</sub>	9
MgCl <sub>2</sub>	7
CMA	1
Other	2

### 2.1.3.3 Anti-icing

Many DOTs have developed a proactive maintenance strategy, which begins with anti-icing, in order to meet the increasing demands of the traveling public during and after winter storms. In fact, 81% of the agencies that responded to the survey practice anti-icing as part of winter maintenance. This covers approximately 33,180 miles or 88% of the 37,706 miles of PCC pavement that will be exposed to anti-icing chemicals annually. The same chemicals used for deicing and pre-wetting are also used as anti-icing chemicals. However, the concentration used varies slightly from that used for deicing purposes. Table 2.3 lists those concentrations used by the participating agencies.

Table 2.3. Anti-icing chemical concentrations used by various agencies

Chemical	Average Concentration (%)	No. of Agencies
NaCl	23	8
CaCl <sub>2</sub>	31.5	5
MgCl <sub>2</sub>	29	13
CMA	26.7	3
KA (Potassium Acetate)	50	1

As previously stated, anti-icing is the application of a liquid, solid, or pre-wetted chemical that reduces the freezing point of water in contact with paved surfaces. Anti-icing prevents the formation of a bond between ice and the pavement, which if formed is difficult to remove even by plowing. Anti-icing chemicals may be applied to the pavement before a storm occurs or at least before too much snow/ice has accumulated. However some guides recommend that the pavement should be cleared of snow and ice prior to applying liquid chemicals to reduce dilution. Many agencies, including the

Montana and Colorado DOTs, also rely on weather forecasts and Remote Weather Information Systems (RWIS) to determine the correct and timely application of these chemicals.

According to Colorado’s Standard Operating Guide, the ideal time to apply anti-icing chemicals is before the accumulation of snow and/or when the pavement temperature is dropping toward freezing. This is to keep snow/ice from bonding to the pavement. Prior to application, the pavement should also be flushed of contaminants such as oil and antifreeze. Late application of anti-icers will likely become diluted from the accumulated snow. Since not all winter storms are alike, the appropriate method of treatment must be decided and implemented prior to the storm. Table 2.4 below indicates the types of operations that may be utilized given the type of storm.

Table 2.4. Operation methods as per storm event.

Anti-Ice	Do Not Anti-Ice
Prior to predicted frost, black ice, light or moderate snow event	When pavement temperature is not predicted to reach freezing, only plowing is necessary
When pavement temperature has dropped near freezing	When accumulation will not be significant
Throughout storm event to maintain a wet road	Under blowing or drifting snow conditions, traffic and wind may be sufficient to prevent accumulation and compaction
Or spray once only and coordinate with plowing and sanding throughout the storm	During heavy snow (1in/hr) events, may need to switch to deicers
Driving lanes only, do not apply to shoulders	After the bond between the snow and pavement has occurred
With tankers over an extended area	Prior to predicted rain, freezing rain or sleet

In addition to the above guidelines for operation, there are several precautions that maintenance personnel should understand and take into consideration during storm events. The precautions listed below are from Minnesota’s DOT Anti-icing Guidelines:

- 1) Use caution especially with low or higher rates of application.
- 2) Re-freezing of bridge deck or pavement surfaces can occur if the applied chemical is significantly diluted or pavement temperature decreases.
- 3) Pavement slipperiness with the use of MgCl<sub>2</sub> and CaCl<sub>2</sub> is possible after application under certain temperature and humidity condition (i.e. temperatures above 30 °F with humidity greater than 40%).

- 4) Refreeze can occur when there is sufficient moisture, such as: humidity, fog, mist or drizzle. This moisture may dilute the chemical and cause re-freezing on the pavement or bridge deck surface.
- 5) When blowing or drifting snow conditions exist, anti-icing chemicals on a dry pavement or bridge deck may cause blowing snow to stick and create slippery conditions.
- 6) Build-up of oils and rubber residues may cause the pavement surfaces and bridge decks to become slippery after the application of liquid anti-icing chemicals.

Other precautions can be found in a study by Williams (2001). For instance, it is recommended to use pre-wetting along with plowing techniques rather than anti-icing in rural environments subjected to windy conditions. This is due to the fact that “anti-icing in wind blown snow will cause snow and icepack to develop on the roadway” (Williams 2001). In addition, the study conducted for Caltrans recommends that anti-icing techniques, particularly with  $MgCl_2$ , should not be applied on roads where the snow has accumulated to more than 1/4 inch deep.  $MgCl_2$  is known to “cause roads to be slippery due to fast melting followed by re-freezing”<sup>3</sup>. This will ultimately lead to more sanding, chemical application, and possibly snow plowing.

Although, there are certain precautions to be aware of, there are also beneficial implications of anti-icing chemicals. One benefit is there are “better pavement conditions early in a storm and a faster return to bare pavement conditions after the storm” (Ice and Snow Technologies, LLC). However, be aware that the mere application of anti-icing will not always result in bare pavement. Although, it will prevent the bond between snow/ice and pavement from forming, allowing easier removal of accumulated snow through plowing. This results in accident reduction, reduction in material and labor cost, reduced accumulation of sand in drainages and thus a reduction in clean-up work (Mn/DOT Anti-icing Guidelines).

As previously stated, a major driving force for amending traditional winter maintenance practices was the concern for the environmental impact that these harsh chemicals were having on air, water, endangered species and vegetation. Because anti-icing requires a lower amount of chemicals to effectively maintain road safety, there has been a significant reduction in the “dust count from sand and 25% less fuel is burned” (Gilfillam, 2001). The quality of the water has improved as it contains less sand and chloride from runoff. In addition, roadside vegetation has improved dramatically in areas where anti-icing is in practice. Claims that road safety increased since the transition to anti-icing, was indicated in the study by Gilfillam (2001) with an 83 percent reduction in accidents in the State of Idaho.

---

<sup>3</sup> <http://www.dot.ca.gov/hq/roadinfo/snwicecontrol.pdf>

## 2.2. Concrete Properties that Affect Freeze-Thaw and Chemical Resistance

To better understand the effects that freeze-thaw cycles and deicing chemicals have on concrete, it is important to have a working knowledge of the basic properties of concrete. The most prominent characteristics to analyze are: permeability; air content; cement chemistry; aggregate properties; and cracking. In addition, it is necessary to understand the physical and chemical interactions that take place on the surface and within the hardened cement paste.

### 2.2.1 Permeability

It is widely understood that the water-to-cement ( $w/c$ ) ratio has the largest influence on the durability of concrete. By having a relatively low  $w/c$  ratio, the porosity of the hardened concrete will decrease and in turn, be less permeable. Porosity is a “measure of the proportion of the total volume of concrete occupied by pores” (Neville 1997). The less permeable concrete is the more durable. This is because permeability of concrete “controls the rate of entry of moisture that may contain aggressive chemicals (i.e. chlorides) and the movement of water during heating or freezing” (Mindess et al. 2003). Therefore, a lower  $w/c$  ratio increases strength and improves resistance to cracking from the internal stresses generated by adverse reactions.

In addition, the  $w/c$  ratio affects the volume of capillary pores as the cement paste hydrates (i.e. volume increases significantly for  $w/c > 0.42$ ). Permeability is therefore controlled by an interconnecting network of capillary pores. During hydration, the capillary network becomes increasingly tortuous as interconnected pores are blocked by the formation of hydration products, most notably calcium silicate hydrate (C-S-H). calcium hydroxide (CH) also continues to grow within the residual pores, forming impermeable regions. At a given degree of hydration, “the time at which complete discontinuity of the capillary pores occurs is a function of the  $w/c$  ratio” (Mindess et al. 2003). Furthermore, permeability decreases as the cement continues to hydrate over time.

Although the hardened cement paste has the largest influence on permeability, it is also controlled by the paste-aggregate interface (Neville 1997 and Mindess et. al. 2003). Shrinkage due to freeze-thaw damage changes the pore-size distribution and allows capillary pores to become partially interconnected again, increasing the permeability of the concrete. Cracking at the paste-aggregate interface increases permeability, creating pathways for the flow of water. In order to ensure the resistance of newly placed concrete to alternating freezing and thawing cycles, it is desirable to allow the concrete to dry out completely before exposing it to harsh winter conditions. In addition, substantial hydration, air-entrainment, and a low  $w/c$  ratio, all contribute to a more impermeable concrete and enhance resistance to freeze-thaw damage (Neville 1997).

#### 2.2.1.1 Chloride Diffusion

One important aspect of concrete permeability regarding the application of deicing chemicals is chloride diffusion. Diffusion is a process by which a fluid can permeate a material such as soil or concrete. The concentration of chloride at the surface is the

principle method of transport in near-saturated concrete (Mindess 2003). However, the movement of chloride in concrete is also a function of several variables. These include pore size and spacing, pore volume fraction, changes in pore size with respect to location within the cement paste, and structure of phases present in the pore system.

To mathematically describe the process of one-dimensional chloride migration, Fick's Second Law of Diffusion can be used for most concrete applications.

$$C_{d,t} = C_0 \left[ 1 - \operatorname{erf} \frac{d}{2\sqrt{D_c \times t}} \right] \quad (2.1)$$

The variables in the equation described above are defined as the following:

- $C$  is the chloride concentration at a depth,  $d$ , and a time,  $t$
- $\operatorname{erf}$  is the abbreviation for error function (a curve that cannot be described by normal mathematical equations)
- $C_0$  is the chloride concentration at the surface of the concrete, where the chlorides are being applied, usually as deicers
- $D_c$  is the diffusion coefficient which expresses concrete's property of resistance to chloride diffusion, also related to concrete's permeability property and the moisture content (Mindess 2003)

By using Fick's Second Law to calculate the diffusion parameters  $C_0$  and  $D_c$  and to estimate chloride ingress in concrete, future changes in chloride concentration can be predicted at any depth from the concrete's surface over any period of time. With such predictions, effective strategies to mitigate damage from chloride ingress can be implemented.

Previous research has described the physics of chloride diffusion through saturated cement as a Fickian diffusion mechanism combined with a Langmuirian adsorption equilibrium process (Pereira 1984). This closely illustrates the action of ionic species penetrating the surface of concrete and migrating into the materials pore structure (Papadakis 1996). The rate of chloride diffusion is usually altered by the reversible process of adsorption and de-sorption of the ions to the hydration products of the matrix and by the binding of chlorides to the hydration products, particularly C-S-H. Further, a considerable amount of the damage in concrete exposed to chlorides results from the interaction of ions with C-S-H since it is the dominant phase in most hydrated cements (Kurdowski 1995). Other evidence of chloride binding is the fact that chlorides may be removed from the mix water via binding to the primary phases, present in the cement paste (Mondal 1975, Jeffery 1952, Barnes 1980, Colville 1971, 1972), and this occurs during the initial set (Lambert 1985).

Additionally, certain ionic species may also get "trapped" (*i.e.* chemically and physically bound) in the structure of the hydration products and react to form new phases, that may even be non-cementitious in nature. In some cases, phase formation can induce severe

stress concentrations and failure because of the formation of expansive by-products. The most well known phase observed resulting from a dissolution-precipitation reaction with  $Mg^{2+}$  is brucite ( $[Mg_x^{2+}(OH)_{2x+2}]^+[OH \cdot nH_2O]$ ) (Hofmeister 1992). Magnesium silicate hydrate (M-S-H), a non-cementitious by-product, is another common phase that has been observed to form and cause damage to concrete exposed to Mg-based deicers (Lee 2000). (The formation of these by-products and other detrimental effects will be discussed further in section 2.3.2.2 Effects of Magnesium Chloride).

In the past, Fick's Second Law has served as a common tool for many concrete applications. The basic technique is to expose a sealed concrete sample (cubic, prismatic, or cylindrical in shape) to an aqueous solution at a fixed chloride concentration. The duration of exposure is determined beforehand for a specific number of intervals. Afterward, the sample is sectioned with a diamond blade or ground with an abrasive perpendicular to the direction of chloride ingress. The concentration of chlorides in each section, or dust, at each depth is measured, and the data is used to generate a concentration-depth profile for the flow of chlorides in one direction. Based on those measurements, equations derived from Fick's Second Law may be applied to calculate the diffusion coefficient. Today, advanced technology has made it more practical to determine the concentration of chlorides at each depth, by using such equipment as x-ray fluorescence (XRF), scanning electron microscopy (SEM), wet chemistry, x-ray microscopy, or electron probe micro-analysis (EPMA), as well as diffusion cells (Andrade 1992, Yu 1993, Sutter 2003).

Generally speaking, Fick's Law accurately describes the physics of atomic and molecular diffusion, but it does not correctly describe the physics of ionic diffusion. This is because ions have both an electrical potential gradient as well as a concentration gradient associated with their presence. Atoms and molecules usually only migrate under the driving force of a concentration gradient. With ionic diffusion, the electrostatic field associated with the electrical potential gradient physically opposes the migration of ions due to the concentration gradient. These forces must be accounted for when assessing the rate of chloride ingress into concrete. Equations later developed by Nernst, Nernst-Planck (Chatterji; Part 1 1994), and Nernst-Einstein (Lu 1997) are now used to better describe the physics of ionic diffusion. Unfortunately, experimental works that support the Nernst equations, for the specific problem of diffusion in concrete, were not published until the mid-1990's (Chatterji; Part 3 1994). Therefore many previous researchers used improper mathematics to calculate diffusion coefficients (Chatterji; Part1, Part 2 1994, Truc 2000). In addition, newer methods for calculating the diffusion coefficient,  $D_c$ , have recently been published (Truc 2000, Nagesh 1998), which mostly support the Nernst equations that more accurately describe the physics of ionic diffusion in concrete than do the equations of Fick.

In addition to the complicated nature of the pore structure and hydration products of the matrix, all concrete regardless of age contains a small volume fraction of cracks that are present around both fine and coarse aggregates (Mehta 1993). The void space in the local vicinity of the cracks may then provide easy pathways for the transport of water and aggressive chemicals, considerably impacting the rate of diffusion of ions (Gerard 2000). The recent development of theoretical and mathematical models, taking the effects of



cracking into consideration, can more accurately predict the rate of chloride ingress through cement paste (Boulfiza 2003). These, like most other mathematical models for diffusion in concrete, usually consider the physics of water transport as one basis for the calculation of the overall amount of chloride ingress over time (Yunping 1994). A working knowledge of the rate of this ingress is extremely useful for determining the long-term durability of a structure (Costa 1999, Mangat 1994, QCL Group *Australia* 1999). Also, by determining the rate of ionic transport, the initial corrosion of reinforcing steel embedded in structural concrete can be predicted (Mangat 1987, Suryavanshi 1998).

Clearly, the complicated nature of the pore structure and hydration products of the matrix can markedly affect the rate of ingress of ions into concrete, but other materials may also affect the overall diffusivity. Most practical concrete is not made only with portland cement, aggregate, water, and air-entrainer, but also contains additional supplementary cementitious materials (SCM) and chemical admixtures (Rezansoff 1988, Roskopf 1975). Most modern cements contain SCMs as fly ash, ground granulated blast furnace slag (GBFS), and/or silica fume, as well as other SCMs. The addition of these types of SCMs is usually done to enhance performance in freeze-thaw environments (Bleszynski 2002) which aids in improving structural durability. Regarding the diffusion of chlorides, nearly all of the SCMs used today, particularly fly ash, GBFS (Stark 1997), and silica fume, have been shown to have a serious impact on the rate of diffusion of chlorides in cement (Byfors 1987, Thomas 1999, Bentz 2000, Bleszynski 2002). Other admixtures are applied as surface coatings, and some of them actually alter the physical properties of concrete like its conductivity and capacity to transmit heat. With respect to deicing, this could potentially save money (Yehia 2003).

In summary, the diffusion of ionic species through the matrix of concrete is a very complicated problem that has many variables. Although diffusion in concrete has been studied extensively, finite and precise diffusion coefficients, that could help predict a structures long-term durability, have not yet been obtained (Yunping 1994, Truc 2000). The mathematics and physics of transport mechanisms in concrete essentially remain unsolved. Future research in this area would aid in the understanding of ionic diffusion into concrete due to the application of aggressive deicing chemicals, commonly applied to roads and bridge decks in northern regions of the United States.

### **2.2.2 Air Content**

Air content has been found to improve frost resistance of concrete. It is also known that the disadvantage of increasing the air content is that it lowers the strength of concrete. In fact, “a strength loss of 10-20% occurs in air entrained concretes” (Mindess et al. 2003). However, to have good frost protection, air entrainment is required.

The required air content is based on the maximum aggregate size, with less air required when larger aggregates are used as shown in Table 2.8 (ACI 1992). These closely spaced air voids “protect concrete during freezing by providing reservoirs for water that exits from the paste on freezing” (Mindess et al. 2003). However, the spacing of air voids greatly depends on the  $w/c$  ratio (i.e. the higher the  $w/c$  ratio, the larger the bubble spacing and the lower the specific surface). It has been found that “a higher specific

surface, which corresponds to smaller bubbles, is desirable so as to minimize the adverse effect of air on the strength of concrete (Neville 1997). In addition, standards specify the maximum value for bubble spacing and the minimum value of the specific surface of the air in concrete in order to ensure the presence of small air bubbles. This gives the most protection from freezing and thawing and the least amount of strength loss.

Other advantages of increasing the air content in concrete include resistance to scaling caused by deicing salts, and improved sulfate resistance. Perhaps the most efficient way to treat concrete with higher air content is to lower the  $w/c$  ratio and compact it better. This will lead to more impermeable concrete with a better resistance to aggressive agents (Mindess et al. 2003).

Table 2.5. Effects of  $w/c$  ratio on the air void system in concrete (Mindess et al. 2003)

$w/c$	Air Content (volume %)	Spacing Factor mm (in)	Linear Expansion per Freeze-Thaw Cycle (%)
0.35	4.8	0.11 (0.0043)	0.00004
0.45	4.7	0.14 (0.0055)	0.00014
0.55	5.2	0.15 (0.0059)	0.00021
0.65	4.9	0.18 (0.0071)	0.00026
0.75	5.3	0.23 (0.0091)	0.00036

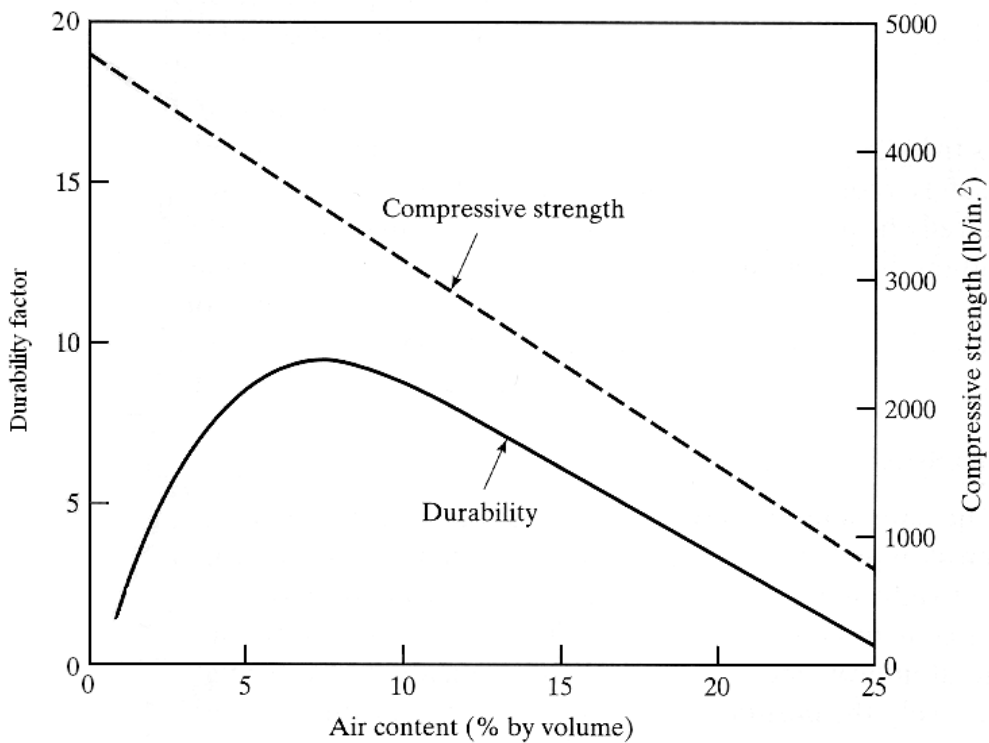


Figure 2.2. Effect of entrained air on durability and strength.

### **2.2.3 Cement Chemistry**

The major constituents of cement are the four compounds: tricalcium silicate ( $C_3S$ ), dicalcium silicate ( $C_2S$ ), tricalcium aluminate ( $C_3A$ ), and tetracalcium aluminoferrite ( $C_4AF$ ). These chemical compounds form at high temperatures within the kiln just before and during the clinkering phase. The calcium silicates make up approximately “three-fourths of the cement and are responsible for the cementing qualities” (Mindess et al. 2003). When mixed with water, the cement undergoes a series of chemical reactions that ultimately hardens the cement into hydrated cement paste. These reactions are commonly referred to as hydration and the hardened cement paste as hydration products (Mindess et al. 2003).

In portland cement, the compounds “contain small impurities of the oxides present in the clinker” (Neville 1997). Impure  $C_3S$  and  $C_2S$  are referred to as alite and belite, respectively. It is known that alite reacts more rapidly than belite, contributing to high early strength, whereas belite is responsible for the ultimate strength. The two major hydration products are calcium silicate hydrate (C-S-H) and calcium hydroxide ( $Ca(OH)_2$ ). Potential problems that can arise with these hydration products due to the application of deicing chemical is discussed later.

One way to mitigate problems with deicing chemicals is to partially replace portland cement with another cementitious material such as fly ash, silica fume or ground granulated blast furnace slag (GGFS). The use of these industrial by-products has many benefits, including their influence on the heat of hydration and strength. More importantly, they aid in the resistance of concrete of chemical attack by improving the chemical nature and microstructure of the hydrated cement paste (Neville 1997) by decreasing the amount of CH and decreasing permeability.

### **2.2.4 Aggregate Properties**

Aggregates that are susceptible to freeze-thaw damage can be reduced in size to improve resistance and durability. Susceptible aggregates cause widespread concrete deterioration in the forms of “pop-outs” and D-cracking on the surface of pavements (Mindess et al. 2003). Aggregates that may suffer pop-outs generally are fine-grained, have high total porosity and are virtually impermeable. When these types of aggregates become “saturated, the critical size of the rocks can become less than the size present in the aggregate” (Mindess et al. 2003). Generally, fracture of the aggregate occurs, leading to pop-outs at the surface.

D-cracking aggregates share similar properties to those susceptible to pop-outs. Moisture accumulates at slab joints, seeping down lower into the concrete and saturating the susceptible aggregates. When this moisture freezes it expands, resulting in fracturing of the aggregate. Thus begins the deterioration process as the concrete is subjected to repeated freezing and thawing cycles (Mindess et al. 2003). This is discussed further in the next section.

While these problems are due to physical attack, most other types of damage result from chemical reactions. For example, reactions between silica in aggregates and alkalis

contained in the cement paste have deleterious effects referred to as alkali-silica reactivity. The overall reaction is a complex four step process. Fundamentally, the alkali-silica reaction will “result in the production of two-component gels – one component is a non-swelling calcium-alkali-silicate-hydrate [C-N(K)-S-H] and the other is a swelling alkali-silicate-hydrate [N(K)-S-H]. The alkali-silica reaction will be safe if only the non-swelling C-N(K)-S-H forms, but unsafe if both gels form” (Mindess et al. 2003).

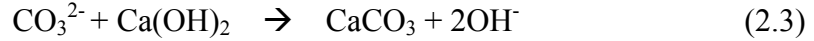
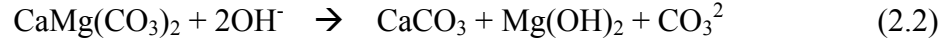
### *2.2.3.1 Dedolomitization*

Another type of deleterious chemical reaction was studied by Cody and Spry (1994), in which they examined a particular type of aggregate and its susceptibility to chemical attack, namely by magnesium. They explained the two ways in which magnesium is introduced into the cement paste. One way is through the application of magnesium-based deicers on pavement surfaces. The other way is dependant on the type of aggregate used in concrete. In their findings, Cody and Spry (1994) reported that dolomite coarse aggregate that undergoes dedolomitization would produce magnesium, which then migrates to the cement paste. Based on previous studies, reactions involving magnesium and hydrated cement paste will have deleterious effects on concrete durability.

In this study, both durable and non-durable concrete containing dolomite rock was investigated with a petrographic microscope, scanning electron microscope, and electron microprobe to determine the differences in the two groups of concrete. It was found that the aggregates in the non-durable or short-service life (less than 15 years) concrete had poor performance due to the fine-grained structure that contained “numerous euhedral and subhedral dolomite rhombohedra, and relatively high porosity” (Cody & Spry 1994). These aggregates were “found to have undergone pervasive chemical reactions with the cement which produced reaction rims on the boundaries of the coarse aggregate particles and in the cement region adjacent to aggregate boundaries” (Cody & Spry 1994).

In contrast, dolomite aggregate in the durable concrete was “coarse-grained, tightly interlocked crystal fabric, anhedral dolomite boundaries, and low porosity” (Cody & Spry 1994). The specimens of durable concrete were extracted from highways that have been in service longer than 40 years. The durable concrete exhibited no remarkable deterioration. Therefore, “textural and porosity differences are believed to be chiefly responsible for different service lives of the two groups of concrete” (Cody & Spry 1994).

The reaction that takes place within the non-durable concrete is generally referred to as alkali-carbonate reactivity (ACR) that occurs between the dolomite coarse aggregate and cement. This reaction occurs when dolomite from the aggregate is attacked by alkali from the high pH portland cement (see Equation 2 below). Consequently, magnesium and carbonate ions are released into the cement paste. The magnesium ions precipitate as brucite,  $Mg(OH)_2$  (see Equation 2 below) as the carbonate ions react with calcium hydroxide from the cement to form calcite,  $CaCO_3$  and hydroxide ions (see Equation 3 below). The formation of brucite and calcite cause crystal growth pressures (among other processes, e.g. hydration state changes of magnesium chloride hydrates) that lead to expansion of the concrete causing premature failure (Cody & Spry 1994).



In this study, the ultimate cause of concrete deterioration was found to result from the alkali-dolomite reaction. However, Cody and Spry (1994) also concluded that “the reaction itself does not produce deterioration”. It is actually the environmental changes, such as slight volume expansions that cause weakening of the aggregate-paste bonding and micro-cracking. In addition to these findings, “there was no evidence of complete dedolomitization” (Cody & Spry 1994) on any of the reaction rims of test specimens. Therefore, even partial dedolomitization may potentially lead to deterioration.

Furthermore, concrete containing such reactive dolomite aggregate may be more susceptible to deicer (i.e.  $\text{MgCl}_2$ ,  $\text{CaCl}_2$ ,  $\text{NaCl}$ ) deterioration under actual winter highway conditions. Enhanced susceptibility to deicing chemicals may develop during dedolomitization because these solutions may have easier access into those concretos in comparison to concrete with less reactive aggregate. The presence of these chloride brines at aggregate-paste boundaries may be especially damaging if bonding at the boundary has already been weakened by dedolomitization and micro-crack formation. Repeated freezing and thawing conditions will enhance deterioration on roads where deicers are used abundantly. This study indicates that concrete, containing aggregate that reacts adversely with cement paste, may be susceptible to enhanced deterioration when exposed to deicing chemicals (Dubberke & Marks 1985).

#### **2.2.4 Cracking**

Although cracking may not cause immediate structural failure, it may provide the onset for deterioration that ultimately leads to failure. As cracking spreads, it promotes the permeability of concrete, leading to surface scaling and further internal stress-related cracking. Table 2.6 lists the leading causes of cracking in concrete due to interactions with its surroundings (Mindess et al. 2003).

Cracking results from various contributing factors. One factor is the loss of water in fresh concrete; this leads to surface cracking due to evaporation and/or suction of water by the subbase or formwork materials. The removal of water from the paste will “generate negative capillary pressures, which will cause the volume of the paste to contract” (Mindess et al. 2003). As the pressures continue to rise within the paste, plastic shrinkage results, leading to differential volume changes, which in turn, “cause cracking under induced tensile stresses” (Mindess et al. 2003). Other types of shrinkage include, drying shrinkage, autogeneous shrinkage, and carbonation shrinkage. It is worth noting that shrinkage is mainly a paste property; the aggregates present within the concrete are able to restrain any volume changes within the paste.

Drying shrinkage is an important phenomenon to consider. The most common example of controlling drying shrinkage is placing contraction joints in pavements and slabs. These control joints prevent shrinkage cracking from occurring across the surface of the concrete by confining it to the area where the joints are located.

Table 2.6. Causes of cracking in individual components of concrete due to interactions with surroundings (Mindess et al. 2003)

Component	Type	Cause of Distress	Environmental Factor(s)
Cement	Unsoundness	Volume expansion	Moisture
Aggregate	Temperature cracking Alkali-silica reaction D-cracking	Thermal stress Volume expansion Hydraulic pressure	Temperature Supply of moisture Freezing and thawing
Cement paste	Plastic shrinkage Drying shrinkage Sulfate attack	Moisture loss Volume expansion	Wind, temperature, relative humidity Sulfate ions

Another type of cracking, due to loading and internal stresses, which can be seen with the aid of a microscope, is called microcracking. Microcracks are very fine cracks that can occur at the interface of the aggregate and cement paste or in the paste itself. This type of cracking may result from “differences in the mechanical properties between coarse aggregates and the hydrated cement paste” (Neville 1997). Microcracking has been known to result from freeze-thaw cycling, as hydraulic and osmotic pressures build up within the hydrated cement paste. This is discussed further in the next section.

As previously mentioned, D-cracking is a type of cracking that result from aggregates susceptible to freeze-thaw damage, and is most often associated with concrete highways and other pavements. It has been defined as “cracking in a slab surface in a pattern that appears first in an orientation parallel to transverse and longitudinal joints and cracks, continues around corners, and may progress into the central area of the slab” (Girard et al. 1982).

### 2.3. Types of Interactions

Both physical and chemical interactions occur within concrete when it is exposed to freeze-thaw conditions and deicing chemicals. Physical interaction is initiated when the saturated concrete freezes, subjecting the concrete to expansion and internal stresses. Chemical interaction results from the application of deicing chemicals, leading to possible degradation of the concrete structure. Combined, physical and chemical interactions disrupt the concrete properties previously discussed.

#### 2.3.1. Physical Mechanisms of Paste Freeze-Thaw Attack

Saturated concrete subjected to freeze-thaw conditions can undergo damaging internal physical alterations due to the development of pressure resulting from ice formation within the pore system. Both the hydrated cement products and aggregates can be vulnerable to freeze-thaw damage, which will produce microcracking and ultimately surface scaling and deterioration. The application of deicing chemicals tends to increase the magnitude of physical deterioration by increasing the development of internal pressures.

At least three separate theories have been forwarded to describe the actions taking place inside the hydrated cement paste during freezing. The most well-known theory, the hydraulic pressure theory, was proposed by T.C. Powers in 1949. The process of the hydraulic pressure theory is illustrated below in Figure 2.3.

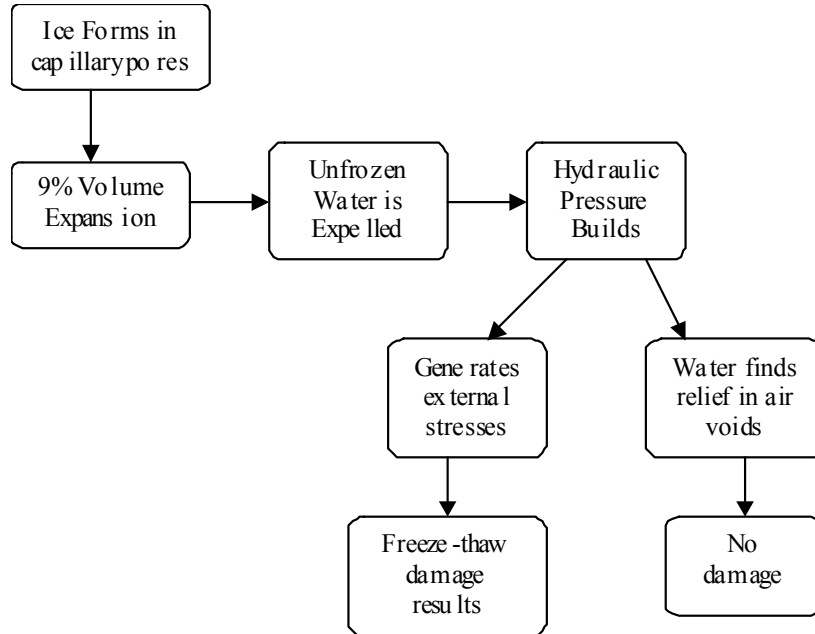


Figure 2.3. Schematic representation of the hydraulic pressure theory.

The phenomenon described by the hydraulic pressure theory begins as the temperature decreases below 0 °C, gradually freezing water in the largest capillary pores first. The 9 percent volume expansion that results as ice forms forces the unfrozen water out of the pores. Hydraulic pressures build in resistance to the outward flow of water, generating excessive internal stresses that will fracture the hydrated cement paste if its strength is exceeded. However, when expelled water is able to find relief at entrained air voids within the cement matrix, it freezes there and damage is avoided.

Powers (1975) forwarded the osmotic pressure theory to address some limitations observed in the hydraulic pressure theory. This theory considers osmotic potential to be the primary cause of paste freeze-thaw damage and partially explains the amplifying deleterious effects of deicing chemicals. The combined affects of surface forces and the alkalinity of deicing salts lower the freezing point of water in the pore system. Then, only pure water forms ice and that is only in the larger pores. Thermodynamic equilibrium is achieved between the ice and the pore water solution in the capillary pores. (This is due to the fact that only pure water freezes, raising the alkaline concentration of the rest of the pore solution and thus lowering the freezing point.) The difference in ionic concentration, or chemical potential, between the solution remaining in the larger pores and the solution in the smaller pores causes migration to larger pores where the ionic concentration is higher. This migration results in a build up of osmotic pressure. This theory also explains why air-entrained paste contracts as it freezes, rather than expanding,

even as ice continues to develop in the capillary pores as the temperature decreases below 0°C (Marchand et al. 1994).

A supporting explanation by Rösli and Harnik (1980) suggests that thermal shock occurs when frozen concrete surfaces are thawed by means of deicing salts. In the case of NaCl, a large amount of heat is required to melt the ice cover and the concrete itself contributes much of this heat possibly resulting in the creation of a significant temperature gradient at the surface. It is also widely regarded that “stress induced in the surface layers by the thermal gradient can surpass the tensile strength of concrete and lead to microcracking” (Rösli and Harnik 1980). They also suggest that a “layer-by-layer freezing could lead to surface scaling. The outer layer of the concrete contains relatively little deicing salt as it is washed out by the liquid water at the surface. In that layer, ice can thus form at temperatures slightly below 0 °C. However, in the layer just beneath it, the salt concentration is high and freezing generally does not occur” (Rösli and Harnik 1980). The difference in salt concentration will create stresses due to different expansion of the two layers, leading to scaling (Rösli 1980, Marchand 1994, Pigeon 1995).

Resulting visual damage from these physical mechanisms of attack are most commonly scaling, map cracking, or paste disintegration. Internal microcracking caused by freeze-thaw damage will eventually progress to scaling on the surface of the pavement. Microcracking is usually first seen around joints, pavement edges, and cracks, since more moisture accumulates in these places. Once cracking begins, the damage gradually worsens, increasing the permeability of the concrete and thus its susceptibility to the further moisture ingress.

Another factor that contributes to the amplifying effect deicers have on physical freeze-thaw damage is that deicers increase the saturation level of concrete increasing hydraulic pressures. This behavior causes concrete subjected to deicer salt application to remain in a critically saturated state for longer periods of time, increasing the likelihood of damage.

Physical degradation caused by NaCl is usually in the form of severe scaling when concrete is subjected to freeze-thaw cycling (Mu et al. 2002). This type of degradation is primarily a result of the supercooling effect that occurs when NaCl reduces the freezing point of water in the concrete pores (Ghafoori and Mathis 1997). This reduces the immediate development of hydraulic pressures in the concrete as the water remains liquid as the temperature drops below 0 °C. However, when the supercooled pore water finally begins to freeze, it does so at a much faster rate, generating a “greater magnitude of hydraulic pressure” (Marchand et al. 1994). Another physical effect of NaCl in the pore solution near the concrete’s surface is the development of increased osmotic pressure that occurs after or during freezing (Marchand et al. 1994).

In addition to the theories already discussed another physical mechanism that can help explain the cause of concrete scaling from the application of deicing salts is that of salt crystallization within the pores (Hansen 1963). It is hypothesized that the pore solution can become supersaturated as wetting and drying cycles concentrate salts in the pores (Harnik 1980, Mindess and Young 1981). Once crystallization begins, salt molecules are drawn out of smaller pores into the larger pores, inducing potentially harmful



crystallization pressures (Ghafoori 1997). An estimation of the magnitude of the crystallization pressure resulting from salt crystal formation has been provided by Winkler and Singer (1972). In their research, they indicated that gypsum and halite crystal growth may exert pressures exceeding 29,000 psi.

In reality, it is likely that the increases in osmotic pressures, thermal stress, level of saturation, and salt crystallization, will result in concrete scaling in the presence of deicer chemicals. As salt concentration increases, the osmotic pressures will also increase because of the higher chemical concentration in the pore solution. Further, thermal stresses will be produced due to the melting of the ice cover and salt crystallization may occur in the pores due to the wetting and drying cycles. Also, the increased level of saturation will provide more water for the generation of pressures. In combination, these mechanisms are far more physically damaging for concrete exposed to deicers when subjected to cyclic freezing and thawing than for concrete that was not exposed to deicers.

### ***2.3.2 Chemical Mechanisms of Paste Freeze-Thaw Attack***

Deicer scaling/deterioration is typically characterized by scaling or crazing of the slab surface due to the repeated application of deicing chemicals. Although the exact causes of deicer scaling are not known, it is commonly thought to be primarily a form of physical attack, possibly resulting from a combination of factors (Mindess and Young 1981, ACI 1992b, Marchand 1994, Pigeon 1994, Pigeon 1995). Some researchers have stated that the presence of deicing chemicals, particularly salts, can magnify or amplify the same mechanisms that lead to freeze-thaw deterioration of the paste (e.g. hydraulic and osmotic pressures) (Ghafoori 1997). Contributing to this effect is the fact that pore water containing a relatively small amount of dissolved salts is more easily absorbed into capillary pores, resulting in increased saturation of the concrete (Pigeon 1995, Ghafoori 1997).

Although most research suggests that salt scaling is primarily a physical deterioration mechanism, some researchers feel strongly that chemical interactions may also be occurring. Marchand (1994) summarized this view stating that more attention should be paid to the chemical interaction between the deicing salts and cement paste hydration products. Recent research indicates that the chemical interaction between deicers and concrete may not be wholly benign as much past research suggests.

It is suggested that the  $\text{Ca}(\text{OH})_2$  dissolution process results in increased porosity at exposed surfaces, increasing the permeability of the concrete. This in turn increases the amount of water available and increases the amount of water available to freeze at 32 °F due to increased pore size (Marchand 1994). One recent study conducted by the Michigan Department of Transportation (MDOT) adds credence to this theory. Muethel (1997) confirmed through laboratory analysis that depletion of calcium hydroxide led to an increase in permeability and reduced alkalinity of the concrete in the vicinity of cracks and joints. The reduction in the concrete pH contributed to corrosion of reinforcing mesh in the jointed reinforced pavements.

It would be expected that factors leading to an increased permeability would be more prevalent at exposed concrete surfaces. In addition to contributing to surface scaling, concrete faces along joint or crack walls would also be adversely affected. A number of studies appear to support this hypothesis. The previously cited study conducted by the Michigan Department of Transportation (MDOT) observed that calcium hydroxide leaching was pronounced in concrete cores obtained at transverse crack locations in jointed reinforced concrete pavements from three different State routes (Muethel 1997). Visual surveys of the concrete pavement surface revealed localized deterioration and staining, while laboratory analysis confirmed that depletion of calcium hydroxide, increased permeability, and reduced alkalinity of the concrete, had occurred.

A study conducted for the Ohio Department of Transportation (ODOT) investigated the joint deterioration observed in many northern tier States (Munoz 1994, Munoz 1995). Termed “coning,” this deterioration is characterized by concrete degradation at joints that progresses from the bottom of the slab upward. The exact cause of this deterioration is unknown, but it is speculated that more than one distress mechanism might be at work. Munoz states that dowel baskets may interfere with proper concrete consolidation, resulting in weaker concrete and increased porosity and permeability. This contributes to a chemical attack mechanism, with dissolution of the concrete paste considered the primary cause. Munoz explored the dissolution mechanism, stating that both the presence of dissolved salts and the velocity of solvent flow through the concrete are important factors. It is speculated that concrete at the joints has increased permeability, with accompanying relatively high solvent velocity. Additionally, potentially high CO<sub>2</sub> content in the solution from melted snow and other factors may lead to an increased solubility of the concrete.

Most past research suggests that salt scaling is primarily a physical deterioration mechanism. However, as this literature reveals, chemical interaction between deicers and concrete may not be as wholly benign as previously believed. In fact, rarely would only one type of degradation be at work. Instead, the principal degradation mechanism is commonly supported by the others, accelerating overall concrete degradation. A study by Jang (1993) found that the use of chemical deicers led to concrete degradation through both their anionic and cationic constituents. In addition to causing dramatic pH shifts, evidence also exists that deicers exacerbate the alkali-silica reaction, aggregate freeze-thaw deterioration (D-cracking), and deicer scaling of concrete.

The use of deicing chemicals has also been implicated in both alkali-silica reactivity (ASR), and alkali-carbonate reactivity (ACR). It is suggested that deicer use contributes to these deleterious reactions due to the increased alkalinity of the pore solution and concrete saturation mainly linked with the use of NaCl (Nixon 1987, Muethel 1997, Crumpton 1989, Gillott 1994).

The following sections describe potential deleterious effects of NaCl, MgCl<sub>2</sub>, CaCl<sub>2</sub>, CMA and the more recently formulated MgCl<sub>2</sub>-based Agricultural Products (M-BAP).

### 2.3.2.1 Effects of Sodium Chloride

At one time, sodium chloride (NaCl), also called rock salt, was thought to be an environmentally friendly, non-corrosive deicer, and became the most commonly used deicer on the market (Ghafoori and Mathis, 1997 and McDonald and Perenchio, 1997). Today, some of the detrimental chemical effects of NaCl deicer are better understood.

One interaction resulting from the long-term application of the popular chemical deicer sodium chloride is the dissolution of calcium hydroxide (Ca(OH)<sub>2</sub>) (Hoffman 1984, Ge'gout 1992, Gagne' 1992). The dissolution equation is stated as follows (Marchand 1994):



When this occurs, increased porosity near the exposed surface results, increasing the permeability of the concrete and enhancing the amount of ice formed near 0 °C. In addition, “soluble calcium chloride produced in the process can also react with the aluminate phases in the cement paste to form chloroaluminate crystals.”



It appears that this reaction would be expansive, although there is no mention in the literature regarding the expansive pressures that would be exerted, or whether it would be damaging in and of itself. This action “may significantly reduce the long-term frost durability of concrete surfaces in service” (Marchand et. al. 1994).

Chloroaluminate (Friedel's salt = monochloroaluminate, CaO·Al<sub>2</sub>O<sub>3</sub>·CaCl<sub>2</sub>·10H<sub>2</sub>O + trichloroaluminate, 3CaO·Al<sub>2</sub>O<sub>3</sub>·3CaCl<sub>2</sub>·32H<sub>2</sub>O) forms from the reaction between the chloride solutions and C<sub>3</sub>A (Ramchandran et al. 1976, Chatterji 1978, Berntsson & Chandra 1982, Ftikos & Parissakis 1985, Worthington et al. 1988, Day 1992, Bonen & Sarkar 1994, Kurdowski et al. 1994, Tumidjski & Chan 1996). This is basically a transformation from the cement hydration product ettringite. The chlorides in solution are thought to cause a replacement reaction in which the sulfate of ettringite is replaced by chloride with the formation of structurally similar trichloroaluminate (Day 1992). An earlier study by Neville (1969) suggests that the chlorides could solubilize the ettringite and deposit calcium chloroaluminate. However, it could transform back to ettringite by later sulfate ingression. This reaction is due to the chloride, rather than the sodium, and can be observed with interactions with MgCl<sub>2</sub> and CaCl<sub>2</sub> solutions as well.

Buck (1985) mentions that chloroaluminate preferentially replaces ettringite when salt is present. Buck also discusses that chloroaluminate formed during initial hydration in the presence of calcium chloride could later convert to ettringite if the solution becomes rich in sulfate ions. Research conducted by Sutter (2000) has demonstrated the presence of chloroaluminate in the form of hydrocalumite (i.e. Friedel's salt) in South Dakota pavements. It was commonly found associated with ettringite in air voids and cracks. Figure 2 below shows a scanning electron microscope (SEM) micrograph and energy dispersive spectrometry (EDS) analysis of a ettringite/Friedel's salt filled air void from I-

94 near Spearfish, SD. This road was badly deteriorated and one of the causes was deicer attack to the cement paste.

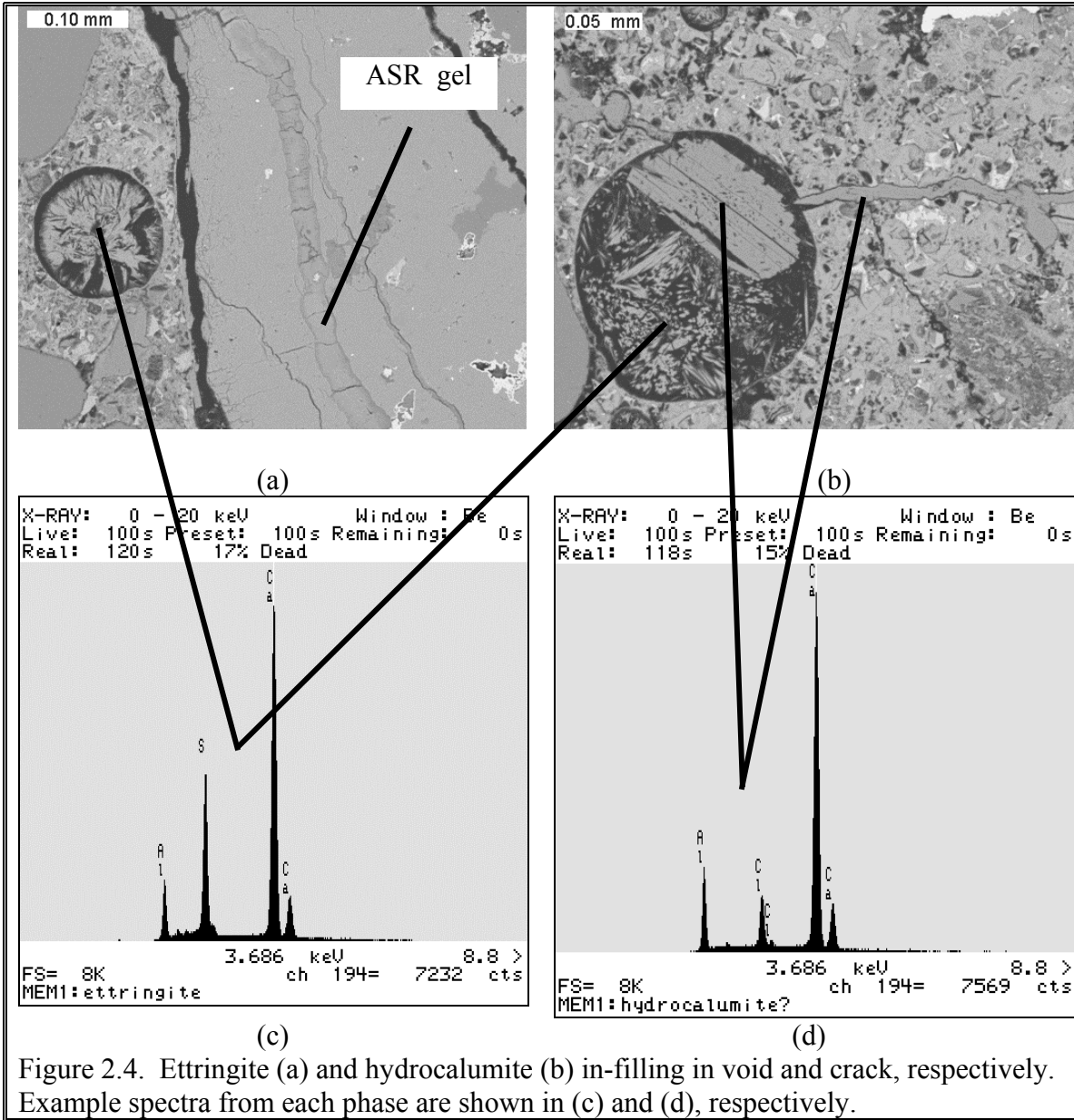
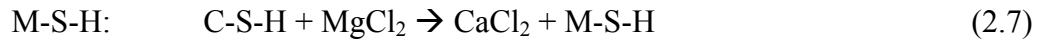


Figure 2.4. Ettringite (a) and hydrocalumite (b) in-filling in void and crack, respectively. Example spectra from each phase are shown in (c) and (d), respectively.

### 2.3.2.2 Effects of Magnesium Chloride

Like other deicers,  $MgCl_2$  effectively reduces the temperature at which water freezes and will have similar physical effects on concrete as  $NaCl$ . In addition, when the  $MgCl_2$  remains in the melt water on the concrete surface, the subsequent chemical interactions that occur may have a negative impact as the solution ultimately penetrates into the concrete. Some interactions of  $Mg^{2+}$  and  $Cl^-$  ions with the cement hydration products in cement paste are known to cause damaging alterations to the cement paste structure,

reducing concrete strength while increasing porosity. These changes result from the ability of  $Mg^{2+}$  and  $Cl^-$  ions to deplete  $Ca(OH)_2$  to form brucite and  $CaCl_2$ . These ions also cause decalcification of the hydration product calcium-silicate-hydrate (C-S-H), making the paste very porous and converting it to the secondary product, magnesium-silicate-hydrate (M-S-H). Problems associated with M-S-H are that it is non-cementitious and tends to develop shrinkage cracks, which lead to crumbling of the hydrated cement paste (Lee et al. 1998). The general reactions for the formation of brucite and M-S-H from  $MgCl_2$  are as follows:



The reaction Equation 2.7 shows that  $Cl^-$  ions cause  $Ca^{2+}$  to leach out from C-S-H, producing very soluble  $CaCl_2$  and weakening the cement paste structure by increasing its porosity.  $Cl^-$  ions will allow the precipitation of expansive chloroaluminates at early stages of hydration (Moukwa 1990). Another study by Santhanam, et al. (2003), shows that the chlorides enter into reaction with  $C_3A$  to produce brucite (Equation 2.6) as well as the chloroaluminate compounds, and they both become incorporated within the C-S-H. Other problems associated with the formation of brucite is that as it expands into the paste-fine aggregate interface, it may cause further debonding of the fine aggregate.

The resulting highly porous cement paste is susceptible to additional  $Mg^{2+}$  ion penetration, which will convert the C-S-H to M-S-H (Ftikos & Parissakis 1985). A rapid decrease in strength is due to its high porosity at early stages of exposure. In addition, a rapid increase in mass results from the large quantity of brucite formed. From SEM observations, M-S-H generally develops under the brucite layer. Many studies indicate that ultimate failure of concrete is the formation of M-S-H from C-S-H (Santhanam et. al. 2003, Snow 2001).

In addition, Cody and Spry (1994) also reported that both durable and non-durable concrete exposed to  $MgCl_2$  were severely deteriorated in their experiment with dolomite aggregates. In the wet/dry cycling, it was seen that the paste and aggregate experienced cracking and precipitation of new mineral, which filled the cracks and other voids. Some laboratory specimens “developed a complex three-layered mineral crack filling” and other stages produced layers of calcite and brucite which was eventually covered by precipitates of “very fine-grained, poorly consolidated minerals containing Fe, Mg, O, Cl, S, and Al” (Cody & Spry 1994). Like other studies, it was reported that the cement paste gained magnesium ions and lost calcium ions through reactions between the aggregates, paste and  $MgCl_2$  deicer.

Furthermore, reaction rims were seen in the paste and aggregate after exposure to  $MgCl_2$ . These rims, when observed electron microprobe, showed voids in the dolomite rims filled with brucite and  $MgCl_2$ ; paste rims were depleted of calcium and enriched with magnesium and the voids and pores were filled with  $MgCl_2$  precipitates (Cody & Spry 1994).

### 2.3.2.3 Effects of Calcium Chloride

Collepari (1994) cited a number of studies that have concluded that  $\text{CaCl}_2$ , another common deicer, is associated with a deleterious chemical reaction with concrete. The chemical attack is accompanied by the formation of a hydrated calcium oxychloride according to the following reaction:



The reaction proceeds most efficiently at temperatures just above freezing (40 °F to 50 °F), with rapid formation of hydrated calcium oxychloride. This reaction is considered to be disruptive to the concrete matrix because of the hydraulic pressures generated.

Collepari (1994) speculates that the damaging nature of this reaction has been masked by corrosion of reinforcing steel and freeze-thaw deterioration of the paste, but states that the chemical degradation that occurs is very detrimental. Collepari cites experimental evidence, based on decreasing compressive strength, suggesting that severe deterioration occurred in non-air entrained concrete exposed to  $\text{CaCl}_2$  deicers even though there was no steel to corrode nor was the concrete subjected to temperatures below freezing.

Collepari has done other research on the chemical effects of  $\text{CaCl}_2$  on cement paste using x-ray diffraction techniques. Analysis of degraded cement paste specimens revealed x-ray diffraction profiles characteristic of the hydrate monochloroaluminate ( $\text{C}_3\text{A} \cdot \text{CaCl}_2 \cdot 10\text{H}_2\text{O}$ ) and also of the oxychloride  $3\text{CaO} \cdot \text{CaCl}_2 \cdot 15\text{H}_2\text{O}$ . The x-ray diffraction profiles corresponding to the oxychloride presence were found only in specimens that were analyzed when moist. Similar analyses were performed with dried samples, but failed to reveal the oxychloride diffraction pattern. Therefore, it is believed that previous researchers had not connected  $\text{CaCl}_2$  paste damage to the oxychloride presence due to the theory that the oxychloride presence in dried cement paste is not discernable by x-ray diffraction (Monosi et. al. 1990).

Other studies have shown another manner in which  $\text{CaCl}_2$  can potentially affect both aggregates and hydrated cement paste within concrete. Concrete containing reactive dolomite aggregates is susceptible to attack when exposed to  $\text{CaCl}_2$  solution. This occurs as the  $\text{CaCl}_2$  solution enhances reactivity in aggregates, releasing  $\text{Mg}^{2+}$ , which then forms destructive brucite and M-S-H as previously discussed. Alteration rims around the aggregates were observed to contain a considerable amount of calcite prior to  $\text{CaCl}_2$  exposure, and afterward it appeared that the expansive brucite formation reduced the amount of calcite (Lee et al. 1998).  $\text{CaCl}_2$  also causes concrete deterioration by inducing fracturing immediately adjacent to the coarse aggregate boundaries and oriented parallel to the aggregate-paste interface (Cody et al. 1996). Concrete containing reactive dolomite aggregates was found to be especially susceptible to  $\text{CaCl}_2$  deterioration by Cody and Spry (1994). This study that focused on dedolomitization, as aforementioned, also experimented with the effects of  $\text{CaCl}_2$  deicer on concrete containing dolomite aggregates. The results on EDAX maps revealed cracks and voids “partially or completely filled with neofomed mineral matter” (Cody & Spry 1994) were rich in  $\text{CaCl}_2$ . Like  $\text{MgCl}_2$ , it was confirmed  $\text{CaCl}_2$  treatment would also cause dedolomitization. In contrast with the  $\text{MgCl}_2$  treatments, however, “ $\text{CaCl}_2$  produced

new, highly visible, reaction rims at the margins of coarse aggregates in non-durable concrete under both wet/dry and freeze/thaw conditions” (Cody & Spry 1994).

One unexpected result of their study was the increased content of magnesium in the dolomite rims. A possible explanation is that “with greater  $\text{CaCl}_2$ -induced dedolomitization in the aggregate interior, the aggregate rim will appear magnesium-rich” (Cody & Spry 1994). Although concrete exposed to  $\text{CaCl}_2$  and  $\text{MgCl}_2$  will result in deterioration, it is important to keep in mind that texture and porosity play a major role in aggregate, and thus concrete, susceptibility.

There are also direct chemical effects of  $\text{CaCl}_2$  on the cement paste. For example, when exposed to  $\text{CaCl}_2$  deicer, chloride concentrations tend to increase within the paste causing discoloration. This may be due to the formation of  $\text{CaCl}_2$  hydrate or to adsorption of  $\text{Cl}^-$  by C-S-H. Iron released from calcium-alumino-ferrite-hydrate also contributes to discoloration (Lee et al. 1998). Also, significant discoloration of the cement paste has been observed in a previous study by Kosmatka and Panarese (1988). They attribute these effects to the formation of calcium chloride hydrate phases ( $3\text{CaO}\cdot\text{CaCl}_2\cdot 12\text{H}_2\text{O}$ ;  $\text{CaO}\cdot\text{CaCl}_2\cdot 2\text{H}_2\text{O}$ ), to adsorption of Cl ion by the C-S-H phase.

As stated previously, all chloride solutions will cause a transformation of hydration products from ettringite to chloroaluminate. Therefore, in the presence of  $\text{CaCl}_2$  solutions, pre-existing ettringite will be transformed to calcium chloroaluminate or trichloroaluminate, which has the same structure as ettringite (Day 1992).

#### *2.3.2.4 Effects of Calcium Magnesium Acetate*

One study on the effects of calcium magnesium acetate (CMA) found that it was not as corrosive as NaCl (McCrum 1989). However, more recent studies have shown that CMA solutions may be the most deleterious deicing chemicals.

A study by Santagata and Collepardi (2000) suggests that CMA causes deterioration of the cement matrix by forming secondary minerals such as M-S-H and brucite. Like  $\text{MgCl}_2$ , CMA solutions transform the cement hydration product C-S-H to non-cementitious M-S-H by depleting the calcium. Potentially expansive brucite also forms as a result of CMA penetration into concrete. The M-S-H layer results in shrinkage cracking and debonding of fine aggregate, making the cement more porous. Secondary brucite is then able to precipitate into the large air voids, where ettringite previously existed, created by the loss of fine aggregate. According to Taylor (1990), the destruction of ettringite occurs due to the decrease in pH caused by the formation of brucite in which magnesium ions consume  $\text{OH}^-$  ions. In addition, calcium ions displaced by the M-S-H forming reaction will precipitate thin layers of calcite on the walls of the air voids and at paste-aggregate interface where brucite also precipitated (Lee et al. 1998). The formation of these secondary minerals results in concrete mass loss, significant decrease in load carrying capacity, and widespread cracking and scaling.

### 2.3.2.5 Background and Effects of M-BAP ( $MgCl_2$ -Based Agricultural Products)

M-BAP contains agricultural by-products such as silage (condensed solubles from grain processors, brewers, and vinters), whey and steepwater (liquor from processing corn). Developers of the newly marketed M-BAP, Ice Ban™, claim that it is “environmentally friendly and non-toxic to vegetation”<sup>4</sup> due to its natural ingredients. It is also stated that another benefit of its natural components is that M-BAP tend to inhibit corrosion of concrete caused by chloride salts. Some appealing physical properties of M-BAP are that they freeze at lower temperatures than most other deicers, possess a high percentage of deicing solids, and mix readily with liquid chloride brines.

There is a downside, however, to using agricultural by-products in winter maintenance. A study conducted by Roosevelt and Fitch (2000) found that Ice Ban™ varies from batch to batch due to the inconsistency of the by-product. As a result of using agricultural by-products, many of the laboratory tests “produced noticeable amounts of mold on the surfaces of the concrete [specimens] where Ice Ban M50™ was used” (Roosevelt and Fitch, 2000). Although, an inhibitor to control mold growth is available, the researchers note that they did not use it for this study.

The main objective of the Roosevelt and Fitch (2000) study was to evaluate the effect of Ice Ban M50™ on NaCl when used as a prewetting liquid. After 20 freeze-thaw cycles for concrete blocks subjected to a variety of combinations of Ice Ban M50™ applied alone, with NaCl, and NaCl with  $MgCl_2$ , the results indicate that Ice Ban M50™ does not significantly contribute to concrete scaling. In fact, it was found that after the 20 cycles, Ice Ban M50™ applied alone resulted in a 1.13 g cumulative scale weight loss compared to the NaCl applied alone resulted in approximately 260 g weight loss due to scaling. In addition, a visual ASTM grading of concrete scaling verifies that Ice Ban M50™ was the least destructive deicer studied, followed by NaCl with Ice Ban™ as a prewetting agent (Roosevelt and Fitch 2000).

Although, the initial cost of M-BAP is very expensive, based on this study it seems that the effects are the least detrimental. Still, there is much to learn about the application of M-BAP as both a deicer and a prewetting agent for other deicing chemicals.

---

<sup>4</sup> [www.iceban.com](http://www.iceban.com)



## **2.4 Pavement Construction Practices – Effects on Deicer Scaling/Deterioration**

### **2.4.1 Overview**

In order to construct durable concrete pavements, it is necessary to approach the mixture design and construction from a holistic point of view. Mehta (1997) presents this concept in a recent paper. He states that current theories on the mechanisms responsible for deterioration of concrete due to various causes are based on a reductionistic approach to science that tries to understand a complex system by reducing it to parts and then considering only one part of the problem at a time. As a result, current material specifications and test methods are focused only on a series of single attributes, failing to consider the system as a whole. Metha (1997) advocates a holistic approach in which loss of water-tightness is the primary concrete deterioration mechanism, which in turn results in loss of strength and stiffness, and materials-related distress. The two primary mix design considerations for producing deicer scaling/deterioration resistant concrete are proper air entrainment and a relatively high cement content with corresponding low  $w/c$ . These and other factors affecting concrete-deicer interaction are presented below.

### **2.4.2 Materials**

#### *2.4.2.1 Cementitious and Supplementary Cementitious Materials*

The selection of cement and supplementary cementitious/pozzolanic material is an extremely important element in designing durable concrete pavements. In many applications, the use of a standard ASTM C 150 Type I cement will provide satisfactory results. But durability should not be taken for granted, and therefore the properties of the cement and supplementary cementitious/pozzolanic materials must be considered in the context of the long-term physical and chemical stability of the concrete pavement.

#### *2.4.2.2 Cement*

The standard specification for portland cements used in the United States is presented in ASTM C 150. The following cement classifications are presented in the ASTM standard:

Type I—For use when the special properties specified for any other type are not required.

Type IA—Air-entraining cement for the same uses as Type I, where air-entrainment is desired.

Type II—For general use, particularly when moderate sulfate resistance or moderate heat of hydration is desired.

Type IIA—Air-entraining cement for the same uses as Type II, where air-entrainment is desired.

Type III—For use when high early strength is desired.

Type IIIA—Air-entraining cement for the same uses as Type III, where air-entrainment is desired.

Type IV—For use when low heat of hydration is desired.

Type V—For use when sulfate resistance is desired.

The most common cement type employed in pavement construction is Type I. The required chemical properties of Type III cements are similar to Type I, but Type III cements are commonly ground finer to promote the development of higher early strengths. Type III cements are gaining more widespread use, particularly in applications where high early strength is needed such as for rapid setting repairs and “fast track” construction. In areas where sulfate attack is a problem, Type V cements are used. Air-entrained cement, designated with an “A,” have small quantities of air-entraining material inter-ground with the clinker during manufacture.

In addition to these cements, ASTM C 595M provides standard specifications for blended hydraulic cements. These specifications recognize the following five classes of blended cements:

Type IS—Portland blast-furnace slag cement

Type IP and Type P—Portland-pozzolan cement

Type I (PM)—Pozzolan modified portland cement

Type S—Slag Cement

Type I (SM)—Slag modified portland cement

These cements are formed through intimately blending portland cement with fine materials such as ground granulated blast-furnace slag (GGBFS), fly ash or other pozzolans, hydrated lime, and pre-blended cement combinations of these materials (PCA 1992). These have not been commonly used on paving projects in the United States, but Type IS, Type IP, and Type I (PM) might be able to be used to produce durable concrete pavements. Each of these three can be further designated as air-entraining (A), moderate sulfate resistant (MS), and/or moderate heat of hydration (MH) through the addition of the proper suffix. For example, an air-entraining, moderate sulfate resistant pozzolan modified portland cement would be designated as Type I (PM)-A(MS).

#### *2.4.2.3 Ground Granulated Blast Furnace Slag*

GGBFS is a byproduct of the production of pig iron, in which the molten slag (at a temperature of 1500 °C) is rapidly chilled by quenching in water. This forms a glassy, sand-like material that is then finely ground to less than 45 µm, producing a surface area of 400 to 600 m<sup>2</sup>/kg Blaine (PCA 1992). GGBFS is nonmetallic, consisting mostly of silicate glass containing calcium, magnesium, aluminum, and silicate with potentially small quantities of crystalline compounds of melilite (Mehta 1993). This rough textured material is cementitious in nature, meaning that it has hydraulic cementing properties on its own. When combined with portland cement, the NaOH or CaOH activates the GGBFS, which hydrates and sets in a manner similar to portland cement (PCA 1992). Specifications for GGBFS for use in concrete are provided in ASTM C 989.

GGBFS may be blended or inter-ground with the cement and classified according to ASTM C 595M as Type IS, Type S, or Type I(SM). Alternatively, it may be added during batching as supplemental cementing materials or as a partial replacement of portland cement.

#### 2.4.2.4 Silica Fume

Silica fume is the byproduct of induction arc furnaces used in the silicon metal and ferrosilicon alloy industries where quartz is reduced to silicon at temperatures up to 2000° C (Mehta 1993). This produces SiO<sub>2</sub> vapors that oxidize and condense to minute spherical, non-crystalline silica. The particle size is roughly two orders of magnitude smaller than fly ash, having an average diameter of 0.1 μm and a surface area of 20,000 to 25,000 m<sup>2</sup>/kg, which is twice that of tobacco smoke (PCA 1992). It is highly pozzolanic, but its incredibly high surface area makes it difficult to handle, significantly increasing the water demand of the concrete unless water-reducing admixtures are used. Standard specifications for silica fume are provided in ASTM C 1240.

Due to its fine size, silica fume is able to pack very tightly into void space between cement and aggregate particles. It can thus be used to significantly reduce concrete permeability, and thus block the ingress of chlorides. For this reason, silica fume concrete has seen extensive use on bridge decks. Its highly pozzolanic nature also converts alkalis and CH into CSH making the concrete less susceptible to chemical attack. It can be used to mitigate ASR and sulfate attack (ACI 1992B; PCA 1992), although its effectiveness must be established through testing using ASTM C 441 for ASR and ASTM C 1012 for sulfate resistance.

Silica fume has not been widely used in pavements because of problems encountered in handling and special concerns related to curing. It is also quite costly and is therefore unlikely to find widespread use in pavement applications, except under special circumstances.

#### 2.4.3 Test Methods to Evaluate Concrete Mixture Designs

##### 2.4.3.1 Diagnostic Methods for Identifying Deicer Scaling/Deterioration

Distress related to deicer use is most often associated with surface scaling and delamination, which is almost unique to this distress type. The deterioration is observed in the paste, exposing the coarse aggregate particles. This is in contrast to a distress such as “popouts” that is characterized by fractured aggregate particles surrounded by intact paste. If the concrete under evaluation is subjected to deicer applications and is showing signs of scaling, deicers are likely contributing to the distress.

Chemical test methods, such as AASHTO T 260 "*Standard method of Test for Sampling and Testing Chloride Ion in Concrete and Concrete Raw Materials*", can be used to measure the chloride ion concentration in relation to depth of a concrete specimen. The presence of a high chloride ion concentration at or near the scaling surface is an indicator that the distress is likely related to deicer applications. In AASHTO T 260 pulverized concrete is dissolved in nitric acid to yield dissolved chloride ions in the concrete. Another approach is a water-soluble method ASTM C 1218 "*Standard Test Method for Water-Soluble Chloride in Mortar and Concrete*", but it has seen limited use. For the same concrete, the average chloride content measured by the water-soluble method is typically 75 percent to 80 percent of its acid-soluble chloride content (ACI 1989). Chloride content is most often expressed as the chloride ion (Cl<sup>-</sup>) present as a percentage

of the mass of cement. It is very important that the chloride content being reported is defined according to the method of testing.

Determination of deicer deterioration at joint and crack locations is a much more difficult task. Rarely is the deicer directly responsible for deterioration. It contributes by increasing the level of saturation, increasing the solubility of some compounds, and potentially increasing the alkalinity of the pore water. Thermal shock may also contribute to the occurrence of distress. Under these circumstances, the concrete becomes more susceptible to other distress mechanisms such as paste and aggregate freeze-thaw deterioration as well as ASR. The deicer may also provide a source of soluble sulfates, resulting in external sulfate attack.

Although the primary distress mechanism may obscure the contribution of the deicer to the deterioration, there are some diagnostic features that are indicators of whether deicer deterioration is at least a contributor to the observed distress. Muethel (1997) examined concrete at crack locations using phenolphthalein to identify calcium hydroxide depletion and permeability measures to estimate coarsening of the paste. He was able to identify zones at the concrete/crack interface that have significantly altered microstructure compared to the mass concrete, speculating that these differences in microstructure have resulted in joint/crack deterioration and staining. He further states that the primary leaching agent is carbonic acid, which aggressively attacks concrete in a high salinity environment. The presence of chemical deicers thus accelerates the leaching process. Marchand et al. (1994) described a similar process.

It is logical to assume that salts would concentrate in joints or cracks due to infiltrating melt water produced from the deicer application. If the chloride ion concentration were mapped from the joint interface into the concrete mass, the gradient would likely be one in which the concentration would be highest at some distance inward from the joint. The concentration at the interface would decrease as the flow of water in or through the crack/joint would have a tendency to wash the deicers away while wetting and drying cycles would concentrate them just below the interface surface. Thus, chemical methods could be employed to determine chloride ion concentrations at various distances from the joint/crack face to measure this phenomenon.

One such method for determining the chloride concentration profile is the "*Bulk Diffusion Test*" (Nordtest NTBuild 443). In this test, the sample is saturated with lime water and an exposed face of a specimen, similar to specimens used for ponding tests, is exposed to 2.8M NaCl for a minimum of 35 days. Then, the sample is mounted in a mill or lathe and layers of approximately 0.02 in are removed in a direction perpendicular to the surface that was exposed to the salt solution. The dust from each layer is gathered and the chloride content is determined in accordance with AASHTO T 260. From this data a diffusion coefficient and surface chloride ion concentration can be determined (Stanish 2000).

Polished concrete slabs can be examined by noting to what depth the cracking is present. Commonly, a pavement undergoing deicer scaling will have microcracking isolated in and parallel to the surface. This is very similar to common paste freeze-thaw

deterioration (Walker 1992), and in fact the mechanisms are closely related. In addition, if the air-void system parameters in the lower portion of the specimen are adequate, and the paste near the finished surface is devoid of air, poor finishing or curing is likely the responsible mechanism. The same polished slabs can be analyzed using an SEM and EDS system too determine chloride ion concentration profiles or areas of the slab can be analyzed using x-ray mapping to show chloride distribution in the concrete.

A relatively new instrument called an analytical x-ray microscope can also be used to analyze chloride concentration profiles in a polished slab. The analytical x-ray microscope produces a "focussed" x-ray beam by passing the x-ray flux generated from an air-cooled x-ray tube through a fine collimator. The collimators are finely produced glass tubes that taper along their length to a final aperture size of 10  $\mu\text{m}$ , 100  $\mu\text{m}$ , or 300  $\mu\text{m}$ , depending upon the collimator selected by the user. The final aperture size determines the point resolution of the image or the point analysis performed on the specimen analyzed. Using the x-ray microscope in a fluoresced x-ray mode, characteristic x-ray maps can be produced showing elemental distributions and point analyses can be performed to determine the composition of individual phases or individual compositions along a line. The advantage of the analytical x-ray microscope over a SEM is that the analyses do not need to be performed in a vacuum and the relatively large spot size (i.e. 100 - 300  $\mu\text{m}$ ) provides an average composition over a line. In the SEM, multiple parallel lines must be averaged to give the same results given the small (i.e. 1-5  $\mu\text{m}$ ) analytical spot size resulting from electron beam excitation of the specimen.

Petrography can also be employed to assist in the diagnosis of deicer deterioration. Carefully prepared polished thin sections could be used to identify salt crystals that might be present in addition to ettringite and hydrocalumite. Also, changes in the paste porosity/texture will be identifiable if care is taken in sample preparation. Some researchers are convinced that common deicers react with cement paste to form chloroaluminates and oxychlorides, compounds that can be observed through optical petrography and electron microscopy.

Deicer distress can appear outwardly similar to ASR and aggregate freeze-thaw deterioration in some manifestations. Wolter speculates that ettringite, in its "amorphous" form, has been confused with alkali-silica gel. An SEM with EDS capability can identify the minerals definitively. In the case of deicer distress, ettringite filling the interstitial pore space can be observed using an SEM (Wolter 1997). The SEM preferably should be a low-vacuum scanning electron microscope (LVSEM) or environmental scanning electron microscope (ESEM) to reduce the drying shrinkage cracking caused by a high vacuum in the conventional SEM.

Wolter (1997) gives the following characteristics of deicer distress that can be identified using optical microscopy:

- Microcracking propagating around aggregate particles and though the paste only.
- Aggregates relatively intact with virtually no reaction rims of silica gel observed,
- Deterioration within the paste only.
- Microcracking within the paste occurring predominantly sub-parallel to the deteriorating surface.
- Secondary deposits of ettringite within the air-void system and microcracks.
- Less microcracking and secondary deposits as distance increases from the deteriorating surface.

When diagnosing possible deicer distress, the orientation of the sample is important. Ideally, the sample should contain the vertical joint surface, so that the conditions with distance from the joint can be noted. Carbonation, microcracking, and the quantity of ettringite often change dramatically over distances of 1 to 2 in, and samples with unknown orientation to the joint are virtually useless (Wolter 1997).

ASTM C 672 "*Standard test method for Scaling Resistance of Concrete Surfaces Exposed to Deicing Chemicals*" is the most common test used to investigate the scaling potential of concrete. It is similar to AASHTO T 259 "*Resistance of Concrete to Chloride Ion Penetration*". In ASTM C 672, a  $\text{CaCl}_2$  solution (other chemical deicers may be used) is ponded on the surface of rectangular concrete specimens that are then subjected to freeze-thaw cycling. The specimens are placed in a freezer (0 °F) for 16 to 18 h and then manually removed to a thawing environment for 6 to 8 h. A surface layer of the water/salt solution is maintained at all times. A visual inspection is made at 5, 10, 15, 20, 25, and 50 cycles. The concrete is rated on a scale of 0 to 5 (e.g. 0 is for concrete surfaces showing no sign of scaling and 5 is for a surface that is severely scaled with coarse aggregate visible over the entire surface). The subjectivity inherent in the rating scale is one problem with this test (Pigeon and Plateau 1995). As a result, it is becoming common for researchers to measure the mass of scaled material to gain a more objective measure of scaling resistance.

This test is most applicable when the concrete pavement will be subjected to deicer applications and supplementary cementitious materials are being used. Concrete made with fly ash and GGBFS have exhibited variable deicer scaling resistance, and therefore mixtures containing these materials should be lab tested if field experience does not exist. Control samples of mixes with known scaling resistance should also be tested, as the results of this test are qualitative.

The Börås method (Swedish Standard SS 13 72 44) is similar to ASTM C 672, but has been modified to more accurately represent field conditions. A freezing front passes from the top of the specimen downward. This test allows for testing of specimens obtained from *in situ* structures as well as those prepared in the lab. A rating is assigned based on the mass of scaled material. Although similar to ASTM C 672, Pigeon and

Plateau (1995) believes that it is a better test for evaluation of scaling resistance. Unfortunately, the correlation between laboratory tests and field performance is not very good (Pigeon 1994; Mehta 1991).

#### 2.4.3.2 Diagnostic Methods for Determining Permeability

It has been shown that concrete subjected to repeated applications of deicers and wetting and drying cycles develops a coarser pore structure, characterized by larger, interconnected pores. Concrete permeability thus increases, making it more susceptible to many other distresses. This connection has been described by a number of researchers. For example, Basheer (1994) has proposed a single deterioration of concrete-permeability interaction model that links concrete permeability to corrosion of steel, frost damage, chloride ingress, carbonation, sulfate attack, salt attack, alkali attack, acid attack, alkali-aggregate reactions, and abrasion. It therefore may be possible to use the increased permeability associated with deicer deterioration as a diagnostic tool by comparing concrete obtained near joint and crack interfaces to that obtained from a slab interior.

Two widely accepted standard test methods for measuring concrete permeability are the British test method (*British Initial Surface Absorption Test*) that is not commonly used in the United States and AASHTO T 277 (ASTM C 1202) "*Electrical Indication of Concrete's Ability to Resist Chloride Ion Penetration*", or rapid chloride permeability test (RCPT). Many other test methods exist, but none has gained greater acceptance than the RCPT. SHRP researchers recommended modification to the AASHTO T 277 test to make it more rapid (Zia et al. 1993). It was also advocated by SHRP researchers that a "pulse pressure" method for concrete permeability be adopted to measure water permeability in the laboratory (Roy et al. 1993a; 1993b). A third SHRP test method was proposed for field evaluations in which the rate of airflow through a concrete surface under an applied vacuum is measured to estimate permeability. Unfortunately, this test is not considered sufficiently quantitative for prediction of actual permeability and thus results should only be used as an indicator of permeability (Whiting et al. 1994). More recently, a concrete sorptivity test has been under development and is under review by ASTM that may provide an indirect method to assess concrete permeability.

Mobasher and Mitchell (1988) published the results of a large study investigating the applicability of the RCPT. They found that the "test is valid and can be used with confidence." They investigated the repeatability of the test, finding the single operator coefficient of variation (COV) of a single test result to be 12.3 percent and the multi-laboratory COV to be 18.0 percent. Misra et al. (1994) report that the RCPT can be used as an important tool for quality control, inspection, and design, although further research is needed to examine the effect that pore solution chemistry has on the results. This is a very important finding from the perspective of using this test as a diagnostic tool, as the pore solution in concrete near joints and cracks will be different than that elsewhere due to the ingress of deicing chemicals.

In their investigation of the RCPT, Feldman et al. (1994) reported how changes in experimental conditions and specimens affected results. It was observed that the test affected the pore structure and resistivity of concrete, particularly relatively young concrete. It was also stated that simple measurement of initial current or resistivity gave

the same ranking for the four concrete specimens tested, and therefore this might be able to replace the RCPT. It is noted that all the concrete produced had a *w/c* of 0.55, and that their findings need to be verified for lower permeability concrete, and that made with blended cements.

Although the RCPT has been embraced by many SHAs due to its ease of use, it suffers some limitations that make it impractical when evaluating some mixtures. The three main limitations are: 1) the current passed is related to all ions in the pore solution and not just chloride ions, 2) the measurements are made before a steady-state migration is achieved, and 3) the temperature of the specimen increases due to the applied voltage (Stanish et al. 2000). The first limitation is most problematic for the assessment of concrete permeability in mixtures containing various admixtures (e.g., accelerators, corrosion inhibitors, etc.) that will affect the ion concentration of the pore solution.

AASHTO T 277 provides excellent correlation to the results obtained by AASHTO T 259 or a wide variety of concrete types and qualities (Perenchio 1994). One exception is concrete made with silica fume because the active pozzolanic nature of the material makes it seem more impermeable to chloride ion penetration than it really is. Another exception is concrete made with certain admixtures that affect the electrical conductivity of the mixture, including calcium chloride or calcium nitrite. Regardless, the rapidity, ease of use, and reliability make this test very attractive when investigating not only the chloride ion permeability characteristics of concrete, but also to assess permeability in general. Table 2.7 can be used to make a general assessment of the chloride ion permeability of the concrete tested using this test method (ASTM C 1202). It is noted that the assessment is not specific, but instead the chloride permeability is assigned a qualitative rating. Pavement concrete should have a qualitative permeability not greater than low, and in aggressive environments (exposure to chemical deicers, sulfates, etc.), a qualitative rating of very low or less is desirable.

Table 2.7. Chloride ion penetrability based on charge passed (AASHTO T 277).

Charge Passed (coulombs)	Chloride Ion Permeability
>4,000	High
2,000-4,000	Moderate
1,000-2,000	Low
100-1,000	Very Low
<100	Negligible

Another approach to understanding the potential susceptibility of concrete to deicer attack is to measure the concrete porosity. Porosity is a measure of the proportion of the total volume of pore space in concrete irrespective of the interconnectivity of the pores (Neville 1996). Absorption tests can be used to measure porosity, but the degree of interconnectivity between the pores influences the measured absorptivity. Thus, although porosity and absorptivity are commonly correlated, there is not a direct relationship. A variety of techniques are used for determining the absorption rate of concrete. One common test is ASTM C 642, *Test Method for Specific Gravity, Absorption, and Voids in Hardened Concrete*, which entails drying a concrete specimen at 212 to 230 °F and then



immersing it in water at 70 °F for at least 48 h. This type of test is commonly used as a quality control test for precast members.

As a result of shortcomings in common absorption testing procedures (e.g., ASTM C 642), there has been movement toward a type of testing known as sorptivity testing. Sorptivity testing measures the rate of absorption by capillary suction of water into the concrete (Neville 1996). Generally, it is too difficult to mathematically model this flow in all but a single direction, and thus sorptivity tests are configured to establish one directional flow into the specimen (Stanish et al. 2000). Sorptivity tests typically require that the sample be at a standard moisture content before testing is begun. The benefits of sorptivity testing are reduced time, low cost of equipment, and simplicity of procedure. The new standard, ASTM C 1585-04 *Standard Test Method for Measurement of Rate of Absorption of Water by Hydraulic-Cement Concretes*, requires only a scale, a stopwatch, and a shallow pan of water. One attractive feature of this approach is that the sample is conditioned for 7 days, with the temperature never exceeding 122 °F. This is important since damage to the concrete microstructure can result at the higher drying temperatures (212 °F or higher) recommended in other test methods, thus biasing the test results. Data reduction includes plotting the gain in mass per unit area over the density of water versus the square root of elapsed time, with the slope of the best-fit line being the sorptivity.

#### **2.4.4 Construction Considerations for Preventing Deicer Distress**

Construction can have a very important impact on the occurrence of materials related distress. As stated, durable concrete must be relatively watertight and non-reactive. From a construction perspective, this means that it must be well mixed, consolidated, and cured under conditions that will produce stable hydration products. Construction practices that have a direct impact on mixing, consolidation, and curing include ambient and seasonal construction conditions, duration of the mixing cycle, method of consolidation, steel placement, finishing, and curing. The following discussion focuses exclusively on those elements of the construction sequence that have a direct bearing on concrete durability.

##### *2.4.4.1 Ambient and Seasonal Construction Conditions*

Ambient and seasonal conditions can play an important role in the durability of concrete through their influence on the development of drying shrinkage cracking, excessive heat of hydration, and inadequate curing prior to deicer application. Hot-weather and cold-weather construction practice as described in *Design and Control of Concrete Mixtures* (PCA 1992) and elsewhere must be followed. It is imperative that drying shrinkage cracking be avoided to maintain the integrity of the concrete surface. This can only be accomplished if an awareness of the relationship between relative humidity, temperature, and wind exists and is acted upon by the construction team.

##### *2.4.4.2 Consolidation*

The goal of consolidation of paving concrete is the removal of entrapped air while avoiding segregation and disruption to the entrained air system. Assuming that a high quality, well-graded, workable mixture is used, it should be easily consolidated through internal and/or external vibration. Internal vibration is applied through immersion-type

vibrators typically located after the strike-off in the paver. Important factors to consider are the frequency of vibration, amplitude, and the speed of paving. Frequency is typically set between 7,000 and 12,000 vpm, although a recent study recommends fixing the frequency at 10,000 vpm (Gress 1997). This same study recommends weekly calibration checks on the vibrators, a negative (down from horizontal) vibrator slope of 30° or to one-half the pavement depth, and a fixed, uniform paver speed. Other sources state that 8,000 vpm is more typical. In any event, it is critical that the vibration is set to consolidate the concrete without segregation.

It is emphasized that undervibration can result in poor consolidation and overvibration may lead to segregation and the disruption of the air void system in the immediate vicinity of the internal vibrator. It has been noted on a number of MRD affected projects that the vibrator trails are visible on the pavement surface and appear to be an initiation point for cracking, spalling, and scaling (Gress 1997). In some instances, petrographic analysis has revealed that the air content in the path of vibration is significantly less than that between the vibrators.

When constructing concrete pavements, considerable attention must be directed to produce a mix that has consistent consolidation characteristics. A paving rate and vibrator frequency must be established early in the project that adequately consolidates the concrete without harmful segregation or disruption to the air void system. If the mix is found to be harsh and difficult to place, construction should be stopped until the problem is corrected. Too often, difficulties in placement are not discovered until a pavement begins to suffer early signs of deterioration at which point little can be done.

#### *2.4.4.3 Steel Placement*

The placement of embedded steel in concrete pavement has a direct bearing on the potential for corrosion. Steel used at joints, such as dowel and tie bars, is typically placed at mid-depth, thus concrete cover is not an issue. But in these applications, the joint provides a direct route for chloride ion and moisture ingress, and thus these bars must be protected with a durable coating to avoid corrosion. Epoxy is the most commonly used protective coating, although the cladding of dowels with plastic and stainless steel has also been used by some agencies.

For reinforcing steel, adequate concrete cover is essential to prevent corrosion. At least 50 mm of quality concrete cover is required in environments where chloride-based deicers are used. To ensure that at least 90 to 95 percent of the reinforcing steel is adequately protected, it is recommended that a design cover of 65 mm be used. Thus, during construction, great care must be exercised to avoid “high steel” which is susceptible to corrosion.

#### *2.4.4.4 Finishing*

In slipform paving, mechanical floating is commonly used immediately following the vibrating pan to embed large aggregate particles, correct small surface imperfections, and “close the surface.” If the entire slipform paving operation proceeded smoothly, no other

finishing other than texturing may be required. But in most cases, additional finishing is needed to correct surface imperfections.

After paving, the surface is checked using a 3- to 4-meter straight edge. Surface imperfections are commonly corrected using a hand-operated float. It is common that little bleed water occurs with stiff, slipformed concrete, but under certain conditions, it may be present. It is emphasized that finishing should not be conducted when bleed water is present, as there is a danger that either bleed water will become trapped beneath the concrete surface creating a plane of weakness or air content in the surface layer will be reduced. In either case, scaling of the surface may occur due to freeze-thaw damage, particularly if chemical deicers are used.

Finishers commonly desire to add more water to the surface to assist in the finishing operation. It is known that this demand must be resisted as working water into the concrete surface will decrease the  $w/c$  and reduce the air content, leading to scaling. If the mix is difficult to work without water being added during finishing, the entire construction operation should be reviewed.

On occasion, a paving edge may slump, requiring correction. In this case, it should be carefully rebuilt with added concrete, working against a bulkhead placed against the slab edge. Care must be taken to avoid over-working or over-finishing the repair.

#### *2.4.4.5 Curing*

Gowripalan (1993) found that improper curing resulted in the surface having a high rate of evaporation that produced a porous, permeable, and weak surface due to insufficient hydration. He also cited research that found that near the surface, the permeability of poorly cured concrete could be as much as ten times that of well-cured concrete.

Ideally, concrete would be cured in such a way that the presence of mixing water is maintained. This requires the continued application of water either through ponding, fogging, or covering the concrete with a saturated cloth such as burlap. Unfortunately, wet curing is not practical for most large paving projects. Instead, the most common curing method is to prevent the loss of mixing water through the application of a membrane-forming curing compound as specified under ASTM C 309. The effectiveness of curing compounds can be assessed through ASTM C 156.

The curing compound should be applied immediately following texturing. Any delay, particularly during hot, windy conditions, can cause significant harm to the concrete resulting in plastic shrinkage cracking. Although these cracks are small and isolated to the concrete surface, they provide access for potentially deleterious compounds into the concrete structure.

Great care should be exercised in the application of curing compounds. The application must be uniform and of sufficient quantity to ensure that the surface is completely sealed. On large paving projects, power-driven spray equipment should be used. It is highly recommended that two coats be applied to ensure complete coverage (PCA 1992).

There are concerns that some curing compounds are not effective. Highway agencies are highly encouraged to test curing compounds to verify their moisture-retention properties. Water-based curing compounds should not be “watered down” during construction. Also, the curing compound should be resistant to damage caused by construction traffic.

Different concrete mixtures will require different lengths of curing prior to opening to traffic. This must be carefully considered when concrete mixtures containing fly ash or GGBFS are used. Temperature also has a major effect on the required length of curing, and the use of maturity concepts to determine appropriate opening times is recommended. In addition to strength gain required for load carrying capacity, newly placed concrete also requires an air-drying period of 1 month before it is subjected to deicer applications. This will add to the scaling resistance of the concrete.

#### ***2.4.5 Preventive Strategies for Controlling Specific Types of Materials-Related Distress***

##### ***2.4.5.1 Deicer Scaling/Deterioration***

In general, deicer scaling is not a concern for properly constructed, high quality portland cement concrete. But even if the concrete is properly constructed and cured, deicers may damage concrete with poor mix characteristics. Pigeon (1994) comments on this by stating that “air entrainment improves to a very large degree the resistance to deicer salt scaling...and as could be expected, scaling decreases with water-cement ratio, and finishing and curing operations are particularly important.” As indicated, the two primary mix design considerations for producing deicer scaling/deterioration resistant concrete are proper air entrainment and a relatively high cement content with corresponding low  $w/c$ .

Air content is an important consideration when trying to prevent deicer scaling. Concrete adequately air-entrained for freeze-thaw may be susceptible to the development of salt scaling. Collepardi (1994) concludes that air contents recommended by ACI for “severe exposure” should be followed if the concrete is to be exposed to calcium chloride deicers, finding that concrete with air contents meeting ACI “moderate exposure” requirements suffered severe degradation in laboratory testing even without being subjected to freeze-thaw action. The ACI recommendations are presented in table 2.8 (ACI 1992).

In addition to the use of entrained air, high cement content, and low  $w/c$ , the use of fly ash has been proposed to enhance deicer scaling/deterioration resistance. The PCA (1992) reports that air entrained concrete containing fly ash has similar freeze-thaw durability to concrete made with portland cement as the sole binder as long as the same compressive strength, air void system, and curing are obtained. The results of a study conducted by Malhortra (1991) agree with those by Malek (1988) in which it was found that the incorporation of fly ash (two ASTM Type F and one Type C) appreciably reduced the permeability of concrete to chloride ions. This study was based on measuring chloride ion permeability using AASHTO T 277 and not on a measure of scaling resistance. Bilodeau (1991) found that concrete containing up to 30 percent ASTM Type F fly ash generally performed well under the combined effect of freezing and thawing in the presence of salt deicer, although performance of the fly ash concrete

was more variable. Although extended periods of moist-curing or drying periods did not seem to significantly effect performance, the use of membrane curing had a decided benefit, particularly for fly ash concrete. In a paper published a year later, Bilodeau (1992) reported on the properties of concrete containing ASTM Type F fly ash as 58 percent of the total cementitious materials content. He noted that in addition to acceptable mechanical properties, high volume fly ash concrete had excellent resistance to chloride ion penetration as compared to plain concrete mixes. He mentioned that further testing is needed to demonstrate scaling resistance.

An experiment conducted by Byfors (1987) examined the influence of fly ash and silica fume addition on chloride ion penetration and pore solution alkalinity. It is reported that the additions of either fly ash or silica fume considerably reduces the rate of chloride ion diffusion. Malhortra (1991) cites a number of studies conducted by CANMET which indicate the incorporation of low calcium fly ash (ASTM Type F) in concrete significantly reduces chloride ion penetration.

Table 2.8. Recommended air contents for freeze-thaw distress resistant concrete (ACI 1992).

Nominal Maximum Aggregate Size, mm (in)	Average Air Content, Percent <sup>1</sup>	
	Moderate Exposure <sup>2</sup>	Severe Exposure <sup>3</sup>
9.5 (3/8)	6	7.5
12.5 (1/2)	5.5	7
19 (3/4)	5	6
25 (1)	5	6
37.5 (1-1/2)	4.5 <sup>4</sup>	5.5 <sup>4</sup>
75 (3)	3.5 <sup>4</sup>	4.5 <sup>4</sup>
150 (6)	3	4

<sup>1</sup> A reasonable tolerance for air content in field construction is ± 1.5 percent.

<sup>2</sup> Outdoor exposure in a cold climate where the concrete will be only occasionally exposed to moisture prior to freezing, and where no deicing salts will be used. Examples are certain exterior walls, beams, girders, and slabs not in direct contact with soil.

<sup>3</sup> Outdoor exposure in a cold climate where the concrete may be in almost continuous contact with moisture prior to freezing, or where deicing salts are used. Examples are pavements, bridge decks, sidewalks, and water tanks.

<sup>4</sup> These air contents apply to the whole as for the preceding aggregate sizes. When testing these concretes, however, aggregate larger than 37.5 mm (1-1/2 in) is removed by handpicking or sieving and the air content is determined on the minus 37.5 mm (1-1/2 in) fraction of the mixture. (The field tolerance applies to this value.) Form this the air content of the whole mixture is computed.

In a large laboratory study, Gebler (1986a) and Klieger (1987) examined the durability of concrete made with both ASTM Type C and Type F fly ash. Both the chloride ion penetration and deicer scaling resistance were measured. It was concluded that fly ash concrete was just as resistant to chloride ion penetration as conventional concrete with similar *w/c*. But it was also found that conventional concrete was more scaling resistant than fly ash concrete, regardless of the type of fly ash used.

Marchand (1994), in a review of salt deicer scaling, reports that many studies are contradictory concerning the scaling resistance of fly ash concrete. He found that many laboratory studies indicate poor scaling resistance of fly ash concrete, yet field studies show adequate performance. He attributes most of these differences to the variable

nature of fly ash and to its slow rate of hydration. He concludes that the maximum recommended amount of fly ash should be limited to 30 percent of the total mass of cementitious material.

Detwiler (1994) found that either a 5 percent addition of silica fume or 30 percent addition of slag led to a far greater reduction in chloride ion penetration than did reducing the  $w/c$  from 0.5 to 0.4. She also noted that increasing the curing temperature over a range from 23 °C to 70 °C creates large differences in performance that indicates “the importance of controlling the curing process if durability is to be achieved.” Her findings seem inconsistent with those of Stark (1997), but this may be explained by Malhortra’s findings in which concrete containing fly ash actually has lower chloride permeability but still had poor scaling resistance (Malhortra 1991). Obviously, more research needs to be conducted to determine if fly ash and/or GGBFS can be used to improve scaling resistance.

#### *2.4.5.2 Corrosion of Embedded Steel*

Chapter 3 in ACI 222R (1989) provides an excellent description of how to protect new concrete construction against corrosion. The following three general categories of protection are considered:

- The use of design and construction practices that maximize the protection afforded by the concrete.
- The use of treatments that penetrate or are applied to the concrete surface that prevent chloride ion penetration.
- The use of techniques that directly protect the reinforcement from corrosion.

For pavement construction, the first and last categories are of most practical merit for prevention of corrosion of embedded steel, as the use of protective coatings on load transfer devices and adequate cover over reinforcing steel should be all that is required if properly constructed, high quality concrete is used.

The most effective pavement design factor for resisting corrosion is to provide adequate concrete cover over the embedded steel. In high quality concrete, the carbonation zone is unlikely to exceed 25 mm and thus a concrete cover of 25 to 40 mm is considered adequate for many structures (Mindess and Young 1981). But tests have shown that structures subjected to severe chloride exposure should have a concrete cover of at least 50 mm (Mindess and Young 1981; ACI 1992b; Mehta 1993). Thus, reinforced concrete pavements constructed in areas exposed to chloride-based deicers should use a minimum 2-in (50 mm) concrete cover. It is noted in ACI 201.2R (1992b) that to achieve the desired 2-in (50 mm) cover in paving for 90 percent to 95 percent of the reinforcing steel, the specified cover should be 65 mm.

It is important that a high chloride ion concentration not be introduced into the concrete through the constituent materials. One potential source of chloride ions in the constituent materials is the aggregate. In one study cited in ACI 201.2R (1992b), quarried stone, gravel, and natural sands were found to contain chlorides of sufficient quantity that the

chloride ion concentration in the concrete exceeded permissible levels. It is noted that chlorides in aggregate are not always available to the corrosion process. Thus, if concrete made with marginal aggregate has had good field performance, higher chloride levels may be tolerated. Calcium chloride accelerator is another internal source of chloride ions and its use should be discouraged if embedded steel is used. The chloride ion concentration of mixing water should also be limited.

Calcium nitrite has been found to be an effective corrosion inhibitor as well as an accelerator (ACI 1992). The nitrite ion chemically interacts with ferric oxides, making them insoluble. This reinforces the passive film, preventing the ingress of chloride ions up to a certain threshold level (PCA 1992). The cost of a corrosion inhibitor can be rather high, adding 8 percent to the cost of concrete (Mehta 1997).

The determination of the chloride ion concentration may be desired since it is an important factor in the corrosion of embedded steel. Chloride ion concentration can be determined using either of two wet chemical analyses. One is used to determine water-soluble chloride whereas the second determines the acid-soluble chloride content. In each case, a concrete specimen is ground to powder, typically using a rotary hammer to avoid the use of cooling fluids. The most common test is the acid solubility test (AASHTO T 260), in which the pulverized concrete is dissolved in nitric acid. The water-soluble method (ASTM C 1218) has seen limited use. For the same concrete, the average chloride content measured by the water soluble method is typically 75 percent to 80 percent of its acid-soluble chloride content (ACI 1989). Chloride content is most often expressed as the chloride ion ( $\text{Cl}^-$ ) present as a percent of the mass of cement. It is very important that the chloride content being reported is defined according to the method of testing.

The permeability of the concrete to chloride ion penetration can be measured in the laboratory. AASHTO T 259, *Resistance of Concrete to Chloride Ion Penetration* was a commonly used test method in which concrete prisms are subjected to ponding of a 3 percent sodium chloride solution for 90 days. The chloride ion concentration is then measured at various depths to assess the degree of ingress.

Due to the long testing period, a rapid test was devised based on the electrical conductivity of the concrete. This test is designated as either AASHTO T 277 *Rapid Determination of the Chloride Permeability of Concrete* or ASTM C 1202 *Electrical Indication of Concrete's Ability to Resist Chloride Ion Penetration*. As discussed previously, it has excellent correlation to the results obtained by AASHTO T 259 for a wide variety of concrete types and qualities (except for concrete made with silica fume) (Perenchio 1994). The rapidity, ease of use, and reliability make this test very attractive when investigating the chloride ion permeability characteristics of concrete. Table 2.6 can be used to make a general assessment of the chloride ion permeability of the concrete tested using this test method (ASTM C 1202). Because of its usefulness, it is recommended that this test be routinely conducted during mix design as an overall assessment of concrete permeability.

Studies cited in ACI 201.2R (1992b) have shown that for similar cover, the level of corrosion successively decreases with decreasing  $w/c$ . For concrete exposed to very severe chloride environments, it is recommended that a  $w/c$  of less than 0.40 be used if possible. In lieu of this, increasing the concrete cover to 100 mm is recommended for cast in place construction in a marine environment having a  $w/c$  of 0.45. Even the most impermeable concrete can become permeable if cracking occurs. These cracks provide easy access, concentrating chlorides, water, and oxygen to form a cell that can initiate corrosion (ACI 1992b).

Torri (1992) studied the effect of pozzolans and supplementary cementitious materials (fly ash, blast-furnace slag, and silica fume) and environmental conditioning on the concrete pore structure and chloride ion permeability. It was concluded that although the pore structure at the surface of concrete containing mineral admixtures was adversely affected by long-term drying, that in all cases, mixtures prepared with admixtures had lower chloride ion permeability than comparable mixtures made of ordinary portland cement.

One interesting study concluded that aggregate can be as much as 1000 times more permeable than a high quality portland cement paste and thus an overabundance of aggregate may adversely affect the ability of the concrete to protect steel (Perenchio 1994). It is therefore suggested that the maximum aggregate size and aggregate permeability are important considerations when designing against corrosion. Perenchio states that the use of large coarse aggregate particles may in effect “short-circuit” the concrete cover by providing a more direct route for harmful agents to permeate into the concrete. This should be studied in detail before adopting new gradation requirements.

Even the most impermeable concrete can become permeable if cracking occurs. Thus sound design practices should be used to minimize cracking and to keep cracks that form in reinforced pavements tight, minimizing the infiltration of deleterious agents. Construction practices should be used that prevent plastic shrinkage cracking of the pavement surface through the application of an approved curing compound at the appropriate time. This is most important during dry, windy days when the evaporation of bleed water can be quite rapid. Poor concrete consolidation must also be avoided through the design of a workable mix and care in selecting the appropriate depth, spacing, and operating frequency for internal vibrators.

In rare cases, it may be determined that an existing concrete pavement is at risk of suffering widespread corrosion before active corrosion has actually taken place. For example, a pachometer survey conducted soon after construction may reveal that the steel was improperly placed and adequate cover does not exist. In such a case, an agency may want to take preemptive measures to prevent the future occurrence of corrosion. Various concrete coatings and sealers are available that will prevent or slow down the penetration of water and salts. Silanes in particular have been found to be very effective.

Concrete cover cannot protect dowels and tie bars because the opening at the joint interface allows for the inflow of chlorides, moisture, and oxygen. It is therefore common practice to protect dowels and tie bars from corrosion by using a protective



barrier coating such as fusion bonded epoxy. The long-term effectiveness of epoxy coating of embedded steel is currently under intense study (Mehta 1993) although many cite it as an excellent preventive measure Perenchio (1994). Some agencies have investigated the use of plastic and stainless steel cladding as an alternative coating for dowel bars.

## 2.5 State-of-the Practice Construction of Concrete Pavements

It is clear from the previous discussion that material selection, mixture proportioning, and construction practices can have a profound effect on the durability of concrete. The need to carefully select materials, properly proportion them, and exercise care in construction is essential when the concrete is to be exposed to a freeze-thaw environment in the presence of deicers. Obvious considerations include the need to select durable aggregates, acceptable portland cement and supplementary cementitious materials, and suitable admixtures, and proportion them to create a dense, relatively impermeable concrete that is not susceptible to physical and/or chemical attack. Excellent information regarding material selection and proportioning to avoid physical and chemical attack is provided in *Design and Control of Concrete Mixtures* (Kosmatka et. al. 2003) and *Guidelines for Detection, Analysis, and Treatment of Materials-Related Distress in Concrete Pavements* (Van Dam et. al. 2002).

From the perspective of the state-of-the-practice, concrete mix design characteristics are particularly important for creating deicer deterioration resistant concrete include low  $w/c$  ratio and air entrainment (Pigeon 1994). A high  $w/c$  ratio produces a weak and permeable hydrated cement paste by increasing the capillary porosity. It is therefore recommended that a maximum  $w/c$  ratio of 0.45 be used to reduce deicer deterioration (ACPA 1992, ACI 1992, Cody 1994). The use of an air entraining agent creates the finely dispersed air bubbles in the hydrated paste that are needed to accommodate the pressures that develop as the concrete freezes and thaws.

It is also a commonly held dictum that a minimum cement content of 564 lbs/yd<sup>3</sup> is needed to increase the scaling resistance of concrete (Kosmatka et. al. 2003). When using ASTM C 672 to evaluate the concrete, Ghafoori (1997) recommended using a minimum cement content of 600 lb/yd<sup>3</sup>. Although the need for a minimum cement content is a common feature of many specifications, this approach has been questioned, with some sources stating that it is more critical to minimize the  $w/c$  ratio while using an aggregate gradation that reduces the cement content (TRB 1999).

One major consideration faced by SHAs when selecting cementitious materials is that portland cements blended with SCM (e.g. pozzolans, GBFS) often require a longer curing time prior to deicer application to prevent scaling. This is due to the slower rate of hydration inherent in many SCM and the decreased permeability characteristic of such concretes, resulting in a longer drying time. Therefore late season paving with concrete containing SCMs is potentially problematic

It is also widely recognized that concrete subjected to a freeze-thaw environment in the presence of deicing chemicals must be air entrained (PCA; ACI 1992; Van Dam et. al.

2002). Barothel-Bouny (2002) reviewed resistance to deicing-salt scaling in terms of different admixtures (such as air-entrainment [AE] admixtures), and the performance of those particular concrete pavements. High performance concretes (HPC) that are not air-entrained performed poorly in the deicing scaling test. The general conclusion of this study, with respect to scaling resistance due to deicing, is that air entrainment has a generally positive effect with respect to scaling resistance.

Air content of concrete was also the primary concern of Collepari et al. (1994). This research looked at the chemical, rather than physical effects, of chemical deicers on concrete structures. Non-air-entrained concrete had increased chemical action as the  $w/c$  ratio decreased, and experienced a significant decrease in durability. The durability performance of air-entrained concretes was considerably better than non-entrained concretes. Their recommendation was to use the ACI “severe exposure” recommendations to prevent attack against  $\text{CaCl}_2$  and freeze-thaw action.

The most critical elements of construction that have an impact on the freeze-thaw durability of concrete subjected to deicers are those that effect the  $w/c$  ratio and/or the air-void system. Any aspect of construction that raises the  $w/c$  ratio can negatively impact durability. Thus the moisture content of the aggregates must be accurately accounted for, the cement must be properly proportioned, and additional mix water must not be added if it will compromise the maximum specified  $w/c$  ratio. Further, water should not be added or “broadcast” onto the concrete during finishing, as this will result in a high  $w/c$  ratio at the surface producing a weak and porous layer susceptible to scaling. Trapping of bleed water by premature floating of the surface can also create a weakened layer of concrete that will be susceptible to scaling.

To ensure adequacy of the entrained air-void system, the air entraining agent must be added at the rate and timing needed to create not only an acceptable air content (Table 2.8), but also an air-void system meeting minimum spacing factor and specific surface requirements (ASTM C 457). Thus standard methods that measure air content may need to be supplemented with methods that measure the actual air-void system parameters such as the air void analyzer (AVA) or ASTM C 457. During placement and finishing, the concrete must not be overworked resulting in the loss of entrained air.

Once placed, the best curing regime possible should be used to facilitate hydration of the concrete surface. Ideally wet curing would be utilized, but this is rarely done on paving concrete. If a curing compound is used, the coverage should be thorough to minimize loss of moisture from the surface. And finally, an adequate curing and drying time must be allowed prior to the first application of deicing chemicals.

Standard specifications for concrete pavement construction used by various SHAs in regions subjected to freeze-thaw cycles in the presence of deicing chemicals have been reviewed and summarized in Appendix B. Table 2.9 presents three key mixture design parameters ( $w/c$  ratio, cement factor, and air content) obtained from the standard

Table 2.9. Concrete mixture parameters obtained from SHA standard specifications.

State DOT	w/c ratio	Cement Content (lbs/yd <sup>3</sup> )	Air Content (percent)
Arkansas	0.45	564	4.0 to 8.0
California	NS	506	4.0
Colorado	NS	656	4.0 to 8.0
Connecticut	0.49	615	4.5 to 7.5
Delaware	0.45	564	4.0 to 7.0
Idaho	NS	560	4.0 to 7.0
Illinois	NS	564	5.0 to 8.0
Indiana	0.45	440	5.7 to 8.9
Iowa	0.43 to 0.488	Varies w/ aggregate	5.0 to 7.5
Kentucky	0.49	564	4.0 to 8.0
Maryland	0.50	580	5.0 to 8.0
Massachusetts	NS	Varies w/ aggregate	6.0 to 8.0
Michigan	NS	564	5.0 to 8.0
Minnesota	NS	Varies w/ aggregate	5.0 to 8.0
Montana	NS	564	4.0 to 7.0
Nebraska	0.42	Varies w/ aggregate	5.0 to 7.5
New Mexico	NS	NS	6.5 to 9.0
New York	0.44	605	5.0 to 8.0
North Carolina	0.559	526	4.5 to 5.5
North Dakota	0.47	564	5.0 to 8.0
Ohio	0.50	600	4.0 to 8.0
Oklahoma	0.48	564	5.0 to 8.0
Oregon	0.48	570	Varies w/ aggregate
Pennsylvania	0.47	587.5	3.5 to 8.0
South Carolina	0.44 to 0.47	588	3.0 to 6.0
South Dakota	0.45	585	5.0 to 7.5
Texas	0.45	NS	Varies w/ aggregate
Utah	0.44	611	5.0 to 7.5
Virginia	0.49	564	4.0 to 8.0
West Virginia	0.49	564	4.5 to 9.5
Wisconsin	0.40 to 0.47	530	5.5 to 8.5

NS: Not specified.

specifications for 31 SHAs that routinely use deicing chemicals. As can be seen, there is considerable variability among the SHAs in specifying these three parameters.

Regarding the w/c ratio, when specified (and often it is not specifically defined), it ranges from 0.40 to 0.559, with an average value of 0.467. Based on ACI 318, concrete elements exposed to freezing and thawing in a moist condition in the presence of deicing chemicals should have a maximum w/c of 0.45. Although a number of SHAs meet this requirement, a significant number do not. Many of the SHAs that have the higher specified maximum w/c ratios are located in regions without notoriously cold winters

(e.g. North Carolina, Kentucky, etc.), yet others (e.g. Ohio) are located in regions with frequent freeze-thaw cycles and moderately cold temperatures.

The minimum specified cement content also varies widely. Many SHAs have adhered to the PCA recommendations of using a minimum cement content of 564 lbs/yd<sup>3</sup> (6 sacks per yard) to prevent scaling. Others have significantly lower minimum values. The air content ranges again vary, but all SHAs reviewed required the use of an air-entraining admixture. Often, SHAs stipulated different air content ranges for different size aggregates, complying with ACI 201 recommendations. New Mexico even stipulated that ASTM C 457 air-void system parameters be met.

Not listed in Table 2.8 is that almost all SHA standard specifications allowed for the use of SCMs, often stipulating a maximum allowable amount of fly ash and/or ground blast furnace slag. Some specifications (e.g. Michigan) recognize that additional curing time is needed for mixtures containing SCMs and therefore had seasonal placement limitations. Illinois required the use of a “protective coating” for all concrete pavement placed after a certain date that will be opened to traffic during the winter months. Finishing and curing requirements were consistent with the state-of-the-practice described previously.

## **2.6 Literature Review Summary**

Traditionally, winter maintenance entails plowing snow and applying chemicals and/or abrasives to melt the ice cover. In the past, many DOTs favored the use of rock salt, although methods of snow and ice removal may vary across the thirty States that practice winter maintenance. Over the years, traditional snow and ice removal methods have been modified in order to comply with environmental regulations, reduce corrosive damage to vehicles, and provide a more economical method to maintain safe roads. Current methods of snow and ice removal include deicing, pre-wetting salt or abrasive material, and anti-icing.

A number of concrete properties affect performance when the concrete is exposed to deicers. The most prominent characteristics to analyze are: permeability; air content; cement chemistry; aggregate properties; and cracking. It is widely understood that the water-to-cement ( $w/c$ ) ratio has the largest influence on the durability of concrete. By having a relatively low  $w/c$  ratio, the porosity of the hardened concrete will decrease and in turn, be less permeable. One important aspect of concrete permeability regarding the application of deicing chemicals is chloride diffusion. The concentration of chloride at the surface is the principle method of transport in near-saturated concrete. However, the movement of chloride in concrete is also a function of several variables. These include pore size and spacing, pore volume fraction, changes in pore size with respect to location within the cement paste, and structure of phases present in the pore system. Air content has been found to improve frost resistance of concrete. It is also known that the disadvantage of increasing the air content is that it lowers the strength of concrete. In fact, a strength loss of 10-20% occurs in air entrained concretes. However, to have good frost protection, air entrainment is required. One way to mitigate problems with deicing chemicals is to partially replace portland cement with another cementitious material such as fly ash, silica fume or ground granulated blast furnace slag (GGFS). The use of these

industrial by-products has many benefits, including their influence on the heat of hydration and strength. More importantly, they aid in the resistance of concrete of chemical attack by improving the chemical nature and microstructure of the hydrated cement paste (Neville 1997) by decreasing the amount of CH and decreasing permeability. Some research has linked concrete distress to deicer degradation of aggregates. Although cracking may not cause immediate structural failure, it may provide the onset for deterioration that ultimately leads to failure. As cracking spreads, it promotes the permeability of concrete, leading to surface scaling and further internal stress-related cracking.

Both physical and chemical interactions occur within concrete when it is exposed to freeze-thaw conditions and deicing chemicals. Physical interaction is initiated when the saturated concrete freezes, subjecting the concrete to expansion and internal stresses. Chemical interaction results from the application of deicing chemicals, leading to possible degradation of the concrete structure. Combined, physical and chemical interactions may disrupt the concrete properties previously discussed.

Saturated concrete subjected to freeze-thaw conditions can undergo damaging internal physical alterations due to the development of pressure resulting from ice formation within the pore system. Both the hydrated cement products and aggregates can be vulnerable to freeze-thaw damage, which will produce microcracking and ultimately surface scaling and deterioration. The application of deicing chemicals tends to increase the magnitude of physical deterioration by increasing the development of internal pressures.

Deicer scaling/deterioration is typically characterized by scaling or crazing of the slab surface due to the repeated application of deicing chemicals. Although the exact causes of deicer scaling are not known, it is commonly thought to be primarily a form of physical attack, possibly resulting from a combination of factors. Some researchers have stated that the presence of deicing chemicals, particularly salts, can magnify or amplify the same mechanisms that lead to freeze-thaw deterioration of the paste (e.g. hydraulic and osmotic pressures). Contributing to this effect is the fact that pore water containing a relatively small amount of dissolved salts is more easily absorbed into capillary pores, resulting in increased saturation of the concrete.

In general, deicer scaling is not a concern for properly constructed, high quality portland cement concrete. But even if the concrete is properly constructed and cured, deicers may damage concrete with poor mix characteristics. As indicated, the two primary mix design considerations for producing deicer scaling/deterioration resistant concrete are relatively low  $w/c$  ratio (with corresponding high cement content) and air entrainment. SHA standard specifications reflect this, although the specified maximum  $w/c$  ratio and minimum cement content varied greatly from state to state, indicating that consensus does not exist among the various agencies. All SHAs included in the review air entrained paving concrete.

### **Section 3. Work to Date**

#### **3.1 Examination of Field Cores**

A total of 56 cores have been received from sites in Idaho, Iowa, Montana, Colorado, and South Dakota. At least two cores were selected from each site to represent the condition of the concrete near joints or cracks and the condition of the concrete away from joints or cracks. The cores were cut into slabs oriented perpendicular to the pavement surface and parallel to the direction of traffic. One slab from each core was polished and examined with a stereomicroscope. Slabs from each core were also cut into billets to represent cross-sections at the pavement surface. One set of billets from each core have been ground flat with a diamond cup wheel and are ready for chloride profiling with the x-ray microscope. Another set of billets from each core have been ground flat with a diamond cup wheel, and the ground face impregnated and stabilized with fluorescent epoxy in preparation for thin sectioning. Only the billets from South Dakota have been fully prepared in thin section.

##### ***3.1.1 Idaho, westbound Interstate Highway 184 west of Boise, near milepost 3.***

A total of 18 cores were received from the Idaho site, nine from the left-most lane, and nine from the right-most lane. Four cores were selected for study, two from each lane. From each lane, one core was selected from the joint, and another core was selected away from the joint. Figures 3.1 through 3.4 show the cores as received. None of the cores exhibited any obvious signs of distress. No photos of the core site were available. Table 3.1 summarizes the results of a modified point-count performed according to ASTM C 457 performed on a polished slab from each of the cores. Figures 3.5 and 3.6 show successively zoomed in images of the core ID\_R07 to illustrate the air void structure.



Figure 3.1. Core as received from Idaho site, left-most lane, at joint, (ID\_L06).



Figure 3.2. Core as received from Idaho site, left-most lane, away from joint, (ID\_L04).



Figure 3.3. Core as received from Idaho site, right-most lane, at joint, (ID\_R07).



Figure 3.4. Core as received from Idaho site, left-most lane, at joint, (ID\_R03).



Table 3.1. Results of modified point-counts on cores from Idaho site.

Sample ID	ID_L06	ID_L04	ID_R07	ID_R03
Location	left-most lane, at joint	left-most lane, away from joint	right-most lane, at joint	right-most lane, away from joint
Raw data				
Total traverse length (mm)	3931.060	3931.060	3931.060	3931.060
Area analyzed (cm <sup>2</sup> )	77.0	77.0	77.0	77.0
Air stops	102	143	100	152
Paste stops	365	358	433	353
Aggregate stops	1038	1004	972	1000
Secondary deposit stops	0	0	0	0
Total stops	1505	1505	1505	1505
Number of air intercepts	875	1630	1178	1949
Number of filled void intercepts	18	0	10	1
Results				
Air vol.%	6.8	9.5	6.6	10.1
Paste vol.%	24.3	23.8	28.8	23.5
Aggregate vol.%	69.0	66.7	64.6	66.4
Secondary deposit vol.%	0.0	0.0	0.0	0.0
Existing average chord length (mm)	0.304	0.229	0.222	0.204
Existing paste/air ratio	3.6	2.5	4.3	2.3
Existing air void specific surface (mm <sup>-1</sup> )	13.1	17.5	18.0	19.6
Existing air void frequency (voids/m)	223	415	300	496
Existing spacing factor (mm)	0.272	0.143	0.240	0.118
Original average chord length (mm)	0.298	0.229	0.220	0.204
Original paste/air ratio	3.6	2.5	4.3	2.3
Original air void specific surface (mm <sup>-1</sup> )	13.4	17.5	18.2	19.6
Original air void frequency (voids/m)	227	415	302	496
Original spacing factor (mm)	0.267	0.143	0.238	0.118

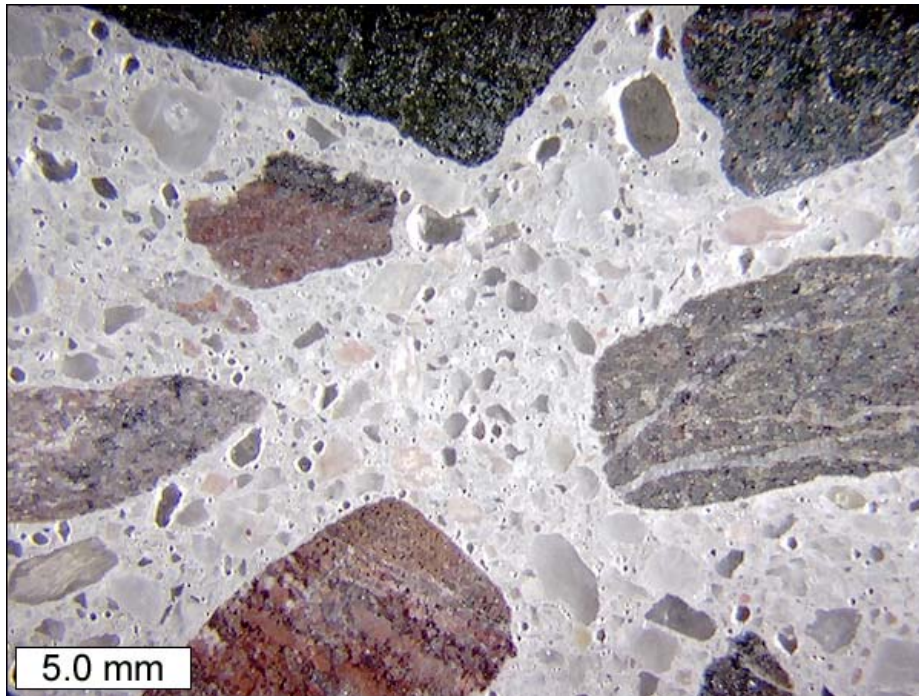


Figure 3.5. Stereomicroscope image of polished surface from core ID\_R07, magnified here approximately 4x

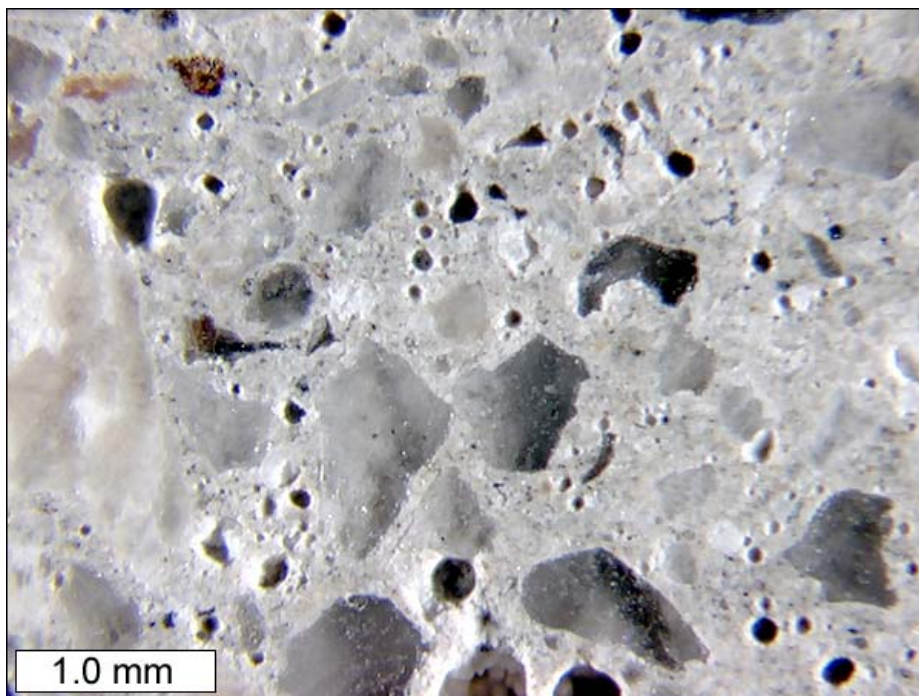


Figure 3.6. Stereomicroscope image of polished surface from core ID\_R07, magnified here approximately 22x.

### 3.1.2 Iowa, eastbound US Highway 34, western end of the Burlington Bridge.

A total of 10 cores were received from the Iowa site, five from the left hand side of the lane, and five from the right hand side of the lane. Two cores were selected for study, one showing a visible crack across the wear-surface of the core, and another without any visible cracks at the wear-surface of the core. Figures 3.7 and 3.8 show the cores as received. Figure 3.9 shows a photograph of a crack at the site. The cores sample approximately the top 4 inches, (10 cm) of the bridge deck. Approximately the top 2 inches, (5 cm) of each the cores consists of a thin concrete overlay. Table 3.2 summarizes the results of a modified point-count performed according to ASTM C 457 performed on a polished slab from each of the cores. Only the concrete overlay was included in the areas sampled by the point count. Figures 3.10 and 3.11 show successively zoomed in images of a polished cross-section of the concrete overlay of core IA\_04 to illustrate the air void structure. Some alkali-silica reactive sand particles were observed on the polished slabs. Figures 3.12 and 3.13 show a reactive sand particle and an adjoining alkali-silica reaction product lined air void before and after staining with sodium cobaltinitrite solution. The area shown in Figures 3.12 and 3.13 is just at the base of the concrete overlay, and the contrast in air void structure between the upper and lower layers of concrete can be seen.



Figure 3.7. Core as received from Iowa site, with surface crack, (IA\_07).



Figure 3.8. Core as received from Iowa site, without surface crack, (IA\_04).



Figure 3.9. Photograph of crack at Iowa site.



Figure 3.10. Stereomicroscope image of polished surface from core IA\_04, magnified here approximately 4x.

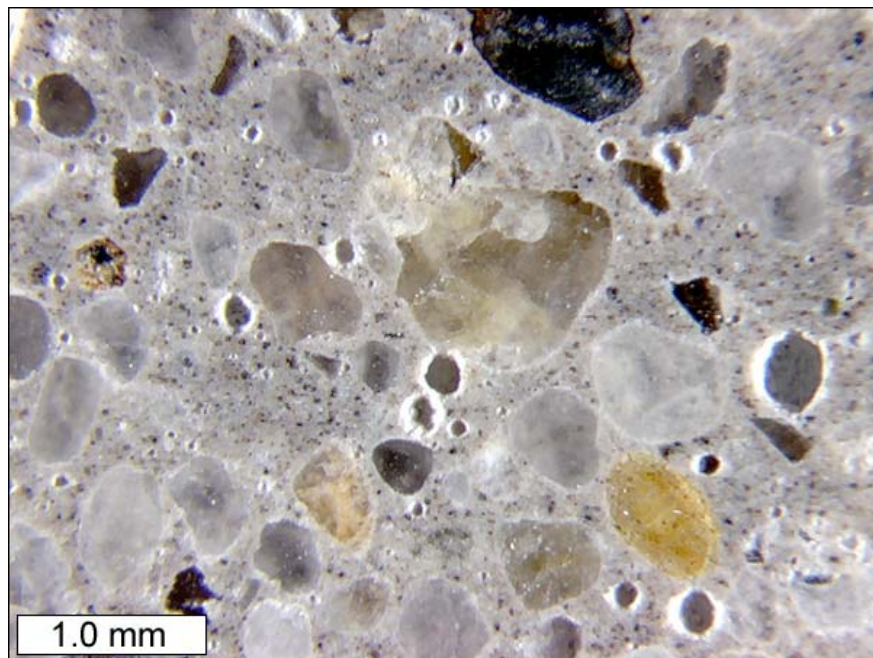


Figure 3.11. Stereomicroscope image of polished surface from core IA\_04, magnified here approximately 22x.

Table 3.2. Results of modified point-counts on cores from Iowa site.

Sample ID	IA_07	IA_04
Location	at crack	away from crack
Raw data		
Total traverse length (mm)	3411.272	4197.484
Area analyzed (cm <sup>2</sup> )	66.8	82.2
Air stops	86	123
Paste stops	400	400
Aggregate stops	817	1083
Secondary deposit stops	3	1
Total stops	1306	1607
Number of air intercepts	835	1198
Number of filled void intercepts	6	5
Results		
Air vol. %	6.6	7.7
Paste vol. %	30.6	24.9
Aggregate vol. %	62.8	67.5
Secondary deposit vol. %	0.2	0.1
Existing average chord length (mm)	0.302	0.268
Existing paste/air ratio	4.7	3.3
Existing air void specific surface (mm <sup>-1</sup> )	14.9	14.9
Existing air void frequency (voids/m)	245	285
Existing spacing factor (mm)	0.269	0.219
Original average chord length (mm)	0.305	0.269
Original paste/air ratio	4.5	3.2
Original air void specific surface (mm <sup>-1</sup> )	14.5	14.9
Original air void frequency (voids/m)	247	287
Original spacing factor (mm)	0.276	0.217



Figure 3.12. Stereomicroscope image of polished surface from core IA\_07 showing alkali-silica reactive sand particle before staining procedure.

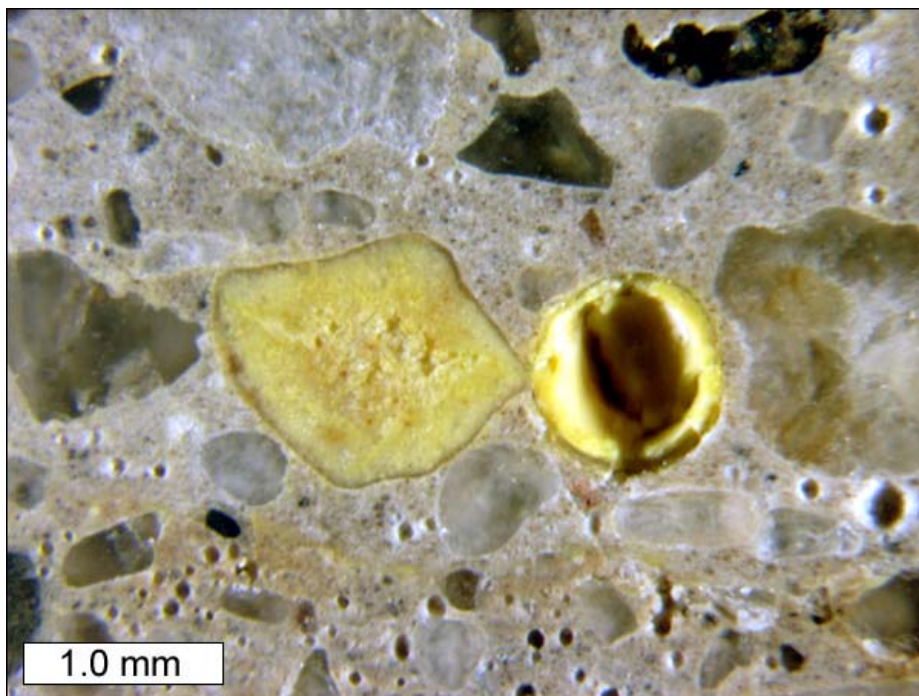


Figure 3.13. Stereomicroscope image of polished surface from core IA\_07 showing alkali-silica reactive sand particle after staining procedure.

### 3.1.3 Montana, westbound Interstate Highway 90 bridge deck near milepost 117.

Eight cores were received from the Montana site. The wear-surfaces were different from core to core. Figure 3.14 illustrates three cores, showing varying degrees of wear at the pavement surface. As shown in Figure 3.14, core MT\_02 still retains the initial tining pattern of the pavement, on core MT\_08, the tining depth is more shallow, and on core MT\_05, the tining has almost completely worn away, and fully exposed the coarse aggregate. Cores MT\_02 and MT\_08 were selected for study. Figures 3.15 and 3.16 show the cores as received. No photographs of the coring site were available. The cores sample approximately the top 5 to 6 inches, (12 to 15 cm) of the bridge deck. Approximately the top 1 to 2 inches, (2 to 5 cm) of the cores consist of a thin concrete overlay. The thickness of the overlay was quite variable from core to core. Table 3.3 summarizes the results of a modified point-count performed according to ASTM C 457 performed on a polished slab from each of the cores. Only the concrete overlay was included in the areas sampled by the point count. Figures 3.17 and 3.18 show successively zoomed in images of the concrete overlay of core MT\_02 to illustrate the air void structure. The air void structure of the concrete overlay would generally be considered inadequate for freeze-thaw environments.



Figure 3.14. Variable wear of pavement surface at Montana site.





Figure 3.15. Core as received from Montana site, with little surface wear (MT\_02).



Figure 3.16. Core as received from Montana site, with some surface wear (MT\_08).



Figure 3.17. Stereomicroscope image of polished surface from core MT\_02, magnified here approximately 4x.



Figure 3.18. Stereomicroscope image of polished surface from core MT\_02, magnified here approximately 22x.

Table 3.3. Results of modified point-counts on cores from Montana site.

Sample ID	MT_02	MT_08
Location	tining intact, little surface wear	tining worn down, some surface wear
Raw data		
Total traverse length (mm)	3400.824	3408.660
Area analyzed (cm <sup>2</sup> )	66.6	66.8
Air stops	47	43
Paste stops	419	424
Aggregate stops	833	836
Secondary deposit stops	3	2
Total stops	1302	1305
Number of air intercepts	419	234
Number of filled void intercepts	24	30
Results		
Air vol. %	3.6	3.3
Paste vol. %	32.2	32.5
Aggregate vol. %	64.2	64.2
Secondary deposit vol. %	0.2	0.2
Existing average chord length (mm)	0.293	0.480
Existing paste/air ratio	9.0	9.9
Existing air void specific surface (mm <sup>-1</sup> )	13.7	8.3
Existing air void frequency (voids/m)	123	69
Existing spacing factor (mm)	0.443	0.758
Original average chord length (mm)	0.295	0.445
Original paste/air ratio	8.4	9.4
Original air void specific surface (mm <sup>-1</sup> )	13.6	9.0
Original air void frequency (voids/m)	130	77
Original spacing factor (mm)	0.432	0.687

### 3.1.4 Colorado, State Highway 83, south of Denver near milepost 57.

Ten cores were received from the Colorado site. Four cores were taken at the joint, and six cores were taken away from the joint. Two cores were selected for study, one core from the joint, and one core away from the joint. Figures 3.19 and 3.20 show the cores as received. Figure 3.21 shows a photograph of cracks in the pavement at the site. Table 3.4 summarizes the results of a modified point-count performed according to ASTM C 457 performed on a polished slab from each of the cores. Figures 3.22 and 3.23 show successively zoomed in images of the core ID\_R07 to illustrate the air void structure. Some alkali-silica reactive sand particles were observed on the polished slabs. Figures 3.24 and 3.25 show a reactive sand particle and an adjoining mass of alkali-silica reaction product both before and after staining with sodium cobaltinitrite solution.



Figure 3.19. Core as received from Colorado site, at joint (CO\_01).



Figure 3.20. Core as received from Colorado site, away from joint (CO\_05).



Figure 3.21. Photograph of cracks in pavement at Colorado site.

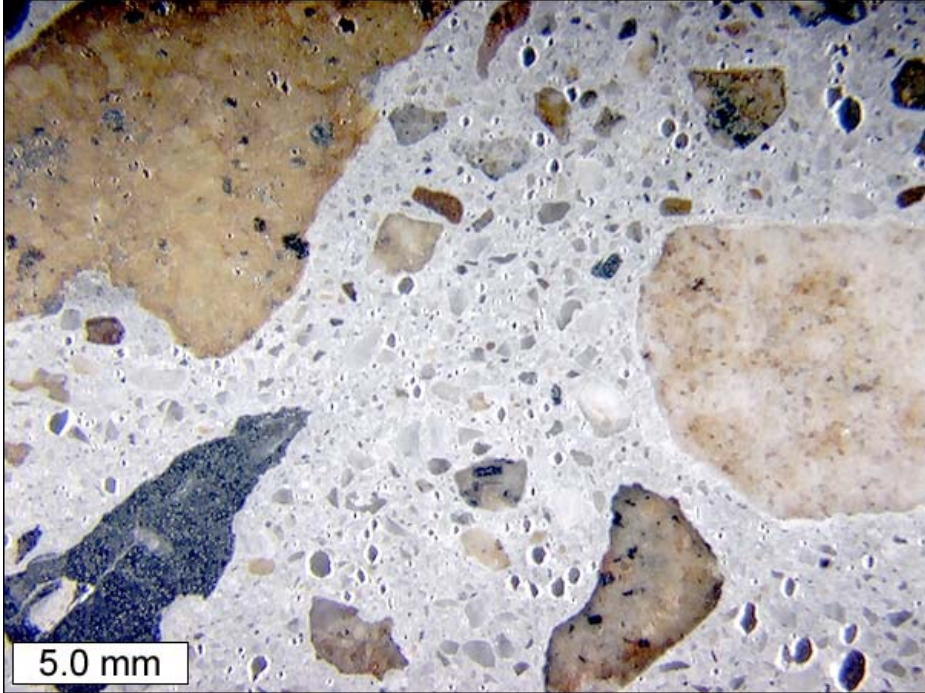


Figure 3.22. Stereomicroscope image of polished surface from core CO\_01, magnified here approximately 4x.

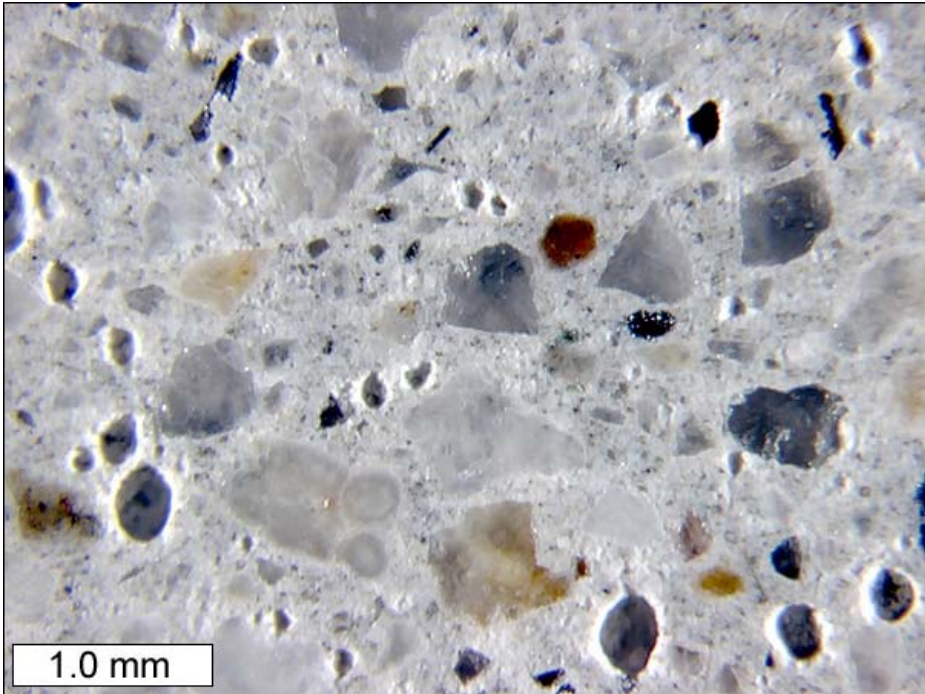


Figure 3.23. Stereomicroscope image of polished surface from core CO\_01, magnified here approximately 22x

Table 3.4. Results of modified point-counts on cores from Colorado site

Sample ID	CO_01	CO_05
Location	at joint	Away from joint
Raw data		
Total traverse length (mm)	3625.456	3625.456
Area analyzed (cm <sup>2</sup> )	71.0	71.0
Air stops	79	83
Paste stops	300	282
Aggregate stops	1009	1023
Secondary deposit stops	0	0
Total stops	1388	1388
Number of air intercepts	1072	1051
Number of filled void intercepts	3	0
Results		
Air vol.%	5.7	6.0
Paste vol.%	21.6	20.3
Aggregate vol.%	72.7	73.7
Secondary deposit vol.%	0.0	0.0
Existing average chord length (mm)	0.192	0.206
Existing paste/air ratio	3.8	3.4
Existing air void specific surface (mm <sup>-1</sup> )	20.8	19.4
Existing air void frequency (voids/m)	296	290
Existing spacing factor (mm)	0.183	0.175
Original average chord length (mm)	0.192	0.206
Original paste/air ratio	3.8	3.4
Original air void specific surface (mm <sup>-1</sup> )	20.8	19.4
Original air void frequency (voids/m)	297	290
Original spacing factor (mm)	0.182	0.175

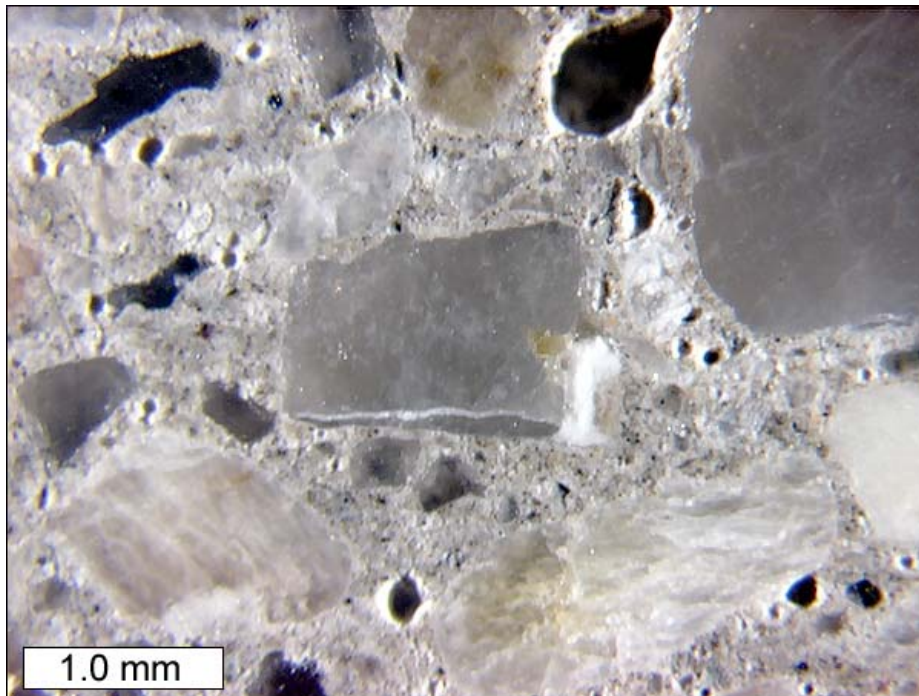


Figure 3.24. Stereomicroscope image of polished surface from core CO\_05 showing alkali-silica reactive sand particle before staining procedure.



Figure 3.25. Stereomicroscope image of polished surface from core CO\_05 showing alkali-silica reactive sand particle after staining procedure.



### **3.1.5 South Dakota, eastbound 26th Street left-turn lane onto northbound Interstate Highway 29.**

Ten cores were received from the South Dakota site. Four cores were taken at the joint, and six cores were taken away from the joint. Two cores were selected for study, one core from the joint, and one core away from the joint. Figures 3.26 and 3.27 show the cores as received. Figures 3.28 and 3.29 show photographs of the coring site. Table 3.5 summarizes the results of a modified point-count performed according to ASTM C 457 performed on a polished slab from each of the cores. Figures 3.30 and 3.31 show successively zoomed in images of the core SD\_04 to illustrate the air void structure.

Preliminary observations of thin sections in epifluorescent mode suggested that the cement paste from core SD\_01 near the joint was slightly more porous than cement paste from core SD\_04 away from the joint. To quantify this subtle observation, 30 epifluorescent mode images were collected from thin sections prepared from core SD\_01, and 30 images were collected from thin sections prepared from core SD\_04. The air voids, cracks, and sand particles were manually removed from each image, so that fluorescence from the cement paste could be isolated and measured. Figures 3.32 and 3.33 show a mosaic of the thirty images collected from the thin sections prepared from core SD\_01, both before and after the masking operation. Figures 3.34 and 3.35 show a mosaic of the thirty images collected from the thin sections prepared from core SD\_04, both before and after the masking operation. Each individual image covers an area of 1.245 x 0.934 mm, and contains 640 x 480 pixels. Figure 3.36 shows a histogram comparing the pixel intensities at the joint and away from the joint. As shown in Figure 3.36, the cement paste fluorescence intensity histogram for the images collected from core SD\_01 near the joint is shifted to the right, and is therefore brighter, than the cement paste fluorescence intensity histogram for the images collected from core SD\_04 away from the joint. The more porous a cement paste is, the more fluorescent dyed epoxy filled pore space there is, therefore more porous cement pastes will fluoresce more brightly than less porous pastes. However, concrete is a heterogeneous material, and some variability in cement paste density might be expected. To investigate further, additional slabs were cut from cores SD\_01 and SD\_04, and more thin sections were prepared. Although quantitative measurements have not been made, the same subtle trend of more porous cement at the joint versus away from the joint was not observed in the second batch. Therefore, the contrast in cement paste porosity has been attributed to variability within the concrete, and may not be related to proximity to the joint.



Figure 3.26. Core as received from South Dakota site, at joint (SD\_01).



Figure 3.27. Core as received from South Dakota site, away from joint (SD\_04).



Figure 3.28. Photograph of South Dakota coring site.



Figure 3.29. Photograph of South Dakota coring site.

Table 3.5. Results of modified point-counts on cores from South Dakota site.

Sample ID	SD_01	SD_04
Location	at joint	away from joint
Raw data		
Total traverse length (mm)	3625.456	3625.456
Area analyzed (cm <sup>2</sup> )	71.0	71.0
Air stops	85	91
Paste stops	396	382
Aggregate stops	907	915
Secondary deposit stops	0	0
Total stops	1388	1388
Number of air intercepts	1577	1420
Number of filled void intercepts	2	0
Results		
Air vol. %	6.1	6.6
Paste vol. %	28.5	27.5
Aggregate vol. %	65.3	65.9
Secondary deposit vol. %	0.0	0.0
Existing average chord length (mm)	0.141	0.167
Existing paste/air ratio	4.7	4.2
Existing air void specific surface (mm <sup>-1</sup> )	28.4	23.9
Existing air void frequency (voids/m)	435	392
Existing spacing factor (mm)	0.158	0.176
Original average chord length (mm)	0.141	0.167
Original paste/air ratio	4.7	4.2
Original air void specific surface (mm <sup>-1</sup> )	28.4	23.9
Original air void frequency (voids/m)	436	392
Original spacing factor (mm)	0.158	0.176

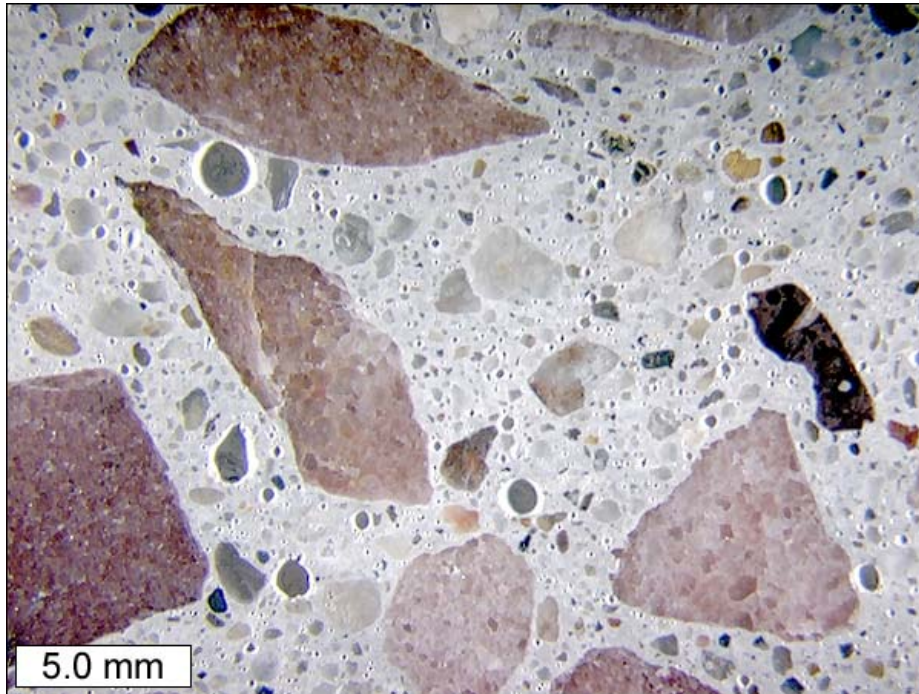


Figure 3.30. Stereomicroscope image of polished surface from core SD\_04, magnified here approximately 4x.

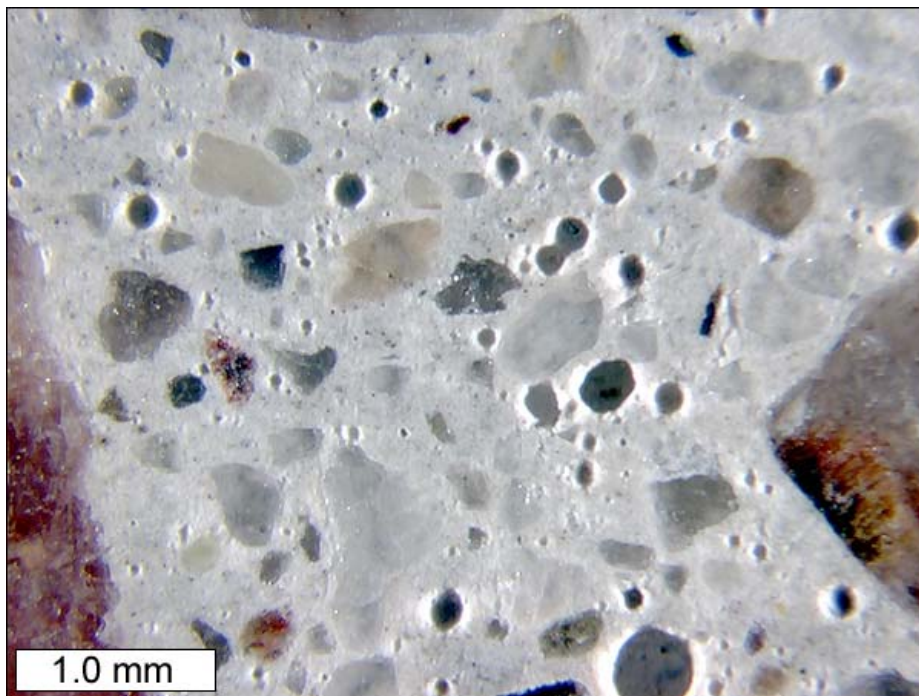


Figure 3.31. Stereomicroscope image of polished surface from core SD\_04, magnified here approximately 22x.

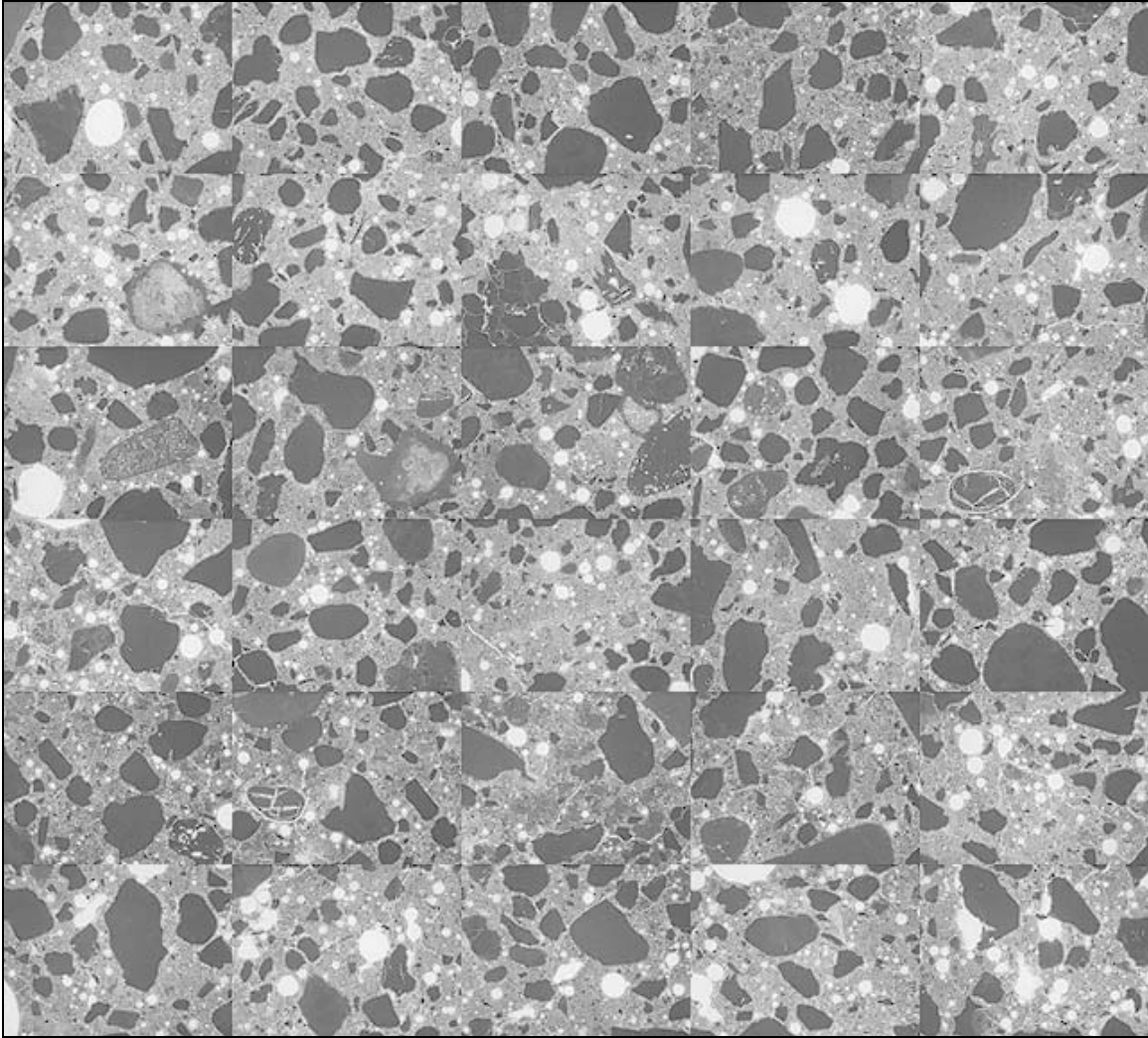


Figure 3.32. A 5 x 6 mosaic of 30 epifluorescent mode images from thin sections prepared from core SD\_01, magnified 17x.

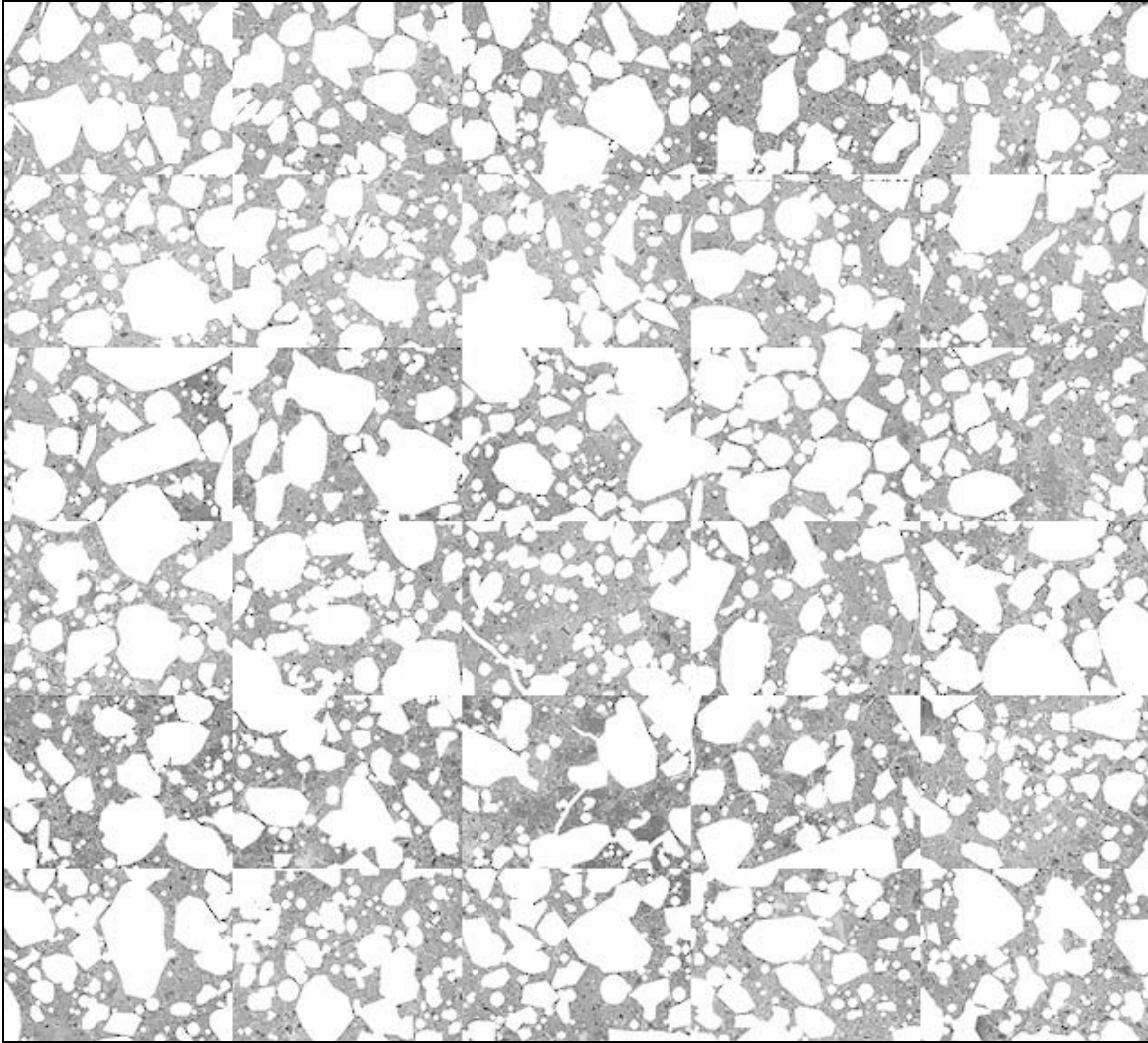


Figure 3.33. A 5 x 6 mosaic of 30 epifluorescent mode images from thin sections prepared from core SD\_01 after masking out sand and air voids, magnified 17x.

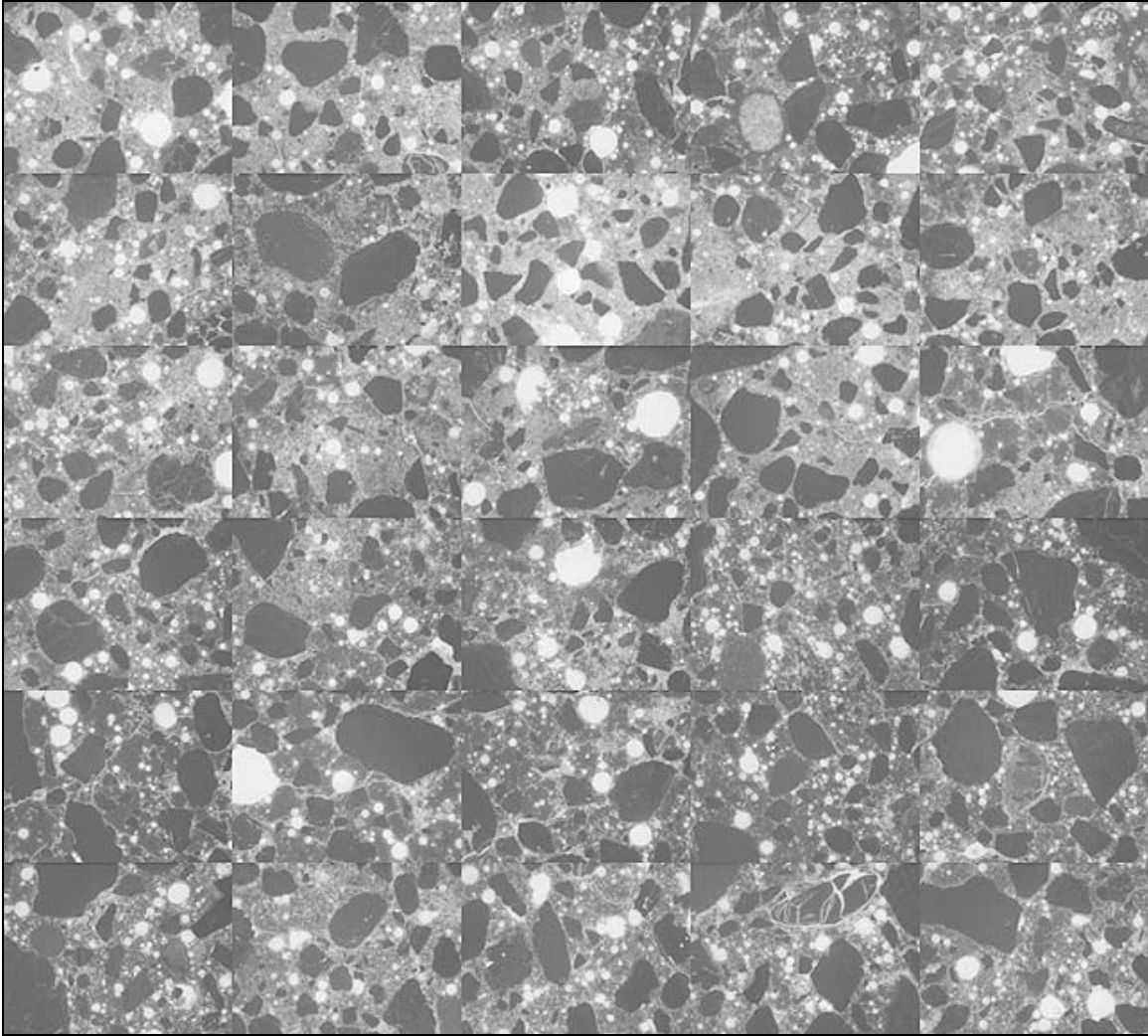


Figure 3.34. A 5 x 6 mosaic of 30 epifluorescent mode images from thin sections prepared from core SD\_04, magnified 17x.



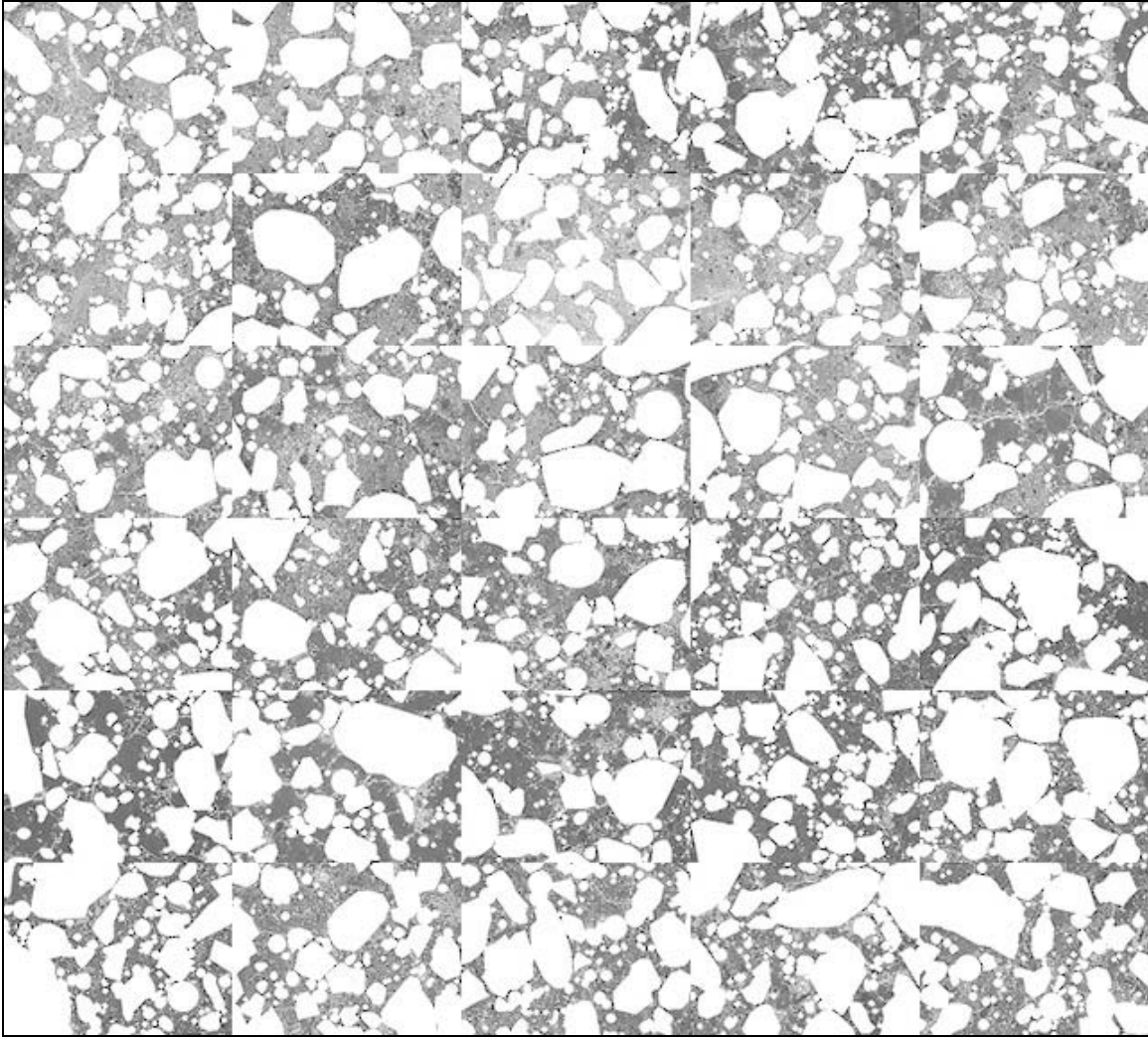


Figure 3.35. A 5 x 6 mosaic of 30 epifluorescent mode images from thin sections prepared from core SD\_01 after masking out sand and air voids, magnified 17x.

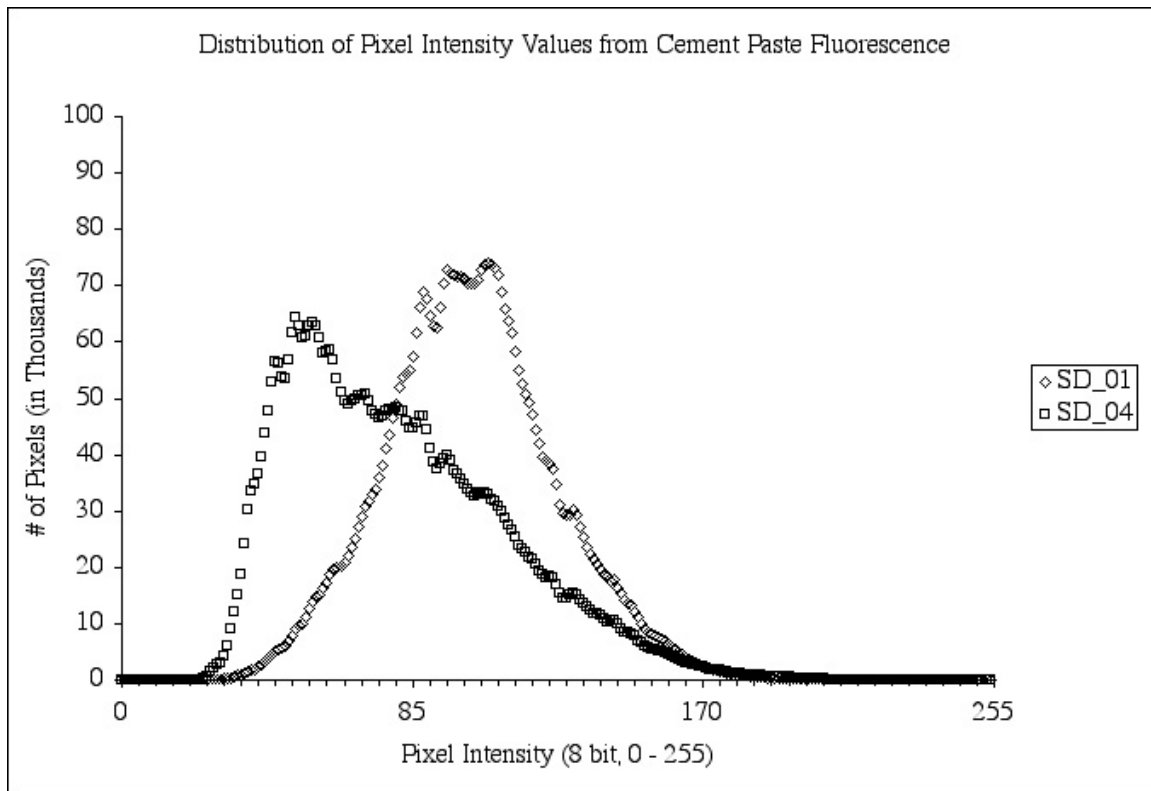


Figure 3.36. Cement paste fluorescence intensity histograms for images collected from cores at joint, (SD\_01) and away from the joint (SD\_04).

### 3.2 Laboratory Experiment - Phase I

#### 3.2.1 Mix Design

In Phase I, three different mortar mixtures were tested under various temperature regimes to examine how deicing chemicals interact with hardened portland cement paste. Also, the results of these tests were used to help identify deicers that may be non-reactive, and bracket material parameters for Phase II where concrete will be tested.

Table 3.6. Testing details associated with the laboratory evaluation.

Test Attribute	Test Code	Test Name & Equipment	Measured Property	Specification
Properties of Fresh Mortar	F	Flow	Mortar workability	ASTM C230
		Unit Weight	Mortar density	ASTM C138
		Air Content	Total air content of fresh mortar	ASTM C185
Material Characterization	C	Split Tensile Strength	Mortar strength	ASTM C496
	P	Stereo Optical Microscopy	Air-void system parameters	ASTM C 457 and C 856
		Petrographic Optical Microscopy with UV dye impregnation	Microstructure analysis, reaction products, and evidence of deterioration	ASTM C 856
		Scanning Electron Microscopy (SEM/EDS)	Microstructure analysis, elemental analysis	ASTM C 856
		X-Ray Microscopy	Bulk elemental analysis	No Standard Test
	R	Rapid Chloride Permeability	Rapid indication of resistance to chlorides	ASTM 1202

Three different mortar mixtures were prepared using Ottawa sand, Type I cement, and water. The mix designs and procedures are presented in Appendix C. The *w/c* was the independent variable with increments of 0.40, 0.50, and 0.60. The paste content was held constant for all mix designs. Appendix D provides a petrographic evaluation of the specimens prepared. Fresh mortar testing was performed on the mixes and the tests performed are listed in Table 3.6. Approximately twenty five hundred 2-in diameter by 4-in high mortar cylinders were made, in addition to twelve 4-in diameter by 8-in high cylinders. The cylinders were cured in lime baths for 28 days, and then placed in a temperature control room at 40 °F until deicer exposure testing began.

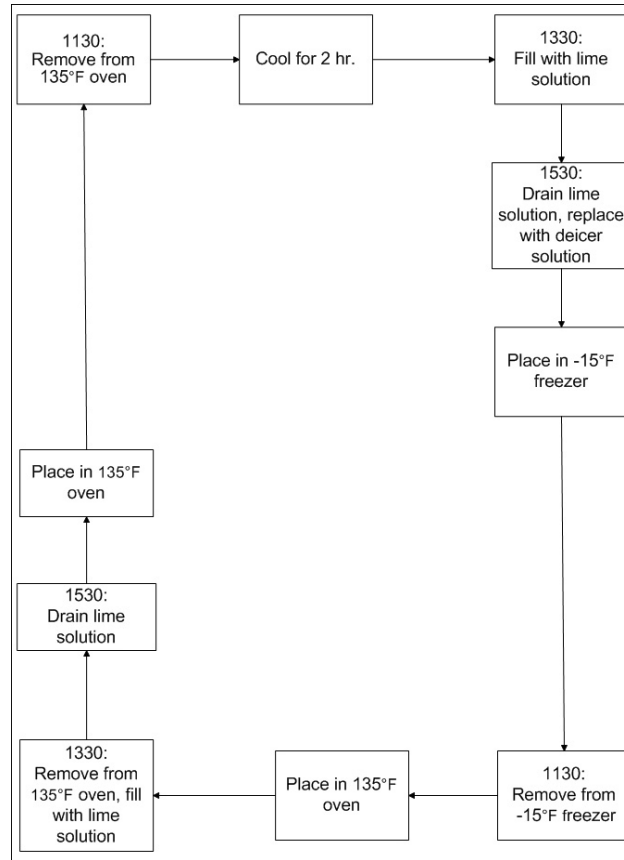


Figure 3.37. Cyclic temperature test procedure for one cycle for cylinders exposed to deicer solutions and a control solution.

### 3.2.2 Testing Regimes

In this experiment, three distinct temperature regimes were used to test the samples. In the first temperature regime, the specimens were cycled between being submerged in salt solution or a control solution at  $-15^{\circ}\text{F}$  for 20 hours, to being in air at  $135^{\circ}\text{F}$  for 20 hours. Figure 3.37 outlines the steps in the cyclic temperature test procedure. In the other two cases, the specimens were submerged in the various deicer solutions and a control solution for a given amount of time (e.g. 0, 7, 14, 28, 56, 84, or 112 days) at a constant, specified temperature ( $40^{\circ}\text{F}$  or  $135^{\circ}\text{F}$ ). Prior to testing, all the cylinders were conditioned by soaking in lime water for 72 hours at  $68\text{-}70^{\circ}\text{F}$ .

### 3.2.3 Deicer Solution Strength

The deicer solution strengths chosen for this study were determined after discussions with the Project Manager at SDDOT. The solution strengths were chosen by first selecting  $15\% \text{MgCl}_2$  as the basis for comparison. This concentration was chosen to represent the dilution that occurs when salt solutions are applied to a road surface. Then, to assess the effects of each deicer on hydrated portland cement paste on an equitable basis, the solutions were normalized on the basis of molal concentration of chloride ion. A solution of  $15\% \text{MgCl}_2$  and water has a molal concentration of  $1.85 \text{ m Mg}^{2+}$  and  $3.7 \text{ m Cl}^-$ . Similarly, a solution of  $17\% \text{CaCl}_2$  and water has a molal concentration of  $1.85 \text{ m Ca}^{2+}$  and  $3.7 \text{ m Cl}^-$ . A solution of  $17.8\% \text{NaCl}$  has a molal concentration of  $3.7 \text{ m Na}^+$  and  $3.7$

m Cl<sup>-</sup>. The CMA solution strength was used at the normal application concentration of 25% CMA by weight, which is a molal concentration of 1.89 m acetate. Molality offers the advantage of equal numbers of moles of each deicer cation per volume solution, which makes determination of diffusion coefficients more straightforward and gives a basis for comparison of deicer chemicals in terms of the chemical interaction only.

The concentrations chosen are all less than the eutectic composition for each solution theoretically resulting in no solid salt in the solution, except for the NaCl solution. The MgCl<sub>2</sub>, CaCl<sub>2</sub> and CMA solutions formed a “slush” that was ice and salt solution. In the case of the NaCl solution, below -5.8 °F only ice and solid NaCl•2H<sub>2</sub>O (hydrohalite) are present. The partial phase diagrams for the deicer solutions are shown in Figure 3.38. A more complete phase diagram for the NaCl - water system is shown in Figure 3.39. Table 3.7 shows the theoretical liquid concentration in the slush mixtures and the abundance of each solid phase in the case of the solid NaCl and water solution. Additionally, the solubility limits for each solution are given. In addition to the four basic deicing solutions, in all testing regimes, specimens were tested in lime water solutions as a control.

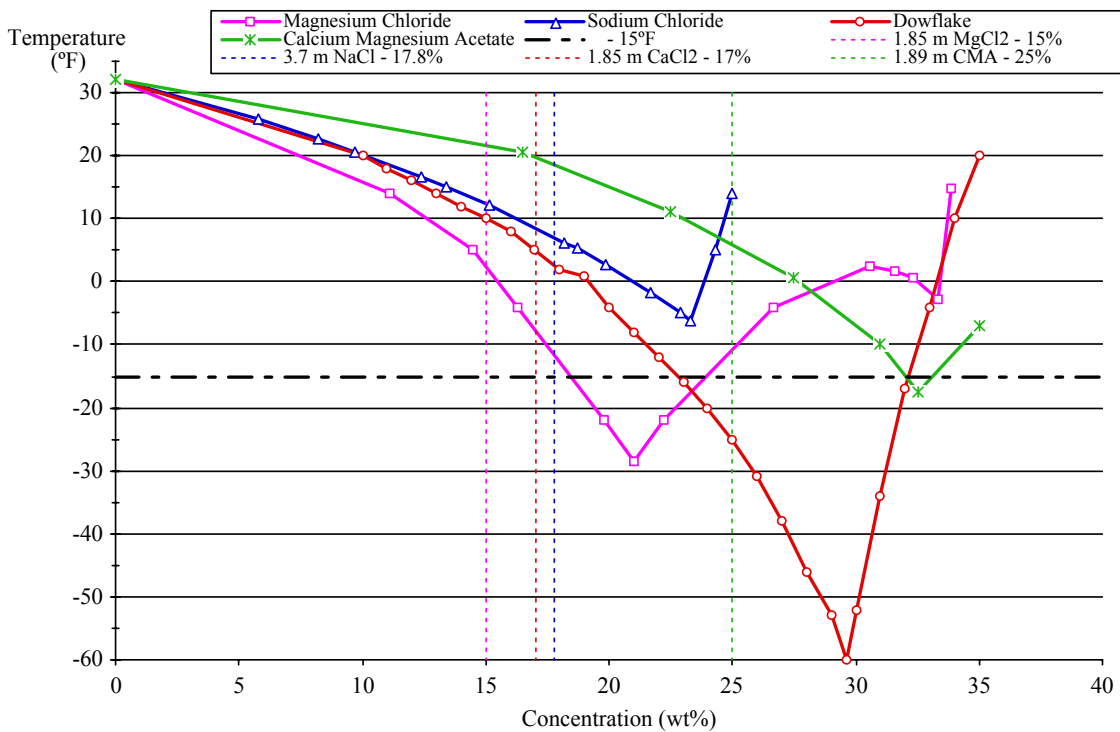


Figure 3.38 The partial phase diagrams for the deicer solutions tested showing the eutectic points for each solution. Concentrations used are shown with vertical dotted lines. The temperature -15 °F is shown as a dotted horizontal line.

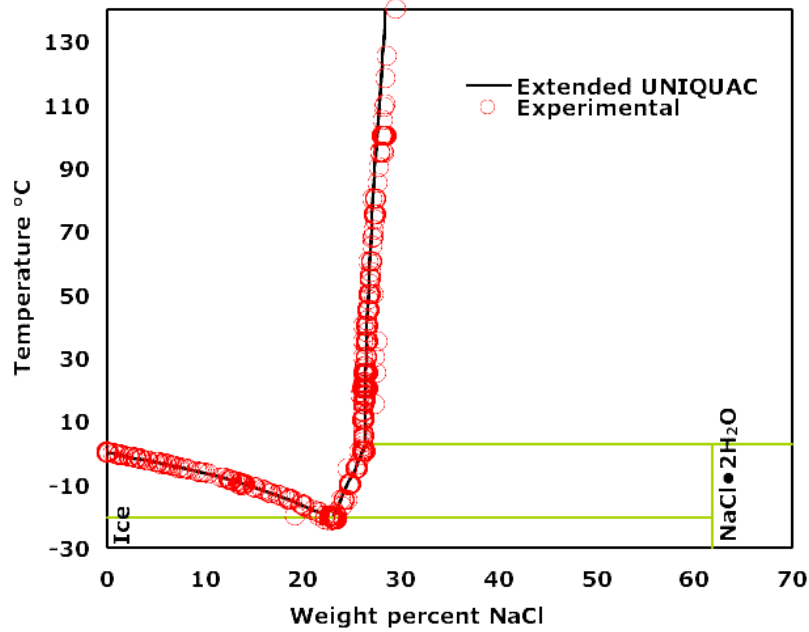


Figure 3.39. A more complete phase diagram for the NaCl - water system (Source: <http://www.phasediagram.dk/binary/>)

Table 3.7 Theoretical volume percent of phases formed in the various deicer solutions used and the composition of the non-ice phase formed. Also, saturation concentrations at two temperatures.

Deicer	Second Phase Abundance in Volume Percent (%)			Second Phase Composition	Saturation Concentration at -15°F	Saturation Concentration at 32°F
	% Ice	% Solid Salt	% Salt Solution	Weight Percent Salt (%)	Weight Percent Salt (%)	Weight Percent Salt (%)
MgCl <sub>2</sub>	18.7%	0	81.3%	18.4% MgCl <sub>2</sub>	24% MgCl <sub>2</sub>	34.6% MgCl <sub>2</sub>
CaCl <sub>2</sub>	29.1%	0	70.9%	24.0% CaCl <sub>2</sub>	34% CaCl <sub>2</sub>	37.3% CaCl <sub>2</sub>
CMA	21.9%	0	78.1%	32.0% CMA	33% CMA	No Data
NaCl	82.2%	17.8%	0	26.4% NaCl·2H <sub>2</sub> O	-	26.3% NaCl

### 3.2.4 Rapid Chloride Ion Penetration Test

The Standard Test Method for Electrical Indication of Concrete's Ability to Resist Chloride Ion Penetration ASTM 1202-97 (AASHTO T 277-93) was performed on 4-in diameter by 2-in high cylinders cut from the 4-in by 8-in cylinder. A literature survey was conducted to investigate the applicability of the RCPT to mortar specimens. It was

found that there is no ASTM or AASHTO standard specifically applicable to the chloride ion penetration test for mortars. According to the reviewed literature, an increase in temperature will increase the conductivity of concrete/mortar and this can lead to erroneous RCPT results. This can be overcome by lowering the voltage (12 volts against ASTM specification of 60 V) while running RCPT on mortars, as suggested by Halamickova (1995).

Three mortar samples representing each of the three different water-cement ratios (0.40, 0.50 and 0.60) were tested at 12 volts. Table 3.8 gives the summarized results. Note that for one 0.40 w/c specimen, an error occurred and the result was eliminated. Therefore, only two results are presented for the 0.40 specimens. As can be seen, there is a clear relationship between the w/c value and the measured chloride permeability.

Table 3.8. RCPT results for different w/c ratio mortars

w/c	Sample ID	Charge at end of 6 hrs, Coulombs	Average charge (for a given w/c ratio)
0.40	4079	842.4	831.6
	4080	820.8	
0.50	5056	1425.6	1490.4
	5056	1598.4	
	5056	1447.2	
0.60	6055	2008.8	1958.4
	6055	1900.8	
	6055	1965.6	

### 3.2.5 Analysis of Specimens Exposed to Deicer Solutions

Random cylinders were removed from the various solutions at the prescribed time intervals and allowed to air dry. These samples were then cataloged and stored in air until testing began. Specimens that best represented the range of conditions were chosen for petrographic analysis from each time interval. The condition of the specimens were such that ASTM C496, the "Standard Test Method for Splitting Tensile Strength of Cylindrical Concrete Specimens" was not able to be performed on specimens from all deicers and time intervals. However, some specimens were selected and tested by ASTM C 496 to assess loss in strength from exposure to the various solutions and temperature regimes. A summary of tests performed is provided in Table 3.6. For each temperature regime test, the results are presented in the following sections.

### 3.2.6 Cyclical Temperature Experiment

#### 3.2.6.1 Observations

The cyclic temperature experiment was initially designed to monitor changes in compressive strength after 14, 28, 56, 84, and 112 days of cyclic treatment. However, it was noticed that after 8 days of cyclic testing, the cylinders immersed in rock salt NaCl deicer solution were beginning to deteriorate. After 28 days, the cylinders had

completely disintegrated. The experiment was repeated a second time, replacing the rock salt NaCl with food grade NaCl to ensure sulfate impurities were not to blame. The results were the same. Figure 3.40 shows three of the cylinders exposed to rock salt NaCl solution after 8 days, and Figure 3.41 shows three of the cylinders exposed to food grade NaCl solution after 8 days. Figures 3.42 and 3.43 show the cylinders in the drained test bins for both the rock salt NaCl and food grade NaCl solutions after 28 days. After 28 days, the NaCl deicer experiments were aborted.

At 28 days the cylinders in the  $MgCl_2$  and  $CaCl_2$  solutions began to show some signs of cracking and expansion. By 56 days, the cylinders in the  $MgCl_2$  and  $CaCl_2$  solutions exhibited advanced deterioration. Figure 3.44 shows three of the cylinders exposed to  $MgCl_2$  solution after 56 days. Figure 3.45 shows three of the cylinders exposed to  $CaCl_2$  solution after 56 days. By 84 days the cylinders exposed to  $MgCl_2$  and  $CaCl_2$  solutions were severely deteriorated, as shown in Figures 3.46 and 3.47. It was decided that instead of running the testing out to the original 112 days, to end the test for all the cylinders at 84 days. The control cylinders exposed to lime water were in good condition at 84 days, as shown in Figure 3.48. The cylinders exposed to the CMA solution were cycled to 84 days. Figure 3.49 shows the cylinders exposed to CMA at 84 days, with limited cracking and crumbling evident near the bases of the 0.60 w/c cylinders. Table 3.9 summarizes the visual ratings for all cylinders exposed to the cyclic temperature experiment over time for both the control (lime water) and deicer solutions.



Figure 3.40. Cylinders exposed to rock salt NaCl solution after 8 days of cyclic temperature test. From left to right: 0.40, 0.50, and 0.60 w/c mortar cylinders.





Figure 3.41. Cylinders exposed to food grade NaCl solution after 8 days of cyclic temperature test. From left to right: 0.40, 0.50, and 0.60 w/c mortar cylinders.



Figure 3.42 Cylinders exposed to rock salt NaCl solution in drained tray after 28 days of cyclic temperature test.



Figure 3.43 Cylinders exposed to food grade NaCl solution in drained tray after 28 days of cyclic temperature test.



Figure 3.44 Cylinders exposed to  $MgCl_2$  solution after 56 days of cyclic temperature test. From left to right: 0.40, 0.50, and 0.60 w/c mortar cylinders



Figure 3.45 Cylinders exposed to  $\text{CaCl}_2$  solution after 56 days of cyclic temperature test. From left to right: 0.40, 0.50, and 0.60 w/c mortar cylinders.

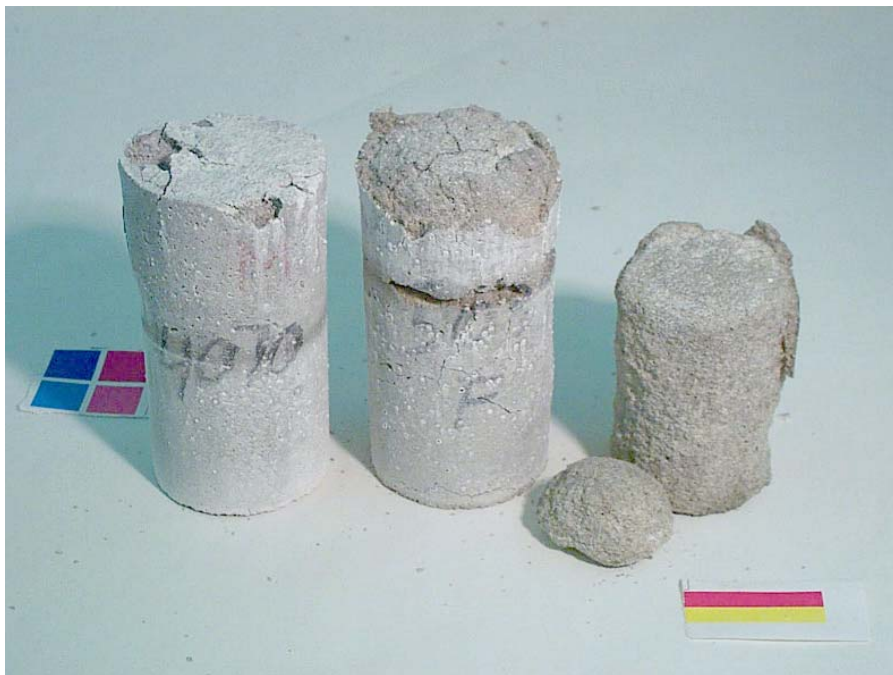


Figure 3.46. Cylinders exposed to  $\text{MgCl}_2$  solution after 84 days of cyclic temperature test. From left to right: 0.40, 0.50, and 0.60 w/c mortar cylinders.



Figure 3.47. Cylinders exposed to  $\text{CaCl}_2$  solution after 84 days of cyclic temperature test. From left to right: 0.40, 0.50, and 0.60 w/c mortar cylinders.



Figure 3.48. Cylinders exposed to CMA solution after 84 days of cyclic temperature test. From left to right: 0.40, 0.50, and 0.60 w/c mortar cylinders.



Figure 3.49. Control cylinders exposed to lime water solution after 84 days of cyclic temperature test. From left to right 0.40, 0.50, and 0.60 w/c mortar cylinders.

Table 3.9. List of visual ratings for all mortar cylinders from the cyclic temperature tests. Rating Scale: 0 - no visible change, 1 – some cracking, 2 - visible expansion and cracking, 3 - severe expansion and cracking, 4 - partial disintegration, 5 - total disintegration, x – test aborted.

Solution	Time in Days											
	w/c = 0.40				w/c = 0.50				w/c = 0.60			
	8	28	56	84	8	28	56	84	8	28	56	84
Lime Water	0	0	0	0	0	0	0	0	0	0	0	0
MgCl <sub>2</sub>	0	0	0-2	1-3	0	0-1	1-2	2-4	0	0-1	2-4	4-5
CaCl <sub>2</sub>	0	0	0-2	2-3	0	0-1	1-3	3-4	0	2-3	3-4	4-5
NaCl	2-3	3-5	x	x	2-4	3-5	x	x	2-4	4-5	x	x
CMA	0	0	0	0	0	0	0	0	0	0	0	1

### 3.2.6.2 Split Tensile Strength Testing

Due to the large amounts of damage sustained during the cyclical testing, it seemed likely that the samples tested for strength would be self-selecting (i.e. the outer surfaces of more susceptible specimens scale off quickly, making them unusable for the split-tensile testing). The less susceptible specimens—with a greater immunity to whatever is causing the destruction—were the only ones able to be tested. Therefore, with the possible exception of the 0.40 *w/c* ratio specimens, this test would not be very useful in drawing conclusions about the damage done to the mortar cylinders as a result of exposure to the different deicers.

### 3.2.6.3 Petrographic Analysis

One of the 0.50 water to cement ratio (*w/c*) cylinders exposed to rock salt NaCl solution, and one of the control 0.50 *w/c* cylinders, were examined in thin section after 8 days of cyclic temperature testing. The cylinders were impregnated with fluorescent dyed epoxy, cut into billets, re-impregnated with fluorescent dyed epoxy, and prepared in polished thin section using anhydrous methods. The thin sections were carbon coated, and examined with a scanning electron microscope equipped with an x-ray energy detector, as well as with a petrographic microscope. The thin sections represent a cross-section through the cylinder in an orientation parallel to the finished surface, at a depth of approximately 2 cm from the finished surface. Figures 3.50 through 3.63 show side by side images comparing the control and deicer-exposed cylinders. The control cylinder exposed only to lime water shows no signs of deterioration, while the cylinder exposed to the rock salt NaCl solution shows severe cracking. The cracks appear empty, with occasional secondary calcium hydroxide crystals.

As the cyclical experiment progressed, and deterioration of the cylinders exposed to CaCl<sub>2</sub> and MgCl<sub>2</sub> solutions became evident, more thin sections were prepared to represent the cylinders after the thaw, (after-thaw), after the lime-soak, (after-lime-soak) and after the oven, (after-oven). The cylinders were pulled during the early onset of deterioration. Three of the cylinders were selected from 0.60 *w/c* ratio mortars exposed to food grade NaCl at eight days, and three more of the cylinders were selected from 0.40 *w/c* mortars exposed to food grade NaCl at ten days. The other six cylinders were selected from 0.50 *w/c* mortars exposed to MgCl<sub>2</sub> and CaCl<sub>2</sub> at twenty days. The deterioration of mortars exposed to the MgCl<sub>2</sub> and CaCl<sub>2</sub> solutions in the cyclic experiment looked very similar to the deterioration of mortars exposed to the MgCl<sub>2</sub> and CaCl<sub>2</sub> solutions from the constant cold temperature experiment. Both the cyclic and constant cold temperature samples exhibited abundant cracks filled with calcium oxychloride or remnant calcium oxychloride. However, for the mortars exposed to the NaCl solution, the crack network appeared clean and empty, with occasional calcium hydroxide crystals. Figure 3.64 shows the early onset of cracking at 20 days in one of the MgCl<sub>2</sub> specimens near the finished surface. White arrows show the calcium oxychloride filling cracks at the left hand side of the image. Figure 3.65 shows the early onset of cracking at 8 days in one of the NaCl specimens. Secondary calcium hydroxide crystals appear in one of the air voids, but the cracks appear empty. In both Figures 3.64 and 3.65, the finished surface of the cylinders runs along the right-hand side of the image.

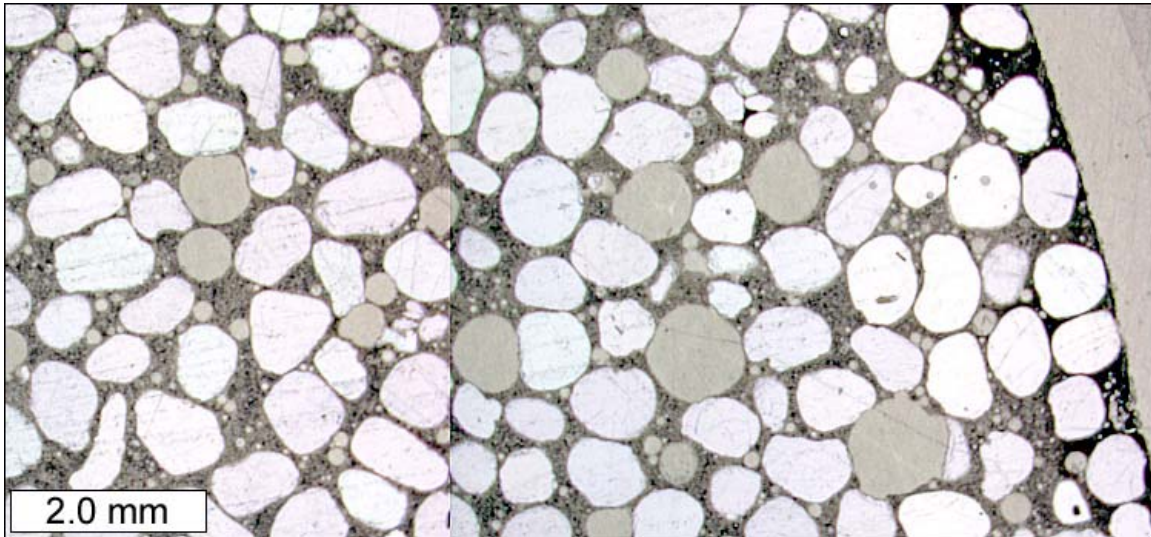


Figure 3.50a: Plane polarized light image from control cylinder.

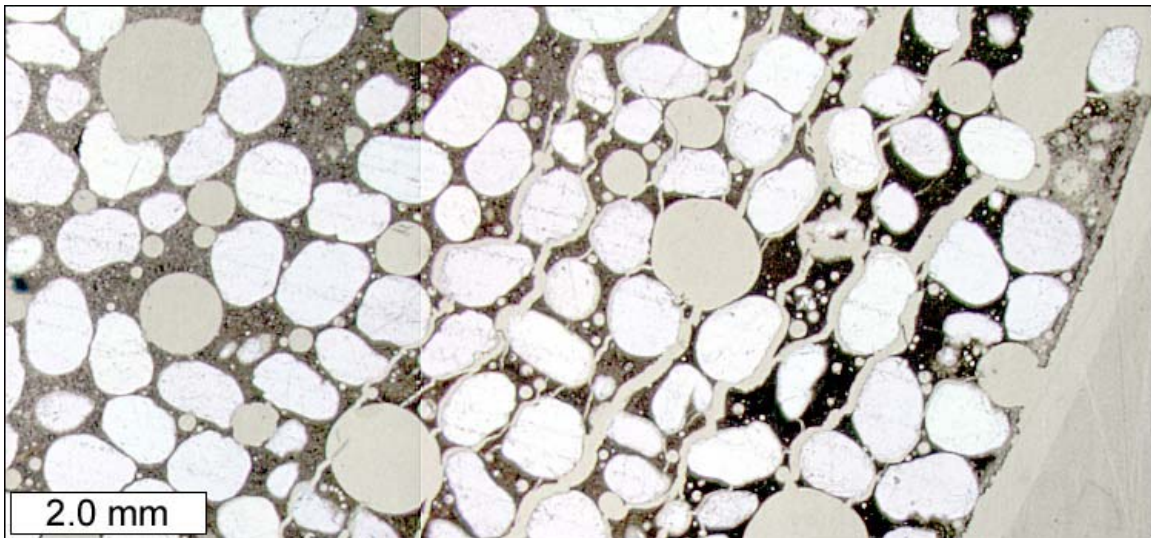


Figure 3.50b: Plane polarized light image from rock salt NaCl deicer-exposed cylinder.

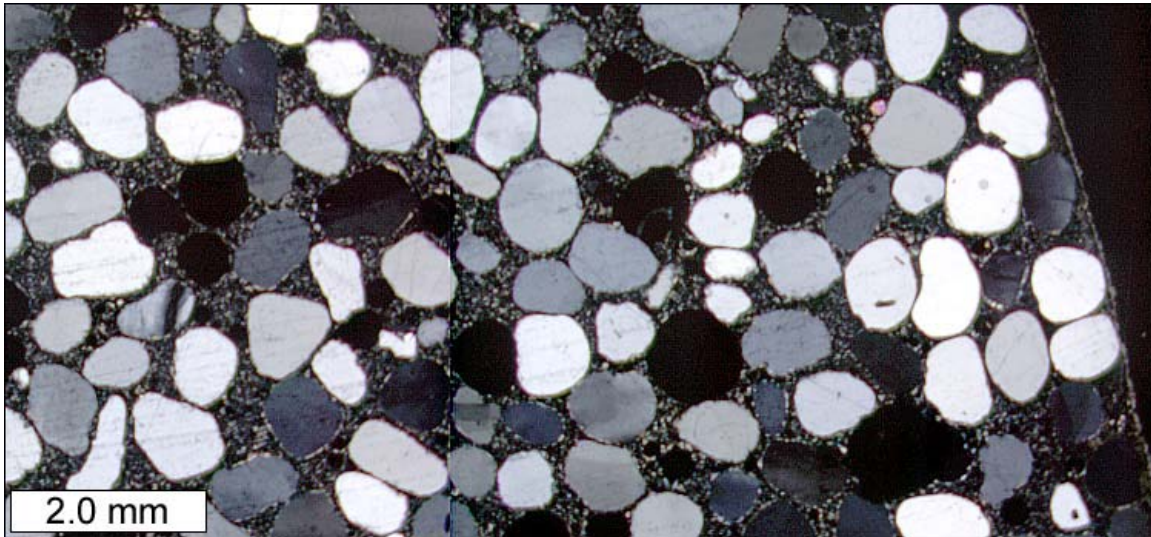


Figure 3.51a: Cross polarized light image from control cylinder.

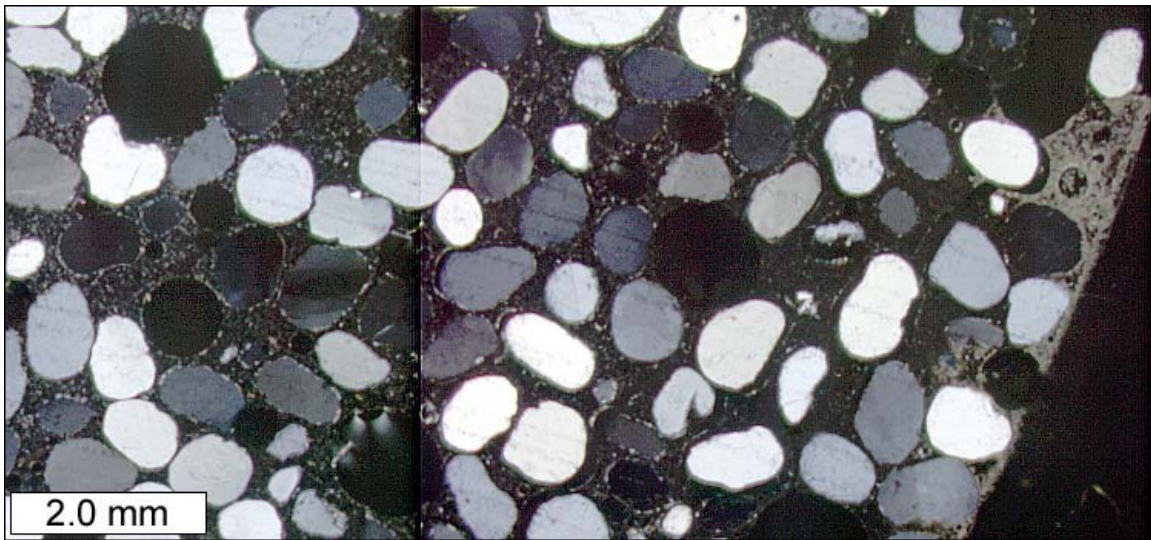


Figure 3.51b: Cross polarized light image from rock salt NaCl deicer-exposed cylinder.



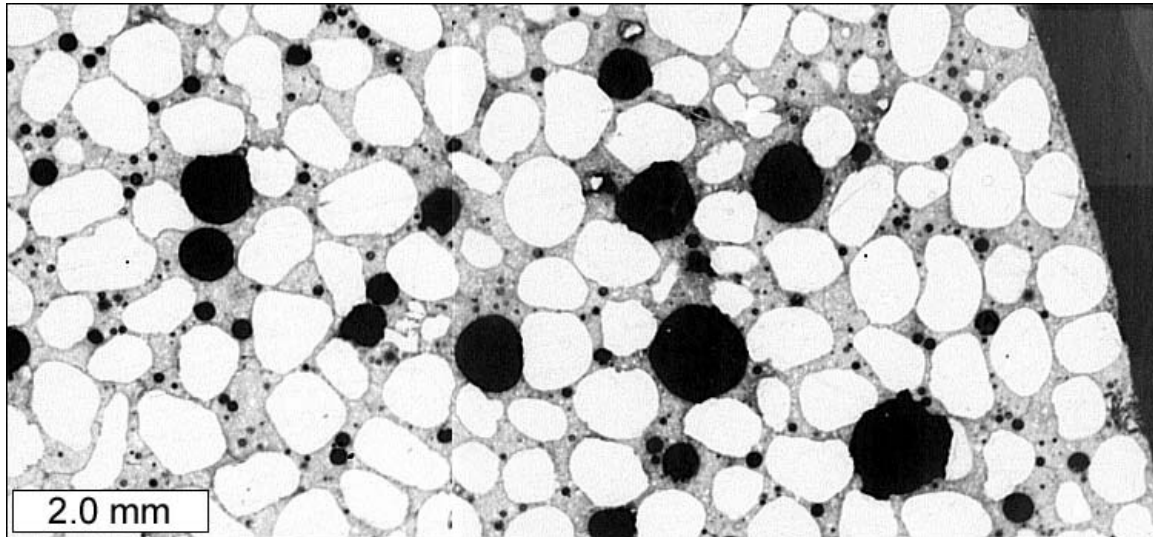


Figure 3.52a: Epifluorescent image from control cylinder.

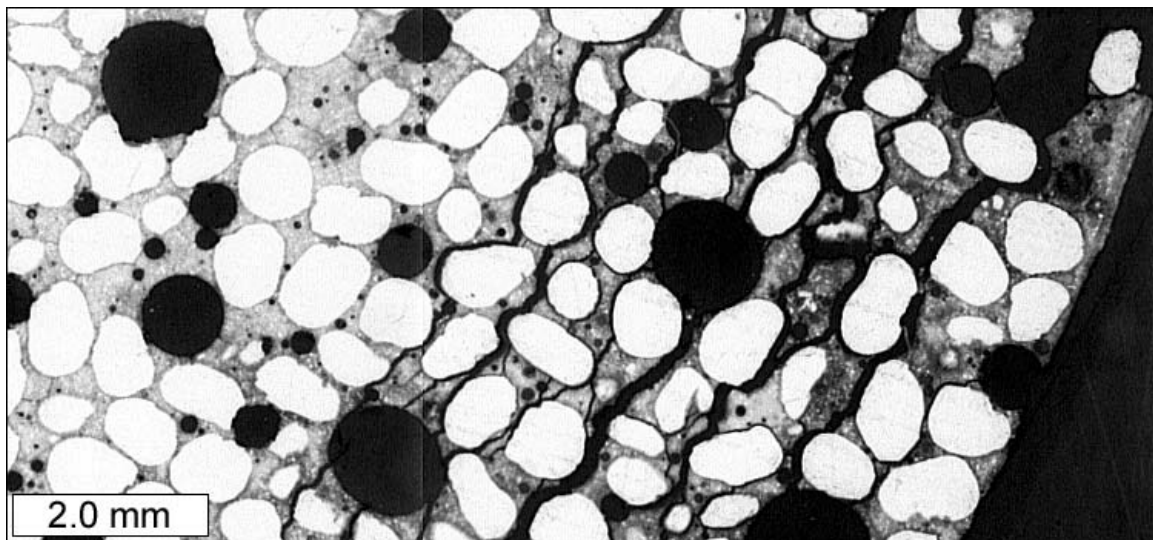


Figure 3.52b: Epifluorescent image from rock salt NaCl deicer-exposed cylinder.

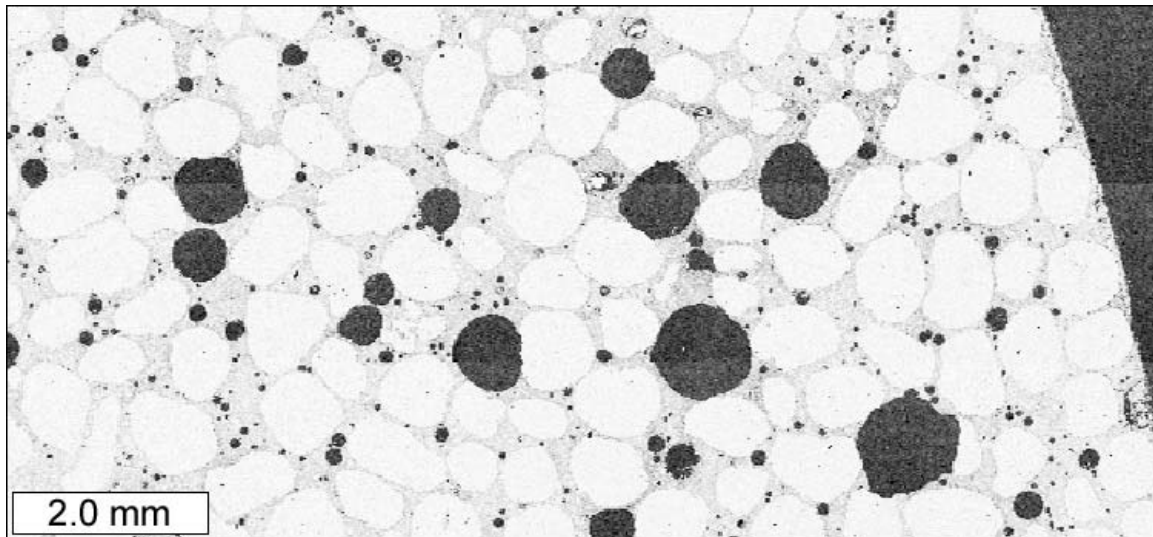


Figure 3.53a: Carbon  $K\alpha$  x-ray map from control cylinder. Darker areas correspond to higher  $K\alpha$  x-ray counts.

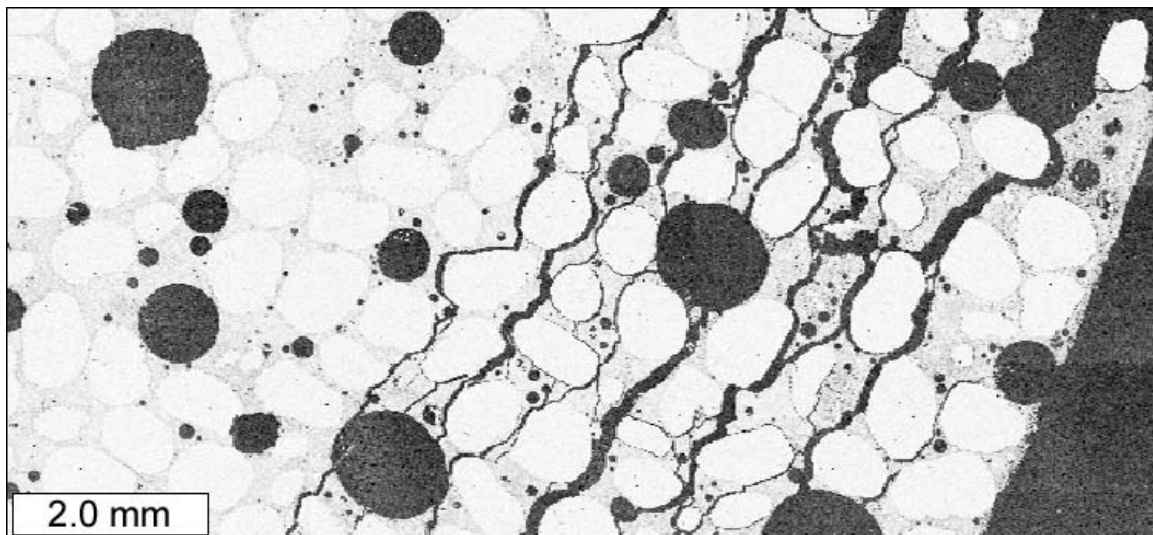


Figure 3.53b: Carbon  $K\alpha$  x-ray map from rock salt NaCl deicer-exposed cylinder. Darker areas correspond to higher  $K\alpha$  x-ray counts.

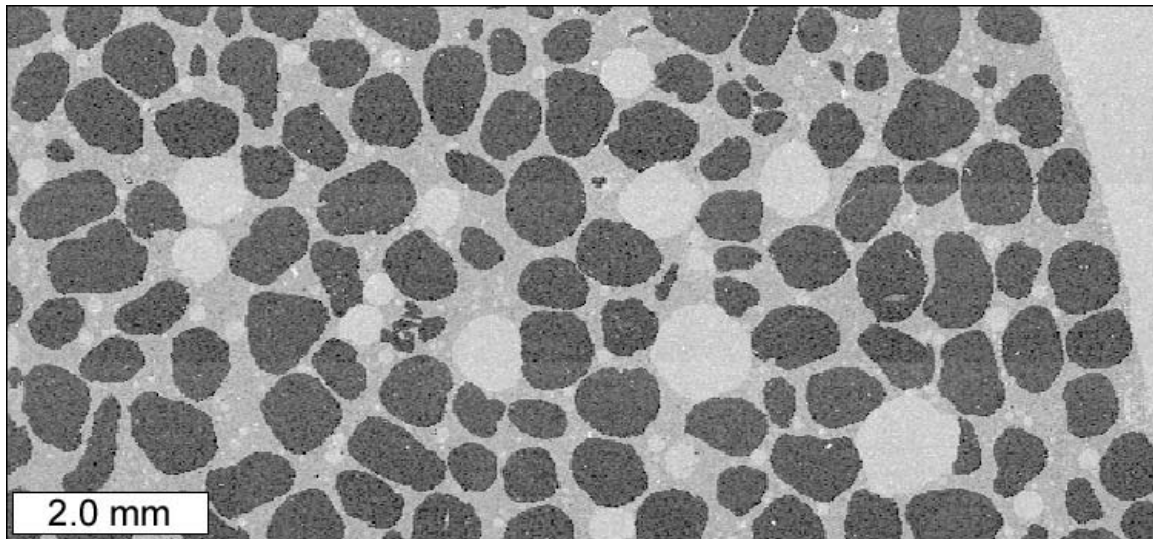


Figure 3.54a: Oxygen  $K\alpha$  x-ray map from control cylinder. Darker areas correspond to higher  $K\alpha$  x-ray counts.

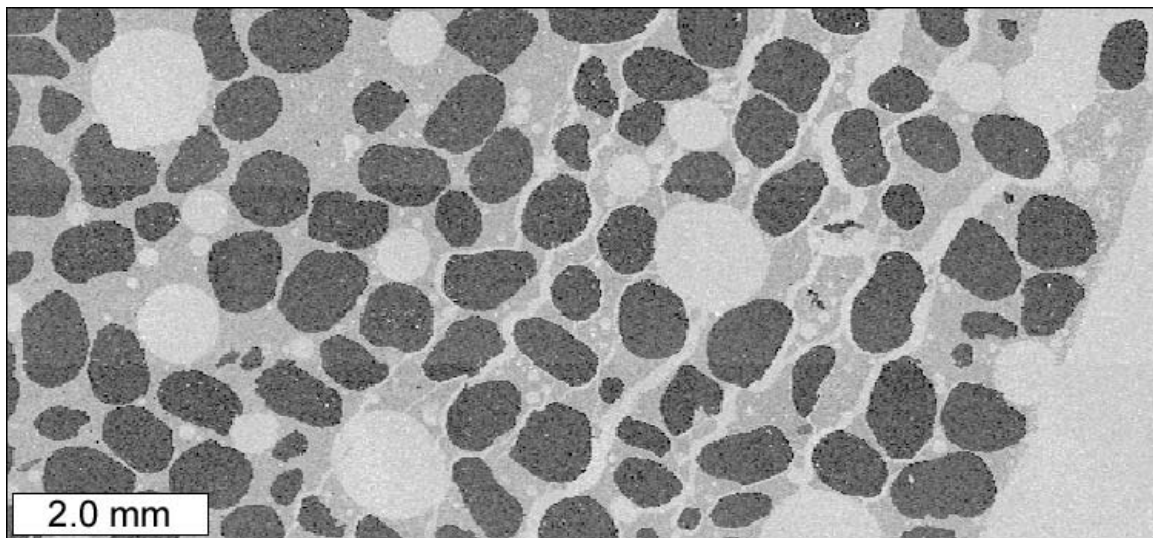


Figure 3.54b: Oxygen  $K\alpha$  x-ray map from rock salt NaCl deicer-exposed cylinder. Darker areas correspond to higher  $K\alpha$  x-ray counts.



Figure 3.55a: Sodium  $K\alpha$  x-ray map from control cylinder. Darker areas correspond to higher  $K\alpha$  x-ray counts.

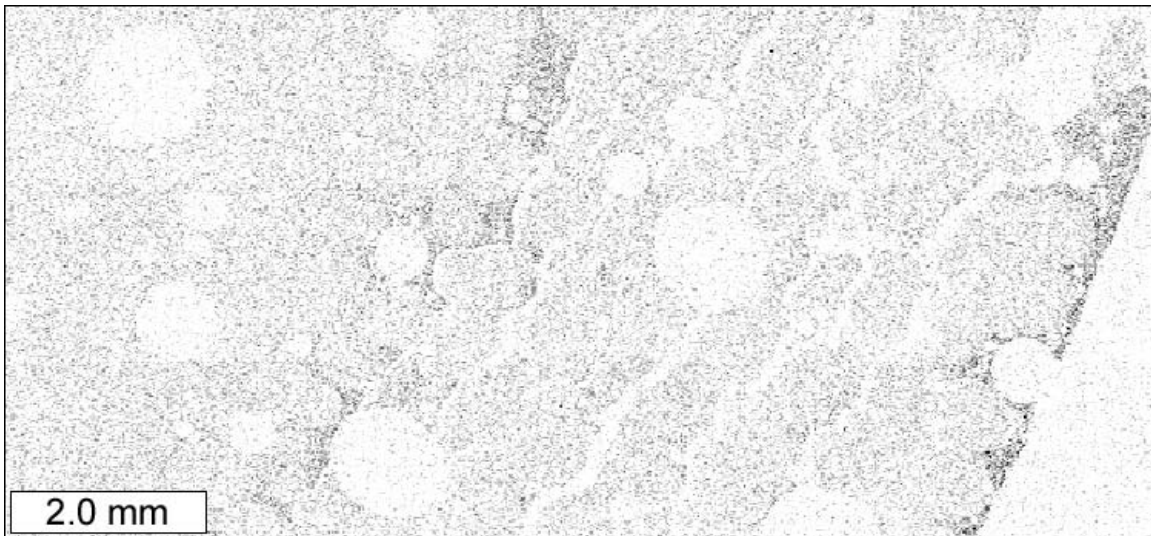


Figure 3.55b: Sodium  $K\alpha$  x-ray map from rock salt NaCl deicer-exposed cylinder. Darker areas correspond to higher  $K\alpha$  x-ray counts.

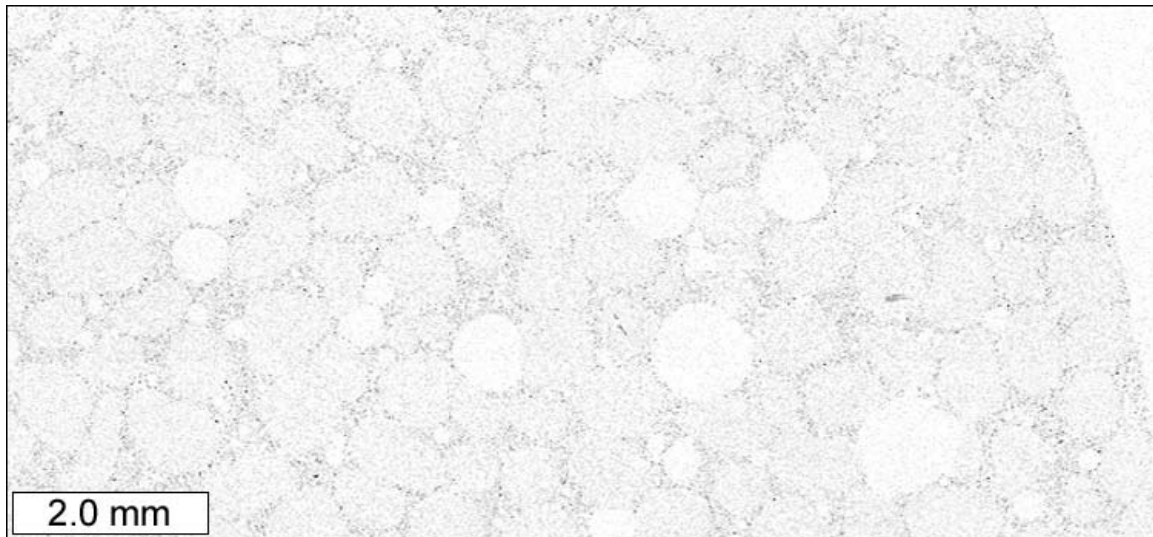


Figure 3.56a: Magnesium  $K\alpha$  x-ray map from control cylinder. Darker areas correspond to higher  $K\alpha$  x-ray counts.

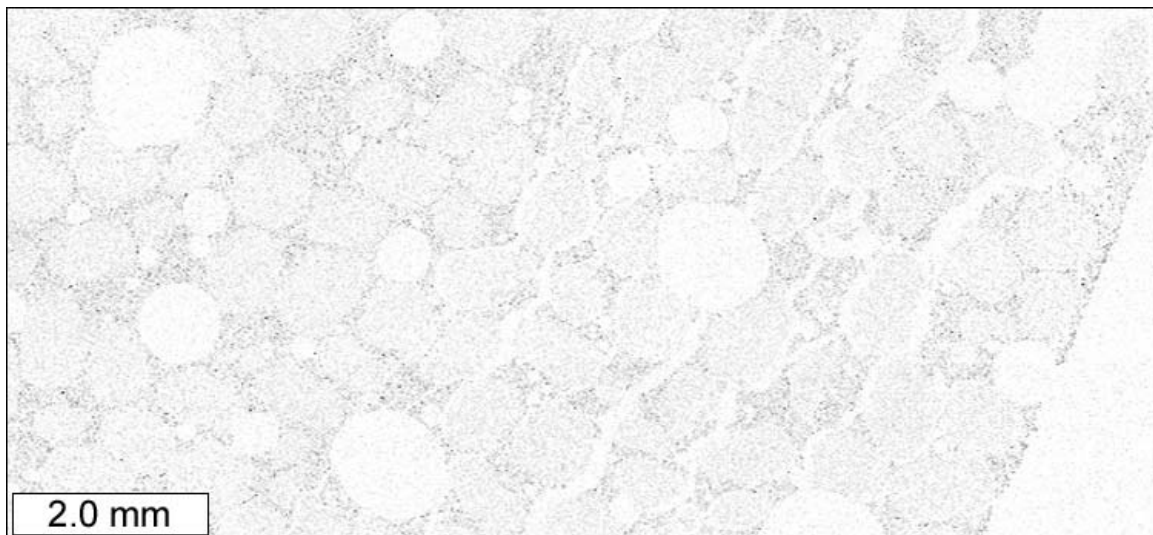


Figure 3.56b: Magnesium  $K\alpha$  x-ray map from rock salt NaCl deicer-exposed cylinder. Darker areas correspond to higher  $K\alpha$  x-ray counts.

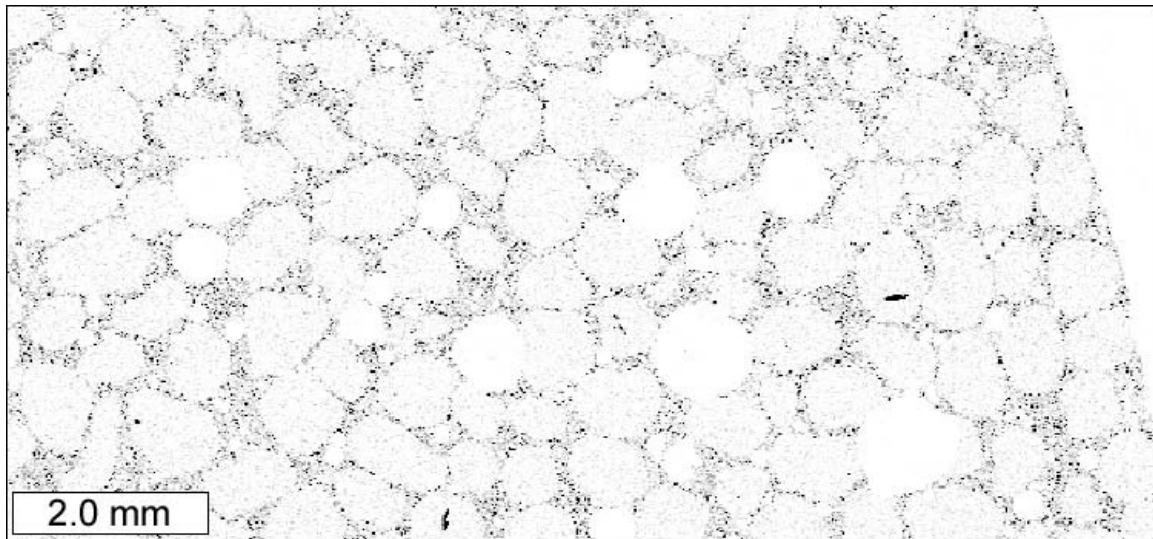


Figure 3.57a: Aluminum  $K\alpha$  x-ray map from control cylinder. Darker areas correspond to higher  $K\alpha$  x-ray counts.

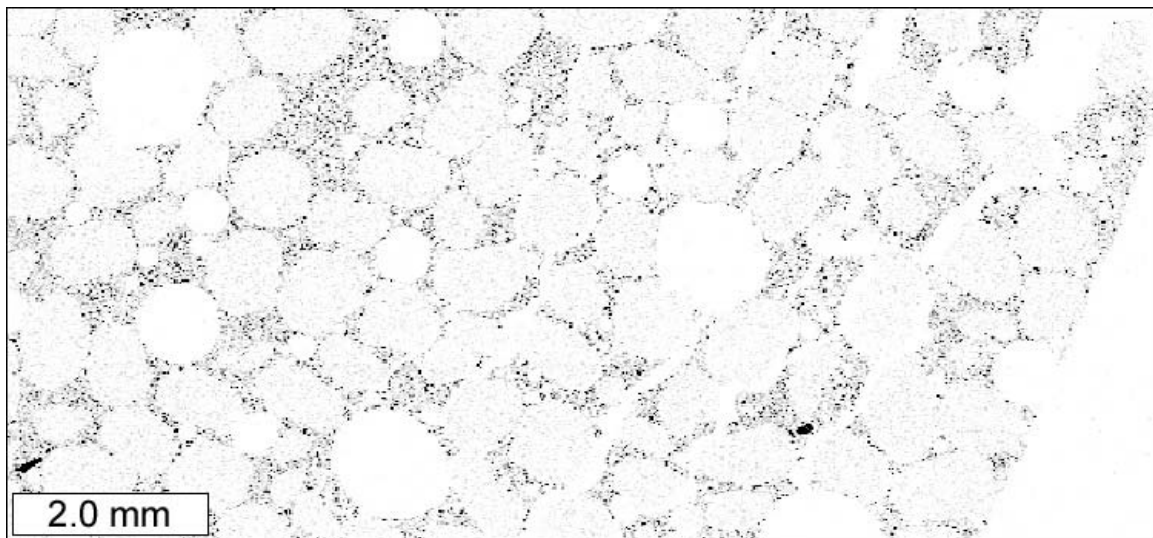


Figure 3.57b: Aluminum  $K\alpha$  x-ray map from rock salt NaCl deicer-exposed cylinder. Darker areas correspond to higher  $K\alpha$  x-ray counts.

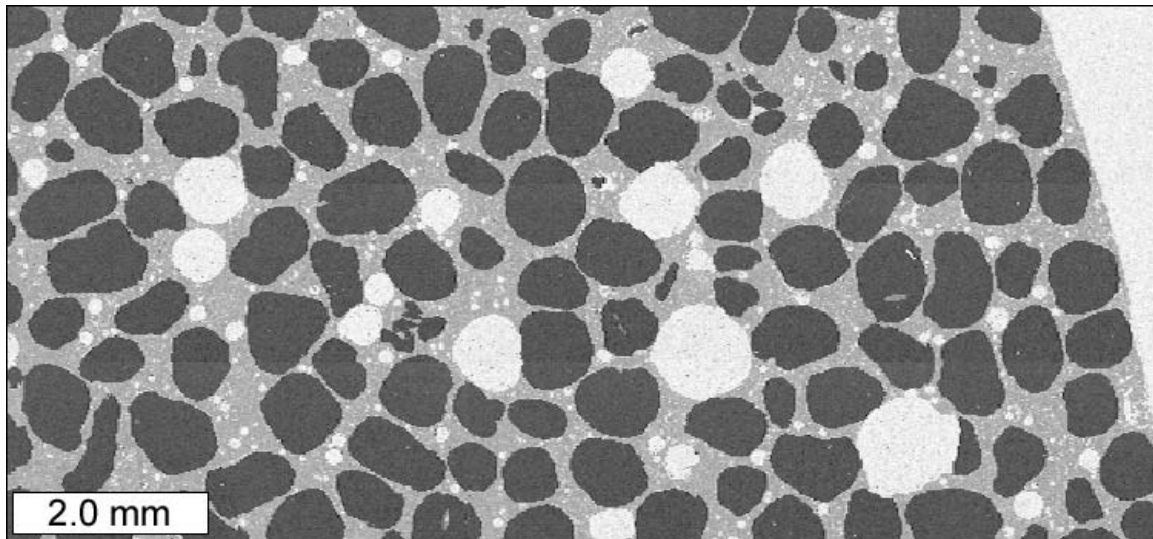


Figure 3.58a: Silicon  $K\alpha$  x-ray map from control cylinder. Darker areas correspond to higher  $K\alpha$  x-ray counts.

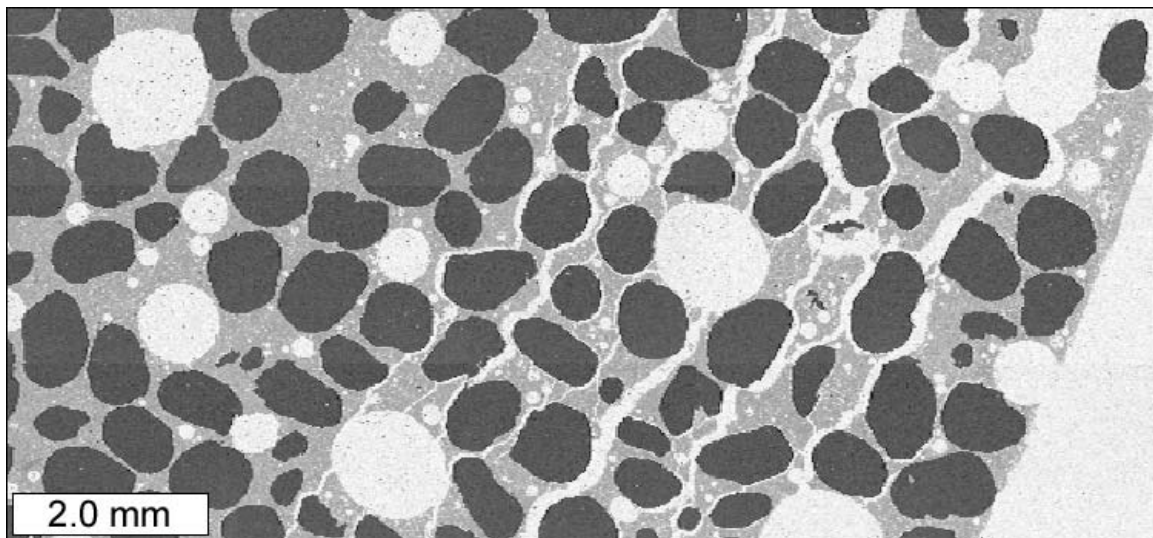


Figure 3.58b: Silicon  $K\alpha$  x-ray map from rock salt NaCl deicer-exposed cylinder. Darker areas correspond to higher  $K\alpha$  x-ray counts.

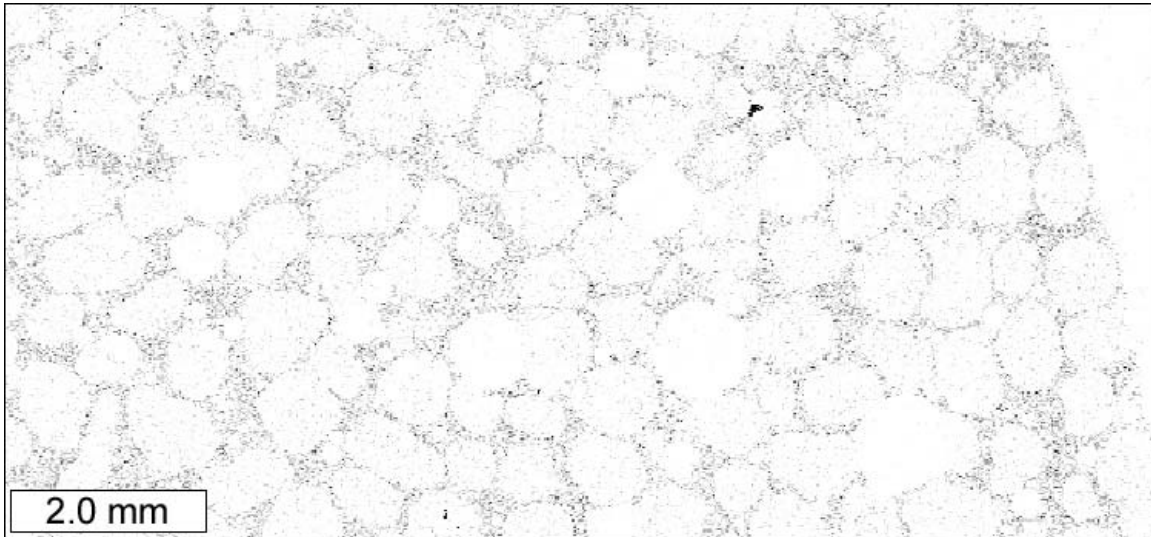


Figure 3.59a: Sulfur  $K\alpha$  x-ray map from control cylinder. Darker areas correspond to higher  $K\alpha$  x-ray counts.

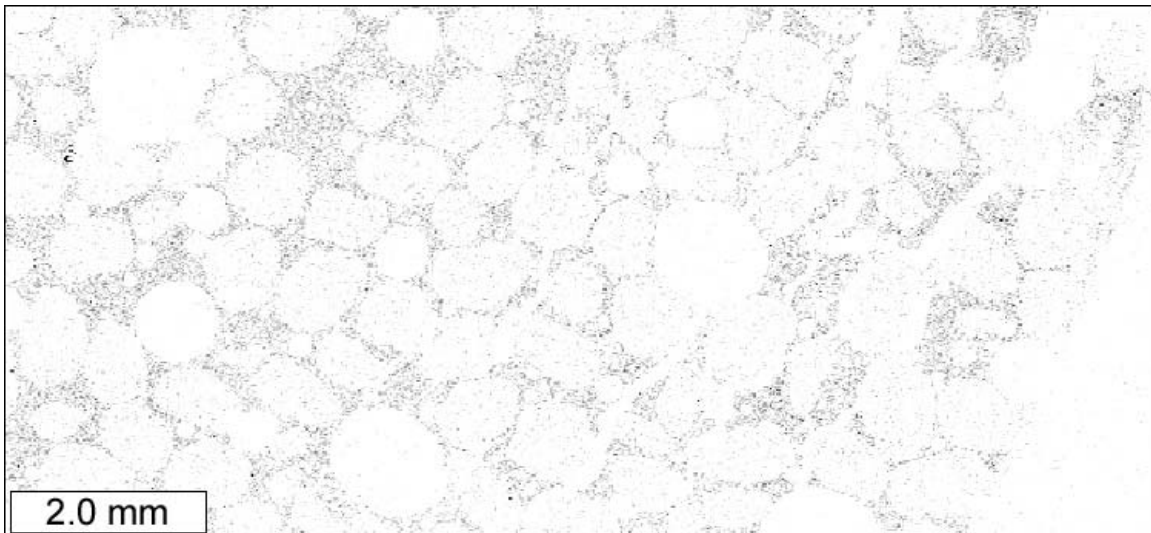


Figure 3.59b: Sulfur  $K\alpha$  x-ray map from rock salt NaCl deicer-exposed cylinder. Darker areas correspond to higher  $K\alpha$  x-ray counts.



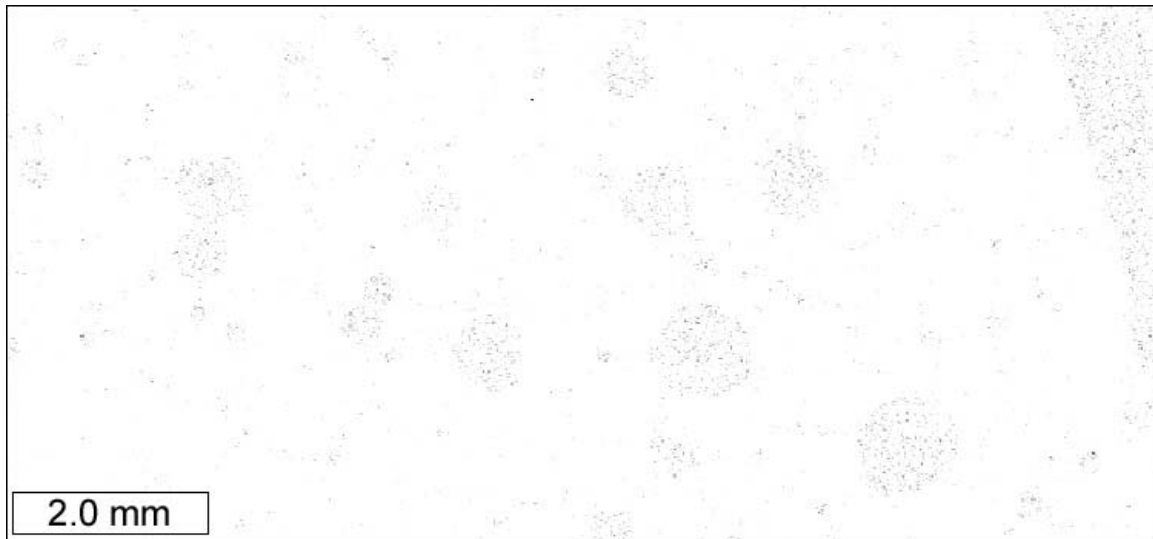


Figure 3.60a: Chlorine  $K\alpha$  x-ray map from control cylinder. Darker areas correspond to higher  $K\alpha$  x-ray counts.

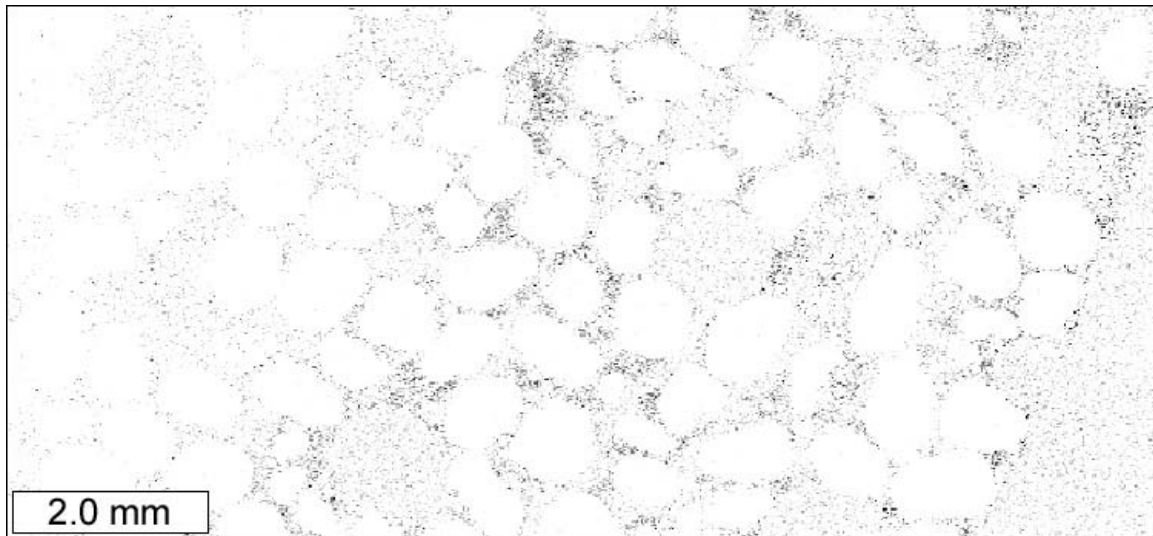


Figure 3.60b: Chlorine  $K\alpha$  x-ray map from rock salt NaCl deicer-exposed cylinder. Darker areas correspond to higher  $K\alpha$  x-ray counts.



Figure 3.61a: Potassium  $K\alpha$  x-ray map from control cylinder. Darker areas correspond to higher  $K\alpha$  x-ray counts.



Figure 3.61b: Potassium  $K\alpha$  x-ray map from rock salt NaCl deicer-exposed cylinder. Darker areas correspond to higher  $K\alpha$  x-ray counts.

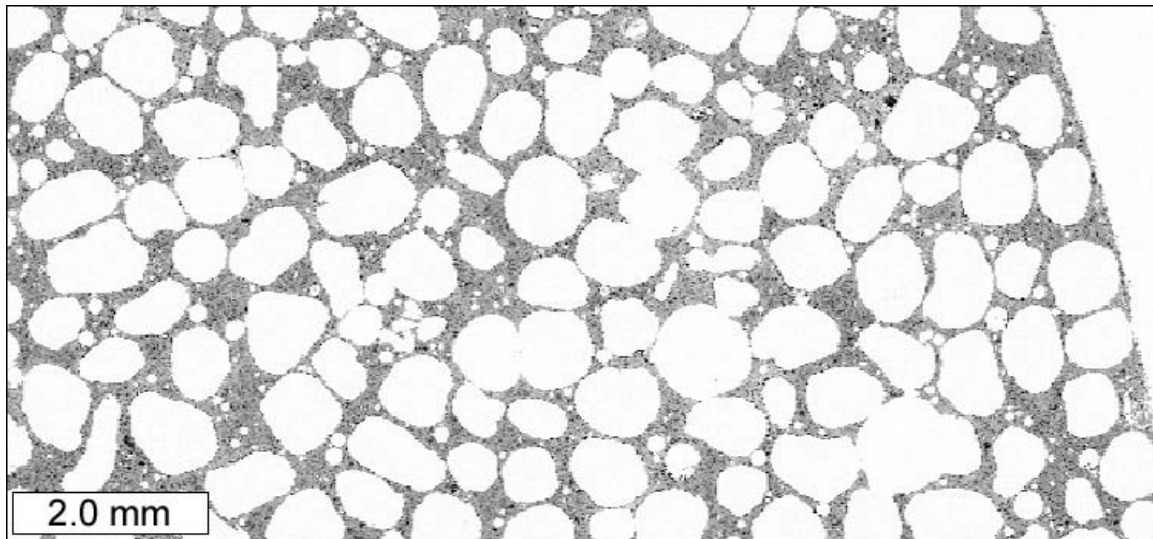


Figure 3.62a: Calcium  $K\alpha$  x-ray map from control cylinder. Darker areas correspond to higher  $K\alpha$  x-ray counts.

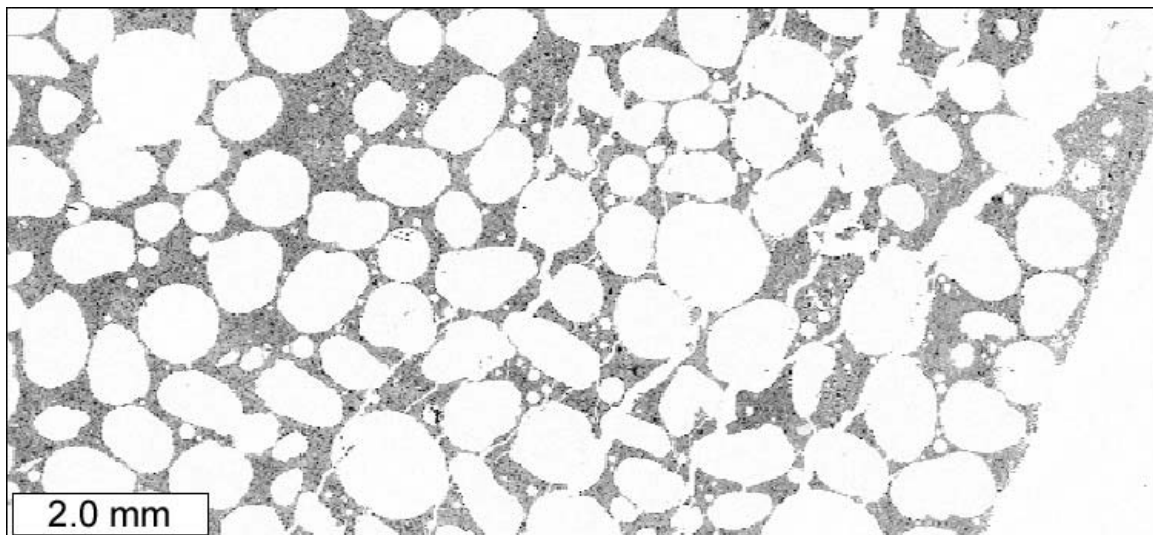


Figure 3.62b: Calcium  $K\alpha$  x-ray map from rock salt NaCl deicer-exposed cylinder. Darker areas correspond to higher  $K\alpha$  x-ray counts.

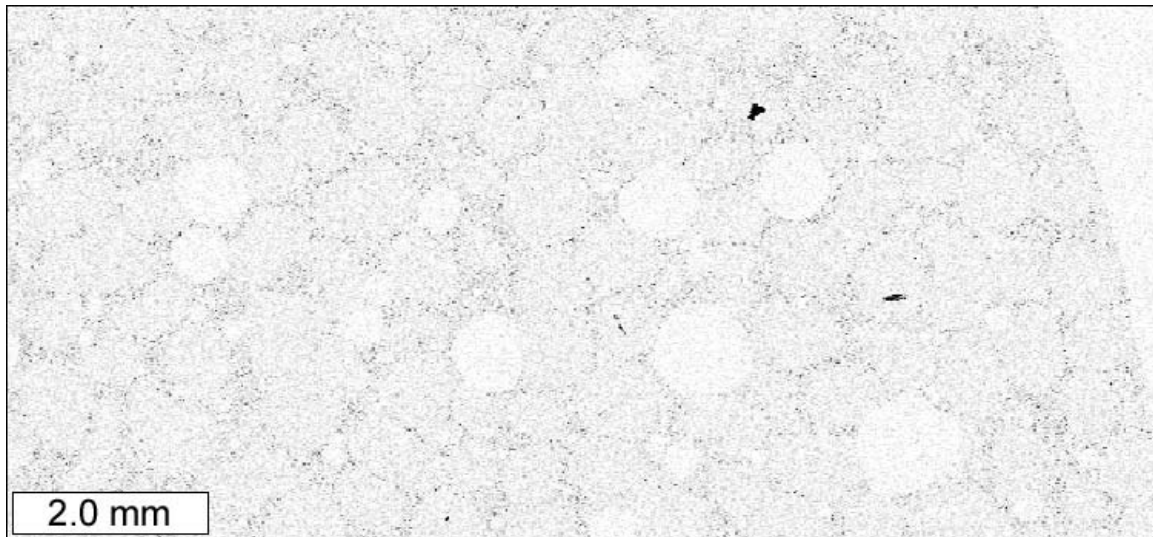


Figure 3.63a: Iron  $K\alpha$  x-ray map from control cylinder. Darker areas correspond to higher  $K\alpha$  x-ray counts.

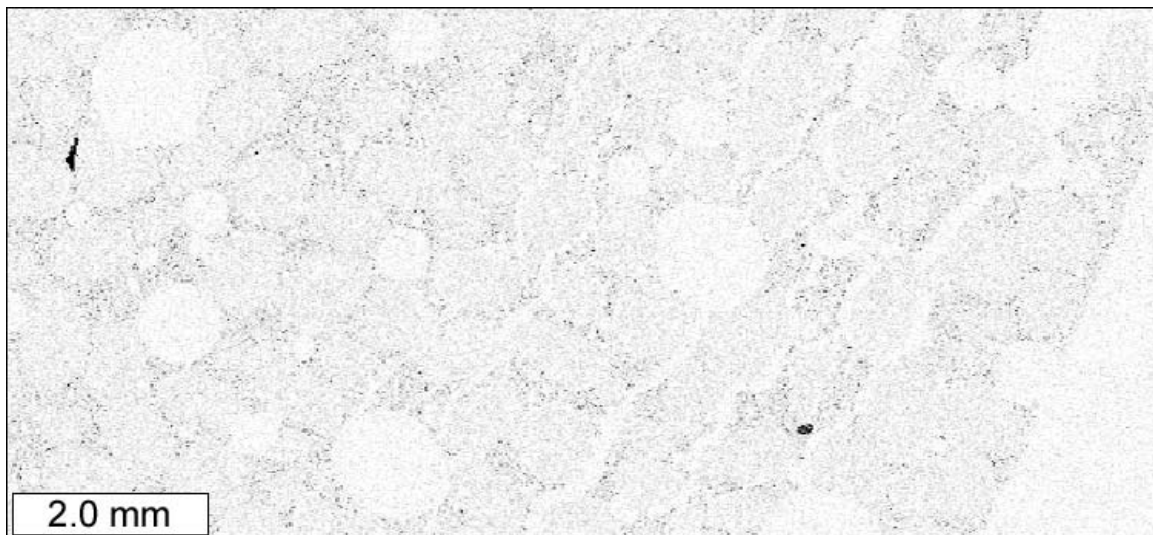


Figure 3.63b: Iron  $K\alpha$  x-ray map from rock salt NaCl deicer-exposed cylinder. Darker areas correspond to higher  $K\alpha$  x-ray counts.

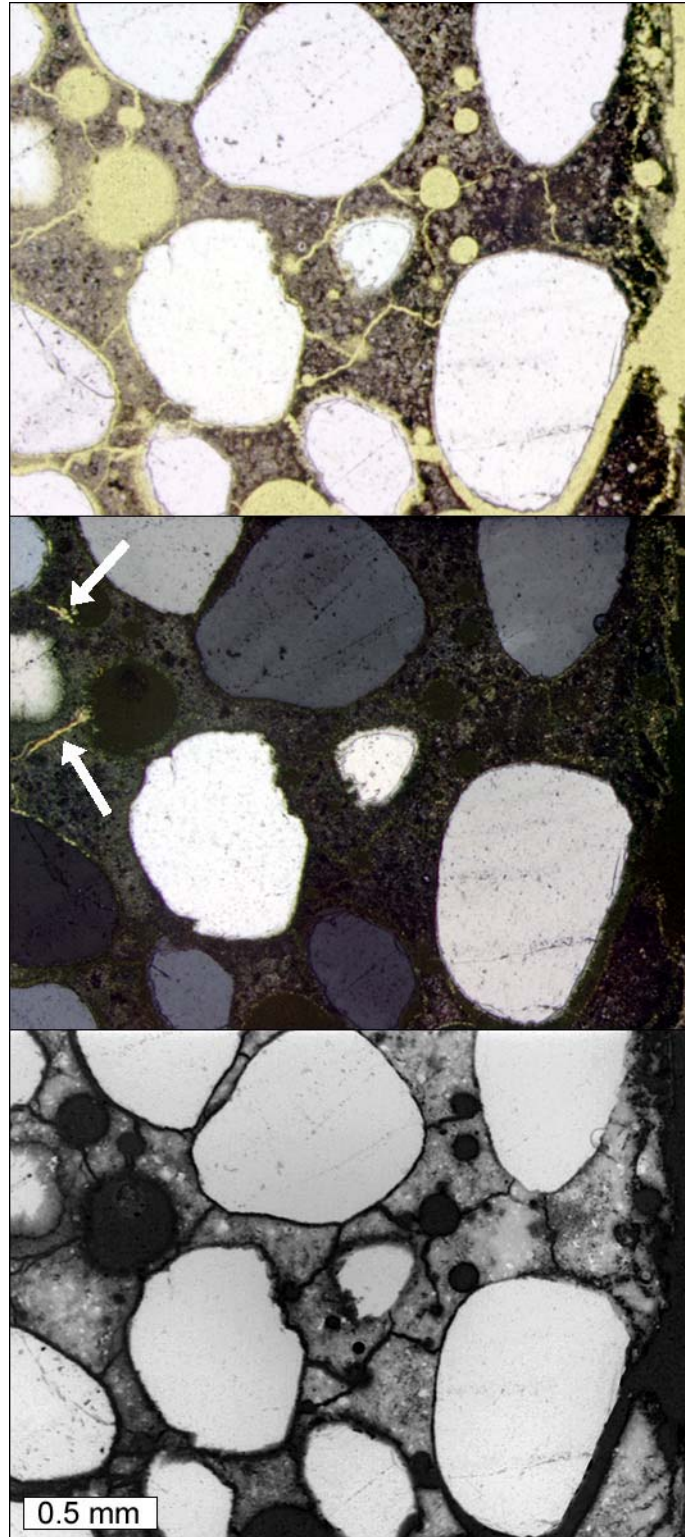


Figure 3.64: Petrographic microscope images of early onset of cracking in  $MgCl_2$  exposed sample from cyclic experiment. White arrows indicate crystalline material filling cracks. From top to bottom: plane polarized light, cross polarized light, and epifluorescent mode.

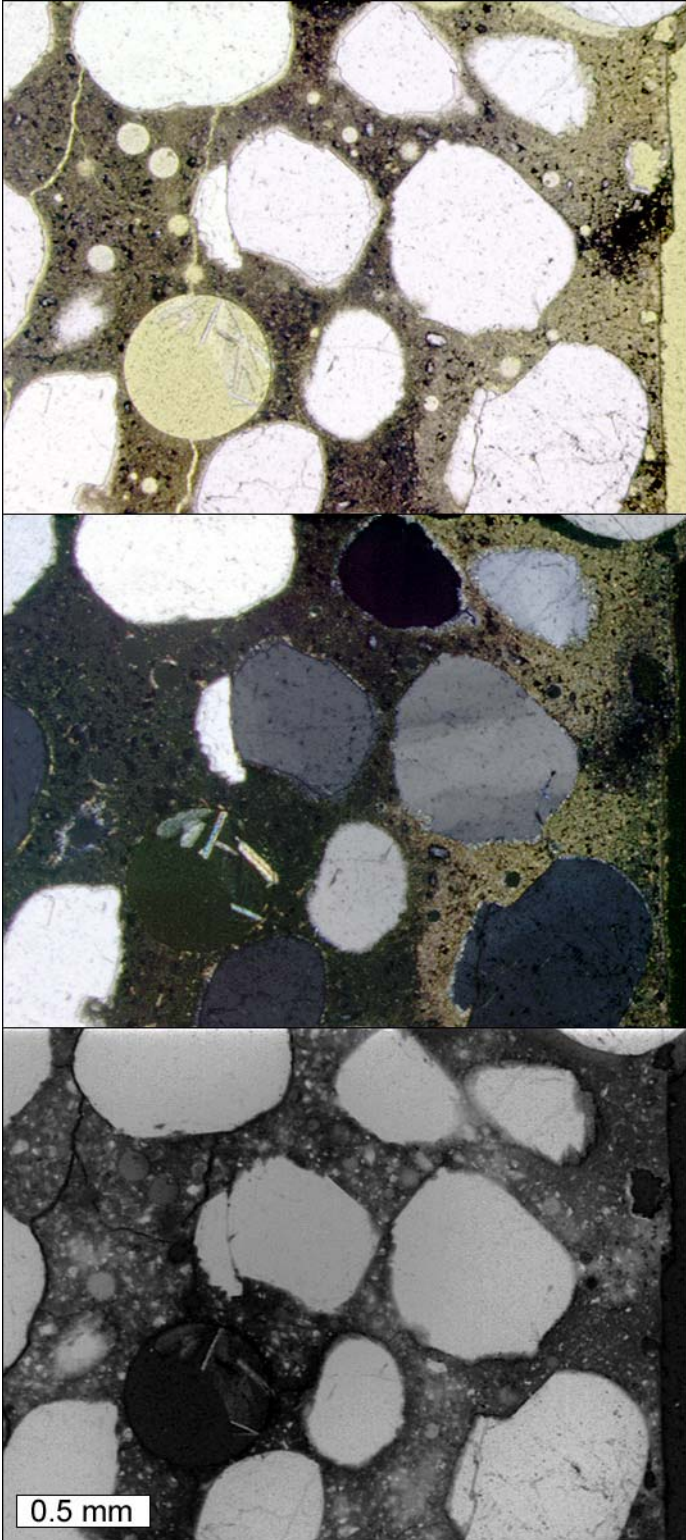


Figure 3.65: Petrographic microscope images of early onset of cracking in NaCl exposed sample from cyclic experiment. From top to bottom: plane polarized light, cross polarized light, and epifluorescent mode.

### 3.2.7 Low Temperature Experiment

#### 3.2.7.1 Observations

The constant low temperature experiment was designed to monitor chloride ingress at 28, 56, and 112 days at a temperature of 40 °F. The cylinders were to be used to determine diffusion coefficients for each mortar and salt solution combination. Some of the cylinders were coated with epoxy on all sides except for the top surface in order to monitor one-dimensional chloride diffusion. Other cylinders were not coated with epoxy, in order to monitor radial diffusion into the sides of the cylinders. As shown in Figures 3.66, the cylinders in the NaCl solution showed no deterioration after 84 days. Figures 3.67 and 3.68 show cylinders from the MgCl<sub>2</sub> and CaCl<sub>2</sub> treatments beginning to show signs of expansion and cracking after 56 days. By 84 days, the cylinders in the MgCl<sub>2</sub> and CaCl<sub>2</sub> solutions were severely deteriorated, as shown in Figures 3.69 and 3.70. It was decided to end the constant temperature experiments for all cylinders at 84 days. The control cylinders in the lime water solution, as shown in Figure 3.71, showed no signs of distress after 84 days. The cylinders in the CMA solution showed little to no distress after 84 days as shown in Figure 3.72, although there was some staining evident in the 0.60 w/c cylinders. Table 3.10 summarizes the visual ratings for the cylinders over time for the low temperature exposure tests.



Figure 3.66 Cylinders exposed to NaCl solution after 84 days of constant low temperature test. From left to right: 0.40, 0.50, and 0.60 w/c mortar cylinders.



Figure 3.67. Cylinders exposed to  $MgCl_2$  solution after 56 days of constant low temperature test. From left to right: 0.40, 0.50, and 0.60 w/c mortar cylinders.



Figure 3.68 Cylinders exposed to  $CaCl_2$  solution after 56 days of constant low temperature test. From left to right: 0.40, 0.50, and 0.60 w/c mortar cylinders.





Figure 3.69 Cylinders exposed to  $MgCl_2$  solution after 84 days of constant low temperature test. From left to right: 0.40, 0.50, and 0.60 w/c mortar cylinders.



Figure 3.70. Cylinders exposed to  $CaCl_2$  solution after 84 days of constant low temperature test. From left to right: 0.40, 0.50, and 0.60 w/c mortar cylinders.



Figure 3.71. Cylinders exposed to CMA solution after 84 days of constant low temperature test. From left to right: 0.40, 0.50, and 0.60 w/c mortar cylinders.



Figure 3.72 Control cylinders exposed to lime water solution after 84 days of constant low temperature test. From left to right: 0.40, 0.50, and 0.60 w/c mortar cylinders.

Table 3.10 List of visual ratings for all mortar cylinders from the low temperature tests. Rating Scale: 0 - no visible change, 1 – some cracking, 2 - visible expansion and cracking, 3 - severe expansion and cracking, 4 - partial disintegration, 5 - total disintegration, x – test aborted.

Solution	Time in Days											
	w/c = 0/40				w/c = 0/50				w/c = 0/60			
	8	28	56	84	8	28	56	84	8	28	56	84
Lime Water	-	0	0	0	-	0	0	0	-	0	0	0
MgCl <sub>2</sub>	-	0-1	1-2	2-3	-	0-1	1-2	1-3	-	0-1	0-1	1-3
CaCl <sub>2</sub>	-	0-1	2-3	3	-	0	2-3	3	-	0-1	1-3	2-3
NaCl	-	0	0	0	-	0	0	0	-	0	0	0
CMA	-	0	0	0	-	0	0	0	-	0	0	0

### 3.2.7.2 Split Tensile Strength Testing

Cylindrical specimens exposed to the constant low temperature treatment in selected chemicals were tested to find the splitting tensile strength. Tests in accordance with ASTM C496 were performed on specimens that had been in the lime water and the four deicing chemicals for 28 days. Three specimens of each w/c ratio were tested, with the exception of calcium magnesium acetate (CMA). An error was made when drawing samples at 28 days for the CMA solution. A 0.40 w/c ratio specimen was taken in place of a 0.60 w/c ratio one. Therefore, four 0.40 w/c ratio specimens and two 0.60 w/c ratio specimens were tested for strength.

The test equipment used was a Model 318.25 load unit manufactured by MTS Systems Corporation (MTS) with a 6.4” stroke and 55 kip actuator. The test was controlled by an MTS TestStar II digital controller, and a PC with accompanying software. The specimen was placed on the bottom platen with a 1”x5”x 1/8” thick wood slat underneath it. Another slat was placed on top of the specimen, and the platen was moved upwards until the specimen was loaded with approximately 20 lbs. Testing was conducted under load control at a loading rate of 2500 lb/min.

Tables 3.11 through 3.15 show the results of each strength test for the various specimens exposed to the constant low temperature treatment in selected chemicals.

Table 3.11 Splitting tensile strength of mortar cylinders exposed to lime water solution for 28 days in the constant low temperature test.						
Lime water Specimens	w/c = 0.40		w/c = 0.50		w/c = 0.60	
	Max Load (lbs.)	Max Tensile Stress (psi)	Max Load (lbs.)	Max Tensile Stress (psi)	Max Load (lbs.)	Max Tensile Stress (psi)
Sample 1	11607.6	924	9704.9	772	8009.2	637
Sample 2	11576.6	921	10396.9	827	8440.9	672
Sample 3	12738.9	1014	10160.7	809	8597.7	684
<i>Average</i>	11974.4	953.0	10087.5	802.7	8349.3	664.3

Table 3.12 Splitting tensile strength of mortar cylinders exposed to NaCl solution for 28 days in the constant low temperature test.						
NaCl Specimens	w/c = 0.40		w/c = 0.50		w/c = 0.60	
	Max Load (lbs.)	Max Tensile Stress (psi)	Max Load (lbs.)	Max Tensile Stress (psi)	Max Load (lbs.)	Max Tensile Stress (psi)
Sample 1	10597.2	843	10655.3	848	9867.45	785
Sample 2	11154.7	888	10812.0	860	8287.96	660
Sample 3	13304.2	1059	10311.7	821	9021.57	718
<i>Average</i>	11685.4	930.0	10593.0	843.0	9059.0	721.0

Table 3.13 Splitting tensile strength of mortar cylinders exposed to MgCl <sub>2</sub> solution for 28 days in the constant low temperature test.						
MgCl <sub>2</sub> Specimens	w/c = 0.40		w/c = 0.50		w/c = 0.60	
	Max Load (lbs.)	Max Tensile Stress (psi)	Max Load (lbs.)	Max Tensile Stress (psi)	Max Load (lbs.)	Max Tensile Stress (psi)
Sample 1	12695.4	1010	9525.8	758	8122.5	646
Sample 2	12490.3	994	9802.6	780	7501.1	597
Sample 3	9616.8	765	10618.5	845	8350.9	665
<i>Average</i>	11600.8	923.0	9982.3	794.3	7991.5	636.0

Table 3.14 Splitting tensile strength of mortar cylinders exposed to CMA solution for 28 days in the constant low temperature test.						
CMA Specimens	w/c = 0.40		w/c = 0.50		w/c = 0.60	
	Max Load (lbs.)	Max Tensile Stress (psi)	Max Load (lbs.)	Max Tensile Stress (psi)	Max Load (lbs.)	Max Tensile Stress (psi)
Sample 1	11858.3	944	10242.0	815	9893.58	787
Sample 2	11446.9	911	10490.7	835	8897.69	708
Sample 3	10592.4	843	11021.1	877		
Sample 4	14278.8	1136				
<i>Average</i>	12044.1	958.5	10584.6	842.3	9395.6	747.5

Table 3.15 Splitting tensile strength of mortar cylinders exposed to CaCl <sub>2</sub> solution for 28 days in the constant low temperature test.						
CMA Specimens	w/c = 0.40		w/c = 0.50		w/c = 0.60	
	Max Load (lbs.)	Max Tensile Stress (psi)	Max Load (lbs.)	Max Tensile Stress (psi)	Max Load (lbs.)	Max Tensile Stress (psi)
Sample 1	11752.8	935	10411.4	829	4363.4	347
Sample 2	11091.7	883	10238.1	815	7343.4	584
Sample 3	10189.7	811	9749.4	776	8367.33	666
<i>Average</i>	11011.4	876.3	10133.0	806.7	6691.4	532.3

There is no apparent correlation between strength and deicer for a particular w/c ratio for anything other than calcium chloride. The calcium chloride, which was the most damaging salt in this particular experiment, decreased the tensile strength of the samples with a 0.60 w/c ratio by nearly 20%. It seems curious that there was no reduction apparent in the other specimens, since visible damage seemed fairly similar for all calcium chloride samples, regardless of w/c ratio. The results may become clearer as further strength testing is performed on specimens with longer exposure times.

### 3.2.7.3 Petrographic Analysis

Thin sections were prepared from the 0.50 w/c mortar cylinders subjected to 56 days of immersion in the five solutions. One cylinder was selected from each of the five solutions: magnesium chloride, calcium chloride, sodium chloride, calcium magnesium acetate, and lime water. The thin sections represent a cross-sectional plane oriented parallel to the finished surface at a depth of about 3/4 of an inch, (2 cm) from the finished surface. Figure 3.73 consists of epifluorescent mode images, Figure 3.74 consists of back-scattered electron images, and Figure 3.75 consists of elemental maps for carbon to illustrate the extensive crack networks of the magnesium chloride and calcium chloride

immersed cylinders as compared to the cylinders immersed in the other three solutions. Near the exteriors of the magnesium chloride and calcium chloride cylinders, the cracks are empty. However, cracks further towards the interior of the cylinders are filled with a crystalline material bearing calcium and chlorine, likely calcium oxychloride or the altered remnants of calcium oxychloride. Figure 3.76 shows cross-polarized light images to emphasize the crystalline nature of the remnant calcium oxychloride filling the cracks. Figures 3.77 and 3.78 show close-up views of regions of the cement paste disrupted by cracks filled with calcium oxychloride for both the magnesium chloride and calcium chloride immersed samples. Figure 3.79 shows calcium oxychloride crystals that have formed at the expense of secondary calcium hydroxide crystals in an air void, yet retained the shape of the original calcium hydroxide crystals. The deterioration of the magnesium chloride and calcium chloride immersed samples appears very similar. Both samples exhibit a region of calcium oxychloride filled cracks and voids associated with calcium hydroxide depleted cement paste. Figure 3.80 shows elemental maps for magnesium for all of the thin sections. Figure 3.80 shows that a magnesium crust is at the exterior of the magnesium chloride immersed sample as well as the calcium magnesium acetate immersed sample. Magnesium is sequestered at the exterior of the magnesium chloride immersed cylinders, likely resulting in a calcium chloride solution in the interior that is similar to the solution in the interior of the calcium chloride immersed cylinders. Figures 3.81 and 3.82 show brucite and magnesium chloride hydrate crystals filling cracks and voids at the exterior of the magnesium chloride immersed cylinder. Figure 3.83 shows elemental maps for chlorine for all of the thin sections. A chlorine gradient is clearly visible for all three of the chloride-based deicers. It should be noted that the epoxy used to stabilize the billets prior to thin sectioning also contains chlorine. A complete set of the elemental maps and petrographic images collected from each of the thin sections is included in Figures 3.84 through 3.108. Figures 3.84 through 3.88 correspond to the cylinder immersed in magnesium chloride solution. Figures 3.89 through 3.93 correspond to the cylinder immersed in calcium chloride solution. Figures 3.94 through 3.98 correspond to the cylinder immersed in sodium chloride solution. Figures 3.99 through 3.103 correspond to the cylinder immersed in calcium magnesium acetate solution. And finally, Figures 3.104 through 3.108 correspond to the cylinder immersed in lime water.

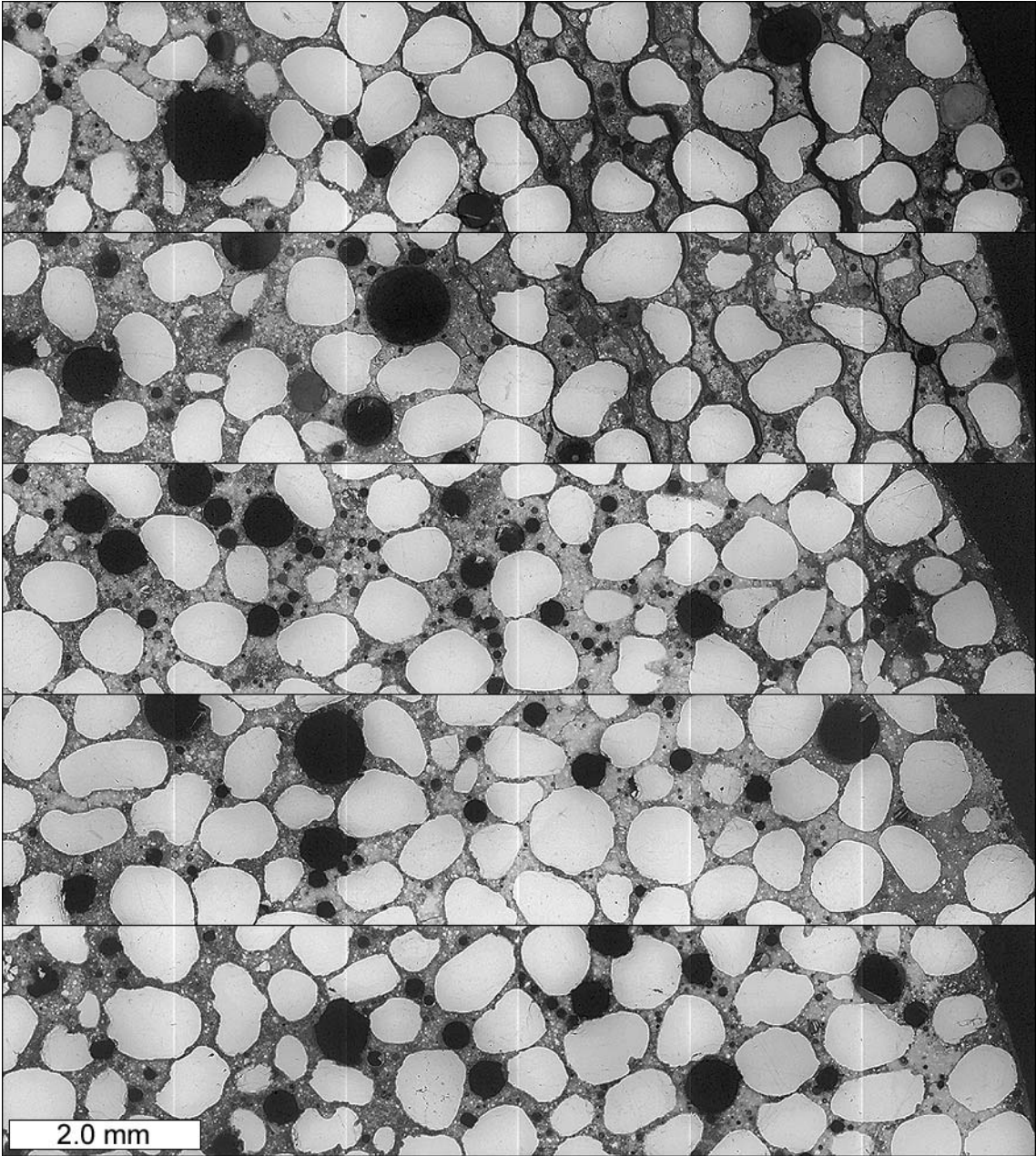


Figure 3.73: Epifluorescent mode images of thin sections prepared from mortar cylinders immersed in the following solutions, from top to bottom: magnesium chloride, calcium chloride, sodium chloride, calcium magnesium acetate, and lime water.

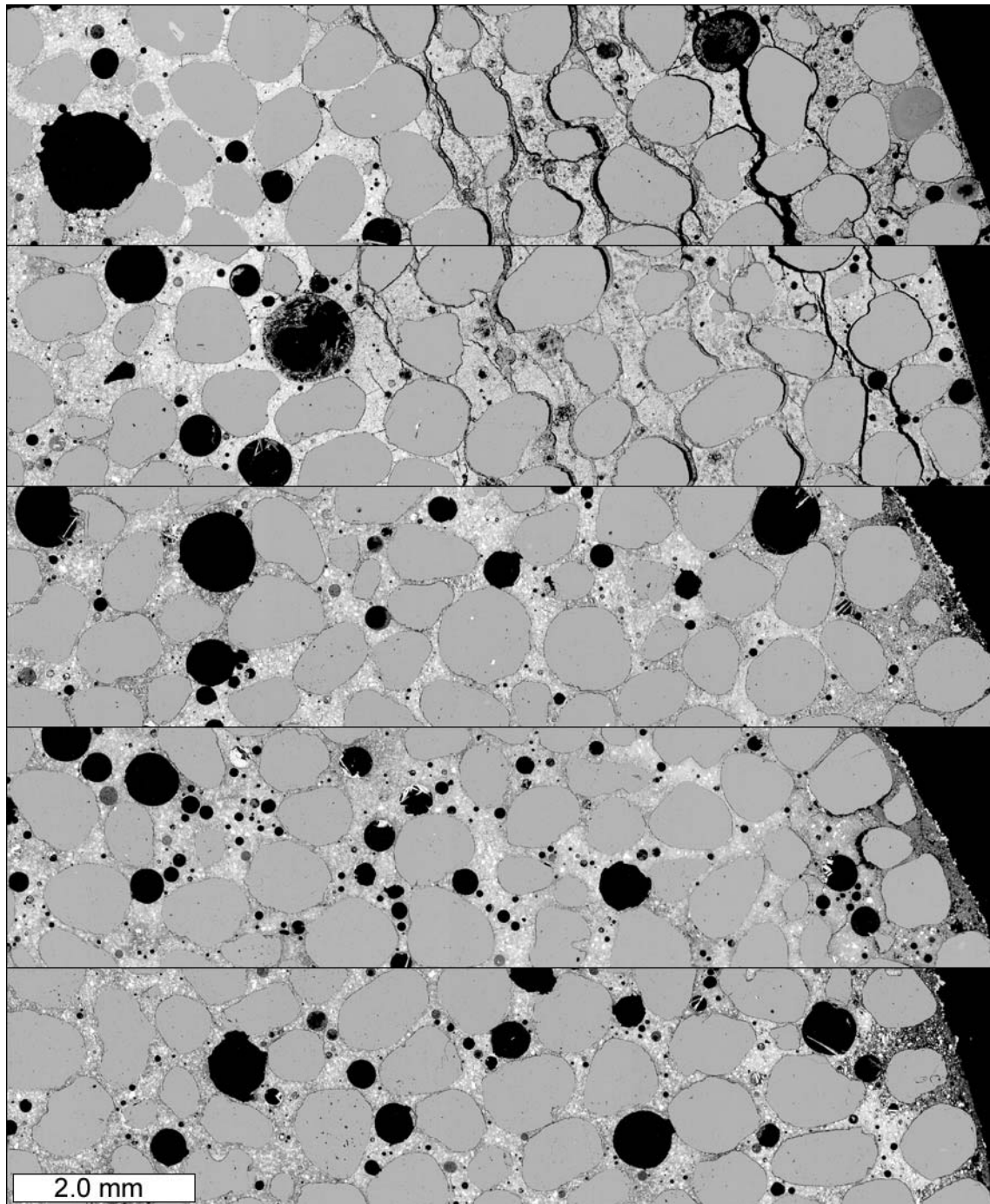


Figure 3.74: Back-scattered electron images of thin sections prepared from mortar cylinders immersed in the following solutions, from top to bottom: magnesium chloride, calcium chloride, sodium chloride, calcium magnesium acetate, and lime water.



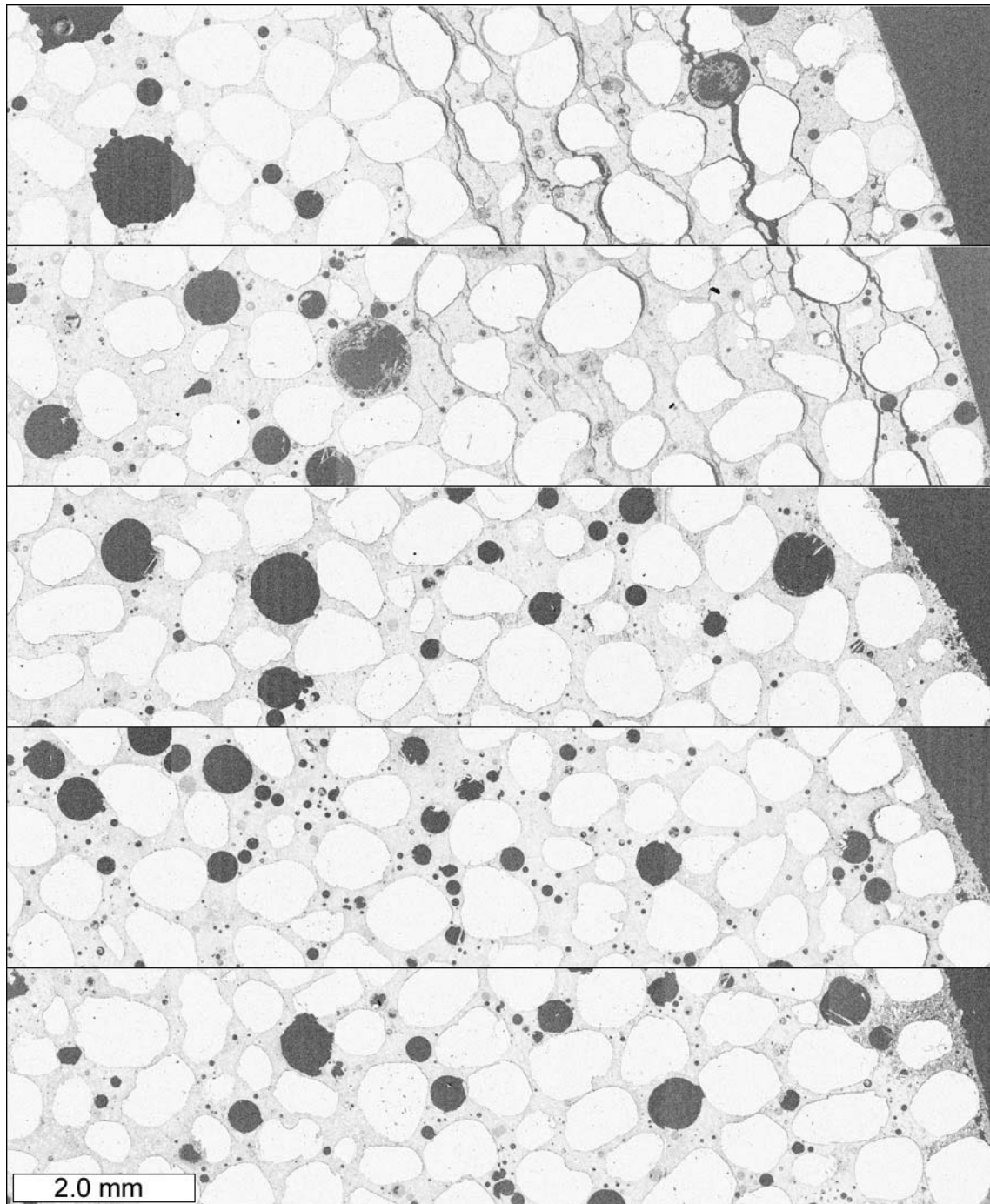


Figure 3.75: Elemental map for carbon collected from thin sections prepared from mortar cylinders immersed in the following solutions, from top to bottom: magnesium chloride, calcium chloride, sodium chloride, calcium magnesium acetate, and lime water.

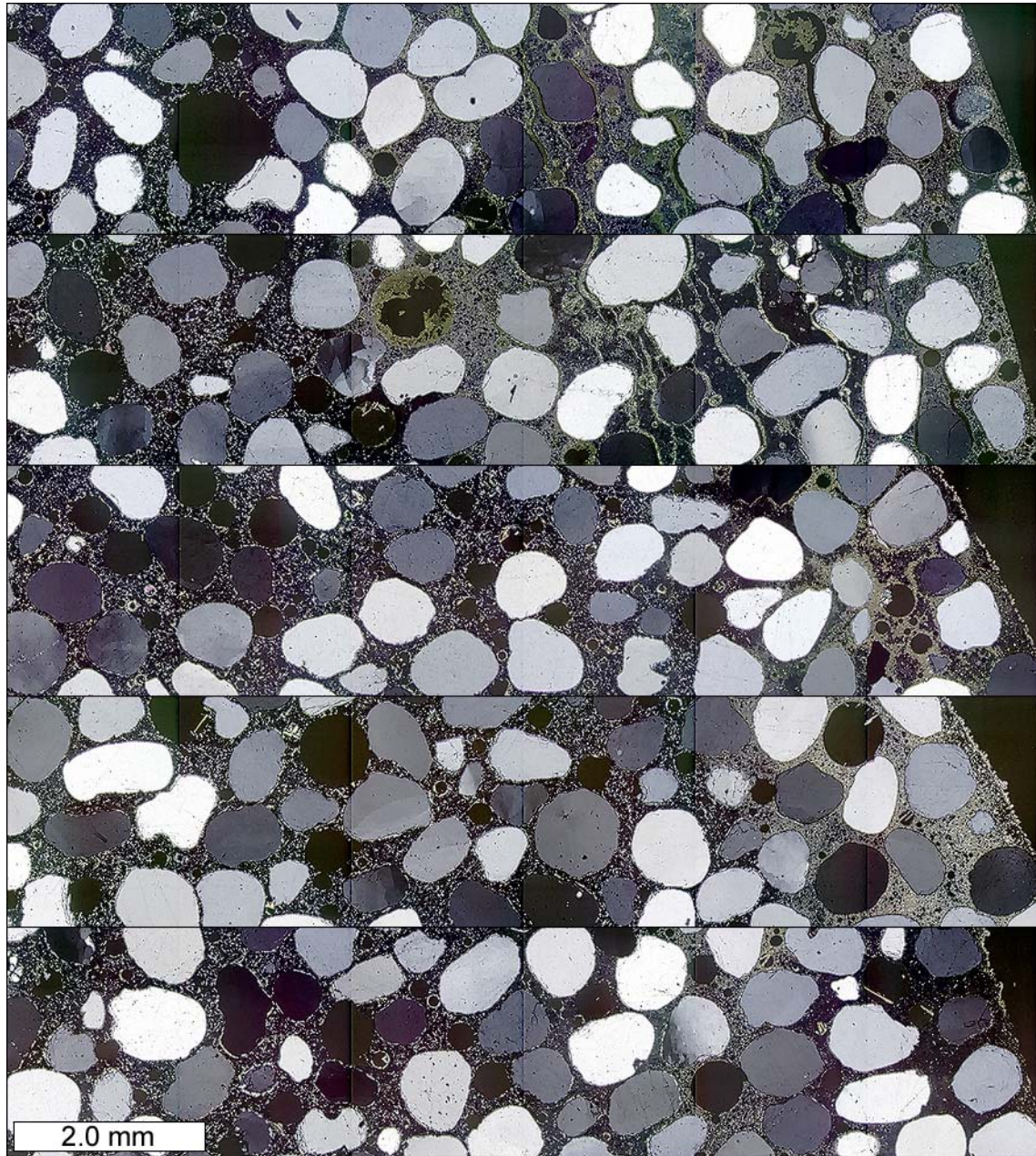


Figure 3.76: Cross-polarized light images of thin sections prepared from mortar cylinders immersed in the following solutions, from top to bottom: magnesium chloride, calcium chloride, sodium chloride, calcium magnesium acetate, and lime water.

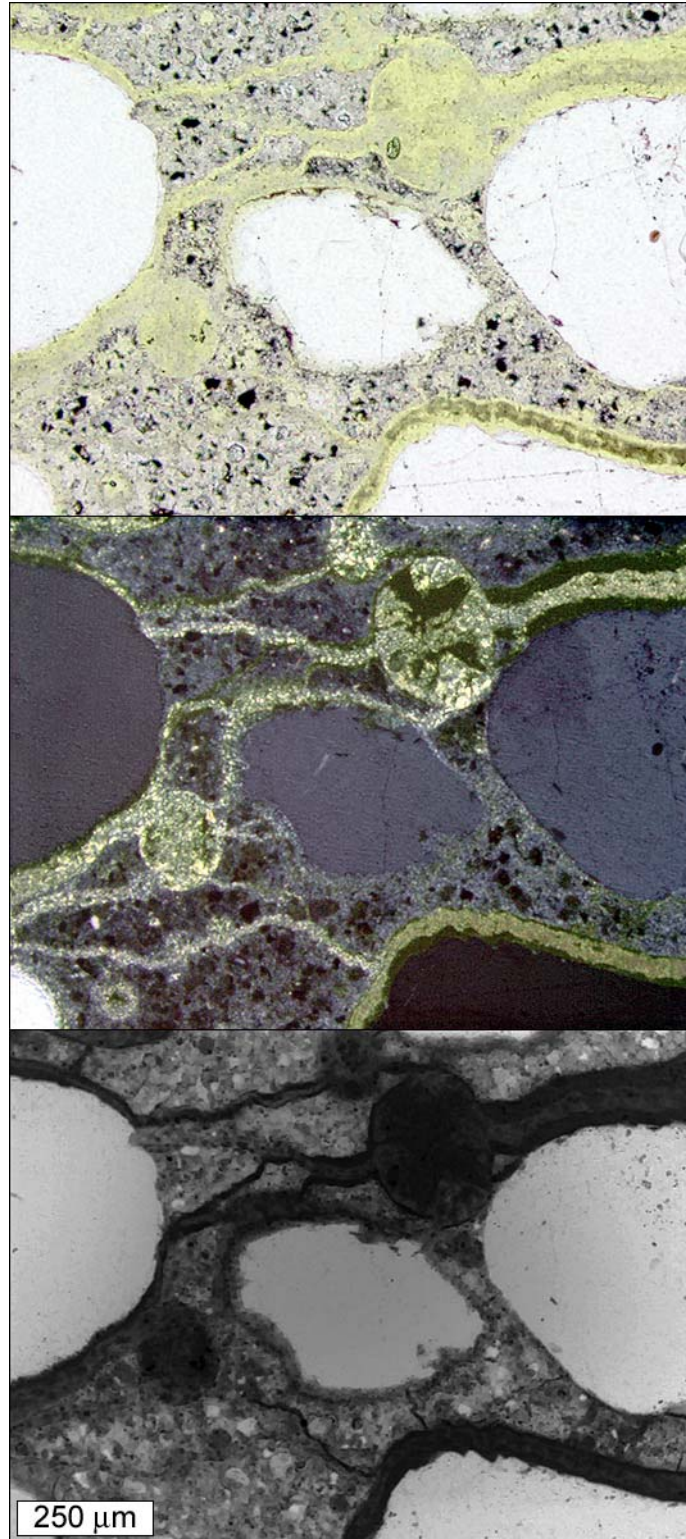


Figure 3.77: Cracks and air voids filled with remnant calcium oxychloride crystals in thin section prepared from magnesium chloride solution immersed sample. From top to bottom: plane polarized light, cross polarized light, and epifluorescent mode.

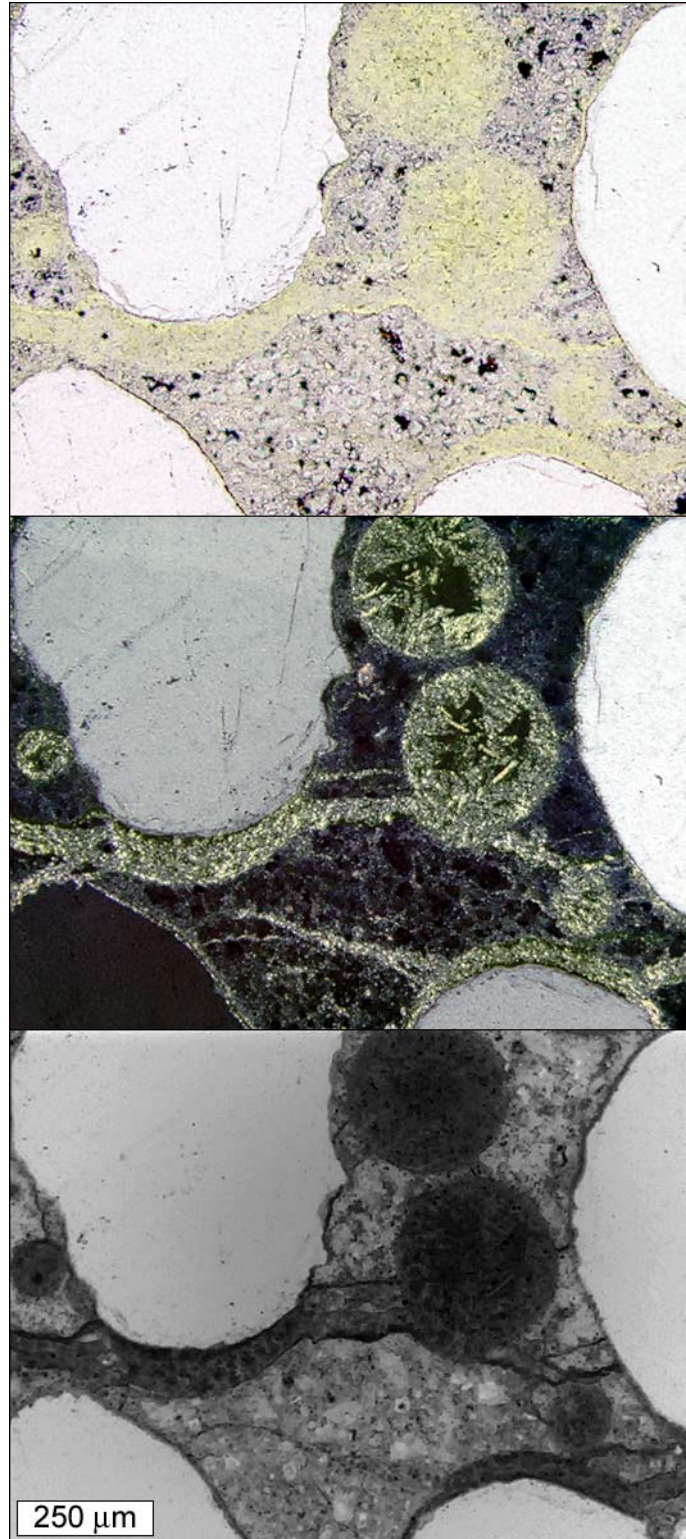


Figure 3.78 Cracks and air voids filled with remnant calcium oxychloride crystals in thin section prepared from calcium chloride solution immersed sample. From top to bottom: plane polarized light, cross polarized light, and epifluorescent mode.

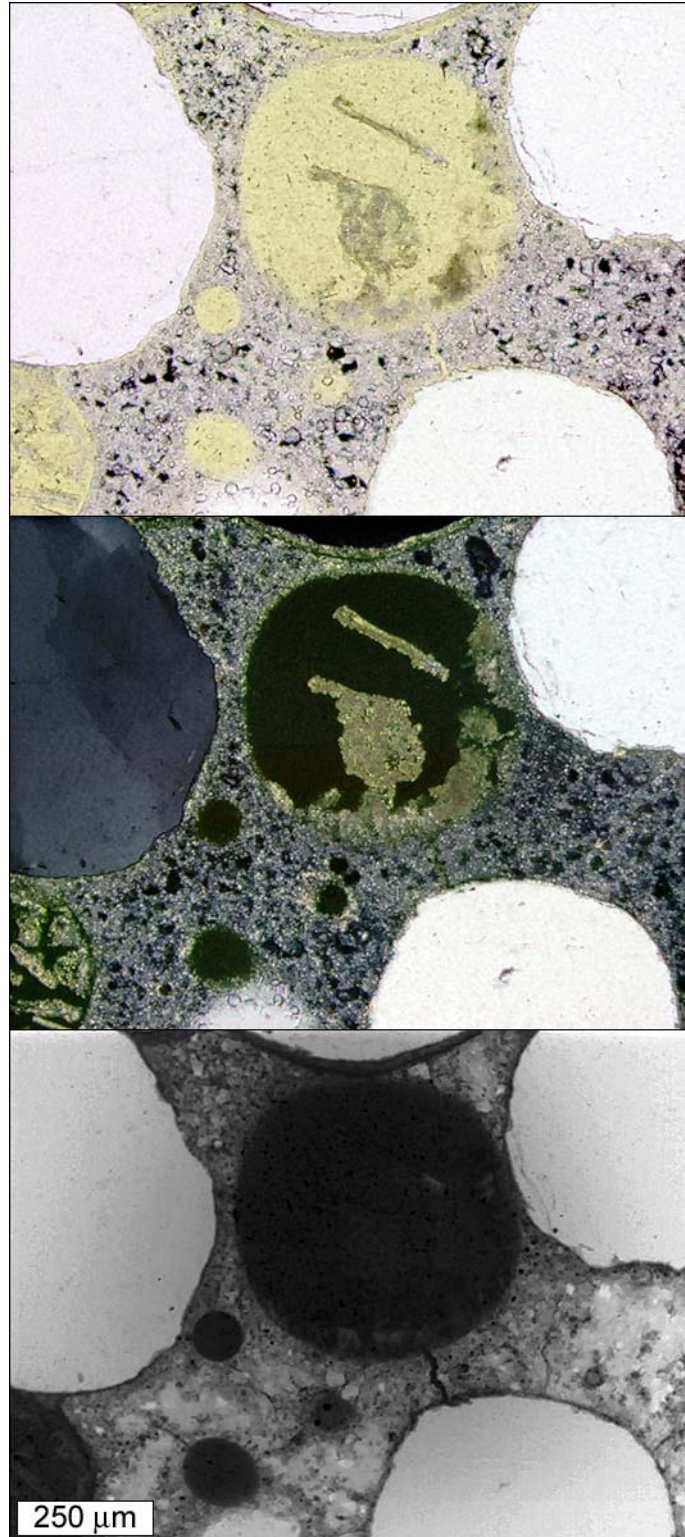


Figure 3.79 Remnant calcium oxychloride crystals that are pseudomorphs of secondary calcium hydroxide crystals initially formed in an air void from thin section prepared from magnesium chloride solution immersed sample. From top to bottom: plane polarized light, cross polarized light, and epifluorescent mode.

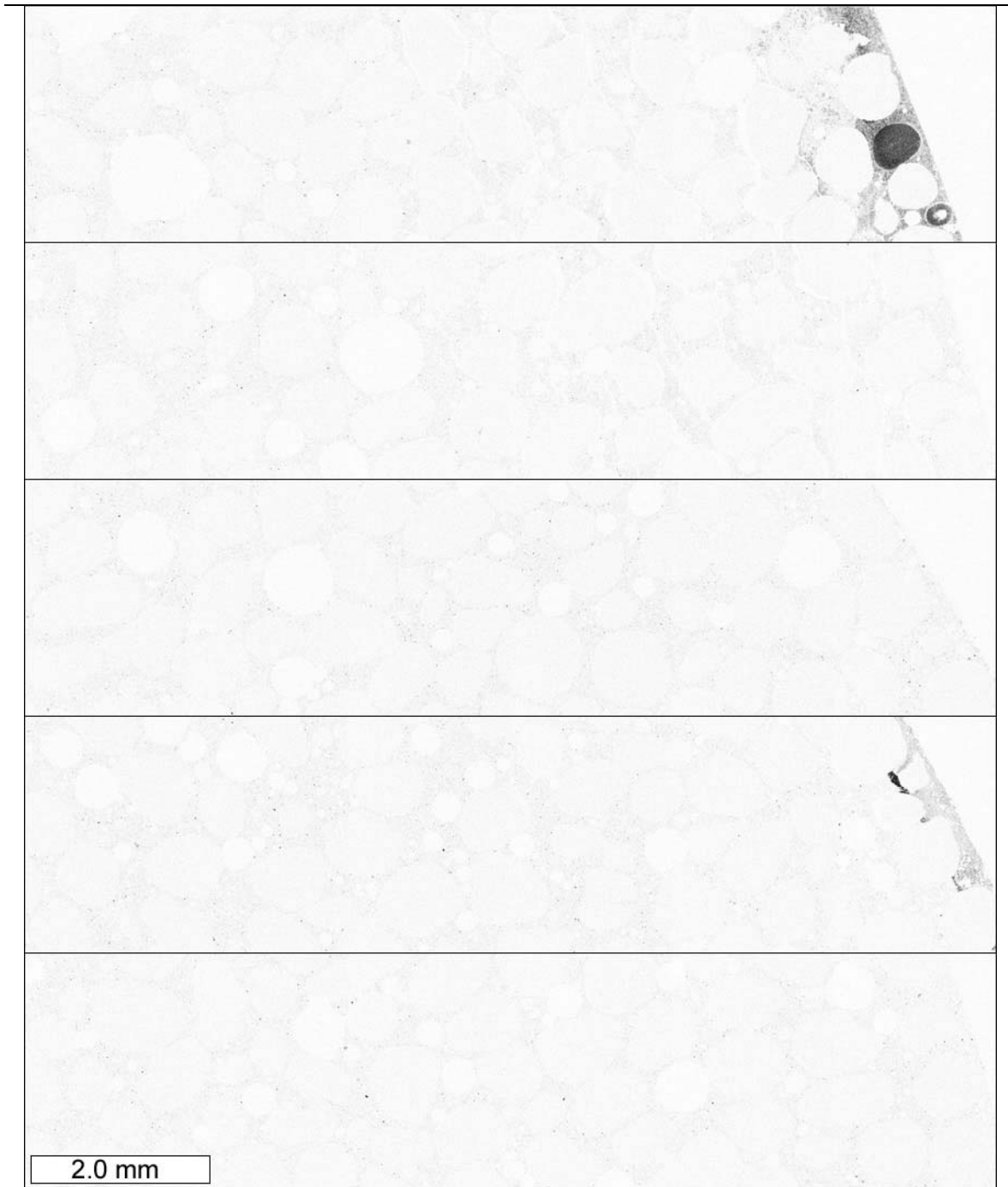


Figure 3.80 Elemental map for magnesium collected from thin sections prepared from mortar cylinders immersed in the following solutions, from top to bottom: magnesium chloride, calcium chloride, sodium chloride, calcium magnesium acetate, and lime water.

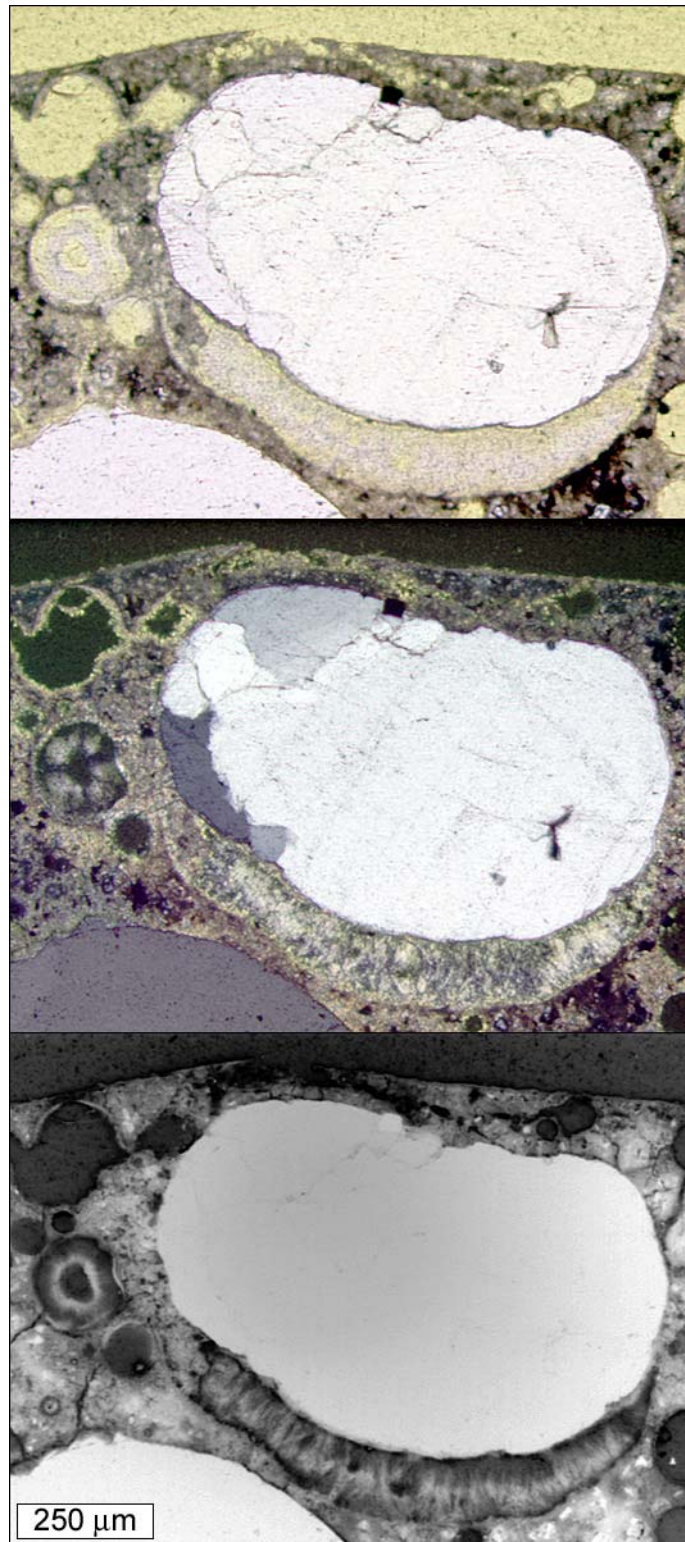


Figure 3.81 Brucite, (magnesium hydroxide) crystals in air void and seam beneath sand grain near exterior in thin section prepared from cylinder immersed in magnesium chloride solution. From top to bottom: plane polarized light, cross polarized light, and epifluorescent mode.

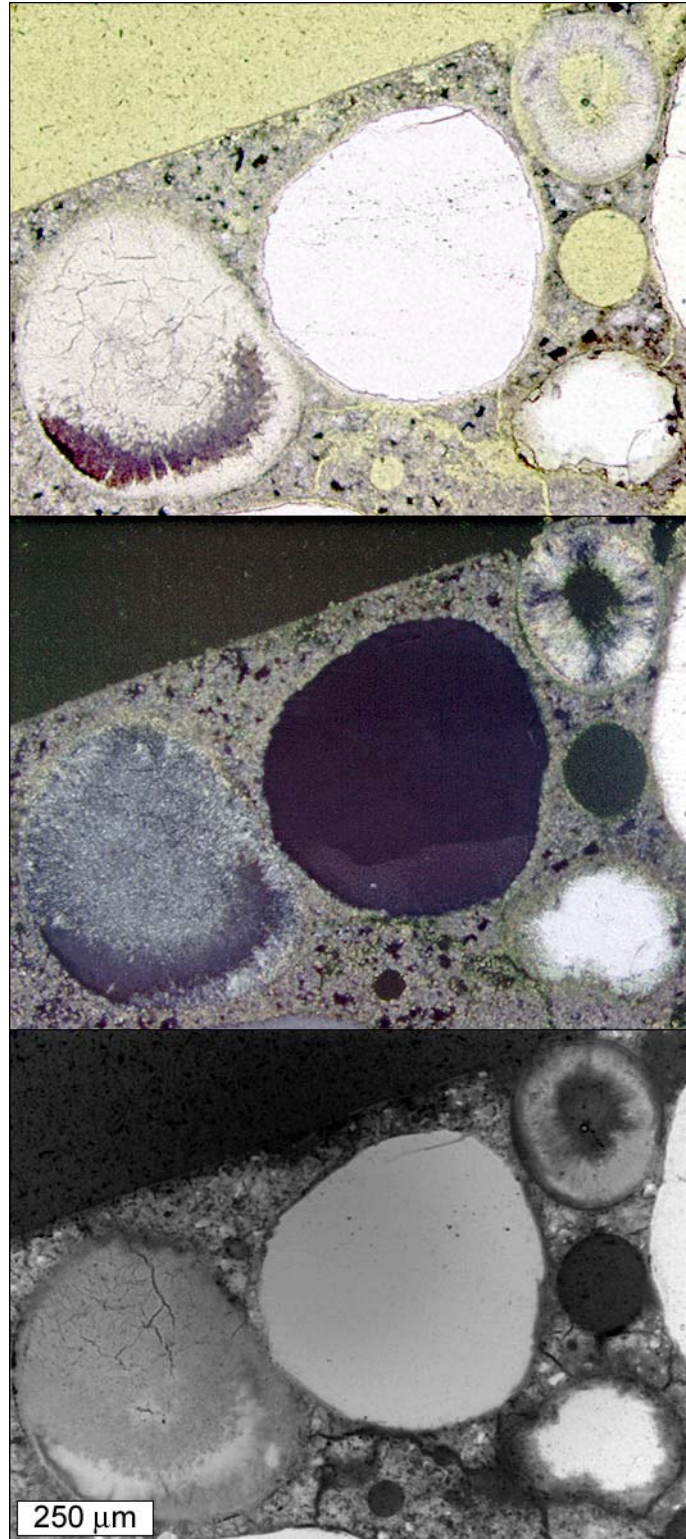


Figure 3.82: Magnesium chloride hydrate crystals in air voids near exterior in thin section prepared from cylinder immersed in magnesium chloride solution. From top to bottom: plane polarized light, cross polarized light, and epifluorescent mode.



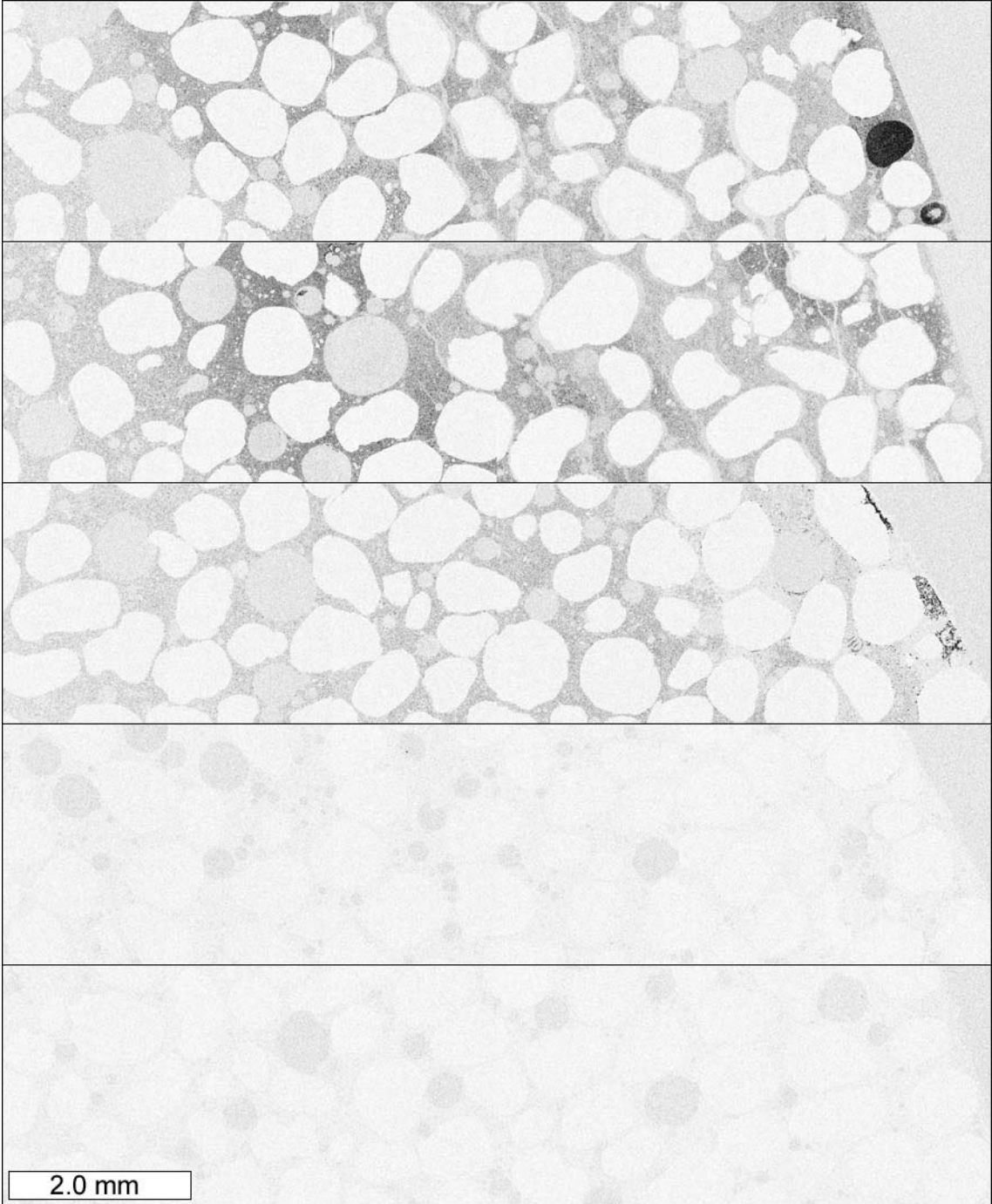


Figure 3.83: Elemental map for chlorine collected from thin sections prepared from mortar cylinders immersed in the following solutions, from top to bottom: magnesium chloride, calcium chloride, sodium chloride, calcium magnesium acetate, and lime water.

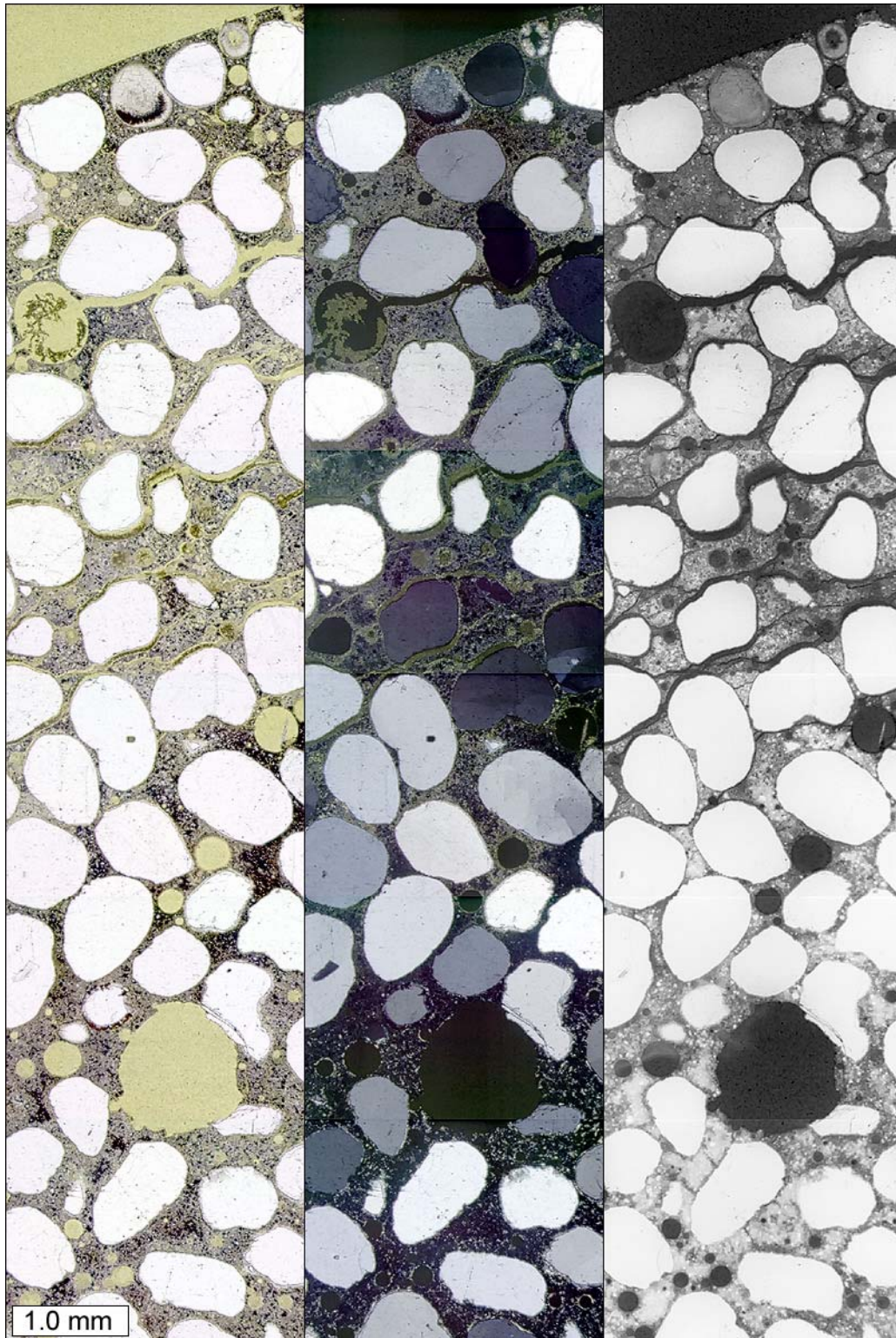


Figure 3.84: From left to right: plane polarized light, cross polarized light, and epifluorescent mode images of a thin section prepared from a cylinder immersed in magnesium chloride solution.

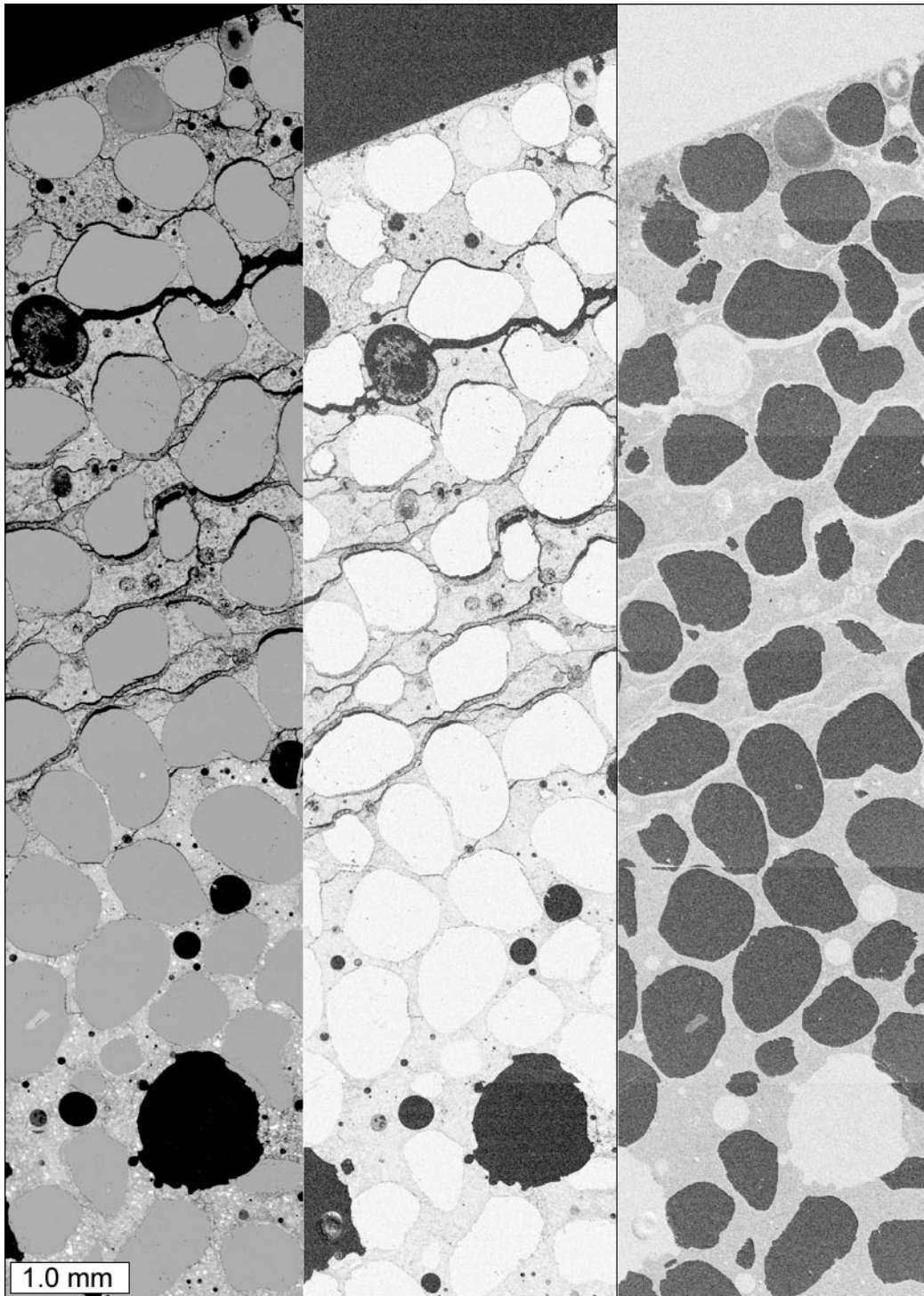


Figure 3.85: From left to right: back scattered electron image, elemental map for carbon, and elemental map for oxygen. Images were collected from a thin section prepared from a cylinder immersed in magnesium chloride solution.



Figure 3.86: Elemental maps, from left to right: sodium, magnesium, and aluminum. The elemental maps were collected from a thin section prepared from a cylinder immersed in magnesium chloride solution.

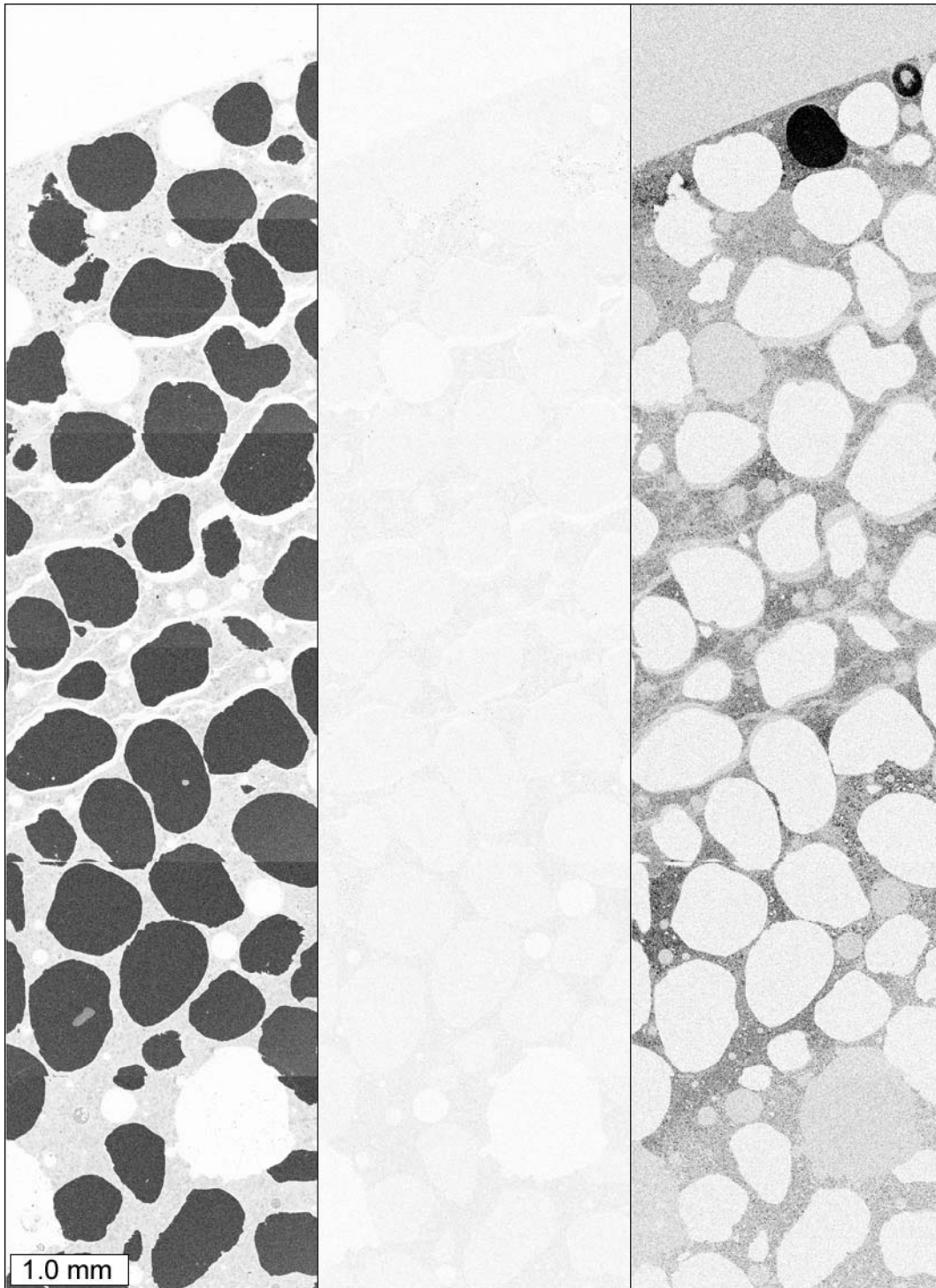


Figure 3.87: Elemental maps, from left to right: silicon, sulfur, and chlorine. The elemental maps were collected from a thin section prepared from a cylinder immersed in magnesium chloride solution.

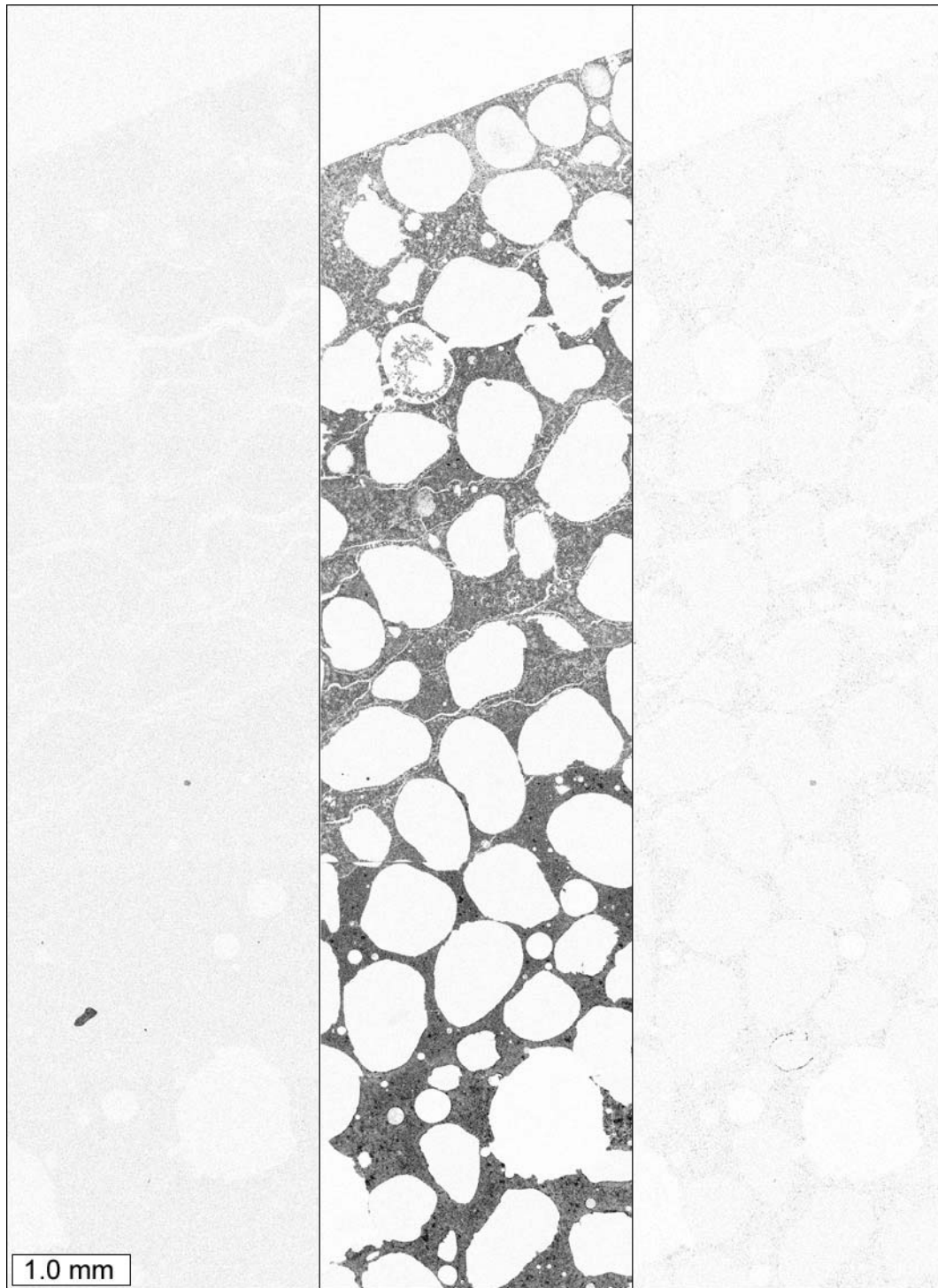


Figure 3.88: Elemental maps, from left to right: potassium, calcium, and iron. The elemental maps were collected from a thin section prepared from a cylinder immersed in magnesium chloride solution.

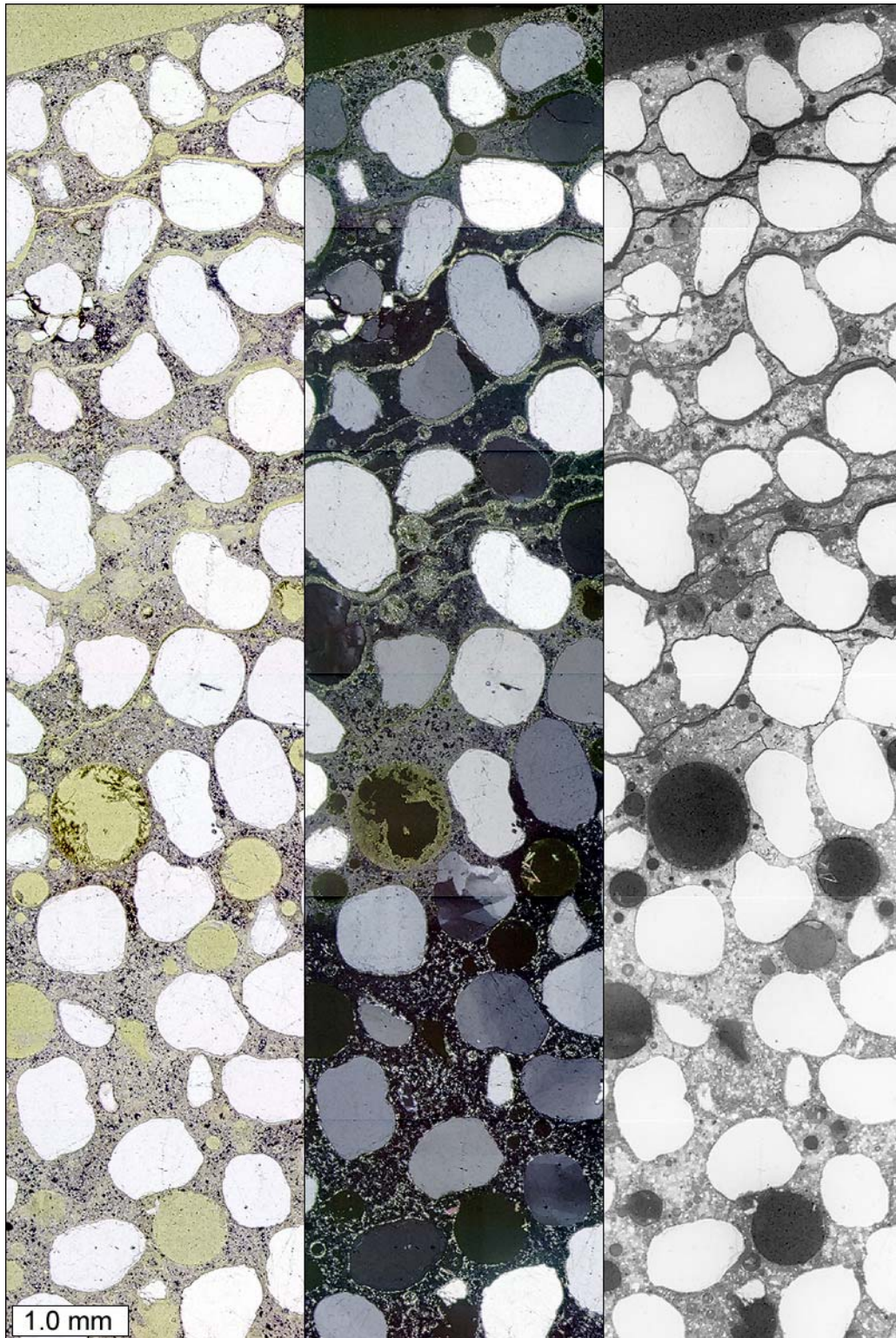


Figure 3.89: From left to right: plane polarized light, cross polarized light, and epifluorescent mode images of a thin section prepared from a cylinder immersed in calcium chloride solution.

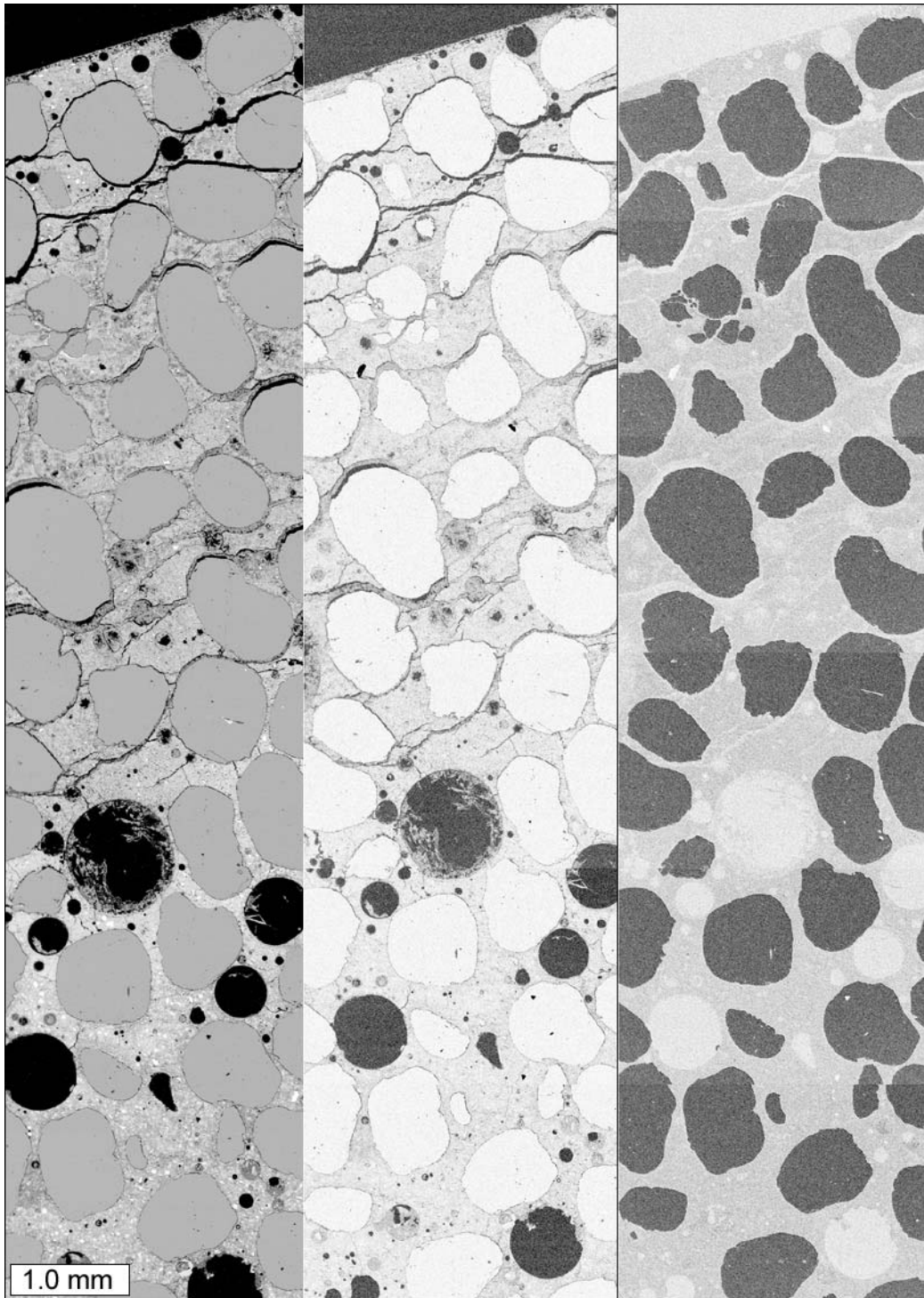


Figure 3.90: From left to right: back scattered electron image, elemental map for carbon, and elemental map for oxygen. Images were collected from a thin section prepared from a cylinder immersed in calcium chloride solution.



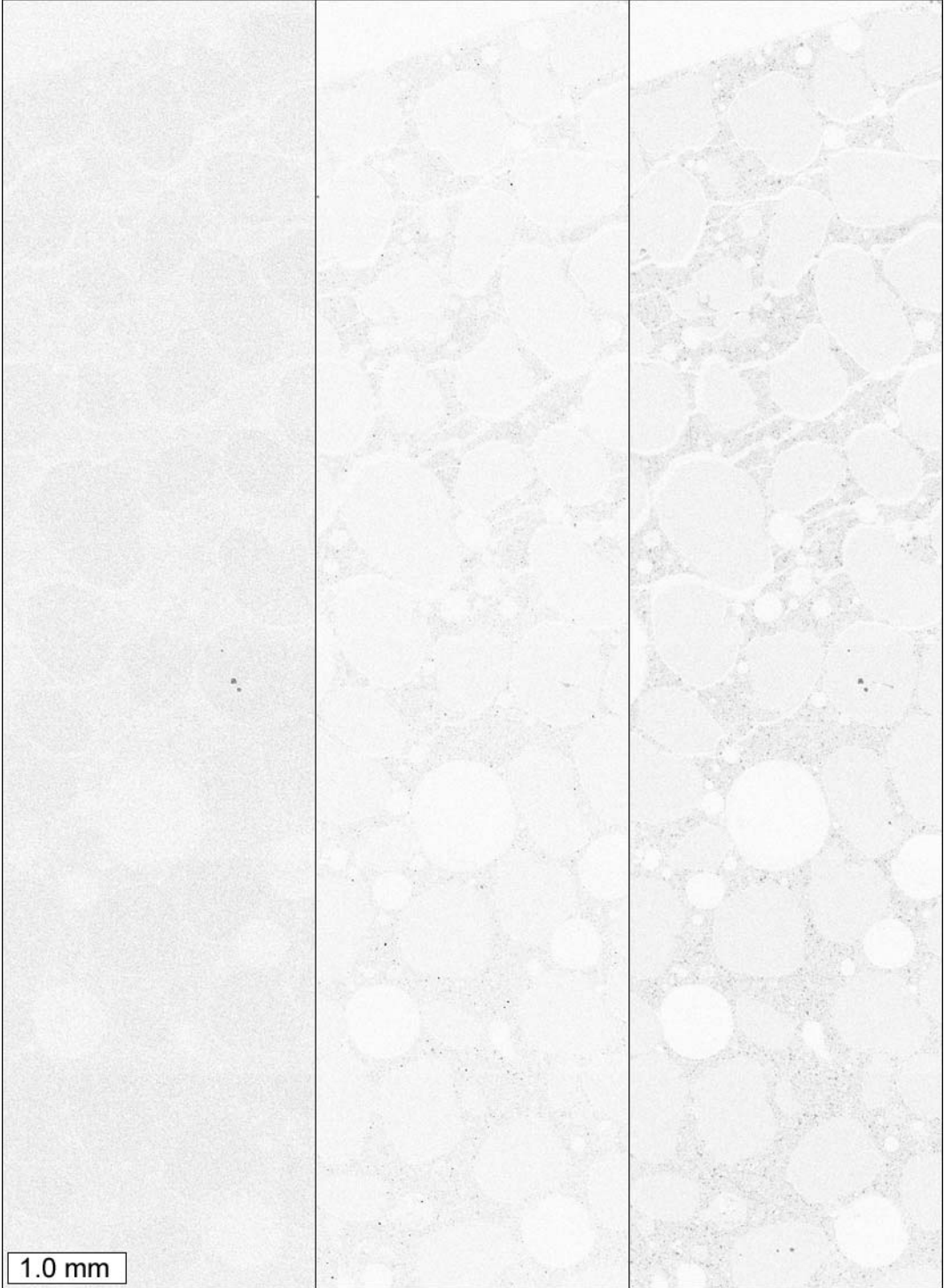


Figure 3.91: Elemental maps, from left to right: sodium, magnesium, and aluminum. The elemental maps were collected from a thin section prepared from a cylinder immersed in calcium chloride solution.

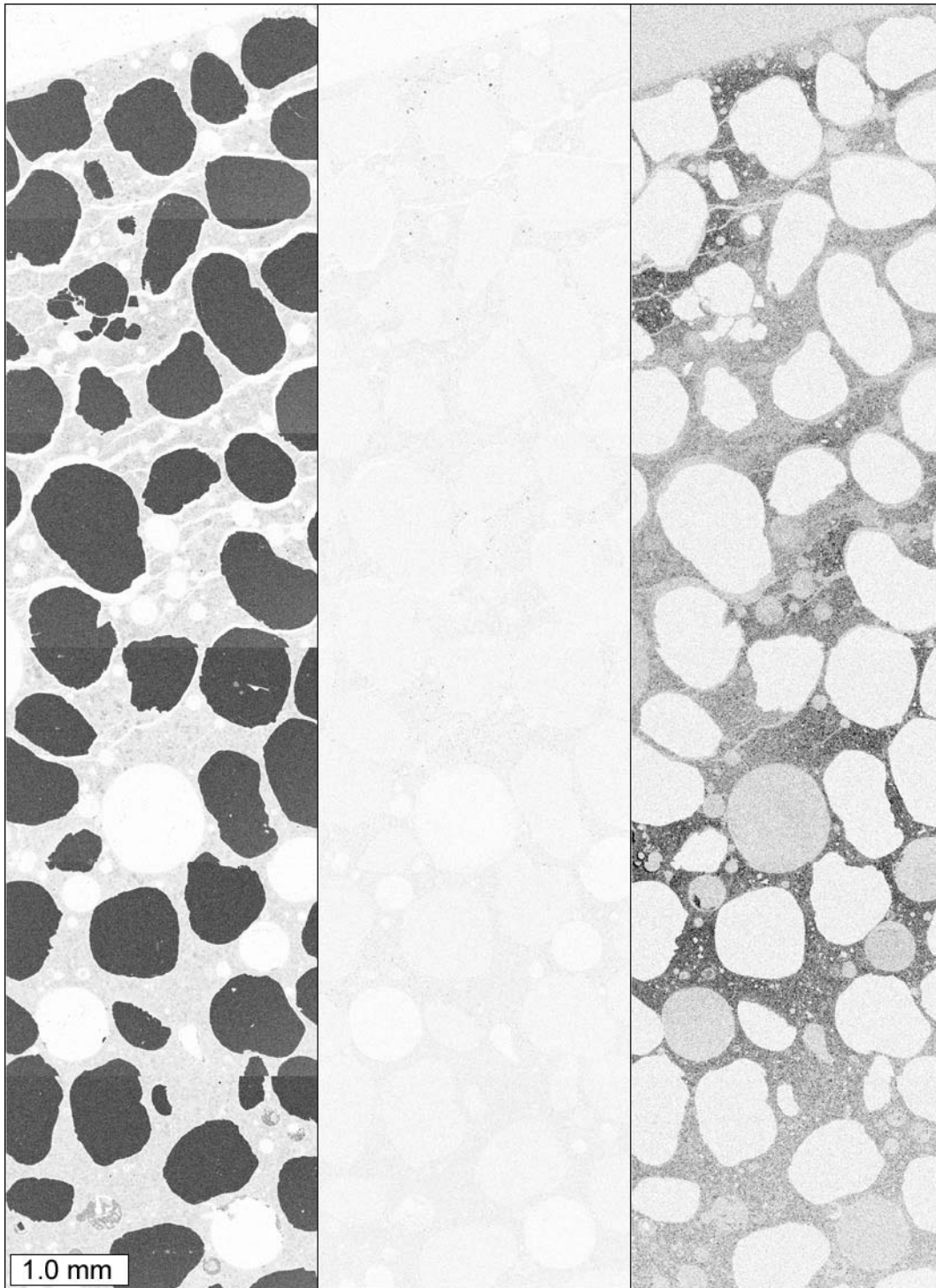


Figure 3.92: Elemental maps, from left to right: silicon, sulfur, and chlorine. The elemental maps were collected from a thin section prepared from a cylinder immersed in calcium chloride solution.

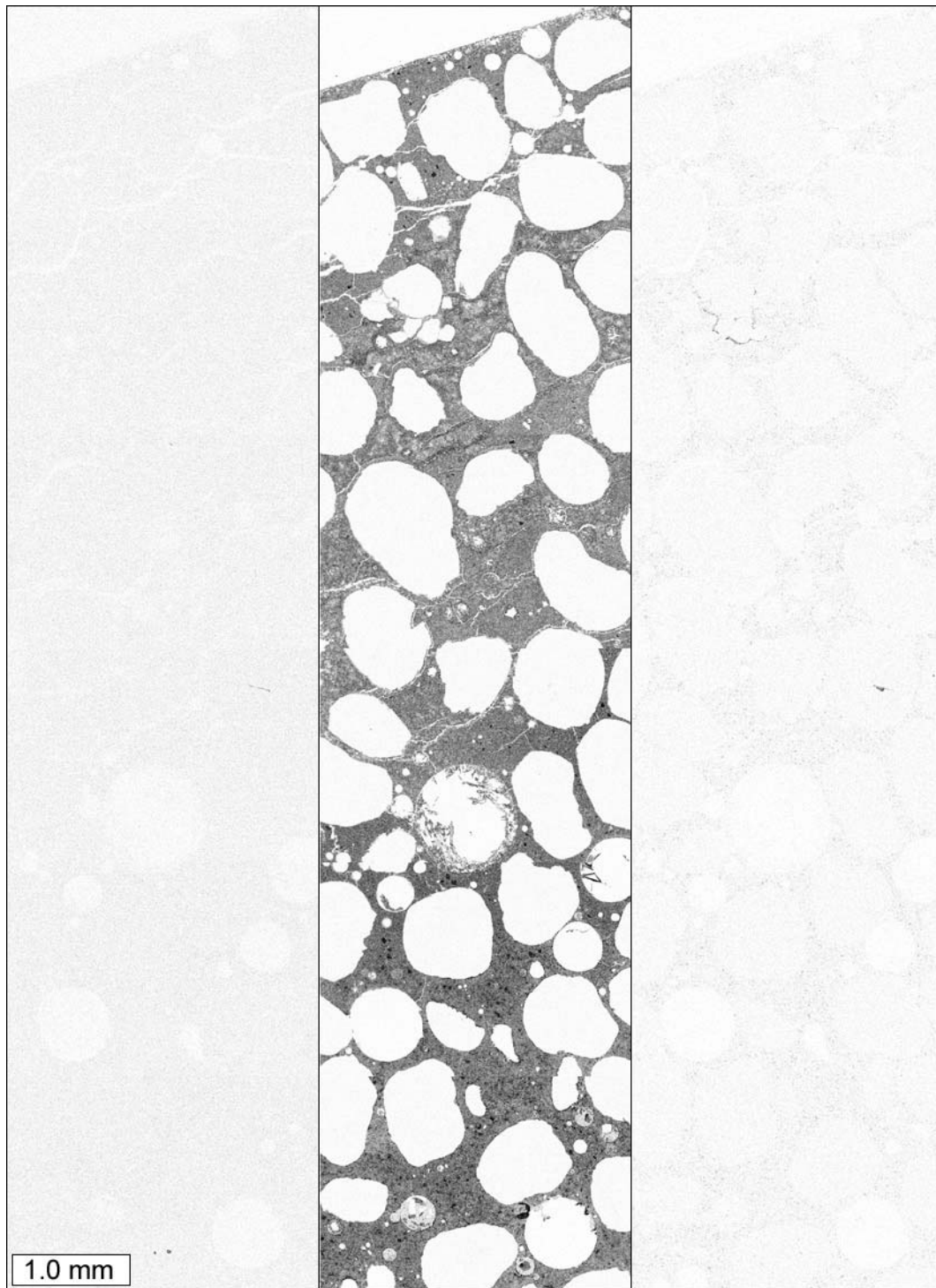


Figure 3.93: Elemental maps, from left to right: potassium, calcium, and iron. The elemental maps were collected from a thin section prepared from a cylinder immersed in calcium chloride solution.

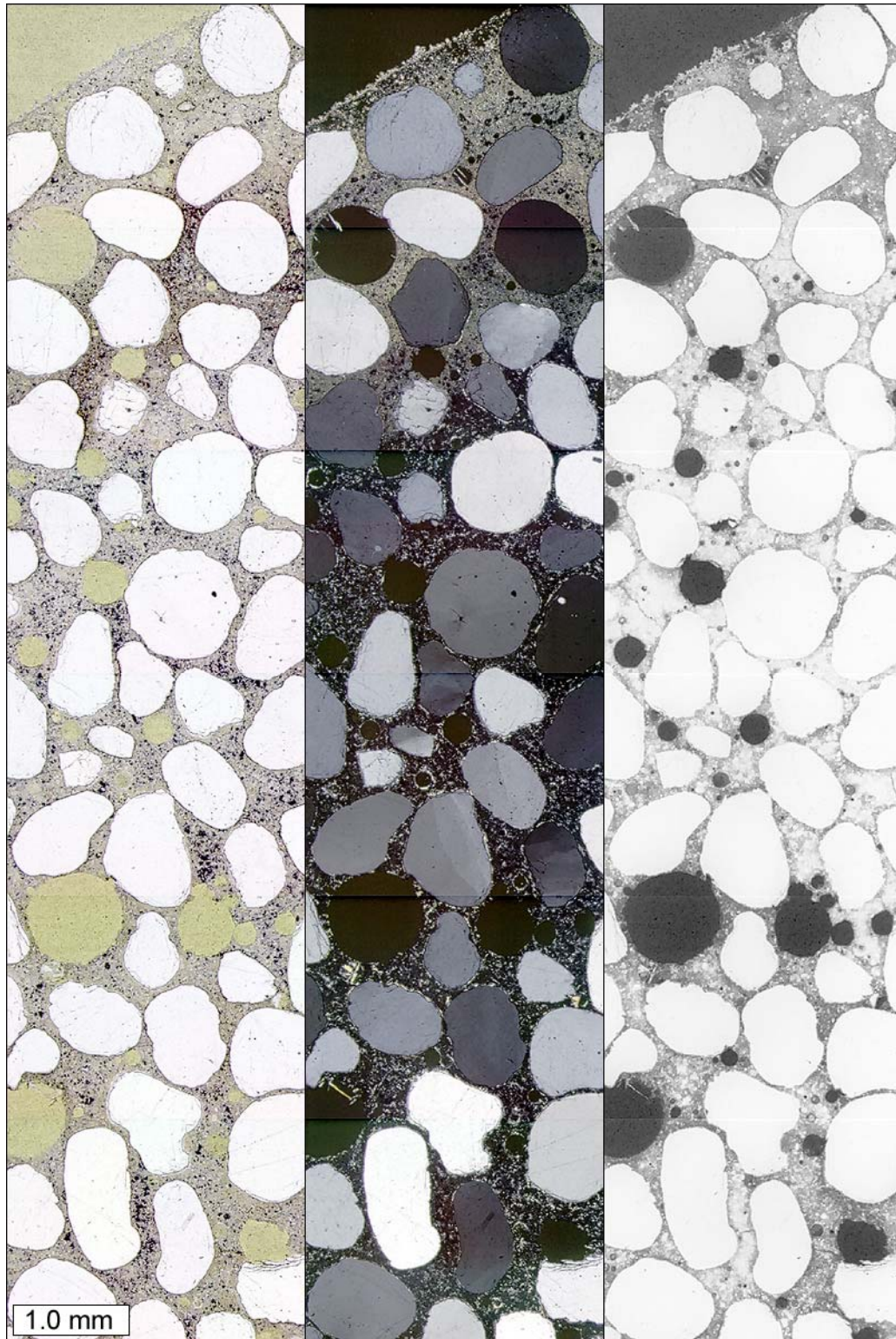


Figure 3.94: From left to right: plane polarized light, cross polarized light, and epifluorescent mode images of a thin section prepared from a cylinder immersed in sodium chloride solution.

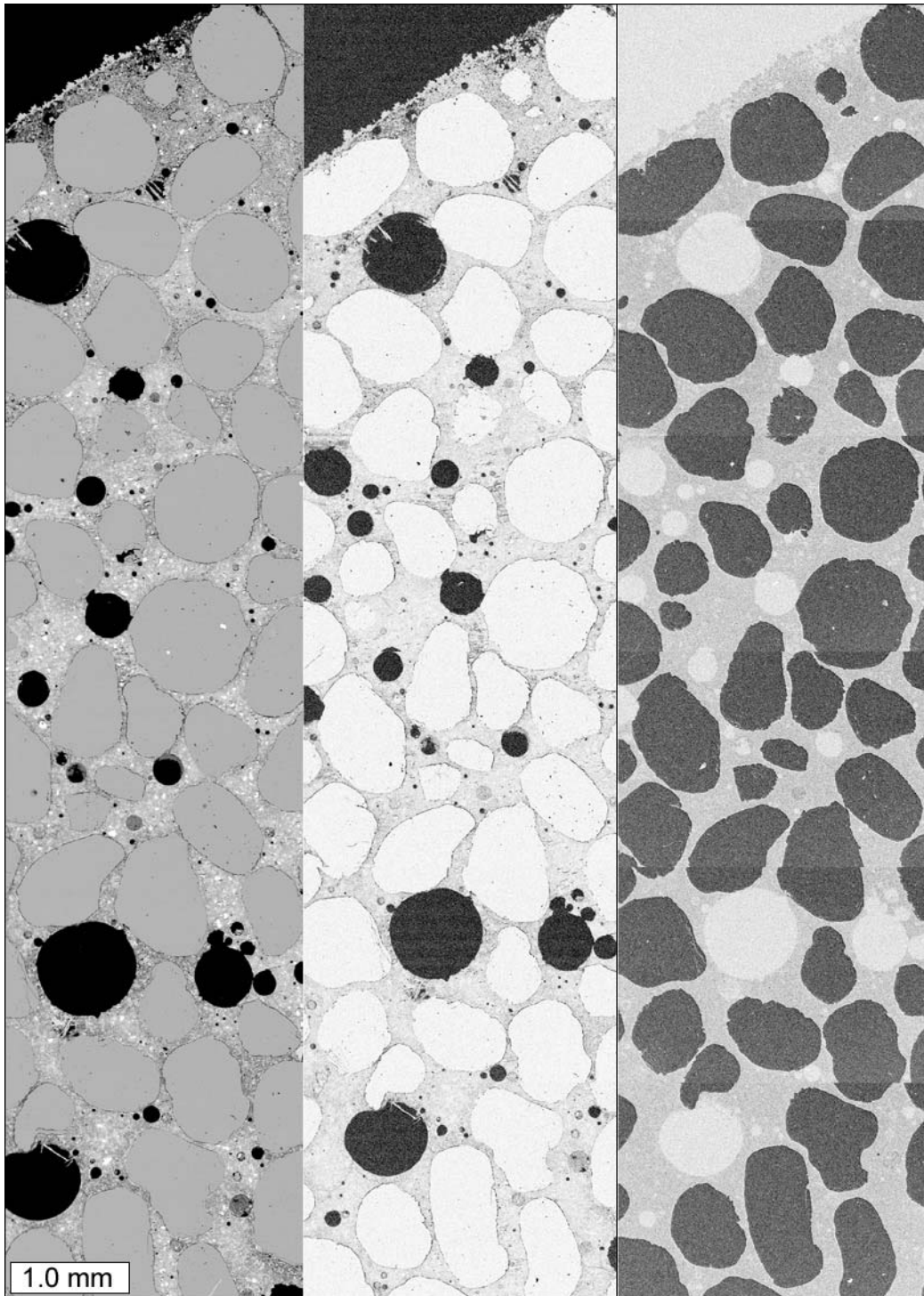


Figure 3.95: From left to right: back scattered electron image, elemental map for carbon, and elemental map for oxygen. Images were collected from a thin section prepared from a cylinder immersed in sodium chloride solution.



Figure 3.96: Elemental maps, from left to right: sodium, magnesium, and aluminum. The elemental maps were collected from a thin section prepared from a cylinder immersed in sodium chloride solution.

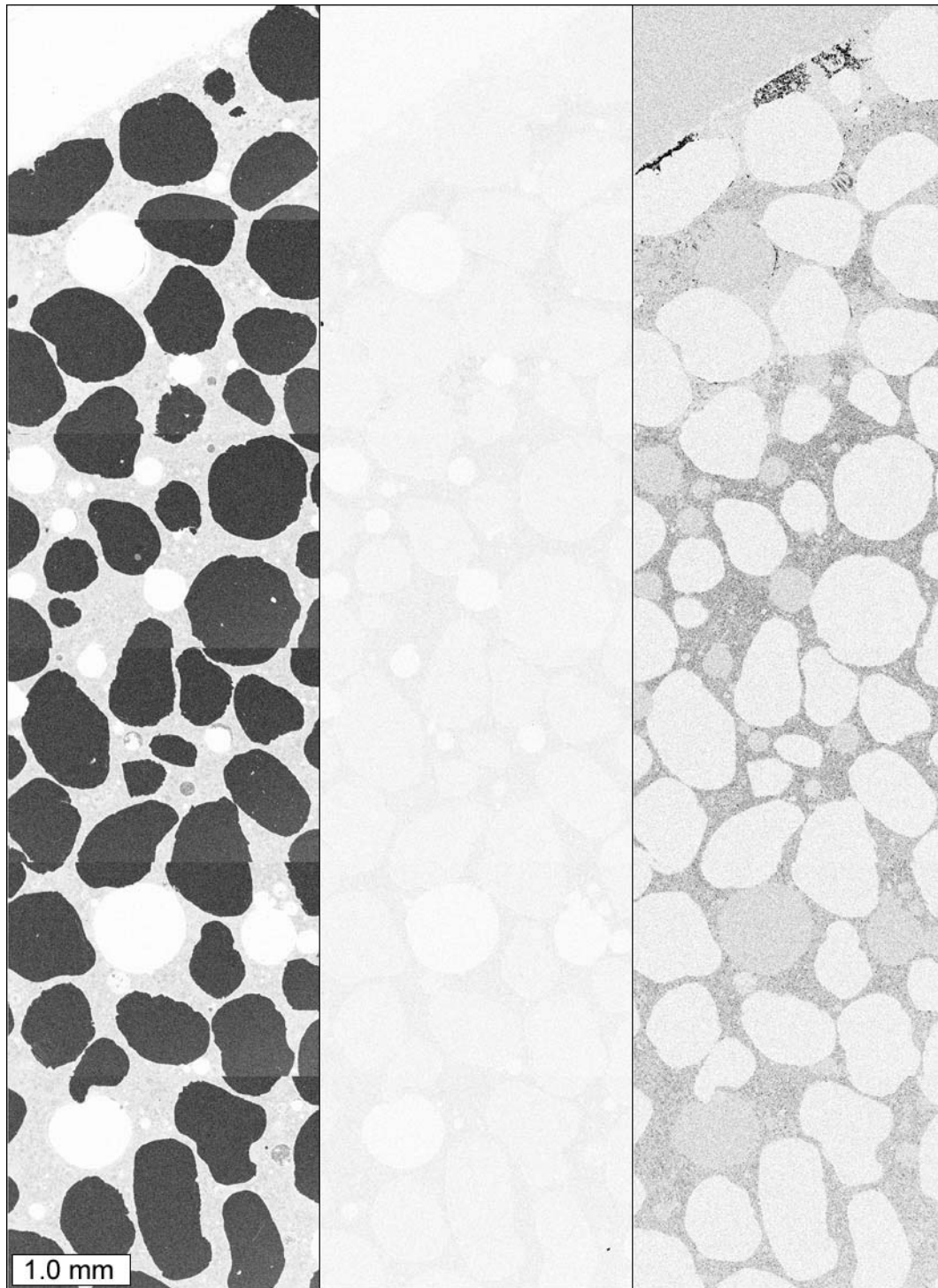


Figure 3.97: Elemental maps, from left to right: silicon, sulfur, and chlorine. The elemental maps were collected from a thin section prepared from a cylinder immersed in sodium chloride solution.

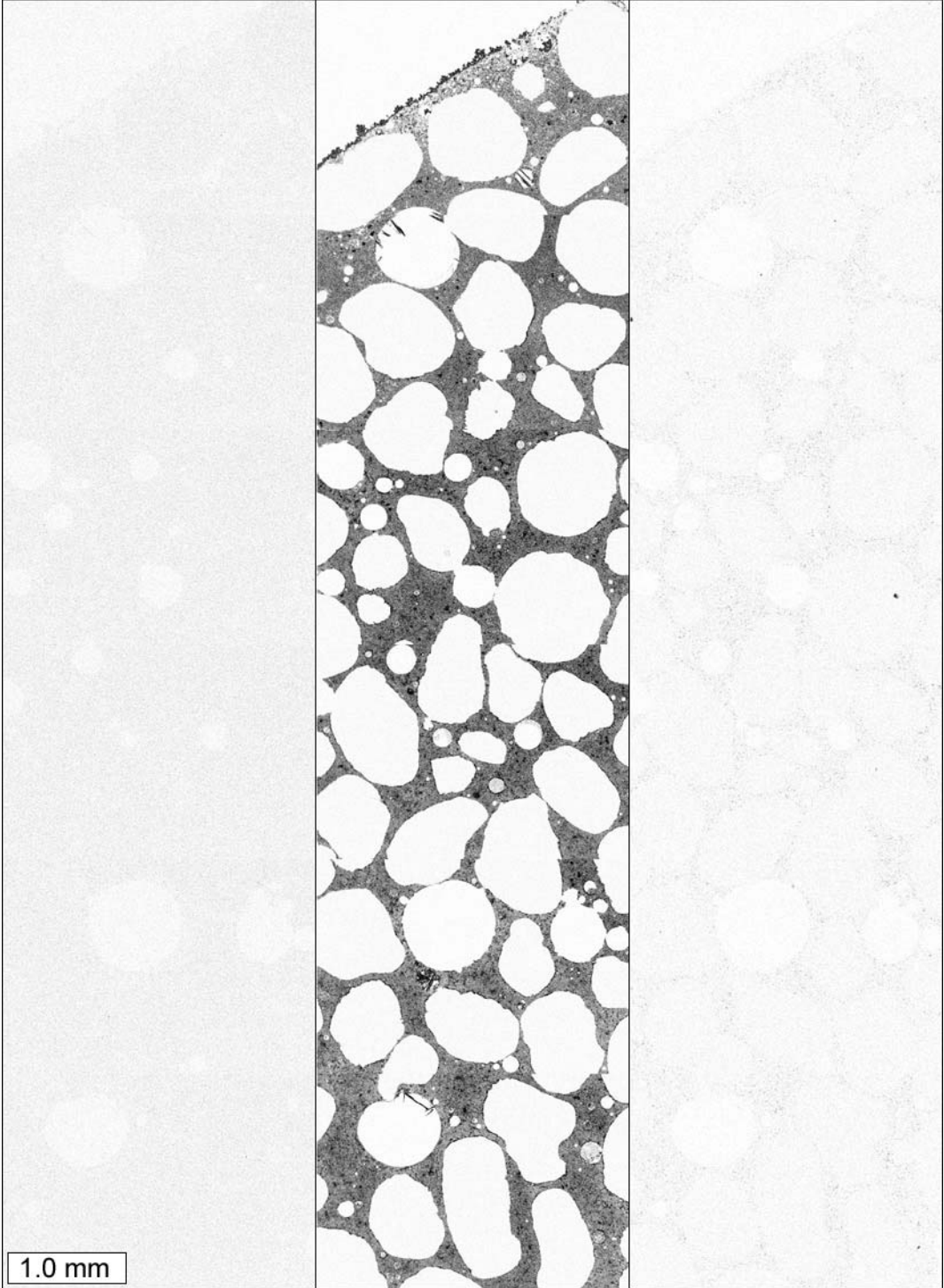


Figure 3.98: Elemental maps, from left to right: potassium, calcium, and iron. The elemental maps were collected from a thin section prepared from a cylinder immersed in sodium chloride solution.



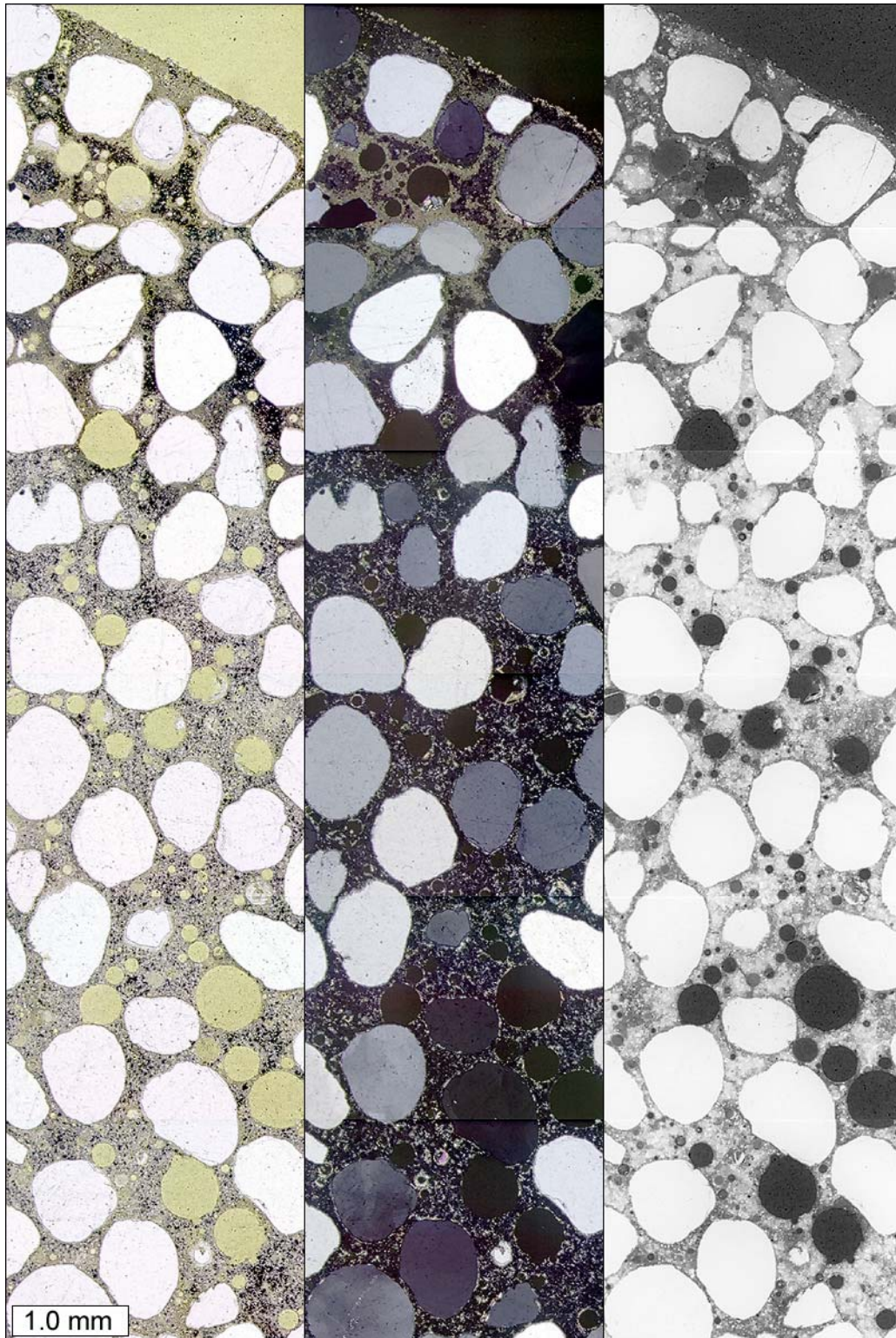


Figure 3.99: From left to right: plane polarized light, cross polarized light, and epifluorescent mode images of a thin section prepared from a cylinder immersed in calcium magnesium acetate solution.

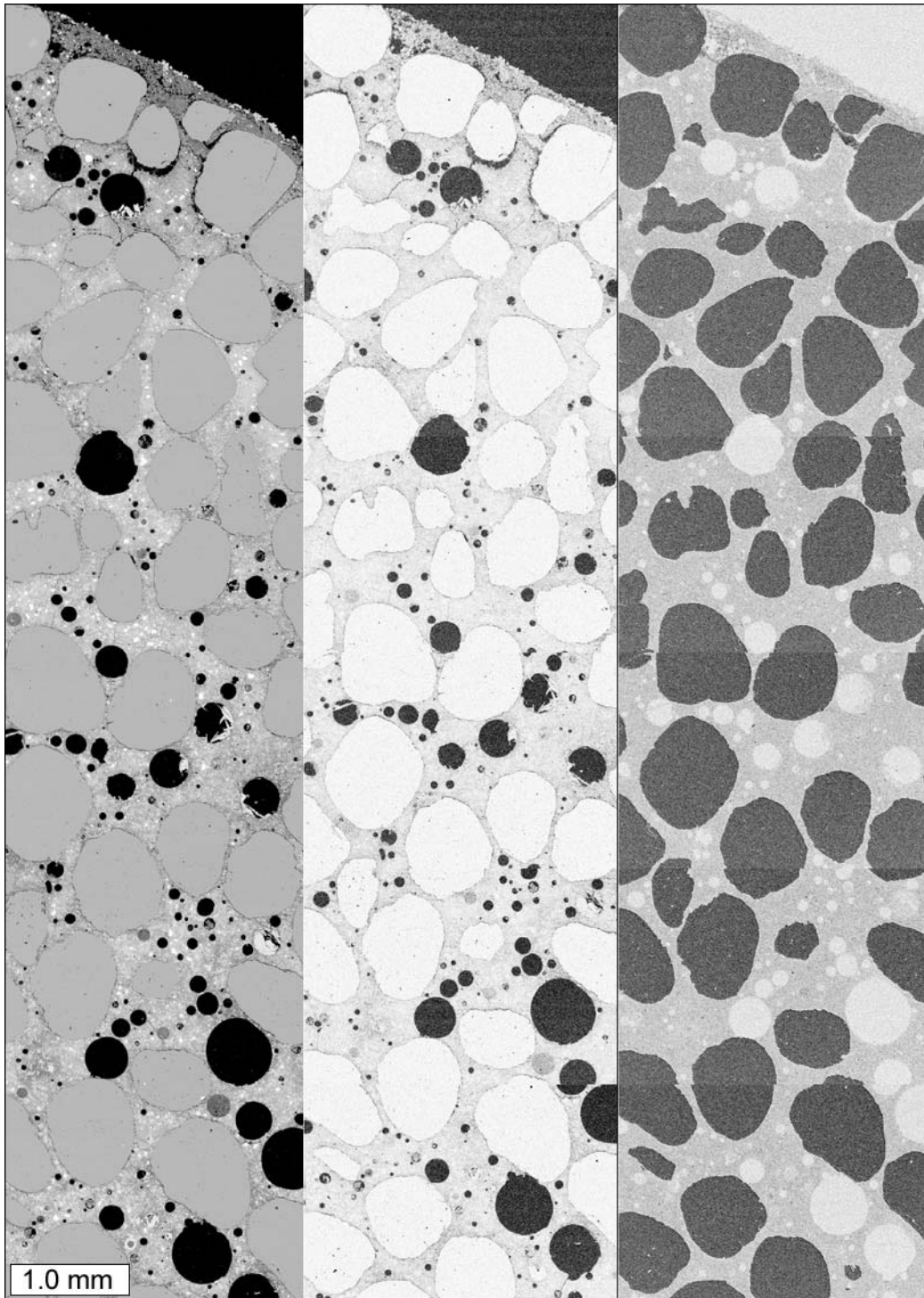


Figure 3.100: From left to right: back scattered electron image, elemental map for carbon, and elemental map for oxygen. Images were collected from a thin section prepared from a cylinder immersed in calcium magnesium acetate solution.

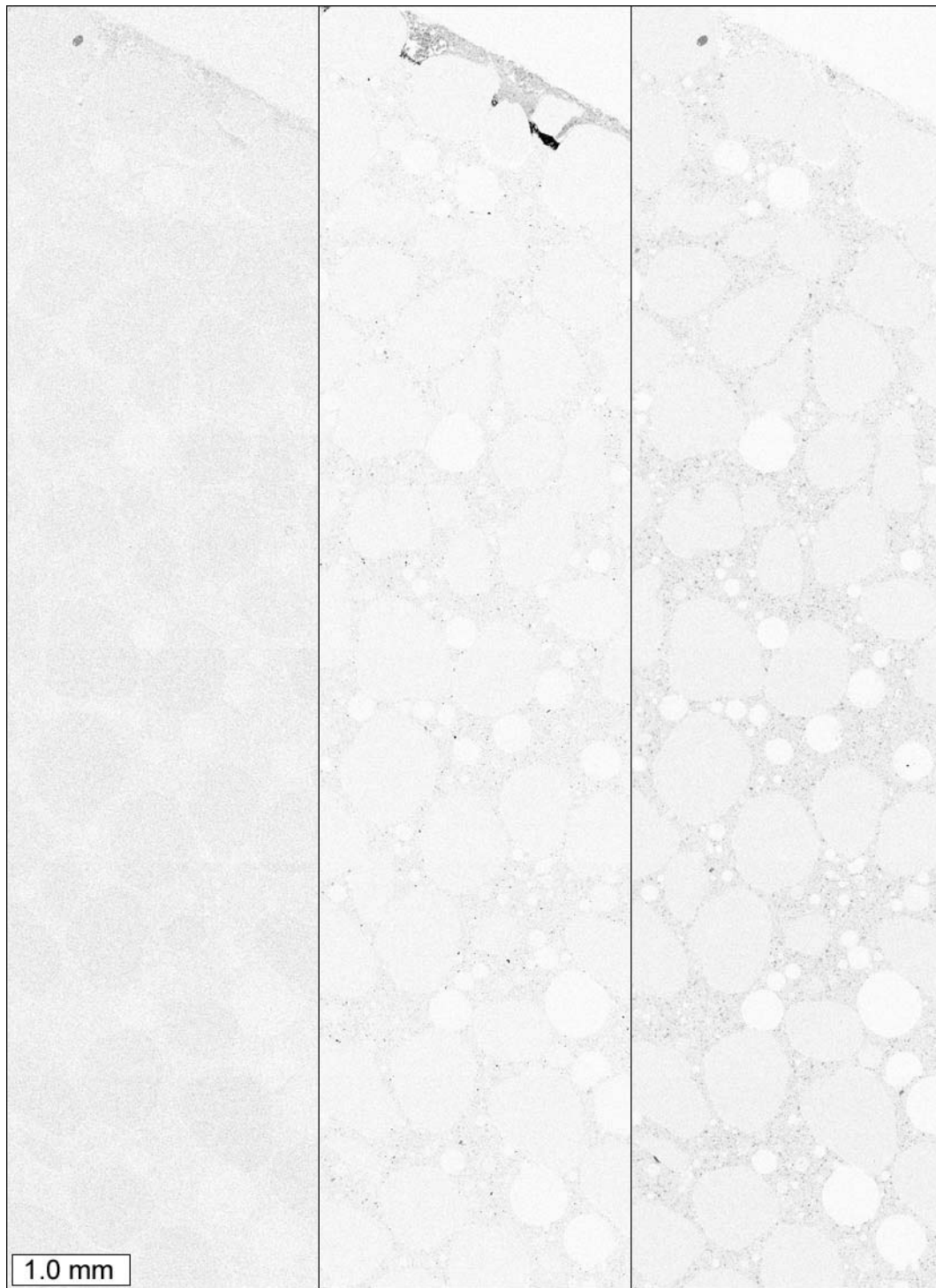


Figure 3.101: Elemental maps, from left to right: sodium, magnesium, and aluminum. The elemental maps were collected from a thin section prepared from a cylinder immersed in calcium magnesium acetate solution.

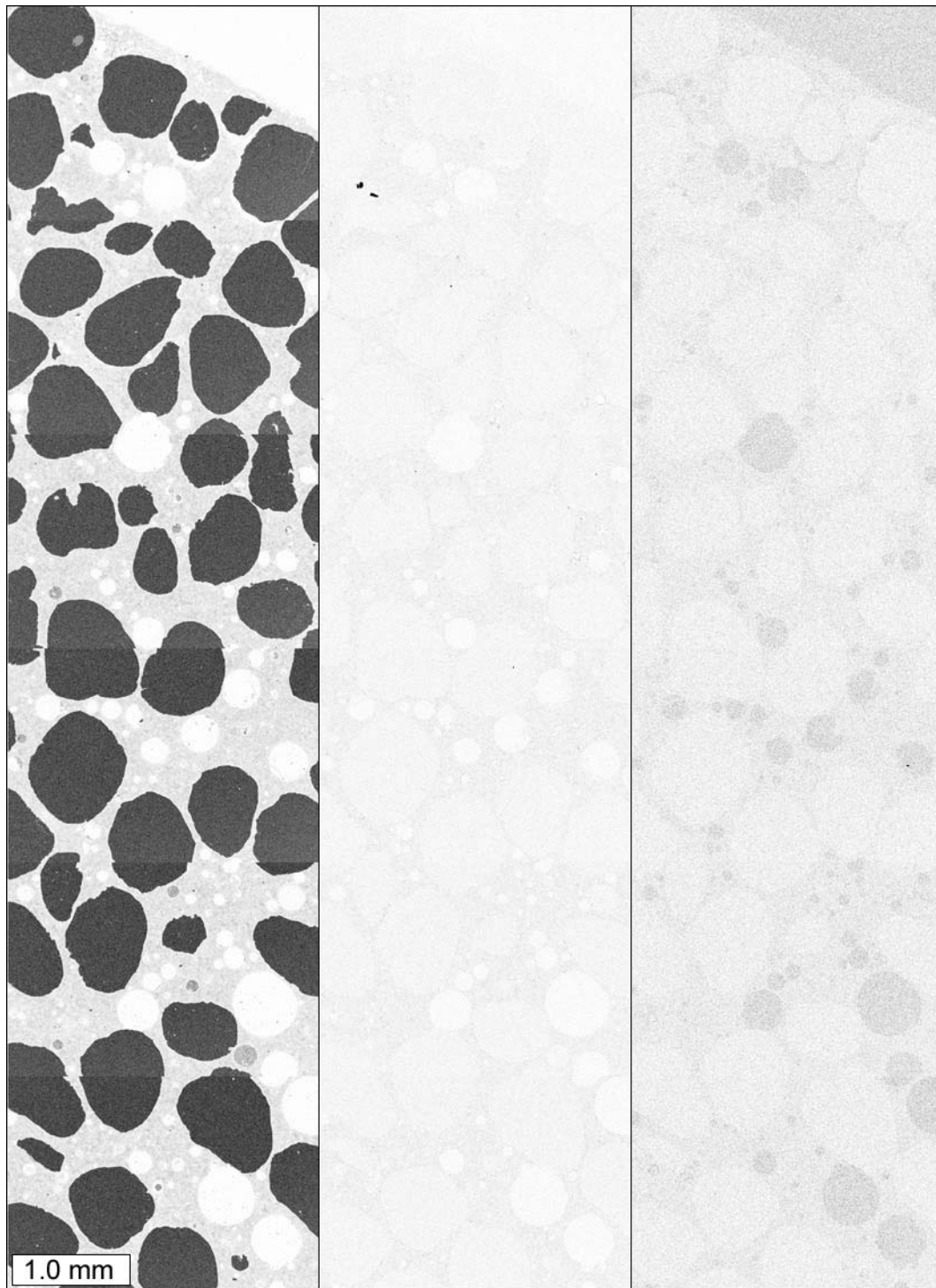


Figure 3.102: Elemental maps, from left to right: silicon, sulfur, and chlorine. The elemental maps were collected from a thin section prepared from a cylinder immersed in calcium magnesium acetate solution.

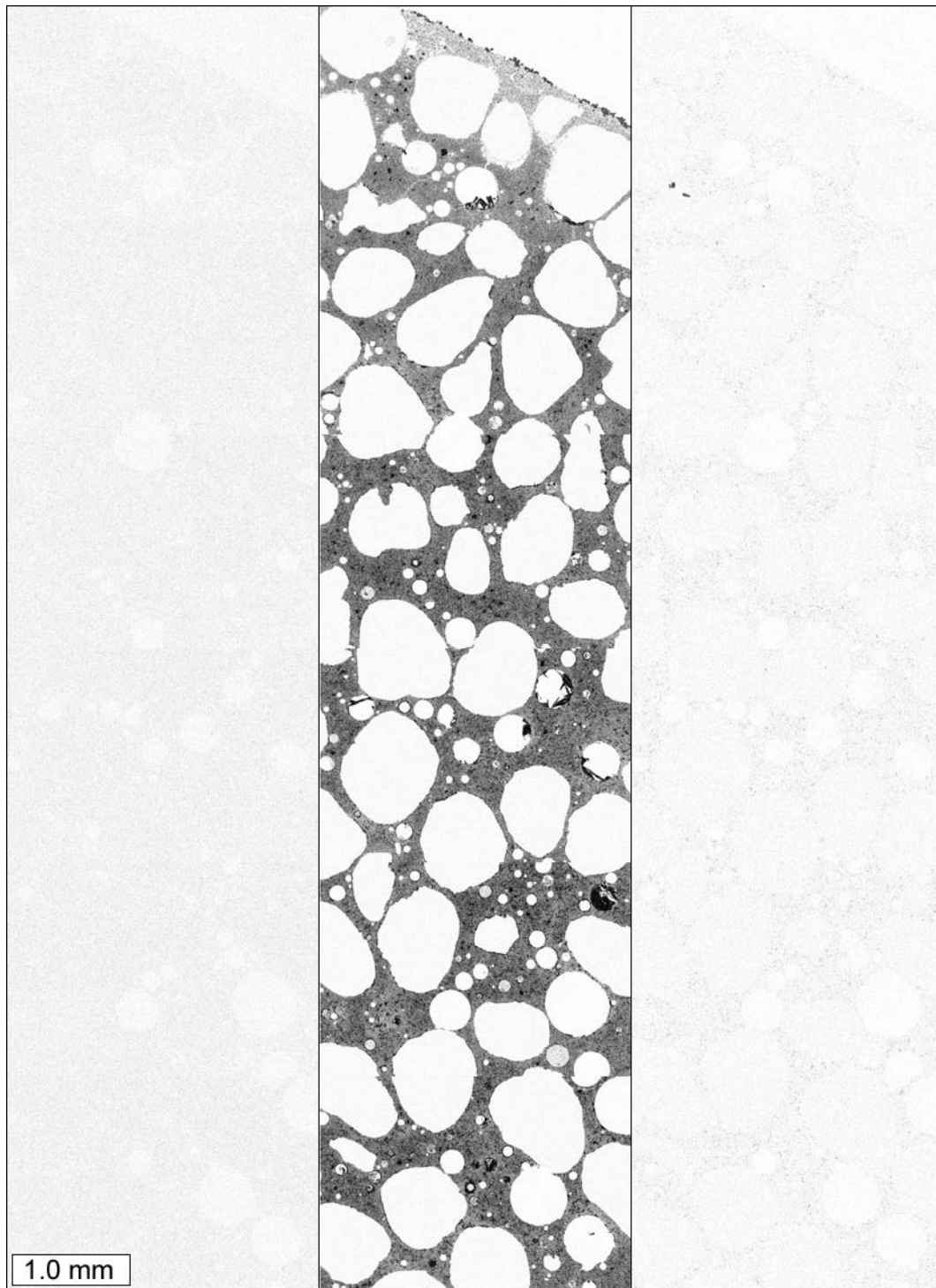


Figure 3.103: Elemental maps, from left to right: potassium, calcium, and iron. The elemental maps were collected from a thin section prepared from a cylinder immersed in calcium magnesium acetate solution.

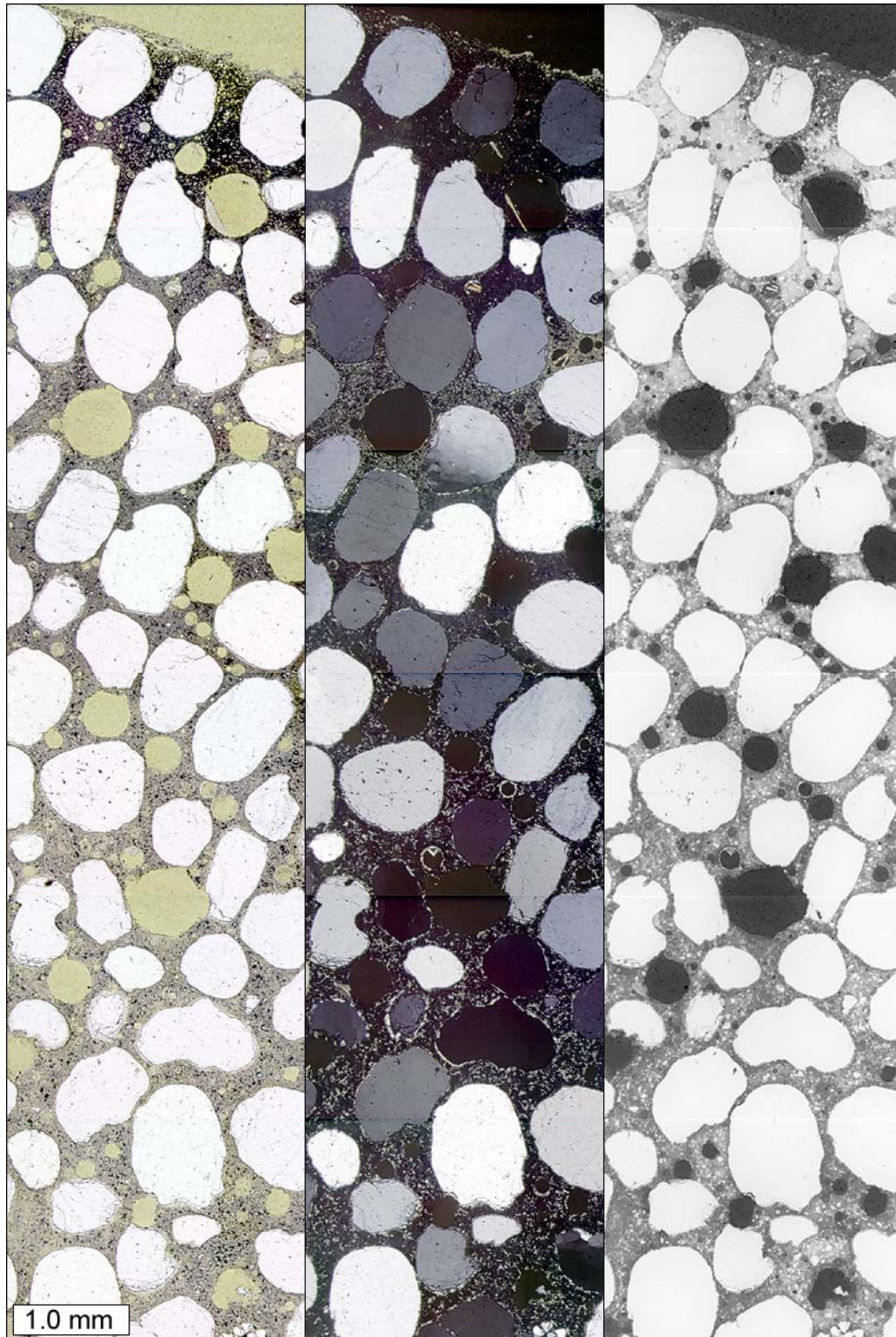


Figure 3.104: From left to right: plane polarized light, cross polarized light, and epifluorescent mode images of a thin section prepared from a cylinder immersed in lime water .

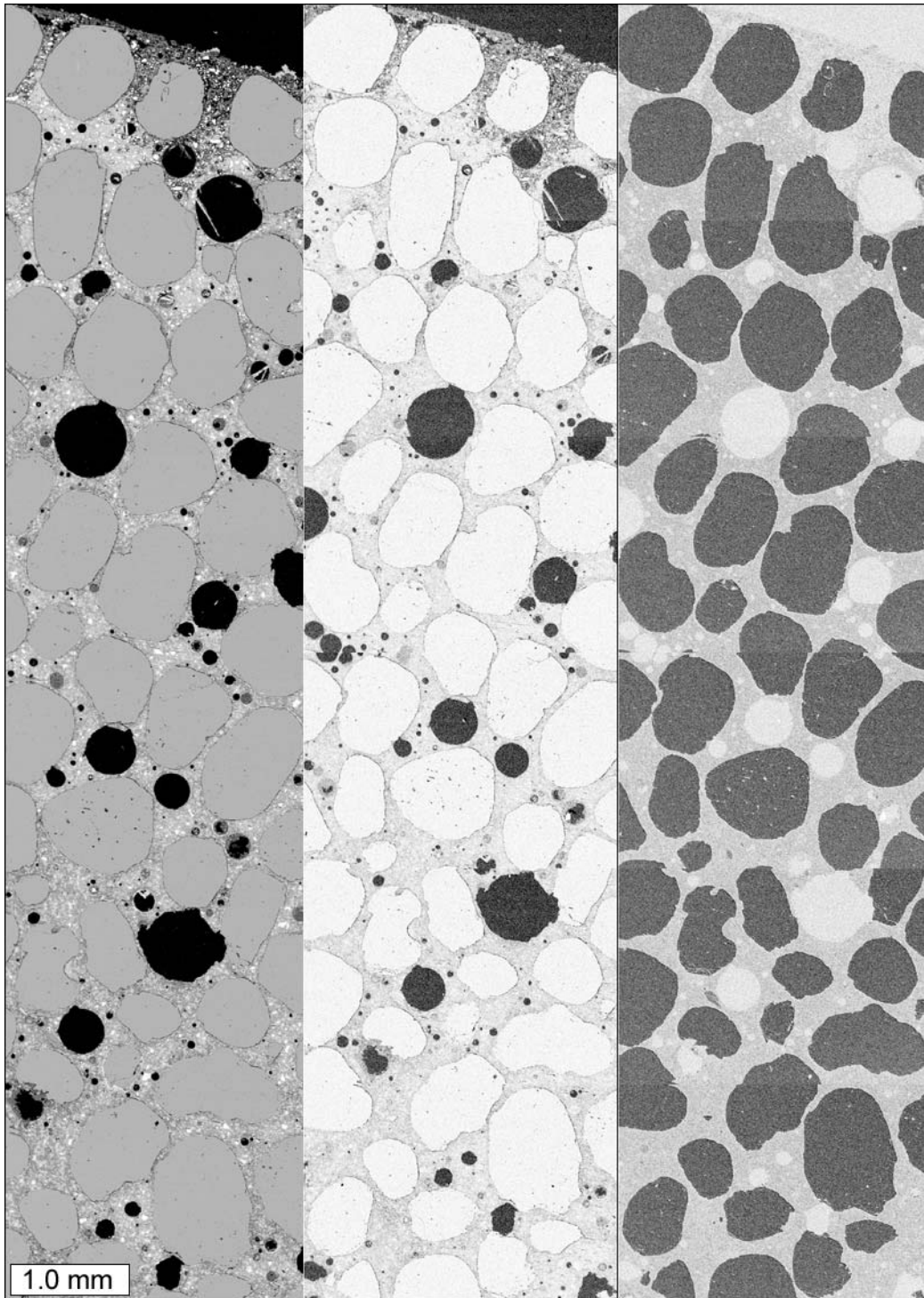


Figure 3.105: From left to right: back scattered electron image, elemental map for carbon, and elemental map for oxygen. Images were collected from a thin section prepared from a cylinder immersed in lime water .

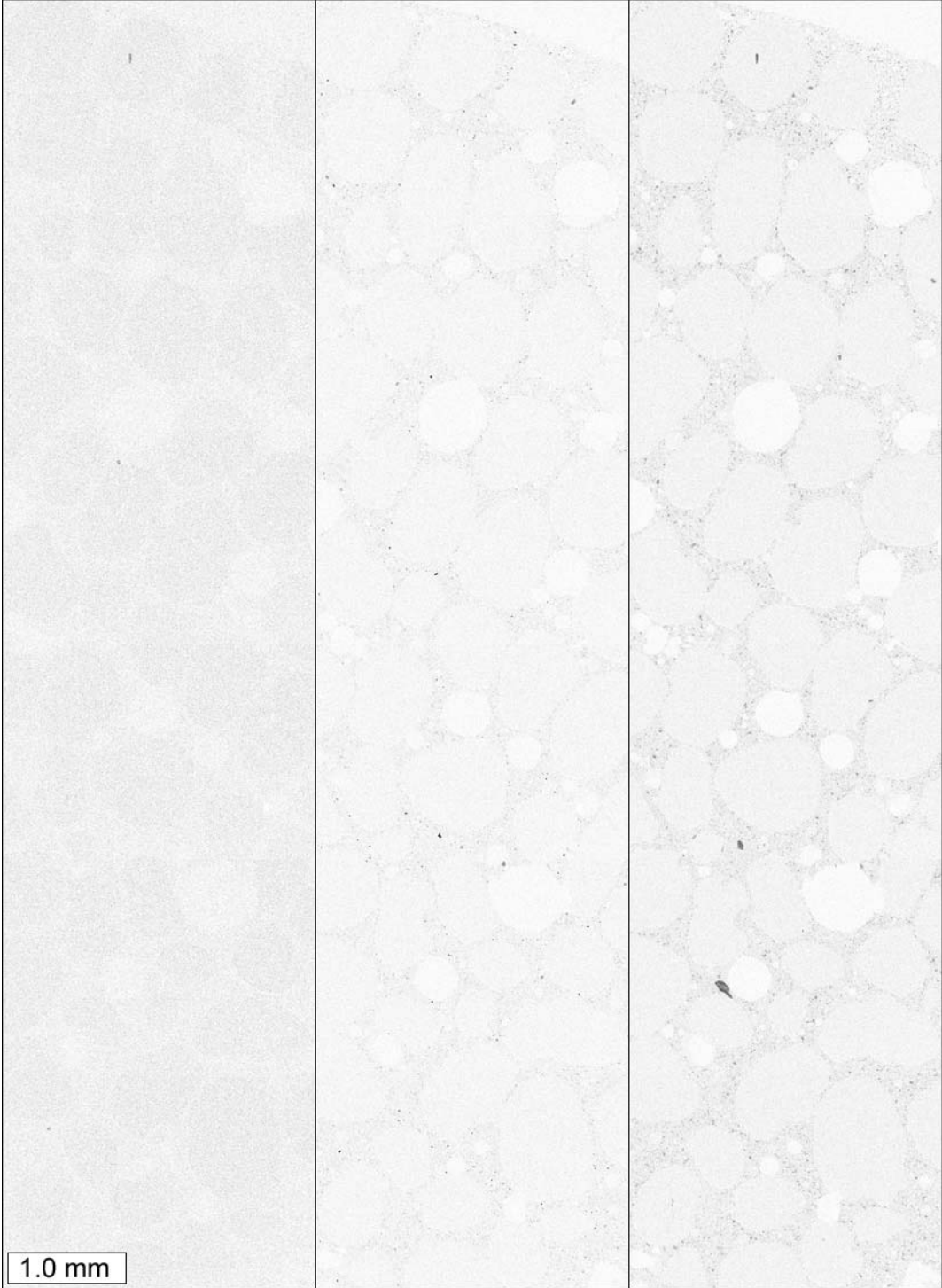


Figure 3.106: Elemental maps, from left to right: sodium, magnesium, and aluminum. The elemental maps were collected from a thin section prepared from a cylinder immersed in lime water .



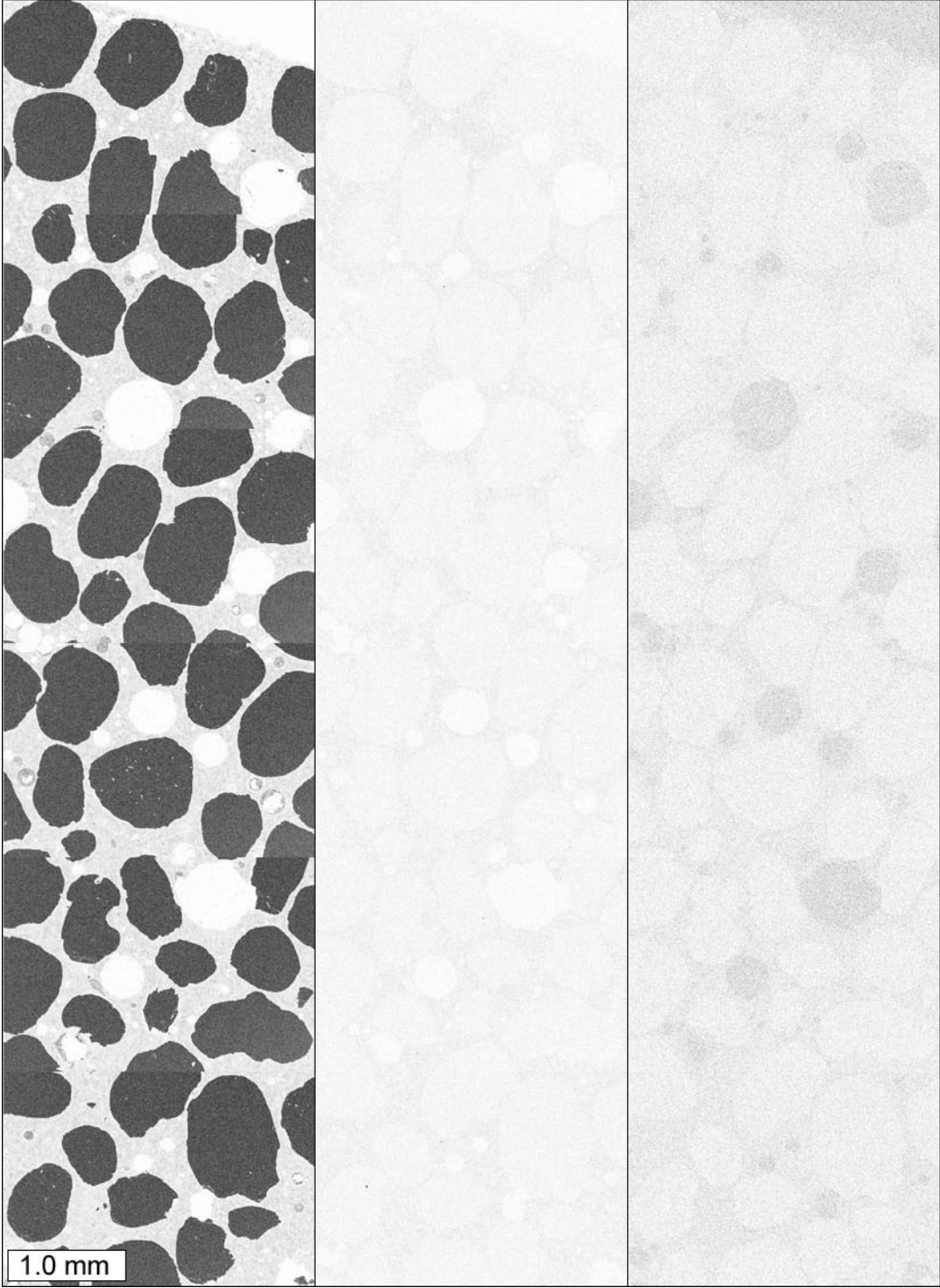


Figure 3.107: Elemental maps, from left to right: silicon, sulfur, and chlorine. The elemental maps were collected from a thin section prepared from a cylinder immersed in lime water .

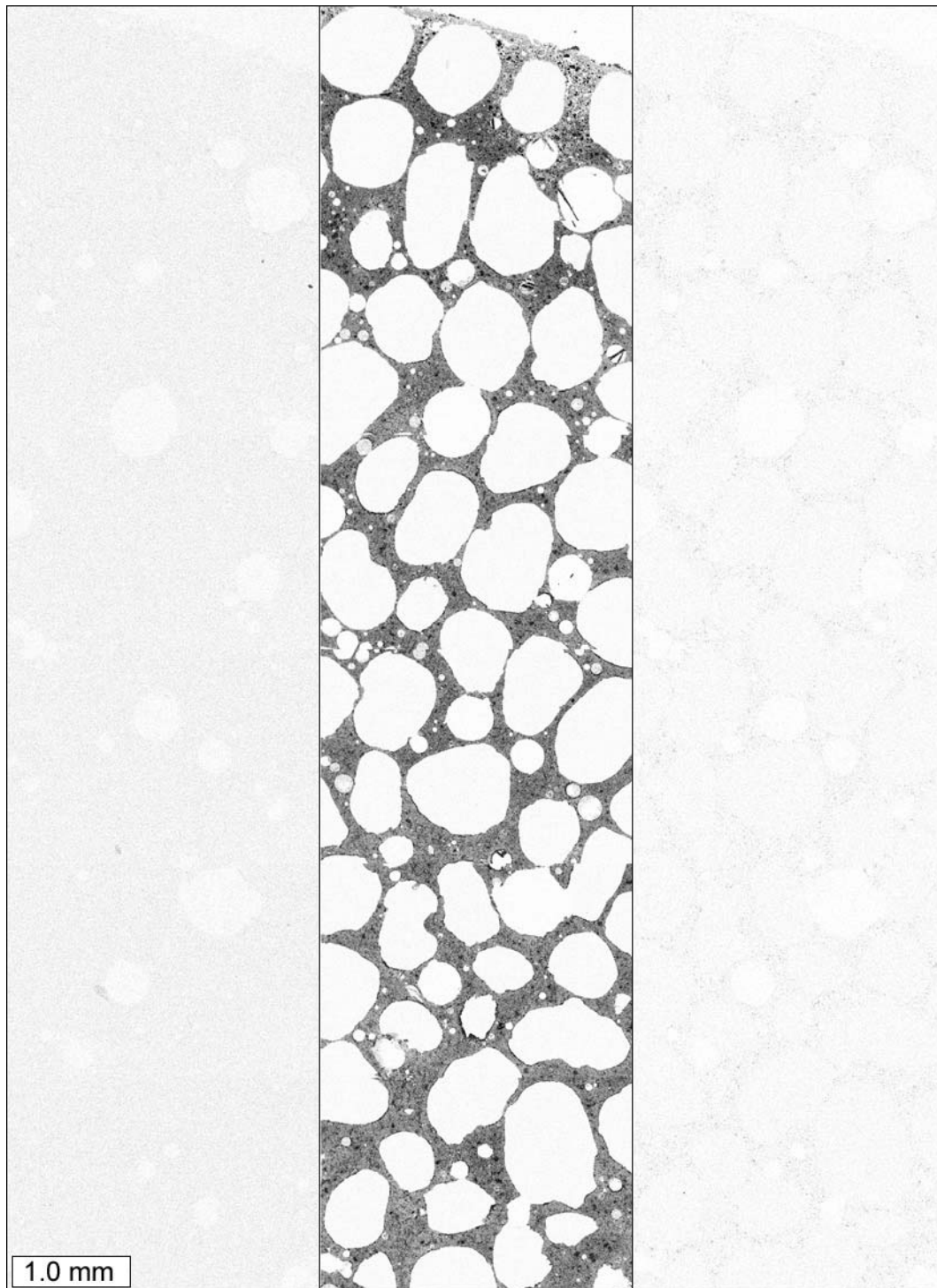


Figure 3.108: Elemental maps, from left to right: potassium, calcium, and iron. The elemental maps were collected from a thin section prepared from a cylinder immersed in lime water .

### 3.2.8 High Temperature Experiment

#### 3.2.8.1 Observations

The constant high temperature experiment was run in the same manner as the constant low temperature experiment, but at an elevated temperature of 135 °F. At 84 days the cylinders in the NaCl solutions showed no distress, as shown in Figures 3.109. The cylinders in the MgCl<sub>2</sub> solution began to show some cracking at 84 days, as shown in Figure 3.110. Figure 3.111 shows the CaCl<sub>2</sub> specimens after 84 days and no visible signs of distress are present. As shown in Figure 3.112, the cylinders in the CMA solution began to disintegrate after 28 days. It was decided to abort the CMA test at 28 days. At 84 days, the control samples in lime water were still unaffected as shown in Figure 3.113. Table 3.16 summarizes the visual ratings for the cylinders over time for all the control lime water and deicer solution exposure tests.



Figure 3.109. Cylinders exposed to NaCl solution after 84 days of constant high temperature test. From left to right: 0.40, 0.50, and 0.60 w/c mortar cylinders.



Figure 3.110. Cylinders exposed to  $MgCl_2$  solution after 84 days of constant high temperature test. From left to right: 0.40, 0.50, and 0.60 w/c mortar cylinders.



Figure 3.111. Cylinders exposed to  $CaCl_2$  solution after 84 days of constant high temperature test. From left to right: 0.40, 0.50, and 0.60 w/c mortar cylinders.



Figure 3.112. Cylinders exposed to CMA solution after 28 days of constant high temperature test. From left to right: 0.40, 0.50, and 0.60 w/c mortar cylinders.



Figure 3.113. Control cylinders exposed to lime solution after 84 days of constant high temperature test. From left to right: 0.40, 0.50, and 0.60 w/c mortar cylinders.

Table 3.16 List of visual ratings for all mortar cylinders from the high temperature tests. Rating Scale: 0 - no visible change, 1 – some cracking, 2 - visible expansion and cracking, 3 - severe expansion and cracking, 4 - partial disintegration, 5 - total disintegration, x – test aborted.

Solution	Time in Days											
	w/c = 0/40				w/c = 0/50				w/c = 0/60			
	8	28	56	84	8	28	56	84	8	28	56	84
Lime Water	-	0	0	0	-	0	0	0	-	0	0	0
MgCl <sub>2</sub>	-	0	0	0	-	0	0	0-1	-	0	0	0-1
CaCl <sub>2</sub>	-	0	0	0	-	0	0	0	-	0	0	0
NaCl	-	0	0	0	-	0	0	0	-	0	0	0
CMA	-	4	x	x	-	4	x	x	-	4	x	x

### 3.2.8.2 Split Tensile Strength Testing

Split tensile testing has not been performed on these specimens. Given the turns that these experiments took, it does not seem prudent to invest resources in testing these specimens at this time.

### 3.2.8.3 Petrographic Analysis

The cylinders immersed at constant high temperature showed no external signs of deterioration after 84 days for any of the solutions, with the exception of the cylinders immersed in the calcium magnesium acetate solution. After 28 days, the exteriors of the cylinders exposed to the calcium magnesium acetate solution began to disintegrate into what could be best described as a mushy gray mass. After removal from the solution, the cylinders developed translucent whisker-like crystals intermixed with the disintegrated mortar. Figure 3.114 shows the crystals intermixed with the disintegrated mortar. A small quantity of the crystals were scraped and collected for x-ray diffraction. Figure 3.115 shows the x-ray diffraction pattern from the crystals. The pattern provided a good match with calcium acetate hydrate. Some crystals were also examined with a scanning electron microscope. Figure 3.116 shows a secondary electron image of some of the crystals. Figure 3.117 shows an energy dispersive x-ray spectrum collected from a crystal with peaks for carbon, oxygen, and calcium. One of the 0.40 w/c cylinders was prepared in thin section. Figures 3.118, 3.119, and 3.120 show petrographic microscope images of a cross-section through the cylinder.

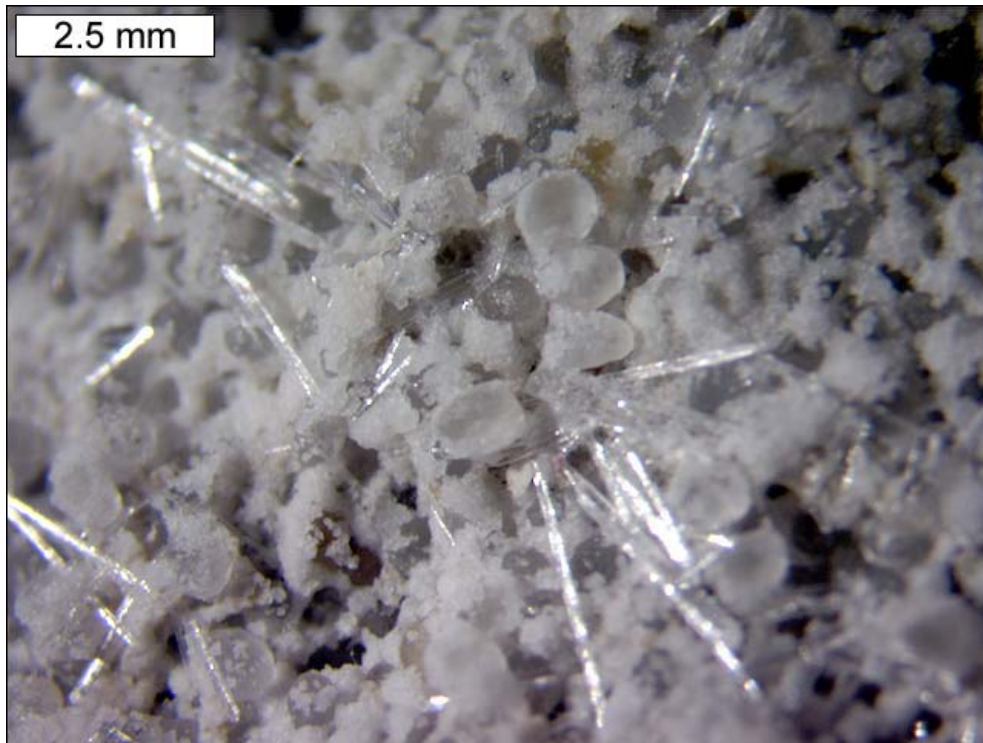


Figure 3.114: Stereomicroscope image of needles of translucent crystals on disintegrated mass of mortar.

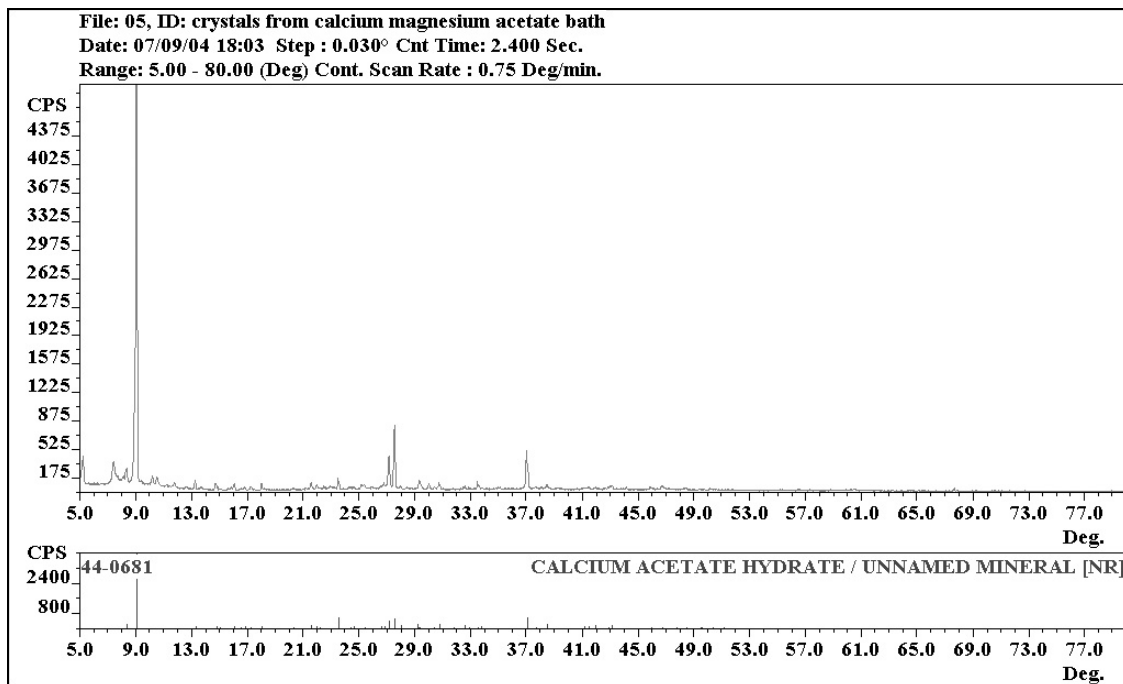


Figure 3.115: x-ray diffraction pattern showing match for calcium acetate hydrate.

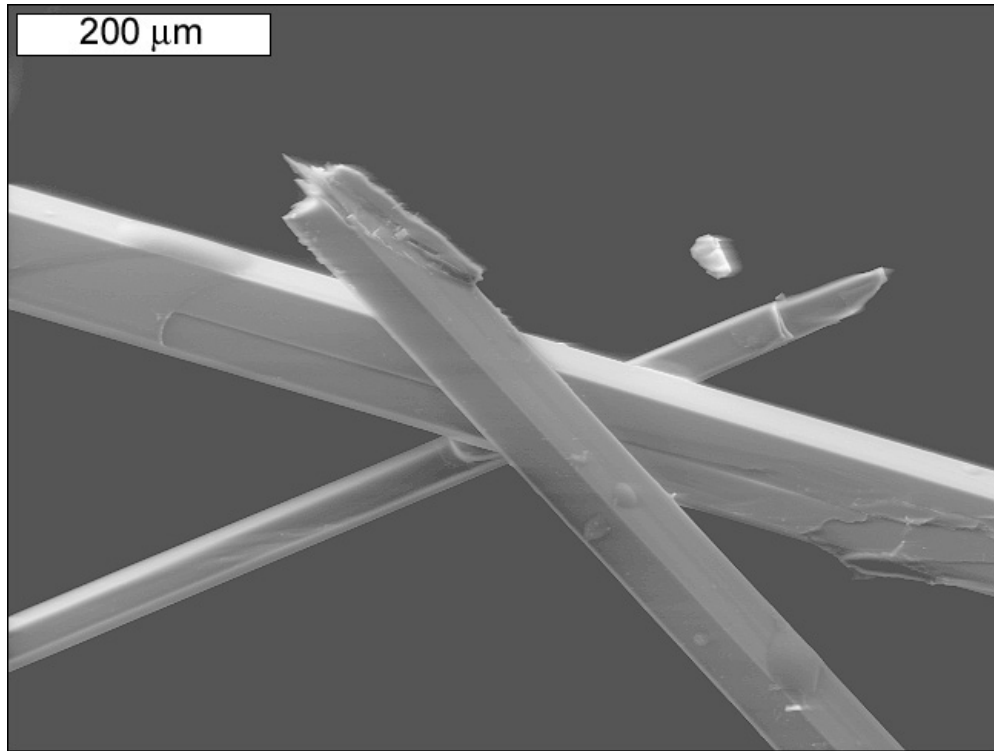


Figure 3.116: Secondary electron image of crystals plucked from disintegrated mortar.

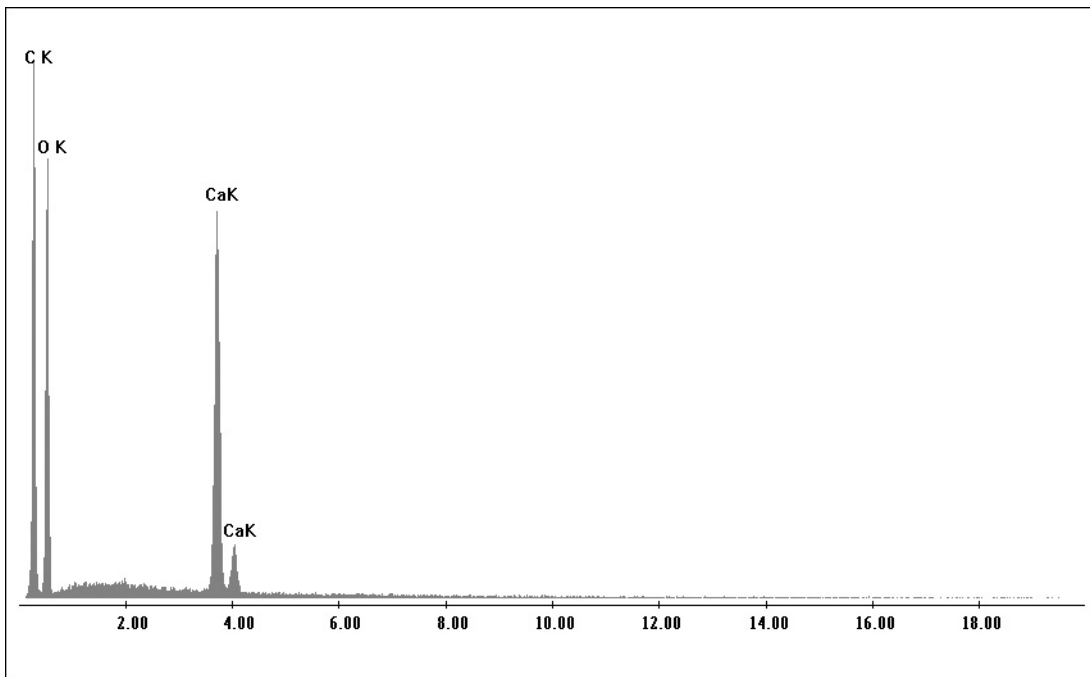


Figure 3.117: X-ray energy spectrum, (in units of kV) showing counts for carbon  $K\alpha$ , oxygen  $K\alpha$ , calcium  $K\alpha$ , and calcium  $K\beta$  x-rays, collected from crystals plucked from disintegrated mortar.



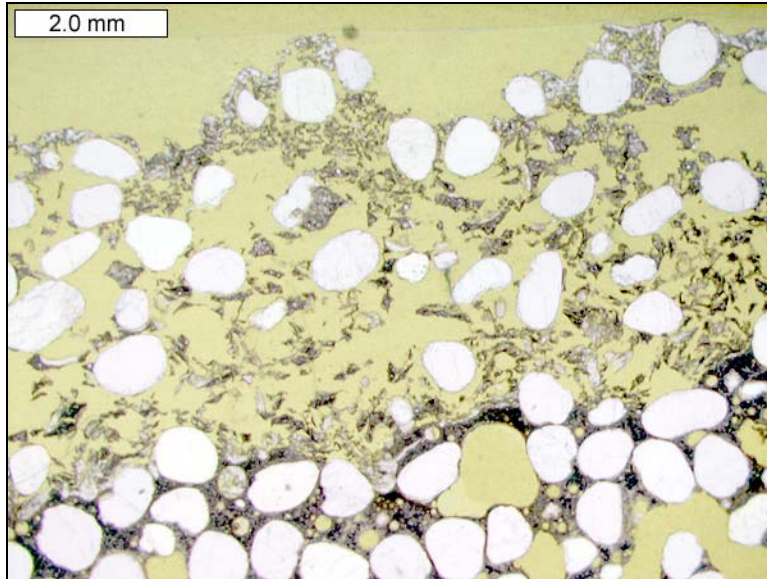


Figure 3.118: Petrographic microscope image, transmitted plane polarized light, of thin section prepared from cylinder from calcium magnesium acetate constant hot temperature experiment.

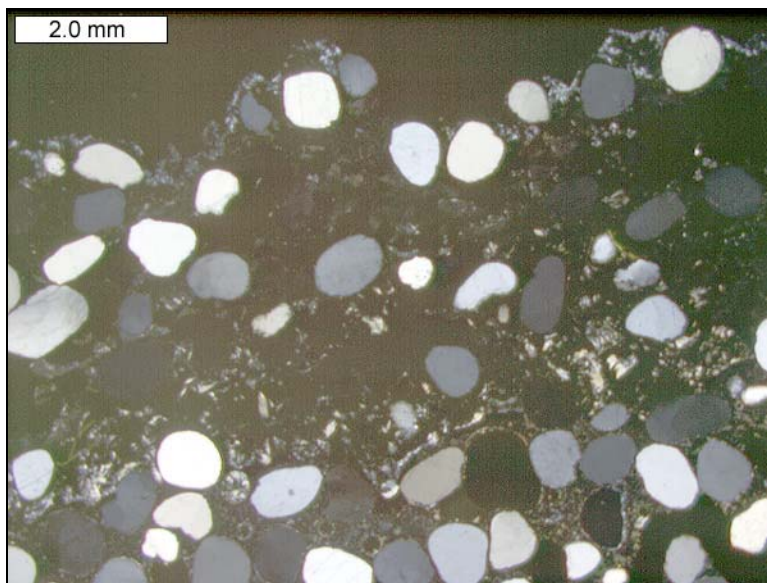


Figure 3.119: Petrographic microscope image, cross polarized light, of thin section prepared from cylinder from calcium magnesium acetate constant hot temperature experiment.

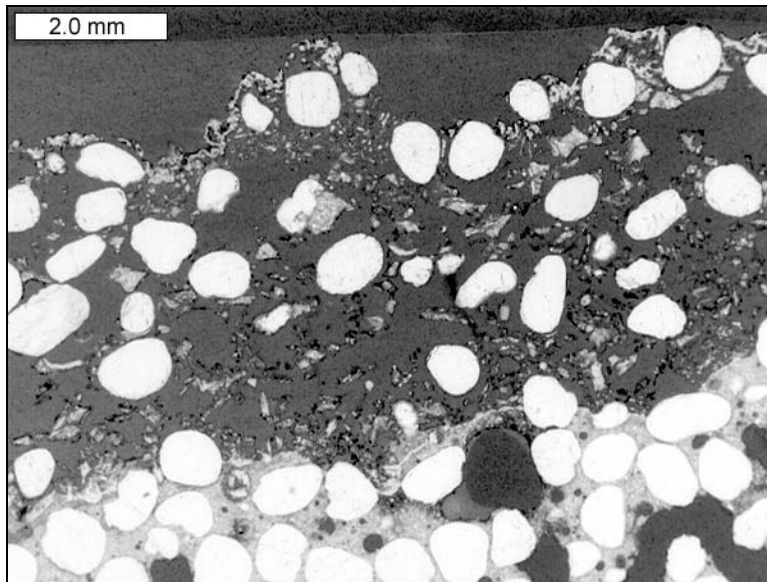


Figure 3.120: Petrographic microscope image, epifluorescent mode, of thin section prepared from cylinder from calcium magnesium acetate constant hot temperature experiment.

### 3.3 Phase I Additional Experiments

#### 3.3.1 Cyclical Temperature Experiments

##### 3.3.1.1 Additional Tests Performed

Given the rapid failure of specimens treated in NaCl solution, it was determined that some follow-on tests should be performed to establish why these specimens failed so dramatically. To this end, two separate tests were conducted. First, the step of placing the specimens in the oven for 20 hours was replaced with allowing the specimens to sit at room temp for that same time. The cyclical temperature experiment was repeated for NaCl and MgCl<sub>2</sub> only. The second experiment was to eliminate the oven step and also eliminate the 2 hours of equilibration in lime water prior to the freezer step and the 20 hours in air. If the distress was associated with drying (i.e. salt crystallization or hydraulic pressure) then the distress should disappear with the elimination of the oven. If distress still occurred, chemical attack of the paste constituents is left as a probable cause. The elimination of the lime water conditioning step was also done to isolate osmotic pressure distress that might result from interactions between the lime water and the ionic pore water of the mortars. Given that the distress in the NaCl specimens occurred so quickly, it was thought that 14 days would be enough time to identify the effects of eliminating the oven and lime water steps, respectively. However, the specimens were exposed for up to 56 days.

##### 3.3.1.2 Results of Additional Tests

As shown in Figures 3.121 and 3.122, eliminating the oven step eliminated the rapid failures seen in the original NaCl cyclic tests. However with extended testing, it was shown that distress would still manifest itself in 56 days as is shown in Figure 3.123.

Eliminating both the oven and the lime water steps greatly reduced the distress even further. However, as can be seen in Figure 3.124, distress did still appear. Therefore, it is postulated that either salt crystallization pressures or hydraulic pressures resulting from water evaporation were the cause of the rapid failures seen in the original experiment. However, no hard evidence of salt crystallization was found as a result of petrographic analysis and a specific mechanism was not identified as the cause of these failures. Further, these tests show that the temperature cycle from sub-freezing to room temperature is adequate to bring on distress and this temperature regime should be investigated further. The next phase of this research will use ASTM C 672, which utilizes a temperature cycle from sub-freezing to room temperature.



Figure 3.121. Cylinders exposed to rock salt NaCl solution after 28 days of cyclic temperature test without the oven step. From left to right: 0.40, 0.50, and 0.60 w/c mortar cylinders.



Figure 3.122. Cylinders exposed to rock salt NaCl solution after 28 days of cyclic temperature test without the oven step or the conditioning in lime water step. From left to right: 0.40, 0.50, and 0.60 w/c mortar cylinders.



Figure 3.123. Cylinders exposed to rock salt NaCl solution after 56 days of cyclic temperature test without the oven step. From left to right: 0.40, 0.50, and 0.60 w/c mortar cylinders.



Figure 3.124. Cylinders exposed to rock salt NaCl solution after 56 days of cyclic temperature test without the oven step or the conditioning in lime water step. From left to right: 0.40, 0.50, and 0.60 *w/c* mortar cylinders.

### ***3.3.2 Cold Temperature Experiment***

#### ***3.3.2.1 Additional Tests Performed***

It was determined that the cold temperature experiment showed the most inexplicable damage and to help understand this, a retest of the CaCl<sub>2</sub> samples was undertaken. The goal of these additional tests was to determine the effect of solution concentration on the observed distress. New constant low temperature CaCl<sub>2</sub> samples were exposed to the solutions at varying concentrations. For this experiment, solution concentrations were chosen at 3, 7, 10, and 14 percent for each solution. The specimens were left in solution for 54 days with random samples being pulled every 7 days for inspection and analysis.

#### ***3.2.2.2 Results of Additional Tests***

As can be seen clearly in Figures 3.125 through 3.129, concentration clearly has an affect on the observed damage at a given time for mortars exposed to the low temperature test.



Figure 3.125. Cylinders exposed to  $\text{CaCl}_2$  solution after 56 days of constant low temperature test. From left to right: 0.40, 0.50, and 0.60 w/c mortar cylinders. Solution strength was 3%  $\text{CaCl}_2$ .



Figure 3.126. Cylinders exposed to  $\text{CaCl}_2$  solution after 56 days of constant low temperature test. From left to right: 0.40, 0.50, and 0.60 w/c mortar cylinders. Solution strength was 7%  $\text{CaCl}_2$ .



Figure 3.127. Cylinders exposed to  $\text{CaCl}_2$  solution after 56 days of constant low temperature test. From left to right: 0.40, 0.50, and 0.60 w/c mortar cylinders. Solution strength was 10%  $\text{CaCl}_2$ .



Figure 3.128. Cylinders exposed to  $\text{CaCl}_2$  solution after 56 days of constant low temperature test. From left to right: 0.40, 0.50, and 0.60 w/c mortar cylinders. Solution strength was 14%  $\text{CaCl}_2$ .



Figure 3.129. Cylinders exposed to  $\text{CaCl}_2$  solution after 56 days of constant low temperature test. From left to right: 0.40, 0.50, and 0.60 w/c mortar cylinders. Solution strength was 17%  $\text{CaCl}_2$ .



## **Section 4. Phase II Proposal**

### **4.1 Phase II Background**

As a result of the Phase I experiments, a number of things were learned. First, the cyclical temperature experiment was too severe and did not provide useful information regarding the effects of deicers on mortar. Therefore, it will have little application to concrete and will not be pursued further. The cold temperature experiment had surprising results and it clearly demonstrated that chemical attack by the various deicers is a real possibility. The high temperature experiment by itself did not shed any light on the effects of deicers on mortar or concrete. Additionally, from the DOT survey, feedback from the panel members, and conversations with practitioners around the upper Midwest and western states, it is clear that scaling is the most common manifestation of distress associated with deicers of all types. Therefore, the remainder of this research will focus on two general areas: scaling and chemical attack to concrete at low temperatures in the presence of deicers. Specifically, the effects of solution strength on chemical attack and must be understood and in the former case, the exact mechanisms of chemical attack must be understood in order to make any realistic predictions of service life. Additional information that must be garnered to complete the research includes the relative diffusivity of the various deicers and the effects of sealers on preventing damage must be understood.

### **4.2 Phase II Experimental Plan**

#### ***4.2.1 Overview***

The next phase of this study will investigate the effect the various deicers have on concrete. To this end, tests will be performed to assess scaling, the mechanisms of chemical attack, and the effects of sealers on preventing distress. Also, fundamental material parameters will be determined including the relative diffusivity of the various deicers in concrete and the role of solution strength on concrete degradation. ASTM C 672, “*Standard Test Method for Scaling Resistance of Concrete Surfaces Exposed to Deicing Chemicals*” will be the basis for the majority of the testing. Both unsealed and sealed specimens will be tested. In addition, constant low temperature testing (at 40 °F) will also be conducted. Diffusion and permeability testing will also be conducted.

#### ***4.2.2 Sample Preparation***

A single concrete mixture will be used in this testing, made with a high quality, partially crushed gravel coarse aggregate (maximum aggregate size of 1 in), natural sand, 564 lb/yd<sup>3</sup> type I cement, a vinsol resin air entraining agent (air content of 6 ± 1 percent), and a water-to-cement ratio of 0.44. The slump will be 3 ± 0.5 in. The concrete will be prepared as one batch using a batch plant operated by Arrowhead Concrete, Duluth, Minnesota. Finishing and curing will be done in accordance with ASTM C 672. These cast samples will be 9-in by 10-in by 3 1/2-in deep. They will be used for ASTM C 672 testing, and also serve as the source of the 2-in by 4-in diameter cylinders needed for the other tests to be conducted. These cylindrical samples will be extracted by coring and will be trimmed to the appropriate thickness using a water-cooled diamond saw.

### 4.2.3 Scaling Resistance Testing

Table 4.1 presents the experimental design for the ASTM C 672 testing to be conducted on unsealed concrete specimens. In accordance with ASTM C 672, two replicate samples will be tested at each concentration resulting in a total of 44 specimens being tested. Specimens will have a minimum surface area of 72 in<sup>2</sup> and a depth of 3 in and subjected to freezing and thawing cycles with the various deicers ponded on the surface. In addition to control specimens that will be ponded with lime water, two levels of concentration for each deicer will be used, as listed in Table 4.2. A total of 4 specimens will be tested for each deicer/concentration combination, two of which will be tested to 50 cycles and two of which will be tested for 100 cycles. In addition to rating the surface in accordance with the standard at 5, 10, 15, 25, and every 25 cycles thereafter, mass loss will also be calculated.

Table 4.1. Experimental design for unsealed ASTM C 672 testing.

Solution	Number of Cycles					
	50	100	50	100	50	100
	Control		Low Concentration		High Concentration	
Lime Water	2	2				
NaCl			2	2	2	2
CaCl <sub>2</sub>			2	2	2	2
MgCl <sub>2</sub>			2	2	2	2
CMA			2	2	2	2
Proprietary			2	2	2	2
Total	2	2	10	10	10	10

Table 4.2. Deicer concentrations to be used in the Phase II testing.

Deicer	Concentration (%)	
	Low	High
Lime Water	Saturated Solution	
NaCl	4.4	17.8
CaCl <sub>2</sub>	4.2	17.0
MgCl <sub>2</sub>	3.6	15.0
CMA	6.4	25.0
Proprietary	TBD	TBD

Similar testing will also be conducted on concrete that has been sealed with one of two silane-based sealants. Table 4.3 summarizes the experimental design for the sealant testing. Once again, two replicates will be used, resulting in a total of 24 specimens being tested. Only the higher concentration of deicer will be used in this investigation. It is anticipated that these specimens will be subjected to 100 freeze-thaw cycles.

Table 4.3. Experimental design for sealed ASTM C 672 testing.

Deicer	Sealant 1	Sealant 2
Lime Water	2	2
NaCl	2	2
CaCl <sub>2</sub>	2	2
MgCl <sub>2</sub>	2	2
CMA	2	2
Proprietary	2	2
Total	12	12

In addition to the scaling ratings and mass loss, upon completion of testing, petrography will be conducted on the various specimens. From this analysis, a measure of deicer penetration will be obtained and any alteration to the concrete microstructure will be assessed. This will allow for direct comparisons to be made regarding the effect of deicer concentration, deicer type, and the impact of sealants.

#### 4.2.4 Low Temperature Test

The low temperature testing conducted in Phase I revealed some interesting results, particularly with respect to the observations of chemical degradation observed in the specimens submerged in CaCl<sub>2</sub> and MgCl<sub>2</sub>. To more fully understand these observations, 4-in diameter by 2-in high cylindrical concrete specimens will be made and submerged in deicer solutions at the same concentrations listed in Table 4.2. Each week, the solution will be replaced and mass loss monitored with the specimens being analyzed after 56 and 84 days of submersion, as indicated in Table 4.4.

Table 4.4. Experimental design for cylindrical specimens tested at 40 °F.

Solution	Number of Days					
	56	84	56	84	56	84
	Control		Low Concentration		High Concentration	
Lime Water	2	2				
NaCl			2	2	2	2
CaCl <sub>2</sub>			2	2	2	2
MgCl <sub>2</sub>			2	2	2	2
CMA			2	2	2	2
Proprietary			2	2	2	2
Total	2	2	10	10	10	10

#### 4.2.5 Diffusion and Permeability Assessment

Additional cylindrical specimens will also be cut for diffusion and permeability testing. Specimens will be prepared and tested for sorptivity, to provide an assessment of permeability. Bulk diffusion will be determined using the NordTest, NTBuild 443. Also, rapid chloride permeability will be determined. Samples with and without sealers will be

tested to assess the effectiveness of sealers at slowing chloride diffusion through concrete.

#### ***4.2.6 Analytical Methods***

For Phase II the same petrographic analysis will be applied as was done in Phase I. Optical microscopy, electron, and x-ray microscopy will be used to characterize the microstructure below the scaled surface on the specimens from the scaling study. In those specimens and the constant cold temperature specimens, a thorough analysis of the specimens will be performed to identify any possible signs of chemical or physical distress. Also, chemical modeling will be conducted and correlated with the Phase I and Phase II petrography results to establish potential degradation mechanisms. This modeling will take into account sorptivity and diffusivity parameters measured in section 4.3.3 but will also rely on fundamental published thermodynamic and chemical data.

### Section 5. Revised Schedule

Shown in Figure 5.1 is the project schedule that is modified slightly from the Revised Work Plan, but is still estimating a September, 2005 completion. Tasks 1, 2, 3, 4 and 11 are complete. Task 5 is approximately 60% complete and Task 6 is approximately 50% complete. Task 5 was scheduled for completion September, 2004 but it will take an additional 3 months to complete Task 5. Task 6 is close to being on schedule and given the academic schedule, it is expected this Task will be completed April, 2005. Tasks 7 and 8 will be done sooner than estimated in the original project schedule. Task 7 will start in month 25, rather than 28. Task 8 will start in month 26, rather than 29.

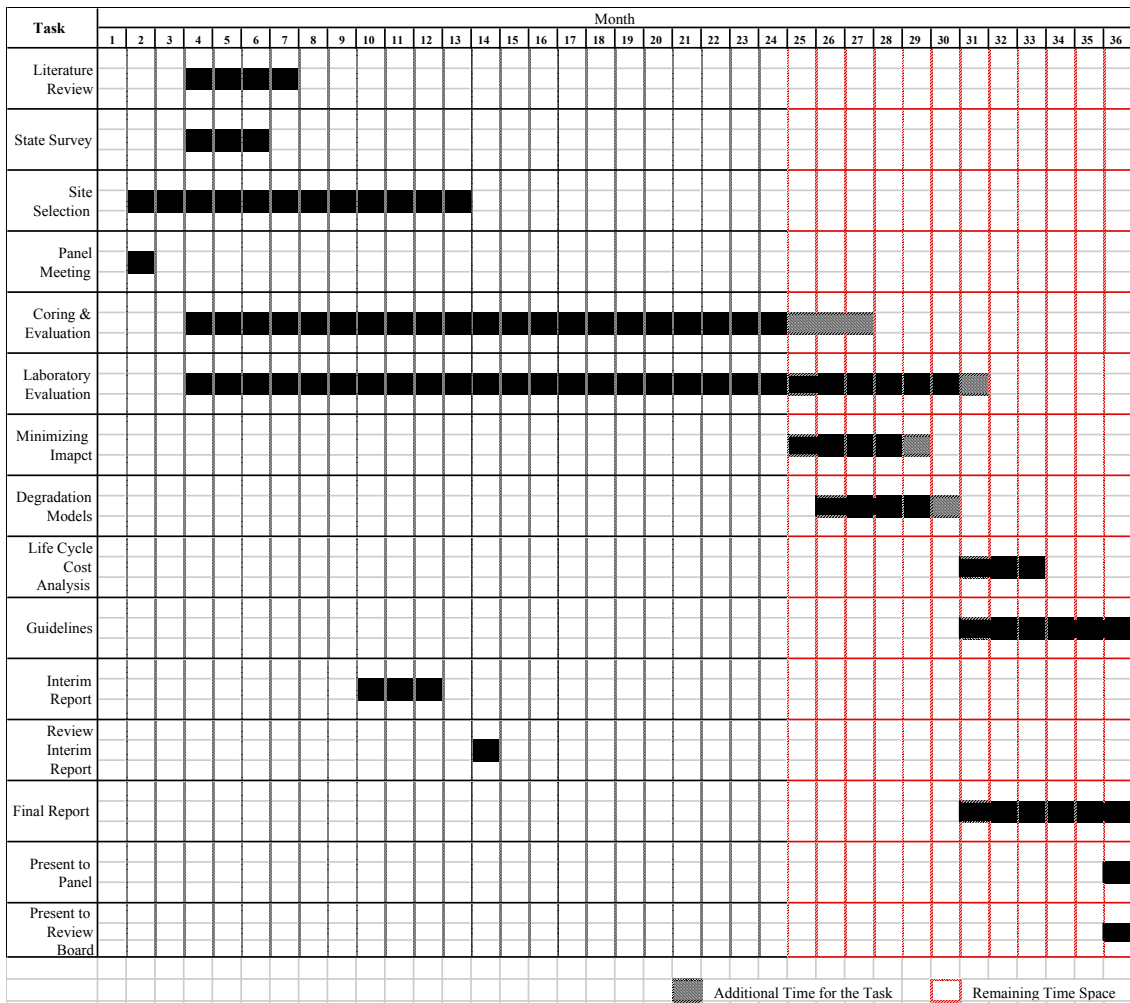


Figure 5.1 Revised project schedule from October 1, 2004 to project end.

## **Section 6. Bibliography**

- ACI (1989). *Corrosion of Metals in Concrete*. ACI Manual Practice ACI 222R-89. American Concrete Institute. Farmington Hills, Michigan.
- ACI (1992a). *Guide to Making a Condition Survey of Concrete in Service*. ACI Manual of Concrete Practice. Part 1. ACI 201.1R-92. ISSN 0065-7875. American Concrete Institute. Farmington Hills, Michigan.
- ACI (1992b). *Guide to Durable Concrete*. ACI Manual of Concrete Practice. Part 1. ACI 201.2R-92. ISSN 0065-7875. American Concrete Institute. Farmington Hills, Michigan.
- ACPA (1992). *Scale-Resistance Concrete Pavements*. Concrete. IS117.02P. American Concrete Pavement Association. Skokie, IL.
- Andrade, C., “Calculation of Chloride Diffusion Coefficients in Concrete From Ionic Migration Measurements”, *Cement and Concrete Research*, 1993 Vol. 23, pp. 724 to 742.
- Barnes, P., Fentiman, C.H., Jeffery, J.W., “Structurally Related Dicalcium Silicate Phases”, *Acta Crystallographica*, 1980, Section A, **36**, pp. 353 to 356.
- Basheer, P. A. M., A. E. Long, and F. R. Montgomery (1994). “An Interaction Model for Causes of Deterioration and Permeability of Concrete.” *Concrete Technology Past, Present, and Future*. V. M. Mohan Malhotra Symposium. ACI. SP-144. American Concrete Institute, Farmington Hills, MI. pp. 213-231.
- Bentz, D.P., “Influence of Silica Fume on Diffusivity in Cement-Based Materials II: Multi-Scale Modeling of Concrete Diffusivity”, *Cement and Concrete Research*, 2000, Vol. 30, pp.1121 to 1129.
- Berntsson, L. & Chandra, S., “Damage by concrete sleepers by calcium chloride”, *Cement and Concrete Research*, 1982, Vol. 12, pp. 87-92.
- Bilodeau, A., G. G. Carette, V. M. Malhotra, and W. S. Langley (1991). “Influence of Curing and Drying on Salt Scaling Resistance of Fly Ash Concrete.” *Durability of Concrete*. Second International Conference, Montreal, Canada. Volume I. ACI. SP-126. pp. 201-228.
- Bilodeau, A., and V. M. Malhotra (1992). “Concrete Incorporating High Volumes of ASTM Class F Fly Ashes: Mechanical Properties and Resistance to Deicing Salt Scaling and to Chloride-Ion Penetration.” *Fly Ash, Silica Fume, and Natural Pozzolans in Concrete*. V.M. Malhotra, Ed. Proceedings, Fourth International Conference. ACI SP-132. pp. 319-349.

Bleszynski, R.F., R.D. Hooton, M.D.A. Thomas, and C.A. Rogers (2002). "Investigations into the Durability of Ternary Blend Concrete Laboratory and Outdoor Exposure Site Studies." *TRB 2002 Annual Meeting CD-ROM*. Transportation Research Board. Washington, D.C.

Bonen, D. & Sarkar, S.L., "Environmental attack on concrete", *Proceedings of the 16<sup>th</sup> International Conference on Cement Microscopy*, Eds. Gouda, G.R., Nisperos, A, & Bayles, J., *International Cement Microscopy Association, Texas*, 1994, pp. 11-23.

Boulfiza, M., Sakai, K., Banthia, N., Yoshida, H., "Prediction of Chloride Ions Ingress In Uncracked and Cracked Concrete", *ACI Materials Journal*, 2003 Vol. 100, No. 1, pp. 38 to 48.

Buck, A. D. (1985a). *A Discussion of the Paper " The Penetration of Chlorides into Hardened Cement Pastes" by H.D. Midgley and J. M. Illston.* Cement and Concrete Research. Vol. 15. No. 5. pp. 933-934.

Buck, A. D. (1985b). *A Discussion of the Paper " The Penetration of Chlorides into Hardened Cement Pastes" By H.D. Midgley and J. M. Illston.* Cement and Concrete Research. Vol. 15. No. 5. pp. 933-934.

Butler, W. B. (1982). *A Critical Look at ASTM C 618 and C 311.* Cement, Concrete, and Aggregates. Vol. 4. No. 2. ASTM. Winter. pp. 68-72.

Byfors, K. (1987). "Influence of Silica Fume and Fly Ash on Chloride Diffusion and pH Values in Cement Paste." *Cement and Concrete Research*. Vol. 17. No. 1. pp. 115-129.

Chatterji, S. (1994). A Discussion of the Paper *The Effectiveness of Supplementary Cementing Materials in Suppressing Expansion Due to ASR. Part 1. Concrete Expansion and Portlandite Depletion.* Cement and Concrete Research. pp. 1572-1573.

Chatterji, S, (1994), "Transportation of Ions Through Cement Based Materials. Part 2: Adaptation of the Fundamental Equations and Relevant Comments", *Cement and Concrete Research*, Vol. 24, No. 6, pp. 1010 to 1014.

Chatterji, S, (1994), "Transportation of Ions Through Cement Based Materials. Part 3: Experimental Evidence for the Basic Equations and Some Important Deductions", *Cement and Concrete Research*, Vol. 24, No. 7, pp. 1229 to 1236.

Cody, R.D., P.G. Spry, A.M. Cody, and G. Gan (1994). *The Role of Magnesium in Concrete Deterioration*. Final Report for Iowa DOT HR-355. Iowa Highway Research Board. Ames, IA. November. pp. 171.

Cody, R.D., A.M. Cody, P.G. Spry, and G. Gan (1996). "Experimental Deterioration of Highway Concrete by Chloride Deicing Salts." *Environmental and Engineering Geoscience*. Volume II, No. 4. Winter. pp. 575-588.

Colleparidi, M., L. Coppola, and C. Pistolesi (1994). "Durability of Concrete Structures Exposed to  $\text{CaCl}_2$  Based Deicing Salts." *Durability of Concrete*. V.M. Malhotra Ed. Third International Conference, Nice, France. ACI SP-145. pp. 107-120.

Colville, A.A., Geller, S., "The Crystal Structure of Brownmillerite,  $\text{Ca}_2\text{FeAlO}_5$ ", *Acta Crystallographica*, 1971, Section B, **27**, pp. 2311 to 2315.

Colville, A.A., Geller, S., "Crystal Structures of  $\text{Ca}_2\text{Fe}_{1.43}\text{Al}_{0.57}\text{O}_5$  and  $\text{Ca}_2\text{Fe}_{1.28}\text{Al}_{0.72}\text{O}_5$ ", *Acta Crystallographica*, 1972, Section B, **28**, pp. 3196 to 3200.

Costa, A, Appleton, J., "Chloride Penetration Into Concrete in Marine Environment. Part II: Prediction of Long Term Chloride Penetration", *Materials and Structures*, 1999, Vol. 32, pp. 354 to 359.

Crumpton, C. F., B. J. Smith, and G. P. Jayaprakash (1989). *Salt Weathering of Limestone Aggregate and Concrete Without Freeze-Thaw*. Transportation Research Record 1250. Transportation Research Board. pp. 8-16.

Day, R.L, "The effect of secondary ettringite formation on durability of concrete: A Literature Analysis", *PCA Research and Development Bulletin RD108T*, 1992, pp. 1-115.

Detwiler, R. J., C. A. Fapohunda, and J. Natale. (1994). Use of *Supplementary Cementing Materials to Increase the Resistance to Chloride Penetration of Concretes Cured at Elevated Temperatures*. ACI Materials Journal. Vol. 91. No. 1. January-February. pp. 63-66.

Dow Chemical Company, "The Very Short Course", *Pamphlet*, August 1999, Dubberke, W. and Marks, V.J., "The Effects of Deicing Salts on Aggregate Durability", *Transportation Research Record, [1031] (Geotechnical Engineering Research)*, pp. 27-34, 1985.

Feldman, R. F., G. W. Chan, R. J. Brousseau, and P. J. Tumidajski (1994). *Investigation of the Rapid Chloride Permeability Test*. ACI Materials Journal. Vol. 91. No. 2. May-June. pp. 246-255.

Ftikos, C., and G. Parissakis (1985). *The Combined Action of  $\text{Mg}^{2+}$  and  $\text{Cl}^-$  Ions in Cement Pastes*. Cement and Concrete Research. Vol. 15. No. 4. pp. 593-599.

Gagne, R., Pigeon, M., Revertegat, E., and Aitcin, P.C. (1992). "Chloride Ions in Cement pastes: Influence of the Cement Type and Long Time Effect of the Concentration of Chlorides." *Cement and Concrete Research*. Vol. 22, No. 2-3, pp. 451-457.

Gebler, S. H., and P. Klieger (1986a). Effect of Fly Ash on the Durability of Air-Entrained Concrete. Research and Development Bulletin RD090.01T, Portland Cement Association, Skokie, IL.



Gegout, P., Revertegat, E., and Moine, G. (1992). "Chloride Ion Attack on Low Water-Cement Ratio pastes Containing Silica Fume." ACI SP-132. Edited by V. Malhotra, pp. 1471-1490.

Gerard, B., Marchand, J., "Influence of cracking on the diffusion properties of cement-based materials Part I: Influence of continuous cracks on the steady-state regime", *Cement and Concrete Research*, 2000, Vol. 30, pp. 37 to 43.

Gerold B. T. (2000). "Estimation of water-cement ratios using fluorescent petrography and extreme value distributions", a thesis submitted for the degree of Master of Science in Civil Engineering, Michigan Technological University.

Ghafoori, N., and R. P. Mathis (1997a). *Scaling Resistance of Concrete Paving Block Surface Exposed to Deicing Chemicals*. ACI Materials Journal. Vol. 94, No. 1. January-February. pp. 32-38.

Gilfillan, Graham, "Road Safety Benefits of Liquid Anti-Icing Strategies and Agents", Kamloops, British Columbia, Canada, *Winter Road Research & Development*, Insurance Corporation of British Columbia, 2000.

Gilfillan, Graham, "Environmental Impacts of New Technology in Winter Maintenance", Insurance Corporation of British Columbia, March 2001.

Gillott, J. E., and C. A. Rogers (1994). *Alkali-Aggregate Reaction and Internal Release of Alkalis*. Magazine of Concrete Research. Vol. 46. No. 167. pp. 99-112.

Girard, R.J., Myers, W., Manchester G.D., Trimm W.L., "D-cracking: Pavement Design and Construction Variables" *Transportation Research Record, [853] (Concrete Analysis and Deterioration)*, pp. 1-9, 1982.

Gowripalan, N., J. G. Cabrera, A. R. Cusens, and P. J. Wainwright (1993). *Effect of Curing on Durability*. Durable Concrete. ACI Compilation 24. pp. 47-54.

Gress, David (1997). Preventing Early Distress in Concrete Pavements. Report No. FHWA-SA-97-045. Final Report. Federal Highway Administration. Washington, D.C.

Halamickova, P., R.J. Detwiler, D.P. Bentz, and E.J. Garboczi, *Water Permeability and Chloride Ion Diffusion in Portland Cement Mortars: Relationship to Sand Content and Critical Pore Diameter*, *Cement and Concrete Research*, 1995, Vol. 25, pp. 790-802.

Hanke, H., "New Experiences with the Use of Abrasives in Germany" *Proceedings from the Xth PIARC International Winter Road Congress*, Lulea, Sweden, Vol. 2, pp. 469-475, March 1998.

Hansen, W. C. (1963). "Crystal Growth as a Source of Expansion in Portland-Cement Concrete." *Proceedings*, American Society for Testing and Materials. Vol. 63. pp. 932-945.

Harnik, A. B., U. Meier, and A. R. Šli (1980). "Combined Influence of Freezing and Deicing Salt on Concrete - Physical Aspects." ASTM STP 691. American Society for Testing and Materials. pp. 474-484.

Hauer, J., Berger, G., Feige, J.M., Feige, D., Reimer, C. & Romness, R., *Snow and Ice Control: A Best Practices Review*, Office of the Legislative Auditor, State of Minnesota, May 1995.

Hoffman, D.W. (1984). "Changes in Structure and Chemistry of Cement Mortars Stressed by a Sodium Chloride Solution." *Cement and Concrete Research*. Vol. 14, No. 1, pp. 49-56.

Hofmeister, W., Von Platen, H., "Crystal Chemistry and Atomic Order in Brucite-Related Double-Layer Structures", *Crystallography Reviews*, 1992, Vol. 3, pp. 3 to 29.

Jang, J. and I. Iwasaki (1993). Effect of Salt Additives on Concrete Degradation. Report No. MN/RD-93/10. Minnesota Department of Transportation, St. Paul, MN.

Jeffery, J.W., "The Crystal Structure of Tricalcium Silicate", *Acta Crystallographica*, 1952, 5, pp. 26 to 35.

Ketcham, S.A., Minsk, L.D., Blackburn, R.R. & Fleege, E.J., *Manual of Practice for an Effective Anti-icing Program: A Guide for Highway Winter Maintenance Personnel*, Federal Highway Administration, 1996.

Klieger, P., and S. Gebler (1987). *Fly Ash and Concrete Durability*. Concrete Durability. ACI. SP-100-56. pp.1043-1069.

Kosmatka, S. H., B. Kerkhoff, and W. C. Panarese (2002). *Design and Control of Concrete Mixtures*. Fourteenth Edition. Engineering Bulletin 001. Portland Cement Association, Skokie, IL. 358 pp.

Kuemmel, D. & Bari, Q, *Benefit/Cost Comparisons of Salt Only Vs. Salt/Abrasive Mixtures Used in Winter Highway Maintenance in the USA*, 4<sup>th</sup> International Symposium on Snow Removal and Ice Control Technology, Reno, Nevada, August 1996.

Kurdowski, W., Trybalska, B., & Duszak, S., "SEM studies of corrosion of cement paste in chloride solution", *Proceedings of the 16<sup>th</sup> International Conference on Cement Microscopy*, Eds. Gouda, G.R., Nisperos, A, & Bayles, J., *International Cement Microscopy Association, Texas*, 1994, pp. 80-89.

Lambert, P., Page, C.L., Short, N.R., "Pore Solution of the Hydrated System Tricalcium Silicate/Sodium Chloride/Water", *Cement and Concrete Research*, 1985 15, pp. 675 to 680.

Lamond, J. F. (1983). *Twenty-Five Years' Experience Using Fly Ash Concrete*. Fly Ash, Silica Fume, Slag & Other Mineral By-Products in Concrete, Volume I. ACI, SP-79. pp. 47-69.

- Lee, Hyomin, Cody, Robert D., Cody, Anita M. & Spry, Paul G., “PCC Pavement Deterioration and Expansive Mineral Growth”, *Transportation Conference Proceedings*, 1998, pp. 71-75.
- Lee, H., Cody, R.D., Cody, A.M., Spry, P.G., “Effects of Various Deicing Chemicals on Pavement Concrete Deterioration”, *Mid-Continent Transportation Symposium Proceedings*, 2000, pp. 151 to 155.
- Lu, X., “Application of the Nernst-Einstein Equation to Concrete”, *Cement and Concrete Research*, 1997, Vol. 27, No. 2, pp. 293 to 302.
- Malek, R. I. A., and D. M. Roy (1988). “The Permeability of Chloride Ions in Fly Ash-Cement Pastes, Mortars and Concrete.” *Material Research Society Symposium Proceedings: Volume 114*. Materials Research Society, pp. 325-335.
- Malhotra, V. M., G. C. Carrette, A. Bilodeau, and V. Sivasundaram (1991). “Some Aspects of Durability of High-Volume ASTM Class F (Low Calcium) Fly Ash Concrete.” *Durability of Concrete*. Second International Conference, Montreal, Canada. Volume I. ACI. SP-126. pp. 65-82.
- Mangat, P.S., Gurusamy, Kribanandan, “Chloride Diffusion in Steel Fibre Reinforced Marine Concrete”, *Cement and Concrete Research*, 1987, Vol. 17, pp. 385 to 396.
- Marchand, J., E. J. Sellevold, and M. Pigeon (1994). “The Deicer Salt Scaling Deterioration of Concrete - An Overview.” *Durability of Concrete*. V. M. Malhotra, Ed. Third International Conference, Nice, France. ACI SP-145. pp. 1-46.
- McCrum, R.L., “Calcium Magnesium Acetate and Sodium Chloride as Highway Deicing Salts”, *Environmental Treatment & Control*, MP Dec. 1989. pp. 24-28.
- McDonald, D.B., Perenchio, W.F., “Effects of Salt Type on Concrete Scaling”, *Concrete International*, 1997, pp. 23-26.
- Mehta, P. K. (1991). *Durability of Concrete - Fifty Years of Progress? Durability of Concrete*. Second International Conference, Montreal, Canada. Volume I. ACI. SP-126. pp. 1-31.
- Mehta, P. K. and P.J.M. Monteiro (1993). Concrete: Structure, Properties, and Materials. Second Edition. Prentice Hall. Englewoods Cliffs, NJ.
- Mehta, P. K. (1997). *Durability—Critical Issues for the Future*. Concrete International. Volume 19, No. 7. July. pp. 27-33.
- Mindess, S., and J. F. Young, Concrete. Englewood Cliffs, N.J.: Prentice-Hall, Inc., 1981.
- Mindess, S., Young, J., & Darwin, D., “Concrete”, 2<sup>nd</sup> ed., Pearson Education, Inc., NY, 2003.

Minsk, L.D., "Snow and Ice Control Manual for Transportation Facilities", McGraw Hill, 1998.

Misra, S., A. Yamamoto, T. Tsutsumi, and K. Motohashi (1994). "Application of Rapid Chloride Permeability Test to Quality Control of Concrete." *Durability of Concrete*. V. M. Malhotra, Ed. Third International Conference, Nice, France. ACI SP-145. pp. 487-502.

Mobasher, B., and T. M. Mitchell (1988). "Laboratory Experience with the Rapid Chloride Permeability Test." *Permeability of Concrete*. ACI. SP-108. pp. 117-143.

Mondal, P. Jeffery, J.W., "The Crystal Structure of Tricalcium Aluminate,  $\text{Ca}_3\text{Al}_2\text{O}_6$ ", *Acta Crystallographica*, 1975, Section B, **31**, pp. 689 to 696.

Monosi, S., and Colleparidi, M., *Research on  $3\text{CaO} \cdot \text{CaCl}_2 \cdot 15\text{H}_2\text{O}$  Identified in Concrete Damage by  $\text{CaCl}_2$  Attack*, IL Cemento, Jan-March 1990, Vol. 87, pp. 3-8.

Moukwa, M., "The Attack of Cement Paste by  $\text{MgSO}_4$  and  $\text{MgCl}_2$  from the Pore Structure Measurements", *Cement and Concrete Research*, 1990, Vol. 20, pp. 148-158.

Mu, Ru, Miao, Changwen, Luo, Xin, Sun, Wei, "Interaction Between Loading, Freeze-Thaw Cycles, and Chloride Salt Attack of Concrete With and Without Steel Fiber Reinforcement", *Cement and Concrete Research*, 2002 Vol. 32, pp. 1061 to 1066.

Muethel, R. W. (1997). *Investigation of Calcium Hydroxide Depletion as a Cause of Concrete Pavement Deterioration*. Research Report R-1353. Michigan Department of Transportation Materials and Technology Division. November.

Munoz, S. R., and E. Y. J. Chou (1994). "Durability of Concrete Materials Under Pavement Joints." *Infrastructure: New Materials and Methods of Repair — Proceedings of the Third Materials Engineering Conference*. ASCE, San Diego, CA, Nov 13-16. pp. 1-7.

Nagesh M., Bhattacharjee, B., "Modeling of Chloride Diffusion in Concrete and Determination of Diffusion Coefficients", *ACI Materials Journal*, 1998 Vol. 95, No. 2, pp. 113 to 120.

Neville, A. M. (1996). *Properties of Concrete*. John Wiley and Sons, Inc., New York, New York.

Neville, A. M. (1997). *Suggestions of Research Areas Likely to Improve Concrete*. Reprint for Transportation Research Board Forum on January 12, 1997.

Nixon, P., and C. Page (1987). "Pore Solution Chemistry and Alkali Aggregate Reaction." *Concrete Durability*. J.M. Scanlon, Ed. Katherine and Bryant Mather International Conference. ACI SP-100. pp. 1833-1863.

- Nixon, William A., "The Use of Abrasives in Winter Maintenance" *Final Report of Project TR 434*, Iowa DOT & Iowa Highway Research Board, March 2001.
- Papadakis, V.G., Fardis, M.N., Vayenas, C.G., (1996), "Physicochemical Processes and Mathematical Modeling of Concrete Chlorination", *Chemical Engineering Science*, **51**, No. 4, pp. 505 to 513.
- PCA (1992). Design and Control of Concrete Mixtures. Thirteenth Edition. Portland Cement Association. Skokie, IL.
- Perchanok, M.S., Comfort, G.A. & Dinovitzer, A., "Winter Sand Application & Stopping Distance on Snow & Ice Covered Highways", *Analysis and Application Paper for 1997 XIII<sup>th</sup> IRF World Meeting*, Ontario Ministry of Transport, 1997.
- Pereira, C.J., Hegedus, L.L., (1984), "Diffusion and Reaction of Chloride Ions in Porous Concrete", *Proceedings of the 8<sup>th</sup> International Symposium of Chemical Reaction Engineering*, Edinburgh.
- Perenchio, W. F. (1994). "Corrosion of Reinforcing Steel." *Significance of Tests and Properties of Concrete and Concrete-Making Materials*. STP 169C. Publication Code Number 04-169030-07. American Society for Testing and Materials, Philadelphia, PA. pp. 164-172.
- Pigeon, M. (1994). "Frost Resistance, A Critical Look." *Concrete Technology Past, Present, and Future*. V.M. Mohan Malhotra Symposium. ACI. SP-144. pp. 141-157.
- Pigeon, M., and R. Plateau (1995). *Durability of Concrete in Cold Climates*. E & FN Spon. ISBN: 0-419-19260-3. 244 pp.
- Powers T.C. (1975). Freezing Effects in Concrete. *Durability of Concrete*. ACI Special Publication SP-47-1. pp. 1-12.
- QCL Group (Australian), "Sulphate Attack and Chloride Ion Penetration: Their Role in Concrete Durability", *QCL Group Technical Notes*, 1999, pp. 1 to 8.
- Ramachandran, V.S., Phill, M.SC., and Ceream, F.I., "Calcium Chloride in Concrete", Applied Science Publishers Ltd, 1976, 207 p.
- Reid Crowther Consulting Inc., "The Economic Impact of Magnesium Chloride Deicer on Concrete Bridge Decks", *A Study for Montana Department of Transportation*, 2000.
- Rezansoff, T. & Scott, D., "Durability of Concrete Containing Chloride Based Accelerating Admixtures", *Canadian Journal of Civil Engineering*, 1988, Vol. 17, pp. 102 to 112.
- Roosevelt, D.S., & Fitch, G.M., "Evaluation of an Ice Ban Product as a Prewetting Agent for Snow Removal and Ice Control Operations", VTRC 00-R12, Jan. 2000.

Rösli, A., & Harnik, A.B., “Improving the Durability of Concrete to Freezing and Deicing Salts”, *Durability of Building Materials and Components*, ASTM STP 691, P.J. Serada and G.G. Litvan, EDS., American Society for Testing and Materials, 1980, pp. 464-473.

Roskopf, P.A., Linton, F.J., Pepler, R.B., “Effect of Various Accelerating Chemical Admixtures on Setting and Strength Development of Concrete”, *Journal of Testing and Evaluation*, 1975, Vol. 3, No.4, pp. 322 to 330.

Roy, D. M., P. D. Cady, S. A. Sabol, and P. H. Licastro (1993a). *Concrete Microstructure: Recommended Revision to Test Methods*. SHRP-C-339. Strategic Highway Research Program. National Research Council, Washington DC.

Roy, D. M., and G. M Idorn (1993b), *Concrete Microscopy*. Publication No. SHRP-C-340. Strategic Highway Research Program, Washington, DC. August.

Santagata, M.C. & Collepardi, M., “The Effect of CMA Deicers on Concrete Properties”, *Cement and Concrete Research*, Vol. 30, 2000, pp. 1389-1394.

Santhanam, Manu, Cohen, Menashi, & Olek, Jan, “Study of Magnesium Ion Attack in Portland Cement Mortars”, *Proceedings from the 11<sup>th</sup> International Congress on The Chemistry of Cement*, 2003, pp. 1460-1474.

Snow, Peter G., “Magnesium Chloride as a Road Deicer: A Critical Review”, <http://www.nrmca.org/engineering/MagChloride/MagchlorideWhitePaper.pdf>, Burns Concrete, Inc., Idaho Falls, Idaho, 2001.

Stanish, K. D., R. D. Hooton, and M. D. A Thomas (2000). *Testing the Chloride Penetration Resistance of Concrete: A literature Review*. FHWA Contract DTFH61-97-R-00022, University of Toronto, Toronto, Ontario, Canada. (June).

Stark, J., and H. M. Ludwig (1997). “Freeze-Thaw and Freeze-Deicing Salt Resistance of Concrete Containing Cement Rich in Granulated Blast Furnace Slag.” *ACI Materials Journal*. Vol. 94, No. 1. January-February. pp. 47-55.

Sutter, L.L., K.R. Peterson, Van Dam, T.J., K.D. Smith, M.J. Wade. “Guidelines for Detection, Analysis, and Treatment of Materials-Related Distress in Concrete Pavements, Volume 3: Case Studies Using the Guidelines”, FHWA Contract No. DTFH61-96-C-00073, Prepared for the Federal Highway Administration, Turner-Fairbank Highway Research Center, McLean, VA, September, 2001.

Sutter, L.L., T.J. Van Dam, K.R. Peterson, and A. Ganguly, “The X-Ray Microscope: A New Tool for Determining Chloride Ion Diffusion in Hardened Concrete”, Proceedings of the Conference on Advances in Cement and Concrete, Copper Mountain, Colorado, August 10-14, 2003.

Suryavanshi, A.K., Swamy, R.N., McHugh, S., “Chloride Penetration Into Reinforced Concrete Slabs”, *Canadian Journal of Civil Engineering*, 1998, Vol. 25, pp. 87 to 95.

Taylor, H.F.W., *Cement Chemistry*: Academic Press Ltd., London, 1990.

Thomas, M.D.A., Bamforth, P.B., "Modeling Chloride Diffusion in Concrete, Effect of Fly Ash and Slag", *Cement and Concrete Research*, 1999, Vol. 29, pp. 487 to 495.

Torri, K., and M. Kawamura (1992). "Pore Structure and Chloride Permeability of Concrete Containing Fly Ash, Blast Furnace Slag and Silica Fume." *Fly Ash, Silica Fume, and Natural Pozzolans in Concrete*. V. M. Malhotra, Ed. Proceedings, Fourth International Conference. ACI SP-132. Istanbul, Turkey, May. pp. 135-150.

Transportation Research Board (TRB) (1999). *Durability of Concrete*. Transportation Research Circular. Transportation Research Board, National Academies of Science, Washington, DC.

Truc, O, Ollivier, J.P., Carcasses, M., "A New Way for Determining the Chloride Diffusion Coefficient in Concrete from Steady State Migration Test", *Cement and Concrete Research*, 2000, Vol. 30, pp. 217 to 226.

Tumidajski, P.J., & Chan, G.W., "Durability of high performance concrete in magnesium brine", *Cement and Concrete Research*, 1996, Vol. 26, No. 4, pp. 557-565.

Van Dam, T.J., L.L. Sutter, K.D. Smith, M.J. Wade, K.R. Peterson, (2002a). *Guidelines for Detection, Analysis, and Treatment of Materials-Related Distress in Concrete Pavements, Volume 1: Final Report*. FHWA-RD-01-163. Federal Highway Administration. Turner-Fairbank Highway Research Center, McLean, VA, March.

Van Dam, T.J., L. L. Sutter, K. D. Smith, M. J. Wade, and K. R. Peterson (2002b). *Guidelines For Detection, Analysis, And Treatment Of Materials-Related Distress In Concrete Pavements - Volume 2: Guidelines Description and Use*. FHWA-RD-01-164. Federal Highway Administration. Turner-Fairbank Highway Research Center, McLean, VA. March. pp. 233.

Walker, H. N. (1980). *Formula for Calculating Spacing Factor for Entrained Air Voids. Cement, Concrete, and Aggregates*. Vol. 2. No. 2. Winter 1980. pp. 63-66.

Whiting, D., M. Nagi, P. Okamoto, T. Yu, D. Peshkin, K. Smith, M. Darter, J. Clifton, and L. Kaetzel (1994). *Optimization of Highway Concrete Technology*. SHRP-C-373. Strategic Highway Research Program. National Research Council. Washington D.C.

Williams, D., "Past and Current Practices of Winter Maintenance at the Montana Department of Transportation (MDT)", Dec. 2001.

Winkler, E. M., and Singer, P. C., (1972). "Crystallization Pressure of Salts in Stone and Concrete." *Bull. Geol. Soc. Am.*, 83 [11 3509-3514

Wolter, S. (1997). *Ettringite: Cancer of Concrete*. American Petrographic Laboratories, St. Paul, MN.

Worthington, J.C., Bonner, D.G., & Nowell, D.V., "Influence of Cement Chemistry on Chloride Attack of Concrete", *Materials Science Technology*, 1988, Vol. 4, pp. 305-313.

Yehia, S.A., Tuan, C.Y., "Conductive Concrete Can Cut Deicing Costs", *Better Roads*, 2003, pp. 66 to 69.

Yunping, X., Bazant, Z.P., Monila, L., "Moisture Diffusion In Cementitious Materials", *Advanced Cement Based Materials*, 1994, Vol. 1, pp. 258 to 266.

Zia, P., M. L. Leming, S. H. Ahmad, J. J. Schemmel, R. P. Elliot, and A. E. Naaman (1993). *Mechanical Behavior of High Performance Concretes, Volume 1: Summary Report*. SHRP-C-361. Strategic Highway Research Program, National Research Council, Washington DC.